Exploring Dark Energy Using Various Probes of Large Scale Structure in the Post-reionization Epoch

THESIS

Submitted in partial fulfillment
of the requirements for the degree of

DOCTOR OF PHILOSOPHY

by

Chandrachud Bijay Vaswar Dash
ID: 2018PHXF0046P

Under the Supervision of

Prof. Tapomoy Guha Sarkar

BITS Pilani
Pilani | Dubai | Goa | Hyderabad

BIRLA INSTITUTE OF TECHNOLOGY AND SCIENCE, PILANI

2024

BIRLA INSTITUTE OF TECHNOLOGY AND SCIENCE
PILANI - 333031 (RAJASTHAN) INDIA

CERTIFICATE

This is to certify that the work reported in the Ph.D. thesis entitled "**Exploring Dark Energy Using Various Probes of Large Scale Structure in the Post-reionization Epoch**", submitted by **Chandrachud Bijay Vaswar Dash**, with ID. **2018PHXF0046P** at the Physics Department, BITS Pilani, Pilani campus for the award of the degree of Doctor of Philosophy (Ph.D.), is a bonafide record of his original work carried out under my supervision. This work has not been submitted elsewhere for any other degree or diploma.

Prof. Tapomoy Guha Sarkar

Professor, Department of Physics
BITS - Pilani, Pilani Campus, Rajasthan, India.

Date:

Dedicated to ...
all those who inspired me

Acknowledgements

I want to start by sincerely thanking my advisor, Prof. Tapomoy Guha Sarkar, for his unwavering support of my Ph.D. research, for his inspiration, passion, and immense knowledge, and for granting me the opportunity to study the field of cosmology in an informal yet adept environment. I could not have imagined having a better advisor and mentor for my doctoral study.

In addition to my advisor, I am grateful to the remaining members of my thesis review committee: Prof. Biswanath Layek and Prof. Madhukar Mishra. Their motivating support, perceptive observations, constructive critique, and valuable suggestions throughout the progress review and thesis drafting process are sincerely appreciated.

I sincerely thank Prof. Rakesh Choubisa, Head of the Department, and Prof. V. Manjuladevi, DRC Convener, for their persistent support. Also, I wish to express my gratitude to all the past HODs, DRC conveners, and faculty members of the physics department for their kind support from time to time. A special thanks to Prof. Jayendra N. Bandyopadhyay for fostering a memorable and enjoyable teacher-student bond. Additionally, I extend my appreciation to Prof. R.R. Mishra for delivering excellent lectures and providing valuable assistance in understanding quantum mechanics and mathematical physics during coursework. The technical staff of the department, Rajeev Ji, Shrikant Ji & Kundan, are also gratefully thanked for their help.

I would humbly express my regards to the Vice-Chancellor, Director and Deans of Birla Institute of Technology & Science (BITS), Pilani, for allowing me to pursue my doctoral studies by providing the necessary facilities and financial support. I extend my heartfelt gratitude to current and former Deans and Associate Deans of AGSRD, with special acknowledgment to Prof. Shamik Chakraborty. All other staff members of AGSRD are also gratefully thanked for their help.

I would like to express my gratitude to (Dr.) Pradeep and (Dr.) Ishan, whose companionship and friendship have enriched these years. Through Pradeep, I've imbibed the true essence of life, while Ishan illuminated the depths of physics and mathematics for me. I would like to thank Amrit and Anju for all the support they have provided me during my toughest times here at BITS Pilani. From paneer recipes to dumb-saraz game nights and from tea

to movie watch, you've made the last five years a lot of fun and something I won't forget. The paragraph would not be complete without thanking my best friend, Lizu, for her love and constant support.

In the same breath, I would also like to thank all the colleagues who have walked alongside me through moments of concern and joy, product launches, and coffees over the years. Thanks to (Dr.) Ram, (Dr.) Chitti, (Dr.) Nikita, Aakash, (Dr.) Khushboo, Aayushi, and all my football team buddies for all the memories we have. A special thanks to (Dr.) Ashis and (Dr.) Anjan for their generous support and guidance in the realm of research.

Last but not least, I want to express my heartfelt gratitude to my family. Their unwavering support has been the cornerstone of my journey, with a special mention to my incredible mother. Her constant belief in my aspirations and unending encouragement has been my guiding light. Over the years, she has imparted the invaluable lesson that diligence knows no bounds and that any goal is within reach through hard work. A shout-out also goes to my brother, Ardhendu, whose genuine and steadfast support has been a constant source of strength.

Finally, despite my love for physics, the work reported in this thesis would not have been possible without the financial support of JRF, BITS Pilani Institute fellowship, for which I am grateful.

There are many more people I could thank, but constraints on space-time and modesty compel me to stop here.

Chandrachud Bijay Vaswar Dash
BITS-Pilani, Pilani campus

ABSTRACT

A large number of recent observations have indicated that the expansion of the Universe is accelerating. The underlying cause of this acceleration is, however, largely unknown. A dark energy component with an equation of state (EoS) $P/\rho = w < -1/3$ remains the classic explanation for cosmic acceleration. Given the diversity of theoretical models with the same general phenomenological implications, it becomes crucial for observations to constrain the parameter space for dark energy models. In our study, we explore the landscape of dark energy models by considering the following approaches (i) model-independent EoS parametrizations, (ii) dark energy as modification of gravity in a $f(R)$ theory, and (iii) specific Quintessence models. Since dark energy affects the late time evolution, we have focused our attention to the post-reionization ($z \leq 6$) probes of cosmology. We consider three probes that imprint the background expansion history and growth of perturbations. We firstly consider weak lensing of background sources by intervening large-scale structure. Here, the quantity of interest is the power spectrum of the distortion field which imprints dark energy through the cosmology dependent geometric quantities and the growth rate of density fluctuations. We also use two probes of the post-reionization neutral hydrogen distribution, namely (i) 21-cm intensity mapping, and (ii) Ly-α forest. These probes act as tracers of the dark matter and provide 3D and 1D tomographic images of the underlying large-scale structure, respectively over a wide range of redshifts. The statistical properties of the weak lensing convergence field, the 21-cm signal and the Ly-α are quantified through their auto and cross power spectra. We have used existing observational parameters for weak lensing experiments, Ly-α forest observational data and considered futuristic observations of the 21-cm signal using presently functioning and upcoming radio telescopes. We have used a Fisher-Cramer-Rao, Monte-Carlo analysis to show what dark energy models can be differentiated from the ΛCDM model with a high SNR. We have further obtained observational bounds and error projections of model parameters. We find that upcoming radio observations shall provide tight bounds on dark energy models and help us understand the nature of dark energy by restricting the parameter space.

Contents

List of Figures

List of Abbreviations/Symbols

c	Speed of light
G, G_N	Newtonian gravitational Constant
$g_{\mu\nu}$	Metric tensor
$T_{\mu\nu}$	Energy-momentum tensor
$\Gamma_{\mu\nu}$	Christoffel symbol
$G_{\mu\nu}$	Einstein tensor
$a(t)$	Scale factor
$H(a) = \frac{\dot{a}}{a}$	Hubble expansion rate
$\chi(z), r(z)$	Comoving distance
$D_A(z)$	Angular diameter distance
$\Omega_{i=m,r,\Lambda,k}$	Matter, radiation, Λ, curvature density
$D_+(z)$	Growing mode of δ
$\delta(\vec{x}, t)$	DM density contrast
$f(z)$, $f_g(z)$	Logarithmic growth rate
c_s	speed of sound
$P(k), P_{3D}(k), P_m(k)$	matter power spectrum
C_l^κ, $C^{\kappa\kappa}$, $P_\kappa(l)$	Convergence power spectrum
C_l^{HI}, $P_{HI}(k)$, $P_{21}(k)$	HI 21cm power spectrum
$j_l(x)$	Spherical Bessel function
$j_l''(x)$	2nd deriv of $j_l(x)$ w.r.t the argument
$\mathbf{k}$	Fourier mode (Mpc^{-1})
$\hat{k}$	Unit vector of $\mathbf{k}$
k_B	Boltzmann constant (Joule/K)
$k_\parallel$	Component of $\mathbf{k}$ along θ (Mpc^{-1})

ℓ	Angular multipole
$\hat{n}$	Unit vector along line of sight
$\vec{U}$	Baseline vector (unit less)
$\bar{x}_{HI}$	Spatially averaged HI fraction
$Y_{\ell m}$	Spherical Harmonics
$\Delta(z, \mathbf{k})$	3D Fourier transform of δ (Mpc^{-3})
μ	Cosine of the angle between the line of sight and the wave vector ($\hat{k}.\hat{n}$)
Φ	Gravitational potential
ϕ	Scalar field
r_ν, χ_ν	Comoving distance from present to the redshift $z = 1420/\nu - 1$ (Mpc)
r'_ν, χ'_ν	$dr_\nu/d\nu$, $d\chi_\nu/d\nu$ (Mpc/MHz)
T_s	Spin temperature of hydrogen in mK
T_g	Gas temperature in Kelvin
T_γ	CMB temperature in Kelvin
$T(\nu, \hat{n})$	Excess 21cm brightness temperature at a ν along $\hat{n}$ (mK)
$\bar{T}(z)$	Spatially averaged Excess 21cm brightness temperature (mK)
$\mathbf{U}$	Baseline vector (unit less)
κ	Convergence field
ψ	Lensing potential
Ψ	Scalar perturbation in conformal gauge
b_T	21cm bias
$s(z_d)$	Sound horizon at drag epoch
$\mathbf{s}$	Redshift space distance
ρ_{2D}	Baseline distribution

CHAPTER 1

Introduction

Since ancient times, there has been a relentless human quest toward understanding the evolution and large-scale structure of the Universe. The question about our place in the cosmos has never ceased to amaze us. With the significant advances in observational astronomy, we now have an immense amount of data probing the Universe on cosmological scales. Future observational milestones, especially in radio astronomy and gravitational wave astronomy, will open new avenues and enrich us with even more information about the Universe. However, we still have a profound lack of theoretical understanding about the Universe, its evolution, composition and structure. Precision cosmology has confronted us with a situation where only $\sim 5\%$ of the matter/energy budget of the Universe can be understood within the paradigm of the standard model of particle physics. The remaining composition of the Universe is largely problematic from both theoretical and observational perspective. This unknown sector of the Universe's energy budget is attributed to dark matter and dark energy. This thesis is concerned with the latter.

Observations of Type Ia supernovae have revealed that the Universe's expansion is accelerating, countering the expectation that gravitational attraction would slow it down. This discovery provides direct evidence for the existence of dark energy [9–11]. Additionally, the distribution of galaxies and other structures in the Universe provide evidence for accelerated expansion [12–14]. Precise measurements of the anisotropies in the Cosmic Microwave Background (CMB) have also indicated that the expansion of the Universe is accelerating [15–18]. This counter-intuitive phenomenon can be explained by positing a dark energy component, with an equation of state $P/\rho = w < -1/3$. The cosmological constant has emerged as a strong candidate for dark energy, as various observations [19] constrain w to be close to -1.

The ΛCDM model [20, 21] is defined by the following simple assumptions:

- The Cosmological Principle: Our Universe is homogeneous and isotropic on large scales (> 100 Mpc)

- The Universe consists of radiation (photons, neutrinos), ordinary matter (baryons and leptons), cold (non-relativistic) dark matter (CDM) and a cosmological constant which can be thought of as a homogeneous form of energy whose density remains constant even in an expanding Universe and is associated with vacuum energy [19]. The cosmological constant is responsible for the accelerated expansion.

- General Relativity (GR) is the correct theory for gravity on cosmological scales.

- The spacetime metric is the Friedmann-Lemaitre-Robertson-Walker (FLRW) metric where the spatial part is flat and scaled by $a(t)$.

$$ds^2 = dt^2 - a(t)^2(dr^2 + r^2 d\theta^2 + r^2 \sin^2\theta d\phi^2) \tag{1.1}$$

  This follows from the cosmological principle, which implies that spatial hypersurfaces must be surfaces of constant curvature.

- The dynamics of the Universe can be derived from Einstein's field equation for this metric, which yields the Friedmann equations given by, [22]

$$\begin{aligned} \left(\frac{\dot{a}}{a}\right)^2 = H^2(t) = H_0^2 \sum_{i=r,m,\Lambda} \Omega_{i0} a(t)^{-3(1+w_i)} \\ \frac{\ddot{a}}{a} = -\frac{4\pi G}{3}\sum_i (\rho_i + 3P_i) \end{aligned} \tag{1.2}$$

  where the density ρ_i and pressure P_i of the i^{th} component are related as $P_i = w_i \rho_i$. The density parameters $\Omega_{io} = \rho_{i0}/\rho_{cr}$ where $\rho_{cr} = 3H_0^2/8\pi G$ sum up to unity assuming spatially flat Universe. The cosmological constant Λ corresponds to $w_\Lambda = -1$.

- A period of rapid accelerated expansion known as inflation is assumed to address the horizon and flatness problems [23, 24]. Gaussian quantum fluctuations from this inflation epoch seeded structure formation.

While it is simple and has reasonable agreement with observations, the cosmological model with Λ remains elusive both theoretically and observationally [20, 25–29]. The cosmological standard model ΛCDM is thus currently under severe scrutiny (see [30, 31]).

The main theoretical difficulty with the ΛCDM model is the fine-tuning issue arising from the large discrepancy between observations and theoretical expectations on the value of the cosmological constant Λ (at least 60 orders of magnitude) [29, 32, 33]. Further, there is the coincidence problem [34, 35]. This concerns the fact that the present values of the densities of dark energy and dark matter are of the same order of magnitude, $\rho_{DE}/\rho_m \sim \mathcal{O}(1)$ despite the two components having dramatically different evolution properties implying that the present epoch is somewhat a special period in the cosmic history

In addition to the above theoretical challenges, there are cosmological observational data that appear to be in some tension (2σ or larger) with the standard ΛCDM model as specified by the Planck-18 parameter values [17, 36]. The main observational anomaly comes from the "Hubble tension ($> 4\sigma$)". H_0 measured from local observations using the distance ladder approach is significantly higher than the best fit H_0 measured from CMB anisotropies. The combined local measurements of H_0 are in $> 5\sigma$ tension with implicit CMB measurements of H_0 [37–39]. Further, measurements of the growth rate of cosmological perturbations (using probes like weak lensing, redshift space distortions, and galaxy cluster counts) predict a slower growth rate than that estimated using a ΛCDM fiducial cosmological parameter estimation with Planck data at a level of about $2-3\sigma$ [40, 41]. The ΛCDM model also faces several anomalies in the analysis of CMBR temperature anisotropy power spectra [42]. There are also several discrepancies between the galaxy and Lyman-α BAO at an effective redshift of $z \approx 2.34$ [43, 44]. There are several other tensions, like the "Age of the Universe" problem [45], lithium problem [46], or the anomalous low baryon temperature [47].

Alternative cosmological models which go beyond the ΛCDM paradigm include

- Scalar-Tensor theories, where Newton's constant is made dynamical through its dependence on a scalar field Φ as $G \to G(\Phi(r,t))$ where the dynamics

of the field its governed by its action [48–51].

- A dynamical cosmological constant through the introduction of a scalar field (quintessence) [52–55].

- Allowing for a time-evolving Fine Structure Constant (Maxwell Dilaton theories) with $\alpha \rightarrow \alpha(\Phi(r,t))$ [56–58].

- Modification of the Einstein-Hilbert action by adding terms with may be functions of the Ricci scalar R, the torsion scalar T and/or other invariants. These theories are called $f(R)$, $f(T)$ theories [59–64].

- Negative cosmological constant models use a scalar field along with a negative cosmological constant for greater freedom on the parameter space and attempts to address some issues like the Hubble tension problem [8, 65, 66].

This thesis aims to investigate alternatives to the ΛCDM cosmology. The question is whether a given observational probe can discern such an alternative theory from the ΛCDM model. There are two problems at hand. Firstly, one has to ascertain that the observational error bars are small enough for an alternative theory such that the signal may be distinguishable statistically from the fiducial ΛCDM predictions with a high SNR. The second problem involves the actual precision error projections on the model parameters for different instruments and observational parameters. Since dark energy affects low redshifts, we are interested in the low redshift probes of cosmology.

Dark energy and dark matter can not be directly observed. However, dark energy affects the background evolution and growth of structures. The aim is to measure the clustering properties of the dark matter field, which shall imprint dark energy models. One can either probe dark matter through its gravitational properties (lensing) or probe baryonic matter (neutral hydrogen) as a biased tracer of the dark matter density field. This thesis focuses on three cosmological probes as tools to test dark energy models. Each of these probes can be used to image the low-redshift Universe tomographically. However, while one gives a line of sight integral (weak lensing), the other two probes

(21-cm and Ly-α) are biased tracers and sample the underlying dark matter field.

1. Weak Lensing :

   Weak gravitational lensing causes subtle shape distortions in the images of distant galaxies or CMBR maps due to intervening gravitational influences of the large scale structure [67, 68]. In particular, it can be used to measure the growth of large-scale structures in the Universe, which is sensitive to the properties of dark energy [69–77]. The statistical properties of the distortion field are sensitive to background evolution, are the growth of perturbations, and are thereby a probe of dark energy. We look at weak lensing in cross-correlation with two probes of the neutral intergalactic medium.

2. The 21-cm intensity mapping of the post-reionization epoch:

   The post-reionization 21cm signal from neutral hydrogen (HI) in the intergalactic medium (IGM) has emerged as a promising tool to probe the nature of dark energy [78–80]. The advancement of large radio telescopes and advanced data analysis methods promises more precise 21cm signal measurements and hopes to shed greater light on the nature of dark energy [81–89]. The post-reionization HI 21-cm signal is yet to be detected. However, several presently functioning and future telescopes aim to map the HI distribution tomographically using the 21-cm signal. It is well accepted that the HI can be treated as a biased tracer of the cold dark matter field in the post-reionization epoch [90–93]. We use this to investigate the possibility of cross-correlating the 21-cm maps with other probes. The predicted cross-correlation signal is then used to constrain various dark energy models.

3. The Lyman-α forest:

   Neutral hydrogen (HI) in the pre-dominantly ionized post-reionization intergalactic medium (IGM) produces unique absorption features in the spectra of background Quasars [94]. The Lyman-α forest is a powerful cosmological probe that maps the density fluctuation field along one-dimensional skewers corresponding to QSO sight lines. On suitable large

cosmological scales, the Lyman-α forest is a biased tracer of the underlying dark matter (DM) distribution [95–99]. It's clustering property is directly related to the dark matter power spectrum and the cosmological parameters. Like the HI 21-cm signal, Lyman-α forest observations can be used as a probe of dark energy [100, 101].

1.1 Outline of the Thesis

With this brief introduction, we now present the thesis outline. The work in this thesis aims to constrain dark energy models using the post-reionization probes of IGM. Forecasts on dark energy model parameters are made by considering a host of probes of the post-reionization IGM. The outline of this thesis is as follows:

- In chapter 2, we present the current theoretical understanding of the observed cosmic acceleration. We discuss the most widely accepted model with a positive 'Cosmological Constant (Λ)'. Later, we discuss the cosmologically viable alternative theories to explain the late-time cosmic acceleration without invoking a Λ. We mainly focus on $f(R)$ gravity theories, Quintessence dark energy, and the model-independent approach to construct the dark energy Equation of State.

- In chapter 3, we discuss the observational probes of the post-reionizaton intergalactic medium (IGM). We mainly focus on "Weak Gravitational Lensing", "21cm Intensity Mapping" and "Lyman-α forest" as the most promising observational tools for probing cosmological models using data from existing and forthcoming experiments.

- In chapter 4, we investigate the prospects of detecting the cross-correlation of CMBR weak-lensing convergence field with the large scale tracers of the underlying dark matter distribution in the post-reionization epoch. The cross-correlation is then used to make error projections for the dark energy equation of state (EoS) for models with a time-evolving dark energy. The cross-correlation of CMBR weak-lensing with the post-reionization probes of neutral hydrogen can give us a valuable understanding of the

nature of evolving dark energy. We study the cross-correlation angular power spectrum of the weak-lensing field with the Lyman-α forest and the redshifted HI 21 cm signal from the post-reionization epoch. The angular power spectra are expressed as a line of sight average over the tomographic slices. We find that on using multiple observations with an extended uGMRT like instrument or with a BOSS-like survey quasar (QSO) survey, the cross-correlation with weak-lensing convergence field can be detected at a very high SNR. The cross-correlation of weak-lensing with Lyman-α forest allows the $1-\sigma$ errors on the dark energy EoS parameters for different parametrizations to be constrained at a level of precision comparable to combined Planck+SNIa+BAO+HST projections. The 21-cm weak-lensing cross-correlation is also found to provide strong constraints on the present value of the dark energy EoS parameters for the 7CPL model.

- In chapter 5, we propose the intensity mapping of the redshifted HI21-cm signal from the post-reionization epoch as a cosmological probe of $f(R)$ gravity. We consider the Hu-Sawicki family of $f(R)$ gravity models characterized by a single parameter $f_{,R0}$. The $f(R)$ modification to gravity affects the post-reionization 21-cm power spectrum through the change in the growth rate of density fluctuations. We find that a radio interferometric observation with a SKA1-Mid-like radio telescope in both auto-correlation and cross-correlation with galaxy weak-lensing and Lyman-α forest may distinguish $f(R)$ models from ΛCDM cosmology at a precision which is competitive with other probes of $f(R)$ gravity.

- In chapter 6, we investigate the possibility of constraining a thawing Quintessence scalar field model for dark energy. We propose using the imprint of baryon acoustic oscillation (BAO) on the cross-correlation of post-reionization 21-cm signal and galaxy weak lensing convergence field to tomographically measure the angular diameter distance $D_A(z)$ and the Hubble parameter $H(z)$. The projected errors in these quantities are then used to constrain the Quintessence model parameters. We find that radio interferometric observation at four observing frequencies 916MHz, 650 MHz, 520MHz and 430MHz with a SKA-1-Mid like radio telescope

in cross-correlation with a deep weak lensing survey covering half the sky may measure the binned D_A and H at a few percent level of sensitivity. The Monte Carlo analysis for a power law thawing Quintessence model gives the $1-\sigma$ marginalized bounds on the dark energy parameters. The constraints improve significantly when a joint analysis with SN and other probes is performed.

- In chapter 7 we investigate a cosmological model involving a negative cosmological constant (AdS vacua in the dark energy sector). We consider a quintessence field on top of a negative cosmological constant and study its impact on cosmological evolution and structure formation. We use the power spectrum of the redshifted HI 21 cm brightness temperature maps from the post-reionization epoch as a cosmological probe. The signature of baryon acoustic oscillations (BAO) on the multipoles of the power spectrum is used to extract measurements of $D_A(z)$ and $H(z)$. The projected errors on these are then subsequently employed to forecast the constraints on the model parameters $(H_0, \Omega_m, \Omega_\Lambda, w_0, w_a)$ using Markov Chain Monte Carlo techniques. We find that a negative cosmological constant with a phantom dark energy equation of state (EoS) and a higher value of H_0 is viable from BAO distance measurements data derived from galaxy samples. We also find that BAO imprints on the 21cm power spectrum obtained from a futuristic SKA-mid like experiment yield a $1-\sigma$ error on a negative cosmological constant and the quintessence dark energy EoS parameters which is competitive with other probes. Further, we use a new quantifier to probe dark energy using the Alcock-Paczynski anisotropy of the redshift space power spectrum.

- Finally, chapter 8 summarizes the thesis and discusses future scopes.

Apart from these main chapters, there are three appendices on the topics related to modified gravity field equations, weak lensing, and 21cm power spectrum, and noise estimation.

CHAPTER 2

Cosmic acceleration and dark energy

In this chapter, we delve into the expansive realm of dark energy models, aiming to provide an overview of some of the frameworks and their respective merits and shortcomings. Despite the considerable strides cosmologists have made in unraveling the mysteries of the Universe, a notable degree of uncertainty still shrouds the established cosmological paradigm. In the last chapter, we mentioned that many independent observations have indicated that the expansion of the Universe is accelerating. The most direct evidence comes from the High redshift Supernova search team [102] and the Supernova cosmology project [103]. Precise cosmological measurements from diverse probes point to the fact that the Universe contains approximately $\sim 70\%$ of the energy density in the form of dark energy and the remaining $\sim 30\%$ in the form of non-relativistic matter (both baryonic matter and dark matter). Baryonic matter constitutes only $\sim 5\%$ of the total matter budget of the Universe. The bulk of the matter in the Universe is non-baryonic and manifests only through their gravitational interaction. This matter is known as dark matter. Although the physics of baryons can be understood using the standard model of particle physics, the dark matter and dark energy sector still needs to be understood.

2.1 The cosmological constant Λ

Among the pantheon of dark energy models, the cosmological constant (Λ) emerges as the simplest and most distinctive. It stands as a form of dark energy characterized by its spatial and temporal unchanging nature, constituting the simplest and most direct explanation for the observed accelerated expansion of the cosmos. This concept was originally introduced by Albert Einstein himself within the framework of his gravitational theory [104]. In the subsequent

sections of this thesis, we shall consider modifications to Einstein's theory of gravity, which is described by the Lagrangian $\mathcal{L} = \sqrt{-g}R$. The Einstein's field equations are obtained by a variation of the following action with respect to the metric g_{ab} we obtain the Einstein's field equation:

$$G_{ab} = R_{ab} - \frac{1}{2}g_{ab}R = \frac{8\pi G}{c^4}T_{ab} \tag{2.1}$$

In an attempt to ensure that the cosmological solutions to these equations produce a static Universe, Einstein introduced a constant term Λ. This maneuver not only adhered to the principles of General Relativity (GR) but also harmonized with the constraints imposed by the Bianchi identity (i.e. $\nabla_b T^{ab} = 0$). The new field equations, reflective of Einstein's inclusion of the cosmological constant Λ, can be expressed as follows:

$$G_{ab} = \frac{8\pi G}{c^4}T_{ab} + \Lambda g_{ab} \tag{2.2}$$

Einstein's original aspiration rested on the notion that conventional matter was the sole agent responsible for curving the fabric of spacetime, a postulate closely linked with Mach's principle. This vision, however, encountered a swift setback when de Sitter formulated a solution to Einstein's equations involving a cosmological constant devoid of any matter content. Notably, the introduced cosmological constant Λ exhibited the behavior of a counteracting force against gravity, unsettling the assumption about the Universe's static nature. This revelation eventually led to the breaking down the concept of a static universe that Einstein had initially envisioned. In 1922, Friedmann proposed an alternative cosmological model dispensing with the staticity assumption. In this novel paradigm, he posited that the Universe demonstrated Homogeneity, Isotropy, and a propensity for expansion. Despite its conceptual innovation, this model faced early resistance due to the prevalent belief in a static universe, which was rooted in observational evidence. In 1927, the Belgian physicist Georges Lemaitre also derived dynamical equations for the radius of the Universe from the field equations involving Λ. Lemaitre was aware of the observations of the recession of the spiral nebulae and the emerging evidence that the nebulae belonged to galaxies other than our own. Lemaitre's

work harmonized these observations with general relativity, as the data suggested that the Universe was expanding. However, the tide turned in 1929, when Hubble's groundbreaking discovery of galaxies receding from one another provided compelling support for an expanding universe. This transformative revelation led to a reevaluation of the cosmological constant Λ's role. Thus, the concept of a static universe was ultimately abandoned, and the pursuit of a dynamically evolving cosmos gained ascendancy. This shift in perspective marked a critical juncture in the understanding of the Universe's behavior, highlighting the indispensable role of the cosmological constant Λ in shaping the course of cosmological theory. Einstein's "greatest blunder" eventually became the most straightforward explanation for the accelerated expansion discovered observationally much later. For a homogeneous and isotropic expanding Universe, the spacetime metric (FLRW metric), has a constant spatial curvature and is characterized by the curvature (hyperbolic, spherical, or flat) and the time-dependent scale factor $a(t)$. The (00) and (aa) components of Einstein's equations give us the Friedmann equations

$$\frac{H^2(t)}{H_0^2} = \sum_{i=r,m,\Lambda} \Omega_i a(t)^{-3(1+w_i)} \tag{2.3}$$

$$\frac{\ddot{a}}{a} = -\frac{4\pi G}{3} \sum_{i=r,m,\Lambda} (\rho_i + 3P_i) \tag{2.4}$$

where we assume a multi-component Universe with each component behaving like a perfect fluid with a i^{th} component having the energy-momentum tensor $T_b^{(i)a} = \mathrm{dig}(-\rho_i, P_i, P_i, P_i)$ Following the conventional notation, we employ the symbol $\Omega_i = \rho_i(0)/\rho_c$ with $\rho_c = 3H_0^2/8\pi G$ to denote various energy density parameters. The energy conservation $\nabla_a T_0^a = 0$ gives,

$$d(\rho_i a^3) = -P_i d(a^3) \tag{2.5}$$

If the pressure density relationship is written as $P_i = w_i(a)\rho_i(a)$ where the equation of state (EoS) parameter $w_i(a)$ can be a function of time, the formal

solution is given by

$$\rho_i(a) \propto \exp\left(-3\int_1^a \frac{da'}{a'}\left[1+w_i(a')\right]\right) \tag{2.6}$$

Absorbing the cosmological constant in the energy-momentum tensor one can envisage a dark energy fluid with the energy momentum tensor given by $T^a_{(\Lambda)b} = -\frac{\Lambda}{8\pi G}\delta^a_b = \mathrm{dig}(-\rho_\Lambda, -\rho_\Lambda, -\rho_\Lambda, -\rho_\Lambda)$, where $\rho_\Lambda \equiv \frac{\Lambda}{8\pi G}$ is the effective energy density of the cosmological constant. The cosmological constant has an equation $P_\Lambda = -\rho_\Lambda$, satisfying the EoS parameter exactly $w = -1$. We know that any component of the Universe with $w < -1/3$ will drive an acceleration. Thus Λ, which corresponds to a negative pressure, can cause an acceleration. Nonetheless, it's worth acknowledging that Λ is not the sole contender to elucidate the observed accelerated expansion of the Universe. Before exploring potential substitutes for Λ (or dark energy), let's examine several pieces of observational evidence supporting its existence.

Observational evidence of Dark Energy (or Λ)

Cosmic Microwave Background [17, 18, 105, 106]:

The Hot Big Bang theory entails that in the very early Universe, matter and radiation were coupled to behave like a single fluid in thermal equilibrium, interacting through Thomson scattering. As the expansion rate cooled down the temperature, at around $z \approx 1100$ (known as the epoch of recombination), proton and electron formed a bound state of the hydrogen atom, and the Universe became transparent to photons, which started to free stream[22]. However, they will keep a memory of their thermal equilibrium and exhibit a black body spectrum. This spectrum of the photons free streaming from the epoch of recombination (CMBR) peaks in the microwave region of the spectrum at the present epoch [22].

Though the CMBR is remarkably homogeneous in temperature and follows a Planck distribution at temperature $T_0 = 2.724 \pm 0.004K$ [107, 108] there are fluctuations at a level of 10^{-5} [109]. These fluctuations are primarily rooted in tiny density fluctuations that form the seeds of structure formation. In the era preceding recombination, the interplay between photon-baryon plasma

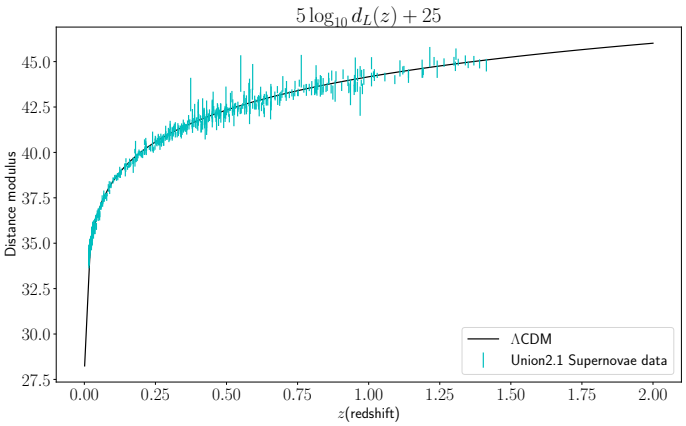

Figure 2.1: The solid black line corresponds to the standard model of cosmology, and the distance modulus from the Union2.1 supernovae survey provides excellent agreement with ΛCDM model.

and the gravitational potential exerted by dark matter governs the evolution of the Universe. This interplay engenders a distinctive phenomenon known as acoustic oscillations. The competing forces of photon-baryon pressure and gravity give rise to these oscillations, which imprint a characteristic scale onto the cosmic microwave background (CMB) radiation. The presence of these acoustic oscillations introduces a specific scale (sound horizon at the decoupling era) on the CMBR temperature anisotropies. The angular measurement of this scale serves as a standard ruler for probing the angular diameter distance, thereby offering insights into the geometry of the universe [105]. The measured statistical properties of the CMBR anisotropies, when used for cosmological parameter estimation strongly supports a ΛCDM Universe [36].

Supernovae Surveys [9–11, 110–113]: By far the most direct probes of dark energy come from the analysis of distance measurement from observation of Supernovae explosions. Supernovae type Ia (SNIa) are thermonuclear explosions of white dwarfs in binary systems with red giants [114]. Supernovae spectra without any hydrogen are called type I. This class is subdivided into types Ia and Ib, depending on the presence or absence of a silicon absorption feature. Supernovae Ia show remarkable uniformity, and their spectra and “light curves” are perfectly matched. Thus, these supernovae serve as "standard candles," enabling astronomers to employ them as reliable tools for esti-

mating cosmic distances [115, 116]. Observations of distant SNIa can be used to measure the luminosity distance as a function of redshift and thus probe the evolutionary history of the universe [117]. The SNIa observations essentially constrain the contents of the Universe by pinning down the combination [118],

$$q_0 \equiv -\frac{1}{aH^2}\left.\frac{d^2a}{dt^2}\right|_{t_0} = \frac{1}{2}\sum_i \Omega_{i0}\left(1+3w_{i0}\right) \tag{2.7}$$

For a -ve value of q_0 corresponds to accelerated expansion and SNIa observations suggest $q_0 \approx -0.6 \pm 0.2$ [119].

Baryon Acoustic Oscillations [1, 120–125]:

Density perturbations in the cosmological fluid drive acoustic waves in the primordial baryon-photon plasma. These waves are frozen once recombination occurs at $z \sim 1000$, leaving a distinct oscillatory signature on the CMBR anisotropy power spectrum. Baryons contribute to 15% of the total matter density. Thus baryon acoustic oscillations are also imprinted in the low redshift clustering of non-relativistic matter. However, the oscillatory effect is suppressed by a factor $\sim \Omega_b/\Omega_m \sim 0.1$ compared to the effect in CMBR anisotropies. The baryon acoustic oscillation (BAO) is a powerful probe of cosmological parameters [3, 126–129]. A characteristic scale corresponding to the sound horizon at recombination sets a standard ruler. This scale will imprint in the clustering of galaxies and will appear as a peak or dip in the correlation function, depending on whether there is an excess or deficiency of clustering at that scale [121]. Observing the BAO feature in correlation function in transverse and longitudinal directions, we can directly measure expansion rate $H(z)$ and angular diameter distance $D_A(z)$, which are sensitive to dark energy [120]. BAO observations are particularly useful as the effect occurs on large scales (~ 150 Mpc), where density fluctuations are in the linear regime. These provide means for estimating cosmological parameters and placing strin- gent constraints on dark energy models [130].

Large Scale Structure [131–135]:

The Large Scale Structure (LSS) of the Universe refers to the distribution of galaxies and matter on scales much larger than individual galaxies or galaxy clusters. This distribution of galaxies in structures like filaments, sheets and

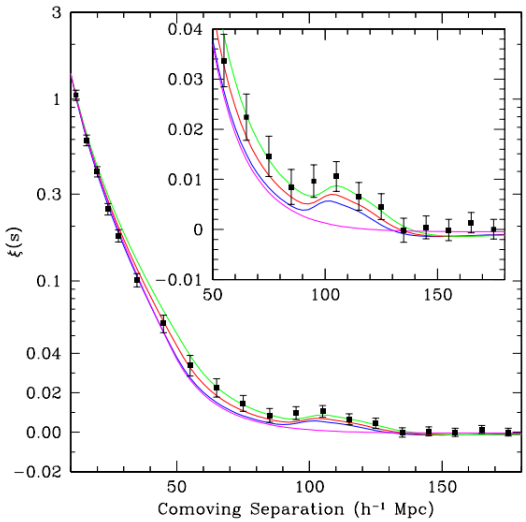

Figure 2.2: From [1] the Baryon Acoustic Peak is a bump in the two-point correlation function (in this case, of SDSS luminous red galaxies). Shown are models with $\Omega_m h^2 = 0.12$ (top), 0.13 (second) and 0.14 (third), all with $\Omega_b h^2 = 0.024$). The bottom line without an acoustic peak is the correlation function in the pure CDM model, with $\Omega_b = 0$.

voids, is known as the cosmic web. These correlated structures can be seen up to billions of light years in length and are created and shaped by gravity. Galaxies are believed to form at the peaks of the dark matter overdensity field. Thus, mapping out the galaxies over a range of redshifts gives a direct probe of structure formation. The clustering statistics is quantified using the $n-$ point functions and their Fourier transforms. The measurement of the galaxy power spectrum/bispectrum and the growth rate of density fluctuations in galaxy redshift surveys like the 2dF Galaxy Redshift Survey (221,000 redshifts, completed 2002) [*]; the Sloan Digital Sky Survey SDSS [†] (approximately 1 million redshifts by 2007), Baryon Oscillation Spectroscopic Survey (BOSS) [‡] points towards a ΛCDM Universe [3, 4, 123, 128].

[*] http://www.2dfgrs.net/
[†] https://www.sdss.org/
[‡] https://www.sdss3.org/surveys/boss.php

2.1.1 Problems with the cosmological constant Λ

The agreement between the theoretical predictions based on the ΛCDM model and observations is impressive. It is then expected that new data from more precision experiments would show compatibility with ΛCDM. The real surprise occurs when this is not seen in reality. There are several observational results where the data seems to be in tension (2σ or larger) with the ΛCDM model [37, 136, 137].

Hubble Tension: Local measurements of the Hubble constant H_0 are measured to values that are higher than those estimated from CMBR anisotropies in the paradigm of the ΛCDM model [39, 136, 138, 139].

Growth Tension: Direct measurements of the growth rate of cosmological perturbations from probes such as Weak Lensing, Redshift Space Distortions, Cluster Counts etc., indicate a lower growth rate than that indicated by the ΛCDM parameter values at a level of about $> 2\sigma$ from CMBR [40, 41, 140, 141]. The value of the growth parameter combination $S_8 \equiv \sigma_8(\Omega_{m0}/0.3)^{0.5}$ is found by weak lensing, cluster counts, redshift space distortion data to be to be lower compared to the Planck CMB value $S_8 = 0.834 \pm 0.016$ [36].

CMB anomalies: The ΛCDM model assumes that the primordial fluctuations are Gaussian, statistically homogeneous, and isotropic. However, diverse anomalies have been noticed in the CMB at large angular scales, which appear to violate these assumption [42, 142, 143].

BAO anomalies: The BAO measurements from galaxy and Ly-α, gives a $2.5-3\sigma$ discrepancy between the BAO peak position in the Ly-α at an effective redshift of $z \sim 2.34$ and the CMB predictions from ΛCDM model [43, 44, 144].

Age of the Universe: The age of the Universe as obtained from local measurements using the ages of the oldest observed stars (Pop II) in the Milky Way appears to be larger and in some tension with the corresponding age of the Universe obtained using the CMB Planck data in the context of ΛCDM [45].

QSO Hubble diagram: The distance modulus-redshift relation for quasars at higher redshift (> 0.5) is in some tension with the concordance ΛCDM model indicating some hints for phantom late time expansion [145–147].

Lithium problem: Measurements of old, metal-poor stars in the Milky Way's halo finds ~ 5 times less lithium than that Big Bang Nucleosynthesis

theory predicts [46].

Other than these observational tensions, the cosmological constant has serious theoretical difficulties. There are two most notable theoretical challenges: (i) fine-tuning problem [29] and (ii) coincidence problem [148, 149] amongst other theoretical issues.

Fine-tuning problem: Since $|\Lambda|^{1/2}$ has the dimensions of inverse length, it will set the scale for the Universe when cosmological constant dominates. It follows that the most stringent bounds on Λ will arise from cosmology when the expansion of the Universe has diluted the matter-energy density sufficiently. The Universe's expansion rate today is usually expressed in terms of the Hubble constant: $H_0 = 100\text{h km s}^{-1}\text{ Mpc}^{-1}$. Converting the unit frequency^{-1} to the corresponding energy in eV and km to Mpc, we obtain:

$$\Lambda \approx H_0^2 = \left(100\text{h} \times 3.24 \times 10^{-20} \times 6.58 \times 10^{-16}\text{eV}\right)^2 \approx (2.13\text{h} \times 10^{-42}\text{GeV})^2$$

Which corresponds to an energy density:

$$\rho_\Lambda = \frac{\Lambda}{8\pi G} \approx \frac{2.227 \times 10^{-84}\text{GeV}^2 \times 1.488 \times 10^{38}\text{GeV}^2}{8 \times 3.14} \approx 0.132 \times 10^{-46}\text{GeV}^4$$

where we put $G \propto m_{pl}^{-2}$ in the last substitution. Since the cosmological constant is equivalent to the vacuum energy density of empty spacetime, we can calculate the vacuum energy by summing over all the zero-point energies of some field mass m, momentum k, and frequency ω up to a cut-off scale [25] $k_{max} >> m$.

$$\rho_v = \int_0^{k_{max}} \frac{d^3k}{(2\pi)^3} \frac{\sqrt{k^2+m^2}}{2} = \int_0^{k_{max}} \frac{4\pi k^2 dk}{(2\pi)^3} \frac{1}{2}\sqrt{k^2+m^2} \tag{2.8}$$

Since the integral is dominated in large k modes ($k >> m$):

$$\rho_v \approx \int_0^{k_{max}} \frac{4\pi k^2 dk}{(2\pi)^3} \frac{k}{2} = \int_0^{k_{max}} \frac{\pi k^3 dk}{4\pi^3} = \frac{k_{max}^4}{16\pi^2} \tag{2.9}$$

A plausible cut-off scale is the Planck scale (m_{pl}), up to which general relativity

is believed to hold, gives:

$$\rho_v \approx \frac{m_{pl}^4}{16\pi^2} \approx \frac{(1.22 \times 10^{19}\text{GeV})^4}{16\pi^2} \approx 0.014 \times 10^{74}\text{GeV}^4 \tag{2.10}$$

We can see the ratio of observed and predicted theoretical value

$$\frac{\rho_v}{\rho_\Lambda} \approx \frac{10^{74}\text{GeV}^4}{10^{-47}\text{GeV}^4} \approx 10^{121} \tag{2.11}$$

differs by 121 orders of magnitude. However, there is another cutoff scale that can be used if one considers the supersymmetry, which breaks down at around 1TeV. Then,

$$\rho_v \approx \frac{(10^3\text{GeV})^4}{16\pi^2} \approx 6.34 \times 10^9\text{GeV}^4 \tag{2.12}$$

which is a value 56 orders of magnitude larger than the observed value. We, however, do not know of any symmetry mechanism or invariance principle that causes Λ to vanish. This discrepancy in the value of the vacuum energy is also called the "smallness" problem [29] and is also referred to as the cosmological constant puzzle [20].

Coincidence problem: The coincidence problem refers to the absence of an explanation for why the density of non-relativistic matter at present is of the same order of magnitude as that of dark energy [150]. Since $\rho_m \propto a^{-3}$ and $\rho_\Lambda \propto a^0$ leads to $\rho_m/\rho_\Lambda \propto a^{-3}$, which indicates that Λ was negligible in the past and will dominate the future. If the cosmological constant is considered to be an initial condition in the early Universe, it seems really unlikely that Λ should have a value comparable to matter at the present cosmological epoch while galaxies and other large scale structures have formed [150]. It's fascinating to note that large-scale structure would not have formed if the energy density of the cosmological constant had been a few orders of magnitude greater or lower. A possible solution to this problem is the anthropic principle, discussed in [25] in details.

Other than these issues, the cosmological constant also has contradictions with String theory [151–153] which finds it difficult to incorporate a small value of Λ.

2.2 Alternatives to the cosmological constant

This section explores a few of the widely used paradigms which explain the cosmic acceleration without invoking the cosmological constant Λ. These alternatives emerge due to theoretical paradoxes or incongruities in observations. Broadly, two avenues are pursued in addressing this challenge. The first approach entails modifications to the theory of gravity on cosmic scales. Alternatively, the second approach involves altering the matter sector within Einstein's field equations. This is accomplished by introducing a dynamic dark energy fluid with nontrivial behaviors or employing a model-independent approach to reconstruct dark energy's equation of state (EoS). These approaches attempt to provide coherent explanations for the observed cosmic acceleration while evading the necessity of resorting to the cosmological constant.

2.2.1 $f(R)$ gravity theory

$f(R)$ gravity represents a fundamental alternative to General Relativity for explaining the late-time cosmic acceleration, inflation, and other cosmological phenomena without invoking the standard cosmological constant. Within the framework of $f(R)$ gravity theory, the Einstein-Hilbert action's Ricci scalar R is replaced by an arbitrary function denoted as $f(R)$, leading to the following transformation:

$$\mathcal{A} = \int d^4x\sqrt{-g}R \rightarrow \int d^4x\sqrt{-g}f(R) \tag{2.13}$$

The standard way to obtain the field equations is by varying the action w.r.t metric $g_{\mu\nu}$. Such theories are called "metric $f(R)$ gravity" theories. Alternatively, one may use the Palatini formalism where the connection is assumed to be independent of metric, and the action is varied w.r.t both metric and the connection Γ^c_{ab}. Such theories are called the "Palatini $f(R)$ gravity" theory. The third and most general approach is called "metric-affine $f(R)$ gravity", where one uses the same Palatini formalism but without assuming the matter action to be independent of the connection. Our work has focused on metric $f(R)$ gravity.

The action in case of $f(R)$ gravity can be written as

$$\mathcal{A} = \frac{1}{2\kappa^2}\int d^4x\sqrt{-g}f(R) + \int d^4x\sqrt{-g}\mathcal{L}_m(g_{\mu\nu},\phi) \tag{2.14}$$

where $\kappa^2 = \frac{8\pi G}{c^4}$ and $\mathcal{L}_m$ is the Lagrangian matter density, which is a function of metric $g_{\mu\nu}$ and matter field ϕ. By varying the action w.r.t metric $g_{\mu\nu}$ we get the modified field equation as the modified version of Friedmann equations:

$$\begin{aligned} H\dot{f}_{,R} - 2\dot{H}f_{,R} - \ddot{f}_{,R} &= \kappa^2(\rho + P) \\ 3H^2 f_{,R} - \frac{1}{2}(Rf_{,R} - f(R)) + 3H\dot{f}_{,R} &= \kappa^2\rho \end{aligned} \tag{2.15}$$

where, we have assumed that the variation of the matter action gives the usual energy-momentum tensor. Here $f_{,R} = \partial f(R)/\partial R$. These equations govern the background dynamics of a flat FLRW universe in a metric $f(R)$ gravity theory. For a FLRW Universe the Ricci scalar is $R = 6(2H^2 + \dot{H})$

Earlier, the model $f(R) = R - \alpha R^{-n}(\alpha > 0, n > 0)$ was proposed to explain the late-time cosmic acceleration in the metric formalism [154–156]. However, this model suffers from several problems [157, 158]. The instability of these models under cosmological perturbations [159–163], the absence of the matter era [164–166], and the inability to satisfy local gravity constraints from Solar system tests [167–172] are some of the issues. The main reason why this model does not work is that the quantity $f_{,RR} \equiv \partial^2 f/\partial R^2$ is negative. The violation of the condition $f_{,RR} > 0$ gives rise to the negative mass squared M^2 for the scalaron field. Hence we require that $f_{,RR} > 0$ to avoid a tachyonic instability. The condition $f_{,R} \equiv \partial f/\partial R > 0$ is also required to avoid the appearance of ghosts. Thus viable $f(R)$ dark energy models need to satisfy [60]

$$f_{,R} > 0, \quad f_{,RR} > 0, \quad for \quad R \geq R_0(> 0), \tag{2.16}$$

where R_0 is the Ricci scalar today. In literature number of authors studied cosmological dynamics for specific $f(R)$ models [154, 156, 173–183]. However, many viable $f(R)$ models that can satisfy both cosmological and local gravity constraints have been proposed [60, 63, 174, 176, 184–188] Since the law of gravity gets modified over large distances in $f(R)$ models, this leaves sev-

eral interesting observational signatures such as the modification to the spectra of galaxy clustering [159–161, 163, 189], CMB [161, 190, 191], and weak lensing [192, 193]. The functional form of $f(R)$ is chosen so that the model is phenomenologically satisfactory. The $f(R)$ cosmology to be indistinguishable from the ΛCDM at high redshifts where the latter is well constrained from CMBR observations. This, for example, requires $f_{,R} \to 1$ as $R \to \infty$ to reproduce the usual evolution history for $z >> 1$.

We use the $f(R)$ gravity model proposed by Hu-Sawicki (HS), where the functional form of $f(R)$ is given by [25, 182]

$$f(R) = R - \mu R_c \frac{(R/R_c)^2}{(R/R_c)^2 + 1} \tag{2.17}$$

Here μ and R_c are two non-negative parameters in the model where R_c is the present-day value of the Ricci scalar. To recover standard GR results in Solar system tests, the present-day value of $f_{,R}$ is restricted to $\log_{10}|f_{,R0}| < -6$ [182].

Looking at the growth of large scale structure (LSS) the quantity of interest is the growth rate of matter density perturbations $f_g(k,z) \equiv \frac{d \ln \delta_m(k,z)}{d \ln a}$. In linear perturbation theory, and on sub-horizon scales ($k/a >> H$) the evolution of matter density perturbations $\delta_m(k,z)$ is dictated by the differential equation [161, 194–196].

$$\ddot{\delta}_m + 2H\dot{\delta}_m - 4\pi G_{eff}(a,k)\rho_m\delta_m \simeq 0 \tag{2.18}$$

where G_{eff} is an effective gravitational constant that is related to the standard Newtonian gravitational constant (G_N) as

$$G_{eff}(a,k) = \frac{G_N}{f_{,R}}\left[1 + \frac{(k^2/a^2)(f_{,RR}/f_{,R})}{1 + 3(k^2/a^2)(f_{,RR}/f_{,R})}\right] \tag{2.19}$$

In $f(R)$ theories G_{eff} is a scale dependent function [197]. The scale dependence of the growing mode can be used to differentiate the structure formation.

2.2.2 Quintessence as Dark Energy

Quintessence models are canonical scalar field models. The theory comprises of a canonical scalar field ϕ with a potential $V(\phi)$ and interacts with all components only through standard gravity. The word quintessence comes from the

Latin words quintus, meaning 'fifth', and essentia, meaning 'being' used by medieval alchemists. In quintessence, some unknown mechanism ensures that the vacuum energy is zero and the scalar particle associated with quintessence is sufficiently light such that the Universe has not settled at the vacuum state yet [32]. As a result, the scalar field predominates the energy density on large scales.

Let us consider quintessence in the presence of non-relativistic matter described by a barotropic perfect fluid $P(\rho)$ described by the Lagrangian density:

$$\mathcal{L} = \frac{1}{2}\partial_\mu\phi\partial^\mu\phi - V(\phi) \tag{2.20}$$

where $V(\phi)$ is the potential energy density of the field ϕ. The stress-energy tensor can be obtained as which reduces to:

$$T_{\mu\nu} = \frac{-2}{\sqrt{-g}}\frac{\delta(\sqrt{-g}\mathcal{L})}{\delta g_{\mu\nu}} = \partial_\mu\phi\partial_\nu\phi - g_{\mu\nu}\left(\frac{1}{2}\partial_\mu\phi\partial_\nu\phi - V(\phi)\right) \tag{2.21}$$

Assuming that the scalar field is close to spatially uniform on cosmological scales, we can neglect its spatial derivatives $\partial_i\phi$ compared to its time derivatives $\dot{\phi}$ we can obtain the energy density and the pressure of the field as:

$$\rho_\phi = T^0_0 = g^{0\mu}T_{\mu 0} = g^{00}T_{00} = \frac{\dot{\phi}^2}{2} + V(\phi) \tag{2.22}$$

$$p_\phi = T^i_i = g^{i\mu}T_{\mu i} = g^{ii}T_{ii} = \frac{\dot{\phi}^2}{2} - V(\phi) \tag{2.23}$$

Thus, the EoS parameter is:

$$w(\phi) = \frac{\frac{\dot{\phi}^2}{2} - V(\phi)}{\frac{\dot{\phi}^2}{2} + V(\phi)} = \frac{\dot{\phi}^2 - 2V(\phi)}{\dot{\phi}^2 + 2V(\phi)} \tag{2.24}$$

If the potential is steep, then $\dot{\phi}^2/2 >> V(\phi)$, then $w(\phi) \approx \frac{\dot{\phi}}{\dot{\phi}} \approx 1$. If $\dot{\phi} << V(\phi)$, then

$$w(\phi) = \frac{\dot{\phi}^2 - 2V(\phi)}{\dot{\phi}^2 + 2V(\phi)} \approx \frac{-2V(\phi)}{2V(\phi)} \approx -1 \tag{2.25}$$

Thus we can effectively obtain the cosmological constant $w = -1$ for $\dot{\phi} \approx 0$.

Quintessence can play the role of dark energy if:

$$w(\phi) < -\frac{1}{3} \implies \frac{\dot{\phi}^2 - 2V(\phi)}{\dot{\phi}^2 + 2V(\phi)} < -\frac{1}{3} \implies 3\dot{\phi}^2 - 6V(\phi) < -\dot{\phi}^2 - 2V(\phi) \implies \dot{\phi}^2 < V(\phi)$$

However, this condition is insufficient since dark energy domination today requires $w = -1$ not only at the present epoch but for an extended period. Thus, it is a requirement that the condition $\dot{\phi}^2 < V(\phi)$ holds for a while. This can happen if the time derivative of this condition is also fulfilled:

$$\left|\frac{d}{dt}\dot{\phi}^2\right| < \left|\frac{d}{dt}V(\phi)\right| \implies \left|\ddot{\phi}\right| < \left|\frac{V'(\phi)}{2}\right| < |V'(\phi)|$$

where $V'(\phi) = dV(\phi)/d\phi$. In summary, a scalar field can play the role of dark energy if: $\dot{\phi}^2 < V(\phi)$ and $\mid \ddot{\phi} \mid < \mid V'(\phi) \mid$. These are the slow-roll conditions. The slow roll parameters are defined as

$$\epsilon_s = \frac{1}{2\kappa^2}\left(\frac{V'(\phi)}{V}\right)^2, \qquad \eta_s = \frac{V''(\phi)}{\kappa^2 V} \tag{2.26}$$

where $\kappa^2 = 8\pi G$. Thus when $\epsilon_s << 1$ and $|\eta_s| << 1$ we have $\dot{\phi}^2 < V(\phi)$ and $\mid \ddot{\phi} \mid < \mid 3H\dot{\phi} \mid$. The equation of state parameter $w(\phi)$ can be written as

$$w(\phi) = -1 + \frac{V'(\phi)^2}{9H^2\rho_\phi(\xi_s + 1)^2} \tag{2.27}$$

where $\xi_s = \ddot{\phi}/3H\dot{\phi}$. Thus, in the slow-roll limit $|\xi_s| << 1$ and

$$w(\phi) \approx -1 + 2\eta_s/3 \tag{2.28}$$

The dynamics of the scalar field is determined by the Klein-Gordon equation:

$$\ddot{\phi} + 3\left(\frac{\dot{a}}{a}\right)\dot{\phi} + \frac{dV}{d\phi} = 0 \tag{2.29}$$

which can be obtained by the varying action $\mathcal{A}_\phi$ (see Appendix): Assuming a flat universe in the presence of matter and the Quintessence field gives:

$$H^2 = \frac{8\pi G}{3}(\rho_m + \rho_\phi) = \frac{8\pi G}{3}\left(\rho_m + \frac{1}{2}\dot{\phi}^2 + V(\phi)\right) \tag{2.30}$$

$$\dot{H} = \frac{4\pi G}{3}\left(\dot{\phi}^2 + \rho_m + P_m\right) \tag{2.31}$$

The wide class of scalar field models are classified broadly into two broad categories [55]:

(i) The Thawing models In this class, the field is nearly frozen by Hubble friction during the early cosmological epoch and it starts to evolve once the field mass drops below the Hubble expansion rate. Example $V(\phi) = V_0 + M^{4-n}\phi^n \ \ (n > 0)$

(ii) The Freezing models Here, the evolution of the field gradually slows down because the potential tends to be shallow at later times. Example $V(\phi) \sim M^{4+n}\phi^{-n} \ \ (n > 0)$

For the inverse power-law potential $V(\phi) \propto \phi^{-n}$ $(n > 0)$, a distinctive phenomenon known as the "tracker solution" emerges [198]. For this solution, the parameter w remains nearly constant during the matter-dominated epoch and subsequently commences a decrement. This case falls within the subclass of freezing models. To achieve present-day cosmic acceleration, the mass $m_\phi (\equiv d^2V(\phi)/d\phi^2)$ of the quintessence scalar field must be exceedingly minuscule, satisfying the condition $m_\phi \leq H_0 \approx 10^{-33}, \mathrm{eV}$. Nevertheless, understanding how such an extremely light mass aligns with the energy scales characteristic of particle physics proves to be a formidable challenge [199]. Furthermore, without certain symmetries, radiative corrections could potentially disrupt the requisite flatness of quintessence potentials, imperative for cosmic acceleration [200]. It's worth noting that the construction of viable quintessence models within the framework of particle physics is not entirely without hope [201–203]. Numerous models have been proposed, introducing scalar fields or incorporating modifications to $T_{\mu\nu}$, and their dynamics have been extensively explored in the literature. However, it is not the primary aim of this thesis to delve into detailed explanations of these models. Additional information can be found in [204] for further insights.

2.2.3 Reconstruction of w

In order to parameterize the equation of state $w(z)$, there are two directions of approach. Either one may calculate the EoS for some specified theory and

then look for its effects on the cosmological expansion, or one may start from the observations of the cosmological expansion and then reconstruct the scalar field physics responsible for the effects observed. However, the latter approach has issues [52]: (i) Unreliability of expansion measurement data (may exhibit inherent uncertainties.), (ii) Translating the measured quantity into ρ_{DE} and w often requires the utilization of one or more derivatives, (iii) The span of the scale factor or equivalently redshift ($z = 1/a - 1$) entails limitations.

There are innumerable possible choices for $w(z)$. However, it has been shown that at most a two-parameter model can be optimally constrained from observations [205]. A commonly used ansatz, proposed by Chevalier-Polarski [206] and Linder [150], allows for dynamical dark energy and is based on an expansion of $w(a)$ around the present value of the scale factor $a = 1$:

$$w(a) = w_0 + w_a(1 - a) \tag{2.32}$$

This can be obtained by expanding $w(a)$ in the Taylor series around $a = 1$ keeping only linear terms:

$$w(a) = w|_{a=1} + (a-1)\left.\frac{dw}{da}\right|_{a=1} + \frac{1}{2}(a-1)^2\left.\frac{d^2w}{da^2}\right|_{a=1} + \mathcal{O}\left[(a-1)^3\right] \tag{2.33}$$

In terms of the redshift z, the EoS $w(z)$ takes the form:

$$w(z) = w_0 + w_a\left(1 - \frac{1}{1+z}\right) = w_0 + w_a\frac{z}{1+z} \tag{2.34}$$

where w_0 is the present value i.e $w(a_0) = w_0 + w_a(1 - a_0) = w_0$ and the value of its slope $dw(a)/da = -w_a$. Many such two-parameter models have been proposed so far. It is found that few of the models are well-behaved and have a bounded function of redshift throughout the entire cosmic evolution [205, 207–210]. In this thesis, we have directed our attention towards a select subset of these models, which will be explored in greater depth later.

We can reconstruct Quintessence fields using the EoS from 2.34. The energy

density may be written as

$$\rho_{DE} = \rho_{DE0} \exp\left[\int_0^z 3\frac{1+w_0+w_a\frac{z'}{1+z'}}{1+z'}dz'\right]$$

and hence the Hubble expansion rate $H(z)$:

$$H^2(z) = H_0^2\left[\Omega_{m0}(1+z)^3 + (1-\Omega_{m0})(1+z)^{3(1+w_0+w_a)}e^{-3w_a\frac{z}{1+z}}\right] \tag{2.35}$$

Using (2.22), we can obtain the potential and kinetic term in terms of redshift:

$$V(z) = \frac{1}{2}(\rho_{DE} - p_{DE}) = \frac{1}{2}[1-w(z)]\rho_{DE}(z) = \frac{1}{2}\left(1 - w_0 - w_a\frac{z}{1+z}\right)\rho_{DE}(z)$$
$$\frac{1}{2}\dot{\phi}^2 = \frac{1}{2}(\rho_{DE} + p_{DE}) == \frac{1}{2}[1+w(z)]\rho_{DE}(z) = \frac{1}{2}\left(1 + w_0 + w_a\frac{z}{1+z}\right)\rho_{DE}(z)$$

Similar way, we can obtain the field (ϕ) in terms of the redshift as:

$$\phi = \int_{t_e}^{t_0} |(1+w(z))\rho_{DE}(z)|^{1/2}dt = \int_0^z |[1+w(z')]\rho_{DE}(z')|^{1/2}\frac{dz'}{(1+z')H(z')}$$

The mechanism described here involving a slowly evolving field along the potential $V(\phi)$, which contributes to the Universe's acceleration bears a resemblance to the concept of slow-roll inflation in the very early Universe. However, a crucial distinction lies in including non-relativistic matter (dark matter and baryons), which cannot be overlooked when delving into the dynamics of dark energy with accuracy. Furthermore, the energy scale of the quintessence potential must align with the order of $\rho_{DE} \approx 10^{-47}, \mathrm{GeV}^4$ today. This value is significantly smaller than that of the inflaton potential [53].

We note here that the cosmological constant, if included, is generally treated as the only cause for cosmic acceleration when taken alone. However, considering a cosmological constant along with a quintessence field infact, allows the cosmological constant to be negative. Such models have been studied and verified against observations [8, 65, 66, 211]. These hybrid models may be useful in easing some of the issues like the Hubble tension.

CHAPTER 3

Probing the post-reionization epoch using weak lensing and the neutral IGM

Dark matter and dark energy, which dominate cosmological background evolution and structure formation, cannot be detected directly. Dark matter is felt primarily through its gravitational influence, and dark energy too, affects the expansion history and growth of structures, and thereby, the imprint of these constituents of the Universe can be seen in any probe of cosmology which is affected by the expansion history and growth of structures. In this thesis, we have considered three different probes of large-scale structure. Firstly, we consider weak lensing, which measures the distortion of images of distant sources due to gravitational lensing by the intervening large-scale structure and emerges as the line of sight integral over the matter distribution between the source and the image plane. The two other probes we use are related to the neutral hydrogen distribution in the post-reionization epoch. Following the completion of complex astrophysical processes characterizing the epoch of reionization, the Universe became predominantly ionized. However, some neutral hydrogen survived and remained housed in two distinct astrophysical systems. Bulk of the neutral gas formed the clumped Damped Lyman Alpha systems which are the source of the 21-cm signal in emission. The diffuse low-density neutral hydrogen in a predominantly ionized IGM formed the Lyman Alpha Forest system, which produces a distinct absorption feature in the quasar spectra. Both these systems become important probes of cosmology through some line transition of the neutral hydrogen. Assuming the gas to be a biased tracer of the underlying dark matter distribution, one may thereby use the emission/absorption of these lines to tomographically map out the dark matter field over a range of redshifts. In the next few sections, we discuss these cosmological probes.

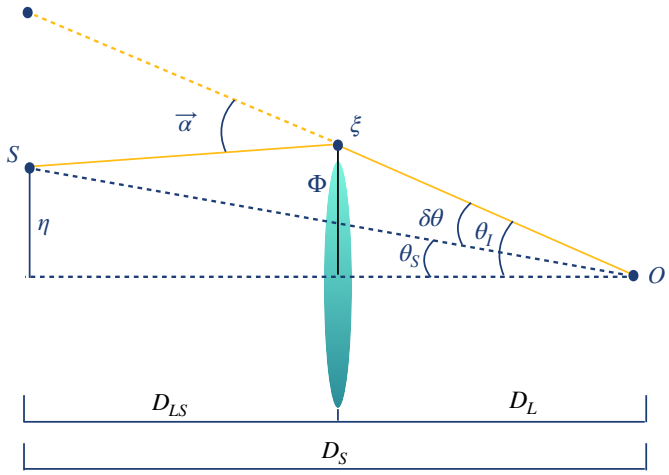

Figure 3.1: Sketch of a gravitational-lens system (adapted from [2]).

3.1 Weak Gravitational Lensing

One of the notable consequences of General Relativity (GR) is the phenomenon of bending of light under gravity [212, 213]. This effect, known as gravitational lensing [214, 215], gives rise to distortions in the images of background sources. Measuring these tiny coherent distortions allows cosmologists to probe the dark sector of the universe [67, 68]. The deflection of light can be derived by examining geodesic curves originating from the field equations within the framework of GR. The deflection of light by gravitational field (potential Φ) is given by the deflection angle and is described as an integral over the path

$$\vec{\alpha} = \frac{2}{c^2} \int \vec{\nabla}_{\perp} \Phi \, d\ell \tag{3.1}$$

In accordance with the illustration presented in Figure (3.1), we can readily derive the ray-tracing equation by considering the intercepts of a light ray concerning the optical axis at the distances D_L and D_S from the observer for the lens and the source, respectively. Let $\vec{\theta_I}$ be the angle between the optical axis and the image, and $\vec{\theta_S}$ be the angle between the optical axis and the source. Through geometrical considerations, we arrive at the relationship for

an infinitesimal lens as

$$D_S\vec{\theta_S} = D_S\vec{\theta_I} - D_{LS}\vec{\alpha} \tag{3.2}$$

where D_{LS} is the distance between the lens and the source. An integral over the comoving distance χ gives the total shift in the sky.

$$\delta\vec{\theta} = \vec{\theta}_I - \vec{\theta}_S = \frac{2}{c^2}\int_0^{\chi_s} \frac{D_{LS}}{D_S}\vec{\nabla}_\perp\Phi \; d\chi \tag{3.3}$$

This equation serves as a foundational component in the ray-tracing analysis of gravitational lensing. In practical observational scenarios, astronomers typically measure this deflection angle or the lensing potential in terms of the angular position $(\vec{\theta})$. This adjustment involves replacing $\vec{\nabla}_\perp$ with $\vec{\nabla}_\theta$ through the relationship $\vec{\nabla}_\perp = D_L^{-1}\vec{\nabla}_\theta$. The factor of D_L^{-1} emerges from the small-angle approximation, where the perpendicular separation from the Line of Sight (LoS) is $D_L\vec{\theta}$. Consequently,

$$\delta\vec{\theta} = \vec{\nabla}_\theta\psi \quad \text{with} \quad \psi(\chi_s\vec{\theta}) = \frac{2}{c^2}\int_0^{\chi_s} \frac{D_{LS}}{D_L D_S}\Phi(\chi,\vec{\theta}) \; d\chi \tag{3.4}$$

Here, we introduce the quantity ψ, referred to as the lensing potential. The lensing potential encapsulates all the imaging properties of a gravitational lens system. We define a magnification matrix $\mathcal{M} = \frac{\partial\vec{\theta_S}}{\partial\vec{\theta_I}}$ with matrix elements

$$\mathcal{M}_{ij} = \frac{\partial\theta_{Si}}{\partial\theta_{Ij}} = \delta_{ij} - \psi_{ij} \tag{3.5}$$

The derivative is taken at the center of the lensed image, and we use the notation $\psi_{ij} \equiv \partial^2\psi/\partial\theta_i\partial\theta_j$. This equation reveals that, in the presence of a lens, the mapping is determined by the curvature of the lensing potential ψ, whereas in the absence of a lens, the mapping remains a simple identity. The second derivatives of gravitational potentials correspond to tidal forces, implying that local deformations caused by the lens mapping are dictated by the gravitational tidal forces generated by the lens. The physical interpretation of magnification matrix $\mathcal{M}$ can be gleaned from its trace:

$$tr\mathcal{M} = 2 - \vec{\nabla}^2\psi = 2(1-\kappa) \tag{3.6}$$

where we have defined $2\kappa = \vec{\nabla}^2\psi$. We can define the shear matrix as the traceless part of the magnification matrix:

$$\Gamma \equiv -\left(\mathcal{M} - \frac{1}{2}(tr(\mathcal{M}))\mathcal{I}\right) \tag{3.7}$$

The shear matrix has the following components:

$$\begin{aligned}\Gamma_{11} \equiv \gamma_1 = \frac{1}{2}(\psi_{11} - \psi_{22}), \Gamma_{22} = -\gamma_1,\\ \Gamma_{12} = \Gamma_{21} \equiv \gamma_2 = \psi_{22}\end{aligned} \tag{3.8}$$

Indeed, the symmetric tensor Γ effectively quantifies the projection of the gravitational tidal field. This projection, in turn, characterizes the distortions experienced by background sources due to the lensing effect. We can express the Magnification matrix in terms of κ and γ, as follows:

$$\mathcal{M} = (1-\kappa)\mathcal{I} - \Gamma = \begin{bmatrix} 1-\kappa-\gamma_1 & -\gamma_2 \\ -\gamma_2 & 1-\kappa+\gamma_1 \end{bmatrix} \tag{3.9}$$

For a non-singular $\mathcal{M}$, we can compute its inverse ($\vec{\delta\theta_I} = \mathcal{M}^{-1}\vec{\delta\theta_S}$), which determines how sources are mapped on images. The determinant of $\mathcal{M}$,

$$\det \mathcal{M} = (1-\kappa)^2 - \gamma^2 \quad \text{with} \quad \gamma^2 \equiv \gamma_1^2 + \gamma_2^2 \tag{3.10}$$

The points where $\det \mathcal{M} = 0$ are known as critical points and play an important role in strong lensing [216, 217]. In the context of weak lensing, we generally assume that the linear lens mapping is invertible, leading to an expression:

$$\mathcal{M}^{-1} = \frac{1}{\det \mathcal{M}} \begin{bmatrix} 1-\kappa+\gamma_1 & \gamma_2 \\ \gamma_2 & 1-\kappa-\gamma_1 \end{bmatrix} \tag{3.11}$$

The inverse of $\det \mathcal{M}$ corresponds to magnification. Therefore, the matrix $M = \mathcal{M}^{-1}$ is commonly referred to as the magnification tensor. With this context, we introduce the quantity μ :

$$\mu \equiv \det M = \frac{1}{\det \mathcal{M}} = \frac{1}{(1-\kappa)^2 - \gamma^2}\mathcal{M} \approx 1 + 2\kappa \tag{3.12}$$

In the last step, we invoke a first-order Taylor expansion. As a result, in weak gravitational lensing, convergence determines how magnified an image will be rather than shear. The eigenvalues of the matrix M (or the inverse of the eigenvalues of the $\mathcal{M}$) quantify the amplification in the direction of the eigenvectors of the shear tensor.

Using Poisson's equation in an expanding Universe that is spatially flat ($\Omega_K = 0$), we can replace the Distances D_{LS}, D_S, D_L with the corresponding distances. Thus

$$\kappa = \frac{4\pi G}{c^2} \int_0^{\chi_s} d\chi \frac{\chi(\chi_s - \chi)}{\chi_s} a^2 \rho(\chi) \tag{3.13}$$

This expression for κ illustrates that it involves a Line of Sight integral weighted by the mass density ρ. By introducing the density contrast $\delta = (\bar{\rho} - \rho)/\bar{\rho}$ and converting ρ to conventional cosmological parameters $\rho = (3H_0^2/8\pi G)\Omega_{m0} a^{-3}$ the expression for κ becomes:

$$\kappa = \frac{3}{2} \frac{H_0^2}{c^2} \Omega_{m0} \int_0^{\chi_s} d\chi \frac{\chi(\chi_s - \chi)}{\chi_s} \frac{\delta(\chi)}{a} \tag{3.14}$$

This is often referred to as effective convergence, as it arises from the actual mass distribution of the Universe. From an observational perspective, κ (or any lensing quantity) cannot be directly inferred due to the unknown matter distribution in a given direction. However, what can be estimated is the extent of correlation between lensing quantities such as lensing potential, deflection angle, convergence, or shear [215].

Conventionally, the angular correlation function ($\xi(\phi)$ is used to quantify correlations in the observable κ, with $\Delta\vec{\theta} = \phi$) :

$$\xi(\Delta\vec{\theta}(= \phi)) \equiv \langle \kappa(\vec{\theta}) \kappa(\vec{\theta} + \Delta\vec{\theta}) \rangle \tag{3.15}$$

This correlation function depends solely on the magnitude of the separation vector $\vec{\phi}$ and not its orientation due to the assumption of statistical isotropy. Taking the Fourier transform of the correlation function $\xi(\phi)$, we obtain the angular power spectrum:

$$C_\kappa^\ell = \int d^2\phi \, \xi(\phi) \, \exp^{-i.\vec{\ell}.\vec{\phi}} \tag{3.16}$$

where $\vec{\ell}$ is the two-dimensional wave vector conjugate to the angular separation $\vec{\phi}$. In the Limber approximation [218], the **weak lensing convergence power spectrum** takes the form (refer to Appendix B for detailed derivation)

$$C_\kappa^\ell(\vec{\ell}) = \frac{9}{4}\left(\frac{H_0}{c}\right)^4 \Omega_{m0}^2 \int_0^{\chi_s} d\chi \, \frac{g^2(\chi)}{a^2(\chi)} \, D_+^2(\chi) P_{3D}\left(\frac{\vec{\ell}}{\chi}\right) \tag{3.17}$$

with $g(\chi)$ being the geometric factor,

$$g(\chi) = \chi \int_\chi d\chi' n(\chi') \left(\frac{\chi' - \chi}{\chi'}\right) \tag{3.18}$$

where $n(\chi)$ is the radial distribution of source galaxies (normalized so that $\int d\chi \, n(\chi) = 1$. If we look at the lensing of the CMBR, then all sources are at a single redshift z_s and the corresponding geometric factor shall be

$$g_{CMB}(\chi) = \chi \left(\frac{\chi_s - \chi}{\chi_s}\right) \tag{3.19}$$

The quantity (C_κ^ℓ) in Eq:(3.17) is the observable quantity which contains rich cosmological information [70]. Firstly, the weak lensing power spectrum imprints the matter (both dark matter and baryonic) distribution through the terms $D_+(z)$ and $P(\ell/\chi)$. Secondly, $g(\chi)$ encapsulates information about the expansion history through $\chi(z), H(z), D_A(z)$, etc. Thus the lensing power spectrum in principle can be used to constrain a host of cosmological parameters [76, 219, 220]. Assuming that the fluctuations form a Gaussian random field, the power spectrum contains the entire statistical information. However, since the weak lensing field is nongaussian on small scales, higher-order correlations may become important on large multipoles [221, 222].

The first detection of weak lensing by large-scale structure was announced and remarkably consistent with theoretical expectations [223–225]. Since then, several further measurements have been collected using ground-based [226–231] and space-based observations [232–235], leading to an increasingly better understanding of the cosmos.

Ground-based surveys currently cover approximately 100 square degrees, while space-based surveys span a few square degrees but incorporate more

distant galaxies with stronger lensing signals. These measurements have enabled the determination of E and B mode correlation functions of shear in real space, resulting in impressive constraints on σ_8 and Ω_{m0} [236]. While weak lensing is a crucial probe of dark energy, it needs to be combined with other potential probes like SNIa, CMB, etc., to produce robust constraints on EoS w [237]. Future weak lensing studies have the potential to quantify dark energy and modified gravity models much more accurately [238]. Gravitational lensing proves to be a powerful tool for probing modified gravity theories since it originates from the sum of two gravitational potentials, $\Phi + \Psi$ [239]. As modifications to gravity impact Φ and Ψ differently, weak lensing can, in principle, distinguish between Λ and modifications of gravity [240].

Weak gravitational lensing is thus a promising technique to study the nature of dark energy and extract other interesting cosmological information simultaneously. Current experiments aim to observe weak lensing signals with wider and deeper surveys. This shall enhance the accuracy and reliability of measurements and put additional insights into dark energy models or modified gravity theories.

3.2 Probes of post-reionization neutral IGM

In the last section, we discussed the use of gravitational lensing to map out the matter distribution. We shall now shift our focus to the probes of the intergalactic medium (IGM). While dark matter has a dominant role is cosmic evolution and structure formation, baryonic matter (neutral hydrogen) is detectable through matter/radiation interactions and can map out the dark matter distribution through their gravitational interaction. Neutral hydrogen in the post-reionization epoch are housed in two kinds of astrophysical systems (i) The dense clumped self-shielded Damped Lyman Alpha clouds which source the 21-cm signal and (ii) diffuse Lyman-alpha forest systems. We shall now discuss the redshifted HI 21-cm signal [81, 85, 86, 241] and the Lyman-α forest [96, 97, 99, 242]. Alongside these, there are other probes of the IGM which are not studied in this thesis. Notable amongst these probes are the probes of the late-time anisotropies of the CMB like the Sunyaev-Zel'dovich

effect [243–246] and the Integrated Sachs Wolfe (ISW) effect [247, 248]. Also, intergalactic medium metallicity [249–251], is also known as a cosmological probe.

3.2.1 Red-shifted 21cm signal

Hyperfine coupling of the proton and electron spins in the ground state of the Hydrogen atom creates a triplet and a singlet state, with the triplet state having a higher energy than the singlet state. The transition of these spin-flip states results in the emission or absorption of radiation with a wavelength of 21-cm (frequency 1420MHz) in the rest frame of the gas.

The radiative transfer equation describes the propagation of radiation through the IGM.

$$\frac{dI_\nu}{ds} = -\alpha_\nu I_\nu + j_\nu \tag{3.20}$$

where I_ν is the intensity of the incident light and α_ν is the absorption coefficient. This equation may be expressed in terms of optical depth $(d\tau_\nu = \alpha_\nu ds)$ and $S_\nu = j_\nu/\alpha_\nu$ is the Source function. In the case when the source function does not include the intensity I_ν the solution of the radiative transfer equation is given by

$$I_\nu = I_\nu(0)\exp(-\tau_\nu) + S_\nu[1 - \exp(-\tau_\nu)] \tag{3.21}$$

In a state of equilibrium, the ratio of occupancy of the hyperfine levels is controlled by the spin temperature T_s defined by

$$\frac{n_1}{n_0} = 3\exp\left(-\frac{T_*}{T_s}\right) \tag{3.22}$$

where n_0 and n_1 denote the populations in the triplet and the singlet states, respectively. Here $T_* = h\nu_e/k_B = 0.068$ K, where h is the Planck's constant, ν_e equals 1420 MHz, and k_B is Boltzmann's constant. Along a line of sight, the CMBR photons interact with the intervening HI through the 21-cm transition. According to the radiative transfer equation and relating the intensity to temperature as $I = 2k_BT/\lambda^2$ (in the Raleigh Jeans limit) we have the CMBR

brightness temperature change as light passes through the gas as

$$T(\tau) = T_\gamma e^{-\tau} + T_s(1 - e^{-\tau}) \tag{3.23}$$

where τ is the 21-cm optical depth, and T_γ is the temperature of the background CMBR. The quantity of observational interest for radio observations of the 21-cm radiation is the excess brightness temperature redshifted to the observer at present, defined as

$$T_b(n, z) = \frac{T(\tau) - T_\gamma}{1 + z} \approx \frac{(T_s - T_\gamma)\tau}{1 + z} \tag{3.24}$$

where we have assumed that $\tau << 1$ and CMBR anisotropies are neglected. The 21-cm optical depth at a redshift z and along a line of sight n and is given by [81–84, 252, 253]

$$\tau = \frac{4.0mK}{T_s}\left(\frac{\Omega_b h^2}{0.022}\right)\left(\frac{0.7}{h}\right)\frac{H_0}{H(z)}(1+z)^3\frac{\rho_{HI}}{\bar{\rho}_H}\left[1 - \frac{(1+z)}{H(z)}\frac{\partial v}{\partial r_\nu}\right] \tag{3.25}$$

where the comoving distance r_ν, and the Hubble parameter $H(z)$ are sensitive to the cosmological model, v denotes the peculiar velocity component along the sight line and $\frac{\rho_{HI}}{\bar{\rho}_H}$ is the ratio of the neutral hydrogen to the mean hydrogen density. We write

$$\delta T_b(\nu, \hat{\mathbf{n}}) = \bar{T}(z)\eta_{HI}(z, \hat{\mathbf{n}}r_\nu) \tag{3.26}$$

where the redshift dependent quantity $\bar{T}(z)$ is given by [253]

$$\bar{T}(z) = 4\mathrm{mK}(1+\mathrm{z})^2\left(\frac{\Omega_\mathrm{b}\mathrm{h}^2}{0.022}\right)\left(\frac{0.7}{\mathrm{h}}\right)\frac{\mathrm{H}_0}{\mathrm{H(z)}} \tag{3.27}$$

and

$$\eta_{HI}(z, \hat{\mathbf{n}}r_\nu) = \bar{x}_{\mathrm{HI}}(z)\left\{\left(1 - \frac{T_\gamma}{T_s}\right)\left[\delta_H(\hat{\mathbf{n}}, z) - \frac{(1+z)}{H(z)}\frac{\partial v(z, \hat{\mathbf{n}}r_\nu)}{\partial r_\nu}\right] + \frac{T_\gamma}{T_s}s\ \delta_H(\hat{\mathbf{n}}, z)\right\} \tag{3.28}$$

The quantity $\bar{x}_{HI}(z)$ denotes the mean neutral fraction at a redshift z, and $\delta_H(\hat{\mathbf{n}}, z) = (\rho_{HI} - \bar{\rho}_{HI})/\bar{\rho}_{HI}$ is the HI perturbations. The function s relates the

fluctuations of the spin temperature to the HI fluctuations.

Around a redshift of $z \sim 1000$, protons and electrons combine and form neutral hydrogen while the decoupled photons free stream and the Universe enters the Dark Ages. A small fraction of electrons that survives the recombination participates in Collisional processes which try to keep the kinetic temperature of the gas T_g at the CMB temperature. At lower redshifts $z \sim 200$ these collisional processes become ineffective in maintaining the gas temperature and in the absence of external heating $T_g \propto (1+z)^2$ while $T_\gamma \propto (1+z)$. The spin temperature T_s, however continues to be coupled to T_g till $z \sim 70$ through the processes of collisional spin flipping after which it matches up with T_γ again.

When gravitational collapse leads to the formation of the first luminous sources at $z \sim 20$, the population of the hyperfine triplet state increases due to Lyman-α scattering, through the Wouthuysen-Field effect [254] causing the spin temperature to rise above the CMB temperature, whereby $T_s >> T_\gamma$ at low redshifts.

The radiative transfer equation tells us that 21-cm radiation will only be seen when $T_s \neq T_\gamma$. In the range of redshifts $30 \leq z \leq 200$ where we have $T_s < T_\gamma$ and thus HI is to be seen as an absorption feature against the background CMBR. At lower redshifts when $T_s > T_\gamma$, the redshifted 21-cm radiation would be seen in emission. The thermal history and the evolution of the temperatures are well studied [255, 256]. From the observational point of view, it implies that the cosmological 21-cm signal will form a background in all radio observations with frequencies $7.1 \leq f \leq 1420$ MHz. The 21-cm line allows tomographic imaging the entire three-dimensional volume in the redshift range $0 \leq z \leq 200$ by suitably tuning the observing frequency of radio telescope.

The redshift range $0 \leq z \leq 200$ is sliced into three epochs corresponding to the major astrophysical events characterizing each of them

- The dark ages ($20 < z < 200$) - Density perturbations are linear, and the gas distribution follows the dark matter distribution. 21-cm signal is seen in absorption [257–259].

- The epoch of Reionization (EoR) ($6 < z < 20$)- With the formation of the first luminous sources, the neutral hydrogen starts to get ionized.

The absence of Gunn-Peterson troughs [260] in the absorption Lyman - α forest spectra of distant quasars indicate that the complex processes of reionization was complete at around $z \sim 6$ [261–263]. Several heating mechanisms [264, 265] causes the spin temperature T_s to rise significantly above the CMB temperature. The 21-cm radiation from the EoR is seen in emission.

- The post-reionization epoch ($0 < z < 6$)- The post-reionization IGM is almost completely ionized. This is the entire era from the end of the reionization process up to the present. The neutral fraction evolves from its value $x_{HI} \sim 1$ in the "dark ages" to its present value $\sim 10^{-3}$ and traces the complex astrophysical processes characterizing each epoch.

We shall now discuss our present understanding of the intergalactic medium in the post-reionization epoch. The IGM for $z < 6$ is mostly ionized. While this is true for the low density gas, which, by the end of reionization is ionized, a small fraction of neutral hydrogen survives in confined, over-dense regions of the IGM which are self-shielded from the background ionizing radiation.

Two astrophysical systems which are related to the HI distribution in the IGM are of immense observational importance

- The optically thin low-density Lyman-α absorbers. They produce distinct absorption lines (which look like a "forest") in the spectra of background quasars called the Lyman-α forest.

- The clumped, dense self shielded, damped Lyman-α systems (DLAs) [266]. These DLAs remain neutral in spite of the background ionizing radiation field. They also store the bulk ($\sim 80\%$) of the HI at $z < 4$ [267] with HI column density greater than $2 \times 10^{20}\mathrm{atoms/cm^2}$ [268–270]. Observation of the distribution and clustering properties of the DLA clouds indicates that these clouds are located in regions of highly non-linear matter over density peaks, which are typically associated with galaxies. [271–273]. These clouds primarily source the 21-cm radiation emission in the post reionization epoch.

In some sense, the DLA's and the Lyman-α forest are complimentary as the DLA's, which source the 21-cm emission, do not contribute to the Lyman-α

optical depth. There is extensive literature on the HI -21 signal from the post-reionization epoch [81–87, 89].

Several assumptions simplify the modeling of the post-reionization HI signal. These are either motivated by implicit observations or from numerical simulations.

- In the post-reionization epoch, there is an enhancement of the population of the triplet state of HI due to the Wouthuysen field coupling. This makes the spin temperature T_s much greater than the CMB temperature T_γ. Thus, the 21-cm radiation is seen in emission in this epoch against the background CMBR [255, 256, 264]. For $z \leq 6$, the spin temperature and the gas the kinetic temperature remains strongly coupled through Lyman-α scattering or collisional coupling [264].

- Extensive study of the Lyman-α absorption lines in quasar spectra indicates that in the redshift range $1 \leq z \leq 3.5$ the cosmological density parameter of the neutral gas has a value $\Omega_{gas} \sim 10^{-3}$ [267]. Thus the mean neutral fraction is $\bar{x}_{\rm HI} = \Omega_{gas}/\Omega_b \sim 2.45 \times 10^{-2}$. which does not evolve in the entire redshift range $z \leq 6$.

- On the large cosmological scales of interest, HI peculiar velocities are assumed to be determined by the dark matter distribution. Thus, peculiar velocity manifests as a redshift space distortion anisotropy in the 21-cm power spectrum.

- The discrete nature of DLA sources is not considered. The corresponding Poisson noise owing to this discrete sampling is neglected, assuming that the number density of the DLA emitters is very large [89].

- HI perturbations are generated by a Gaussian random process. We do not consider any non-gaussianity and thereby the statistical information is contained in the two-point correlation or the power spectrum.

- Galaxy redshift surveys and numerical simulations show that the galaxies are a biased tracers of the underlying dark matter distribution [274–276]. If we assume that HI in the post-reionization epoch is housed predominantly in dark matter haloes, we may expect the gas to trace

the underlying dark matter density field with a bias $b_T(k,z)$ defined as $b_T(k,z) = \left[\frac{P_{\rm HI}(k,z)}{P(k,z)}\right]^{1/2}$ where $P_{\rm HI}(k,z)$ and $P(k,z)$ denote the HI and dark matter power spectra, respectively. The bias function quantifies the nature of HI clustering in the post-reionization epoch. Further, the fluctuations in the ionizing background may also contribute to $b_T(k,z)$ [81]. On scales below the Jean's length, the linear density contrast of HI gas is related to the dark matter density contrast through a scale dependent function [277]. However, on large scales, the bias is known to be scale-independent, though the scales above which the bias is linear, is sensitive to the redshift being probed. Several authors have now demonstrated the nature of HI bias using N-body simulations [91–93, 278]. The simulations are based on the principle of populating dark matter halos in a certain mass range with gas and thereby identifying them as DLAs. These simulations show that the large scale linear bias grows monotonically with redshift for $1 < z < 4$ [279]. This feature is shared by galaxy bias as well [275, 280, 281]. There is a steep rise of the 21-cm bias on small scales. This is because of the absence of small mass halos as is expected from the CDM power spectrum, and, consequently, the HI being distributed only in larger halos. A fitting formula for the bias $b_T(k,z)$ as a function of both redshift z and scale k has been obtained from numerical simulations [91, 92] of the post-reionization signal as

$$b_T(k,z) = \sum_{m=0}^{4}\sum_{n=0}^{2} c(m,n)k^m z^n \tag{3.29}$$

We have used these simulation results in our modeling of the post-reionization epoch.

- The 21-cm flux from individual clouds is extremely weak ($< 10\mu$Jy) and it is rather difficult for these clouds to be ever detected in radio observations, even with futuristic telescopes and in spite of signal enhancement due to the effect of gravitational lensing [282]. However, intensity mapping experiments aim to map out the diffuse collective radiation from the clouds without attempting to resolve individual sources.

Adopting all the assumptions discussed above, the power spectrum of post-reionization HI 21-cm brightness temperature fluctuations from redshift z is given by [256, 283] (see Appendix C for detail analytical derivation)

$$P_{\rm HI}(\mathbf{k}, z) = \bar{T}(z)^2 \bar{x}_{\rm HI}^2 b_T(k, z)^2 (1 + \beta_T(k, z)\mu^2)^2 P(k, z) \tag{3.30}$$

where $\mu = \hat{\mathbf{k}} \cdot \hat{\mathbf{n}}$, $\beta_T(k, z) = f_g(k, z)/b_T(k, z)$. The term $f_g(z, k)\mu^2$ has its origin in the HI peculiar velocities [83, 256] which, as we mentioned, are sourced by the dark matter fluctuations.

Observations and challenges

The fact that the collective 21 cm signal forms a diffused background in all radio observations at frequencies of observation $f \leq 1420$ MHz makes is a powerful tomographic tool. The fluctuations of this background emission on the sky plane (angular variations) and across redshift (frequency), maps out the tomographic image of the Universe. The statistical properties of the fluctuations have a direct imprint on cosmological evolution history, growth of perturbations, and the astrophysical properties of the IGM.

It is possible to study the nature of dark energy by using the redshifted 21-cm signal from the post-reionization epoch (i.e. low redshift measurements) [78, 81, 85, 87, 283–285]. As it traces the dark matter distribution the post-reionization 21-cm intensity mapping [80] can be a tool for cosmological parameter estimation [85–87, 283, 284]. Measurement of the redshift space distortion parameter has been suggested as a method to separate the astrophysical component from the cosmology [84]. The measurement of the BAO imprint through its oscillatory signature in the post-reionization power spectrum is a powerful probe of dark energy. This has been studied by [286] for $z > 3$ and in the low redshift range ($z < 2$) range as well [80].

The first detection of the intensity mapping of 21-cm signal was achieved in 2010 [287]. Using the Green Bank Telescope (GBT), they detected a 3D 21-cm intensity field in the redshift range $z = 0.53 - 1.12$. This discovery served as the first observational evidence that the 21 cm intensity field traces the distribution of galaxies at $z \approx 1$ [288]. Extension of GBT, Masui et al. detected a cross-power

spectrum at $z \approx 0.8$ between 21-cm and galaxies in the WiggleZ Dark Energy Survey [289] and Switzer et al. provided an upper limit on the 21 cm auto-power spectrum for the first time [290]. The 21-cm power spectrum in auto-correlation has yet to be discovered. This is a primary scientific objective of several operational and planned radio interferometric arrays, including Giant Metrewave Radio Telescope (GMRT), the Ooty Wide Field Array (OWFA), the Canadian Hydrogen Intensity Mapping Experiment (CHIME), the Meer-Karoo Array Telescope (MeerKAT), the Square Kilometer Array (SKA) are focused on detecting the cosmological 21cm signal.

The possibility of 21-cm intensity mapping experiments as a precision probe of cosmology faces several observational challenges. The signal is buried is foregrounds from galactic and extragalactic sources that are ≈ 5 orders of magnitude larger [291, 292]. The foregrounds primarily arise from astrophysical sources like Synchrotron radiation from our own galaxy, free free emission, or extra-galactic radio point sources [293–295]. The Galactic synchrotron foreground scales as $\approx (1+z)^{2.6}$, and thus lower redshifts are least affected by the galactic foreground. Secondly, in the low redshift range $(z \leq 6)$ the complex astrophysical processes of the Reionization epoch are absent. Still, foreground removal is the key challenge towards detecting the signal. It turns out that the spectral properties of the foregrounds are strikingly different from the 21-cm signal, which allows for the two to be separated. Several techniques attempt to remove the foregrounds from the measured visibilities (e.g. [296–300], by assuming the smooth nature of the foregrounds. The multi-frequency angular power spectrum (MAPS) [301] has been proposed as a tool for foreground removal by several groups [295, 302]. Some other groups adopt a 'foreground avoidance' strategy where only the region outside the foreground wedge is used to estimate the 21-cm power spectrum (e.g. [303–307]). Further, one requires extremely precise bandpass, calibration for the detection of the signal. Calibration introduces spectral structure into the foreground signal, making it further difficult to effectively remove foregrounds. This difficulty has led to many proposals for precise bandpass calibration [308–317]

The cosmological signal is also plagued by terrestrial RFI (radio frequency interference) from mobile phones, satellite broadcasts, and other instrumental

effects.

In this thesis, we focus on the proposal of cross-correlating the 21-cm signal with other tracers as a way to bypass the foreground issue to some reasonable extent. Before doing so, let us consider another very promising observational probe of IGM, the Lyman-α forest.

3.2.2 Lyman-α forest: A cosmological probe

The Lyman-α forest is an absorption phenomenon in the spectra of background quasistellar objects (QSOs) [96, 97, 100, 101, 318–322]. This observable event manifests across ultraviolet (UV) and optical wavelengths, spanning from the local Universe to the highest ascertainable redshifts where QSOs are observable (currently around $z \approx 5$). It probes the distribution of spatial fluctuations of the HI optical depth in the intergalactic medium (IGM).

On its way to the observer through an expanding Universe, the light from a bright, distant QSO passes through intervening intergalactic diffuse neutral hydrogen. The absorption process induced by these gas entities alters the spectra of the background objects, imparting a detailed record of the physical and chemical conditions of the gas clouds onto the observable spectra of both the background QSOs and galaxy sources. A neutral hydrogen cloud in the line of sight (LOS) will cause absorption of the QSO continuum for a frequency redshifted to the Lyman-α ($1215.67\mathrm{A}^\circ$) UV resonance line in the rest frame of the gas. The inhomogeneous HI distribution in an expanding Universe thus leads to the formation of a series of absorption lines blue ward of $1215.67\mathrm{A}^\circ$, known as the Lyman-α forest. The optical depth of the Lyman-α forest is a tracer of the underlying dark matter distribution and thus, the absorption spectra map out the one-dimensional dark matter inhomogeneities. The term 'Lyman-α forest' characterizes the visual aspect of optical spectra obtained from QSOs, displaying a dense assemblage of numerous sharp absorption lines. The vast majority of lines within the Lyman-α forest correspond to the identical atomic transition at a wavelength of $1215.67A$. However, a small number of the absorption lines in the Lyman-α forest are caused due to absorption by heavier elements. These metal line contaminations do pose observational challenges.

The Lyman-α forest is a powerful cosmological probe [100, 323]. Detailed

literature is available on the use of Lyman-α forest for the estimation of matter power spectrum [242, 324], cosmological parameter estimation [101, 325, 326], constraining small scales clustering properties of dark matter [327], constraining neutrino mass [242, 326] and probing the reionization history of the Universe [328–330].

The Lyman-α forest was initially theorized and observed by Gunn and Peterson in 1965 [260]. The basic idea is as follows: going back in time, an increasing fraction of the total baryonic mass of the Universe must be in the form of neutral gas. The absorption cross-section of the Lyman-α line of neutral hydrogen is large enough that even if only a small fraction of the total mass of the Universe were in the form of HI the redshifted Lyman-α lines should completely absorb a part of the spectrum of any background light source. The absorption should essentially assume the shape of an absorption trough in a QSO spectrum, extending blueward from the Lyman-α emission of the QSO. This distinctive absorption pattern is referred as the **Gunn Peterson effect**. The absence of a large Gunn Peterson absorption (trough) for redshifts $z < 6$ implies that the Universe must be ionized at these epochs.

QSO surveys subsequently demonstrated that the collective ionizing radiation emitted by all known QSOs at high redshift potentially generates a potent UV radiation field capable of maintaining a significant portion of the universal baryonic matter in a highly ionized state. This proposition hinges on the assumption that the gas within the Universe achieves an approximate photoionization equilibrium with the cosmic UV background. This equilibrium entails that the recombination rate of electrons with protons to form neutral hydrogen equals the rate of ionizations from the ground state of HI:

$$n_e n_p \alpha(T) = n_{HI} \Gamma \tag{3.31}$$

In this equation, Γ denotes the rate of photoionizations per neutral hydrogen atom. The variables n_e, n_{HI}, and n_p correspond to the number densities of electrons, neutral hydrogen atoms, and protons (ionized hydrogen), respectively.

Observations of QSOs characterized by higher spectral resolutions revealed a jagged "forest" comprised of numerous individual absorption lines. This indicates that the distribution of neutral hydrogen within the Universe exhibits

inhomogeneity, extending to the typical width of a Lyman-α line. The degree of this clumpiness affects the observable quantity, which is the transmitted flux of the QSO, denoted as $\mathcal{F}$. This flux is proportional to $\exp(-\tau)$, where τ is the Lyman-α optical depth.

Assuming approximate photoionization equilibrium, the optical depth τ depends on the baryon density fluctuations δ_b, IGM temperature T , and photoionization rate Γ as [95, 96, 319, 331]

$$\tau \propto \langle A \rangle (1+\delta_b)^2 \, T^{-0.7} \, \Gamma^{-1} \tag{3.32}$$

Here, $\langle A \rangle$ encompasses all factors dependent solely on the background cosmology. The temperature follows a power-law relationship with baryon density, defined as [331]:

$$T(z) = T_0(z)(1+\delta_b)^{\gamma(z)-1}, \qquad \gamma(z) \approx 1 - 1.6 \tag{3.33}$$

This power-law expression characterizes the thermal state of the intergalactic medium (IGM) [332–334]. The key assumptions are therefore that (i) Γ, T_0 and γ have no spatial fluctuations, and (ii) the neutral hydrogen density is fully determined by the local matter density via gravity.

The standard normalized quantity used for calculating correlations and power spectra is the flux contrast $\delta_{\mathcal{F}}$ of the Lyman-α forest. It is defined as:

$$\delta_{\mathcal{F}} = \frac{\mathcal{F}(\hat{n}, z)}{\bar{\mathcal{F}}} - 1 \tag{3.34}$$

where $\mathcal{F}$ is the transmitted flux fraction, and $\bar{\mathcal{F}}$ is its mean value, indicating the average transmission through the intervening IGM.

Most analytical studies of the Lyman-α forest assume that the transmitted-flux fluctuations through the forest is believed to be as a tracer of the underlying dark matter distribution with a possible bias. Hydrodynamical simulations [99, 335–338] and analytical modeling [339–345] are also extensively used to study the properties of the Lyman-α forest. The simulations and semi-analytical modeling of the Lyman-α forest do support the idea that the transmitted flux is indeed a tracer of dark matter. The primary observable of the

Lyman-α forest is the one-dimensional flux power spectrum $P_{1D}^{\mathcal{F}}$ defined by [242, 318, 346, 347]

$$P_{1D}^{\mathcal{F}} = \frac{1}{2\pi}\int_{k}^{\infty} dk'\, k'\, P^{\mathcal{F}}(k') \tag{3.35}$$

$P^{\mathcal{F}}$ is the 3D power spectrum of the Lyman-α transmitted flux $\mathcal{F}$.

Quasar surveys like SDSS III Baryon Oscillation Spectroscopic Survey (BOSS) [348–350] aims to measure the absorption spectra of $\sim 160,000$ QSOs and the data may improve significantly in future surveys. Thus the idea is then to treat the Lyman-α forest as sampling a continuous 3D density field along skewers corresponding to sight lines.

Many observational issues come in the way of constraining theoretical models using the Lyman-α forest. Some of the key sources of observational uncertainty include: inadequate modeling of the of the background ionizing field, errors in QSO continuum fitting, uncertainties in the slope of the temperature-density relationship in the diffuse IGM and its inevitable fluctuations about the mean relation, metal line contamination in the quasar spectra, and our lack of knowledge about the effects of galactic super winds.

3.3 The cross-correlation of weak lensing the post-reionization tracers of IGM

In this section, we explore the possibility of cross correlating the weak lensing convergence field with tracers like the 21cm signal or Lyman-α forest. Simulations indicate that on large cosmological scales, both the Lyman-α forest and the 21-cm signal are biased tracers of the underlying dark matter (DM) distribution [91–93, 278, 351]. This has allowed the possibility of studying cross-correlations between Lyman-α and post reionization 21-cm signal [278, 352–355]. The cross between Lyman-α and post reionization 21-cm signal which was proposed by [352, 353] has now been observationally detected [356]. Here, we investigate the cross-correlation of weak lensing and 21-cm, originally proposed as a cosmological probe in [357]. We show the general spherical sky formulation and also derive the flat-sky result used earlier [357] from more general considerations.

- There is a crucial difference between the weak lensing and tracer fields. The former measures the integrated effect along the LoS of a geometric kernel from redshift $z = 0$ to the last scattering surface and, is hence sensitive to the fluctuations of the density field on large scales. The tracers (Lyman-α forest and redshifted 21-cm intensity maps) on the contrary, are tomographic probes of small-scale fluctuations. Thus, cross-correlation quantifies the evolution of small wavelength modes of the fluctuations on top of the long wavelength modes.

- It may be possible to lessen the severe impact of foreground contaminants and other systematic effects that plague the signal by cross-correlating the 21 cm signal with other probes [357, 358]. The systematic noise that arises in the individual surveys pose less threat in the cross-correlation signal as they appear in the variance [278, 352–355]. Further, the foregrounds and contaminants of individual surveys are, in most cases, uncorrelated and hence do not bias the cross-correlation signal [359].

- Further, a cross-correlation signal may be detected at a greater Signal to Noise Ratio (SNR) as compared to the HI auto-correlation [360].

It should be noted that using cross correlation won't offer any new benefits if all of the different probes' observations are accurate. However, even after subtraction, we anticipate that the first generation observations of the redshifted HI 21cm signal will contain significant systematic errors and foreground residuals.

Cross-correlation angular power spectrum: Formalism

On large scales, the Lyman-α forest and the redshifted 21-cm signal from the post-reionization epoch are both known to be biased tracers of the underlying dark matter distribution. We denote $\delta\mathcal{F}$ to denote the fluctuations in the Lyman-α transmitted flux $\delta\mathcal{F} = (\mathcal{F} - \bar{\mathcal{F}})/\bar{\mathcal{F}}$. In the post-reionization era, the neutral fraction remains constant [268, 361–363] and photo-ionization equilibrium leads to a power-law, temperature density relationship [328]. Numerical simulations validate the Fluctuating Gunn-Peterson effect [343, 348, 364, 365]

whereby it is reasonable to assume that on large scales the smoothed flux fluctuations $\delta_{\mathcal{F}} \propto \delta$, where δ denotes the dark matter overdensity field.

The HI 21-cm emission signal also arises from the same redshift range as the Lyman-α forest. However, they are sourced by the DLAs which are believed to contain most of the HI during the post reionization era. The Lyman-α forest, on the contrary, arises from the low-density HI in a predominantly ionized IGM. On large scales, the HI 21-cm signal also traces the underlying dark matter distribution. We use δ_T to denote the redshifted 21-cm brightness temperature fluctuations.

Including a redshift space distortion, we may write both $\delta_{\mathcal{F}}$ and δ_T in Fourier space as

$$\delta_i(\mathbf{r}) = \int \frac{d^3\mathbf{k}}{(2\pi)^3}\, e^{i\mathbf{k}.\mathbf{r}} \Delta_i(\mathbf{k})\,. \tag{3.36}$$

where $i = \mathcal{F}$ and T refer to the Ly-α forest transmitted flux and 21-cm brightness temperature, respectively, with

$$\Delta_i(\mathbf{k}) = \mathcal{A}_i[1 + \beta_i \mu^2]\Delta(\mathbf{k}) \tag{3.37}$$

where $\Delta(\mathbf{k})$ is the dark matter density contrast in Fourier space and μ is the cosine of the angle between the line of sight direction $\hat{\mathbf{n}}$ and the wave vector ($\mu = \hat{\mathbf{k}} \cdot \hat{\mathbf{n}}$). β_i is the linear redshift distortion parameter. For the 21-cm signal, we have

$$\mathcal{A}_T = 4.0\,\mathrm{mK}\, b_T\, \bar{x}_{\mathrm{HI}} (1+z)^2 \left(\frac{\Omega_{b0}h^2}{0.02}\right)\left(\frac{0.7}{h}\right)\left(\frac{H_0}{H(z)}\right) \tag{3.38}$$

where $\bar{x}_{\mathrm{HI}}$ is the mean neutral fraction. In the post-reionization epoch $z < 6$, $\Omega_{gas} \sim 10^{-3}$ and the neutral hydrogen fraction remains with a value $\bar{x}_{\mathrm{HI}} = 2.45 \times 10^{-2}$ [268, 361–363]. We may write $\beta_T = f(z)/b_T$ where b_T denotes a bias and $f(z)$ is growth rate of density perturbations. The bias function $b_T(k, z)$ is scale-dependent below the Jeans scale. There is also additional scale dependence arising from the fluctuations in the ionizing background [81]. The bias is also a monotonically growing function of redshift [92]. Several studies indicate that on large scales, a constant linear bias model is reasonably valid [91–93]. We adopt the bias function b_T from simulation results [92]. The function $\beta_T(z)$ crucially imprints the dark energy parametrizations through its dependence of

$f(z)$ and has a redshift dependence arising from both $f(z)$ and $b_T(z)$.

The interpretation of the linear distortion parameter, $\beta_{\mathcal{F}}$ for the Lyman-α forest, is different owing to the non-linear relation between the Lyman-α transmitted flux and the underlying dark matter density field [348]. Contrary to the parameters for the HI 21-cm signal, the parameters $(\mathcal{A}_{\mathcal{F}}, \beta_{\mathcal{F}})$ are independent of each other and are sensitive to parameters like the IGM temperature-density relationship (γ) and the flux probability distribution function (PDF) of the Lyman-α forest. Analytical work [366] and extensive numerical simulations [278, 318, 367–369] demonstrates that in the absence of primordial non-gaussianity the Lyman-α forest can be described by a linear theory with a scale independent bias on large scales. We adopt an approximate values $(\mathcal{A}_{\mathcal{F}}, \beta_{\mathcal{F}}) \approx (-0.15, 1.11)$ from the simulations of Lyman-α forest[318].

We consider the cross-correlation of post-reionization tracers with the weak lensing convergence field. There is a crucial difference between the weak lensing field and the tracer fields. The former measures the integrated effect along the line of sight of a geometric kernel from redshift $z = 0$ to the last scattering surface and, is, hence sensitive to the fluctuations of the density field on large scales. The tracers, namely the Lyman-α forest and redshifted 21-cm intesity maps, on the contrary are tomographic probes of small-scale fluctuations. The cross-correlation thereby quantifies the evolution of small wavelength modes of the fluctuations on top of the long wavelength modes. Further, the noise and systematics that affect the auto-correlation signal appear only in the variance of the cross-correlation and may pose less of a challenge towards detecting the cross-correlation signal . The 21-cm signal is buried deep under galactic and extra-galactic foregrounds. Even after significant foreground removal, the cosmological origin of the 21 cm signal can only be ascertained only through a cross-correlation. To formulate the cross-correlation angular power spectrum, we expand the convergence field in terms of spherical harmonics as

$$\kappa(\hat{\mathbf{n}}) = \sum_{\ell,m}^{\infty} a^{\kappa}_{\ell m} Y_{lm}(\hat{\mathbf{n}}) \tag{3.39}$$

The expansion coefficients a^{κ}_{lm} can be obtained by inverting Eq.(3.39) as

$$a^{\kappa}_{\ell m} = \int d\Omega_{\hat{\mathbf{n}}}\, \kappa(\hat{\mathbf{n}}) Y^{*}_{\ell m}(\hat{\mathbf{n}}) \tag{3.40}$$

Thus, on using the expression for $\kappa(\hat{\mathbf{n}})$ we have

$$a^{\kappa}_{\ell m} = \int d\Omega_{\hat{\mathbf{n}}}\, Y^{*}_{\ell m}(\hat{\mathbf{n}}) \frac{3}{2} \left(\frac{H_0}{c}\right)^2 \Omega_{m_0} \int_0^{\chi_s} g(\chi)\, \chi\, \frac{\delta(\chi\hat{\mathbf{n}}, \chi)}{a(\chi)} d\chi \tag{3.41}$$

Writing

$$\delta(\chi\hat{\mathbf{n}}, \chi) = \int \frac{d^3\mathbf{k}}{(2\pi)^3}\, e^{i\mathbf{k}.\hat{\mathbf{n}}\chi} \Delta(\mathbf{k}) D_{+}(\chi) \tag{3.42}$$

and using the Raleigh expansion

$$e^{i\mathbf{k}\cdot\mathbf{n}\chi} = 4\pi \sum_{\ell,m} (-i)^{\ell} j_{\ell}(k\chi) Y^{*}_{\ell m}(\hat{\mathbf{k}}) Y_{\ell m}(\hat{\mathbf{n}}) \tag{3.43}$$

along with the normalization

$$\int d\Omega_{\hat{\mathbf{n}}}\, Y^{*}_{\ell m}(\hat{\mathbf{n}}) Y_{\ell m}(\hat{\mathbf{n}}) = 1 \tag{3.44}$$

we have

$$a^{\kappa}_{\ell m} = 4\pi(-i)^{\ell} \int \frac{d^3\mathbf{k}}{(2\pi)^3} \int_0^{\chi_s} d\chi\, \mathcal{A}_{\kappa}(\chi) D_{+}(\chi) j_{\ell}(k\chi) \Delta(\mathbf{k}) Y^{*}_{\ell m}(\hat{\mathbf{k}}) \tag{3.45}$$

where

$$\mathcal{A}_{\kappa}(\chi) = \frac{3}{2} \left(\frac{H_0}{c}\right)^2 \Omega_{m_0} \frac{g(\chi)\, \chi}{a(\chi)} \tag{3.46}$$

For the post reionization tracers Lyman-α and redshifted 21-cm signals we define two fields on the sky by integrating $\delta_i(\chi\hat{\mathbf{n}}, \chi)$ along the radial direction

$$F_i(\hat{\mathbf{n}}) = \frac{1}{\chi_2 - \chi_1} \sum_{\chi_1}^{\chi_2} \Delta\chi\, \delta_i(\chi\hat{\mathbf{n}}, \chi) \tag{3.47}$$

Previous works [357, 370] consider these fields at a given redshift, where the radial information is retained for tomographic study. The weak-lensing convergence, on the contrary, consists of a line of sight integral whereby the redshift information is lost. We consider an average over the signals from red-

shift slices and thus lose the redshift information but improve the SNR when cross-correlating with the weak-lensing field. The expansion coefficients for Lyman-α and redshifted 21-cm signals can be generally written as

$$a_{\ell m}^{F_i} = 4\pi(-i)^\ell \int \frac{d^3\mathbf{k}}{(2\pi)^3} \frac{1}{\chi_2 - \chi_1} \sum_{\chi_1}^{\chi_2} \Delta\chi \;\; \mathcal{A}_i(\chi) D_+(\chi) \\ \times \left(j_\ell(k\chi) - \beta_i \frac{d^2 j_\ell(k\chi)}{d(k\chi)^2} \right) \Delta(\mathbf{k}) Y_{\ell m}^*(\hat{\mathbf{k}})$$

Defining the cross-correlation angular power spectrum as

$$\langle a_{\ell m}^{\kappa} a_{\ell' m'}^{F_i *} \rangle = C_\ell^{\kappa F_i} \delta_{\ell,\ell'} \delta_{m,m'} \tag{3.48}$$

we have

$$C_\ell^{\kappa F_i} = \frac{2}{\pi(\chi_2 - \chi_1)} \int_0^{\chi_s} d\chi \sum_{\chi_1}^{\chi_2} \Delta\chi' \mathcal{A}_\kappa(\chi) D_+(\chi) A_i(\chi') D_+(\chi') \\ \times \int dk \; k^2 j_\ell(k\chi) J_\ell(k\chi') P(k) \tag{3.49}$$

where

$$J_\ell(k\chi) = \left(j_\ell(k\chi) - \beta_i \frac{d^2 j_\ell(k\chi)}{d(k\chi)^2} \right) \tag{3.50}$$

Similarly, the auto-correlation angular power spectra may be written as

$$C_\ell^{\kappa\kappa} = \frac{2}{\pi} \int_0^{\chi_s} d\chi \int_0^{\chi_s} d\chi' \mathcal{A}_\kappa(\chi) D_+(\chi) A_\kappa(\chi') D_+(\chi') \int dk \; k^2 j_\ell(k\chi) j_\ell(k\chi') P(k) \tag{3.51}$$

and

$$C_\ell^{F_i F_i} = \frac{2}{\pi(\chi_2 - \chi_1)^2} \sum_{\chi_1}^{\chi_2} \Delta\chi \sum_{\chi_1}^{\chi_2} \Delta\chi' \mathcal{A}_i(\chi) D_+(\chi) A_i(\chi') D_+(\chi') \\ \times \int dk \; k^2 J_\ell(k\chi) J_\ell(k\chi') P(k) \tag{3.52}$$

We shall now look at a simpler approximate calculation of the angular power spectrum using the flat-sky approximation. Instead of using the basis of spherical harmonics, we shall use the Fourier basis. This approximation is expected to work if the observational field is not too large.

Visibility based approach in “flat-sky" approximation

Radio interferometric observations of the redshifted 21-cm signal directly measure the complex Visibilities which are the Fourier components of the intensity distribution on the sky. The radio telescope typically has a finite beam which allows us to use the "flat-sky" approximation. Instead of expanding the fields κ and δ_i in the basis of spherical harmonics, we shall now obtain a simplified expression for the angular power spectrum by considering the flat sky approximation, whereby we can use the Fourier basis. We define Visibilities as

$$V_{F_i}(\vec{\mathbf{U}}) = \int d^2\vec{\theta}\, a(\vec{\theta}) F_i(\vec{\theta})\, e^{-2\pi i \vec{\mathbf{U}}.\vec{\theta}} \tag{3.53}$$

$$V_{\kappa}(\vec{\mathbf{U}}) = \int d^2\vec{\theta}\, \kappa(\vec{\theta})\, e^{-2\pi i \vec{\mathbf{U}}.\vec{\theta}} \tag{3.54}$$

where $a(\vec{\theta})$ denotes the beam function of the telescope measuring the angular coverage of the 21-cm or Lyman-α forest survey. Thus

$$V_{F_i}(\vec{\mathbf{U}}) = \frac{1}{\chi_2 - \chi_1} \sum_{\chi_1}^{\chi_2} \Delta\chi \int d^2\vec{\theta}\, \mathcal{A}_i(\chi) \int \frac{d^2\mathbf{k}_\perp dk_\parallel}{(2\pi)^3} [1 + \beta_i(\chi)\mu^2] \Delta(\mathbf{k}) D_+(\chi) \times e^{ik_\parallel \chi}\, a(\vec{\theta})\, e^{i(\mathbf{k}_\perp \chi - 2\pi \vec{\mathbf{U}}).\vec{\theta}}$$

where $\mu = k_\parallel / k$. Performing the $\vec{\theta}$ integral, we have

$$V_{F_i}(\vec{\mathbf{U}}) = \frac{1}{\chi_2 - \chi_1} \sum_{\chi_1}^{\chi_2} \Delta\chi\, \mathcal{A}_i(\chi) \int \frac{d^2\mathbf{k}_\perp dk_\parallel}{(2\pi)^3} [1 + \beta_i(\chi)\mu^2] \Delta(\mathbf{k}) D_+(\chi) \times e^{ik_\parallel \chi}\, \widetilde{a}_i \left(\frac{\mathbf{k}_\perp \chi}{2\pi} - \vec{\mathbf{U}} \right) \tag{3.55}$$

Where the aperture function $\widetilde{a}_i(\vec{\mathbf{U}})$ is the Fourier transformation of the telescope beam function $a(\vec{\theta})$. Similarly, for the convergence field, we have

$$V_{\kappa}(\vec{\mathbf{U}}) = \int_0^{\chi_s} d\chi\, \mathcal{A}_\kappa(\chi) \int \frac{d^2\mathbf{k}_\perp dk_\parallel}{(2\pi)^3} \Delta(\mathbf{k}) D_+(\chi)\, e^{ik_\parallel \chi}\, \delta_D \left(\frac{\mathbf{k}_\perp \chi}{2\pi} - \vec{\mathbf{U}} \right) \tag{3.56}$$

where we have assumed an almost full sky weak-lensing survey. We are interested in the Visibility-Visibility correlation

$$\langle V_{F_i}(\vec{\mathbf{U}})V^*_{\kappa}(\vec{\mathbf{U}}')\rangle = \frac{1}{\chi_2-\chi_1}\sum_{\chi_1}^{\chi_2}\Delta\chi\int_0^{\chi_s} d\chi'\,\mathcal{A}_i(\chi)\mathcal{A}_\kappa(\chi')D_+(\chi)D_+(\chi')\int\frac{d^2\mathbf{k}_\perp dk_\parallel}{(2\pi)^3}e^{ik_\parallel(\chi-\chi')}$$
$$\left[1+\beta_i(\chi)\frac{k_\parallel^2}{k_\parallel^2+\mathbf{k}_\perp^2}\right]\widetilde{a}_i\left(\frac{\mathbf{k}_\perp\chi}{2\pi}-\vec{\mathbf{U}}\right)\delta_D\left(\frac{\mathbf{k}_\perp\chi'}{2\pi}-\vec{\mathbf{U}}'\right)P(k)$$

Defining $C^{F_i\kappa} = \langle V_{F_i}(\vec{\mathbf{U}})V^*_{\kappa}(\vec{\mathbf{U}}')\rangle$

$$C^{F_i\kappa} = \frac{1}{\pi(\chi_2-\chi_1)}\sum_{\chi_1}^{\chi_2}\Delta\chi\int_0^{\chi_s}\frac{d\chi'}{\chi'^2}\,\mathcal{A}_i(\chi)\mathcal{A}_\kappa(\chi')D_+(\chi)D_+(\chi')\int_0^\infty dk_\parallel\cos k_\parallel(\chi-\chi')$$
$$\left[1+\beta_i(\chi)\frac{k_\parallel^2}{k_\parallel^2+\left(\frac{2\pi\vec{\mathbf{U}}'}{\chi'}\right)^2}\right]\widetilde{a}_i\left(\frac{\chi\vec{\mathbf{U}}'-\chi'\vec{\mathbf{U}}}{\chi'}\right)P\left(\sqrt{k_\parallel^2+\left(\frac{2\pi\vec{\mathbf{U}}'}{\chi'}\right)^2}\right)$$

If the aperture function $\widetilde{a}_i$ is peaked, we may approximately write the visibility correlation on the same baseline as

$$C^{F_i\kappa}(U) = \frac{1}{\pi(\chi_2-\chi_1)}\sum_{\chi_1}^{\chi_2}\frac{\Delta\chi}{\chi^2}\,\mathcal{A}_i(\chi)\mathcal{A}_\kappa(\chi)D_+^2(\chi)\int_0^\infty dk_\parallel\left[1+\beta_i(\chi)\frac{k_\parallel^2}{k^2}\right]P(k)$$
$$\text{with}\quad k=\sqrt{k_\parallel^2+\left(\frac{2\pi\vec{\mathbf{U}}}{\chi'}\right)^2} \tag{3.57}$$

The auto-correlation angular power spectrum may be similarly written as

$$C^{F_iF_i}(U) = \frac{1}{\pi(\chi_2-\chi_1)^2}\sum_{\chi_1}^{\chi_2}\frac{\Delta\chi}{\chi^2}\,\mathcal{A}_i^2(\chi)D_+^2(\chi)\int_0^\infty dk_\parallel\left[1+\beta_i(\chi)\frac{k_\parallel^2}{k^2}\right]^2P(k)$$
$$C^{\kappa\kappa}(U) = \frac{1}{\pi}\int_0^{\chi_s}\frac{d\chi}{\chi^2}\,\mathcal{A}_\kappa^2(\chi)D_+^2(\chi)\int_0^\infty dk_\parallel P(k) \tag{3.58}$$

We often use the Eq: (3.57) in the thesis. Using the cross-correlation signal, we study some of the popular dark energy models and constrain model parameters. We note here that working in the Fourier basis necessarily makes the signal non-ergodic when one looks at correlation between two time slices (due to time evolution of all the relevant quantities). Further, one also notes

the inseparability of the baseline **U** (transverse) from the frequency (radial) in this formalism [90]. The formulation developed in this section shall be used in the next chapter to constrain dark energy models.

We note that the cross-correlation signal is itself affected by the 21-cm foregrounds [371–373], which degrades the signal. We have not incorporated this effect in our analysis.

CHAPTER 4

Constraining dark energy using the cross correlations of weak lensing with post-reionization probes of HI [§]

4.1 Introduction

We have seen that though observations have indicated that the expansion of the Universe is accelerating [25, 374], the cause of what is driving this late time acceleration is still an open question. Precision cosmological measurements indicate that the Universe contains approximately $\sim 70\%$ of the energy density in the form of dark energy [15, 16, 375, 376] and the remaining $\sim 30\%$ in the form of non-relativistic matter (both baryonic matter and dark matter). A natural candidate for constant dark energy is the cosmological constant Λ. This model with $w = -1$ is well tested by many observations. In this model the cosmological constant Λ is to be interpreted as a non-zero vacuum energy density [19]. We have discussed several theoretical difficulties pertaining to the cosmological constant (like the 'fine tuning' problem). We have also mentioned recent results from low redshift measurements of H_0 [27] which seems to be in tensin with the Planck-2015 predictions for flat ΛCDM model. Further, there are indications that a varying dark energy model maybe preferable over the concordance ΛCDM model [28] at a high level of statistical significance. Our understanding of the cosmic acceleration thus still remains cloaked in mystery. Dark energy models differing from the standard cosmological constant typically involves a scalar field [21, 24, 55, 64, 377–385] whose dynamics with suitable initial conditions is used to model the cosmic acceleration. It is generally a difficult program to constrain the immense diversity of such scalar field models from observations. It is convenient to use some parametrization of these mod-

[§]The chapter is adapted from *Constraining dark energy using the cross correlations of weak lensing with post-reionization probes of neutral hydrogen, Chandrachud B.V Dash, Tapomoy Guha Sarkar, Journal of Cosmology & Astroparticle Physics, 016, (2021).*

els which mimic their general behaviour. The dynamic EoS with $p/\rho = w(z)$ is one such commonly used parametrization [206, 382, 386–388]. The most popular and widely used parametrization of the EoS is a two-parameter model by Chevallier-Linder-Polarski (CPL), [150, 206]. In this study we shall also use two important variants of the CPL model called the 7CPL model [388] and Barboza-Alcaniz (BA) model [207].

Weak gravitational lensing by intervening large scale structure [67, 68, 215] distorts the images of distant background sources, over large angular scales. This is caused by the deflection of light by the fluctuating gravitational field created by the intervening overdensity field. We have discussed that precise quantitative measurement of these distortions opens a window towards our understanding of the large scale matter distribution and geometry of the Universe. Late time cosmic history is governed largely by dark energy, either through a modification of the growing mode of density perturbations or through clustering properties of dark energy or both. Weak-lensing studies can be used to impose constraints on dark energy models [74, 76] since the lensing distortions manifest as a line of sight integral of a 'kernel' which is sensitive to background evolution and structure formation. Weak-lensing also distorts the CMBR photon distribution and manifests as secondary anisotropy in the CMBR maps [389]. The CMBR temperature and polarization maps may be used to extract the effect of lensing [390–392]. Delensing of the CMBR is crucial in quantifying the imprint of gravitational waves in the B modes [393].

Neutral hydrogen (HI) in the post-reionization epoch ($z < 6$) [81–85] is housed in two important astrophysical systems of interest. We have seen that the predominant fraction of the neutral gas is found in the dense self shielded Damped Lyman-α (DLA) systems [266, 267]. These DLA clouds are the source of the redshifted 21-cm signal, to be seen in emission. Intensity mapping of the large scale HI distribution using observations the redshifted 21-cm radiation [241, 394] aims to map out the collective diffuse emission without resolving the individual DLA sources [78]. The statistics of these intensity maps is a potentially rich probe of cosmological background evolution and large scale structure formation [80, 283, 284, 286]. Several studies look at the possibility of using 21-cm intensity mapping to constrain dark energy models [395, 396].

It is also a key science goal of many radio telescopes like the GMRT [*] OWFA[†], MEERKAT[‡], MWA[§], CHIME[¶], and SKA [||] to detect the cosmological 21-cm signal for a tomographic imaging [397] at observing frequencies $\nu \leq 1420\text{MHz}$.

The Lyman-α system comprises of the diffuse HI in the dominantly ionized post-reionization inter galactic medium (IGM), which produces distinct absorption features in the spectra of background QSOs. These absorption features known as the Lyman-α forest, provides one dimensional maps of the underlying HI fluctuation field along QSO sight lines. The Lyman-α forest is known to be a powerful cosmological probe [100, 101, 242, 329, 398–400]. The Baryon Oscillation Spectroscopic Survey (BOSS) [349, 350] has measured the BAO imprint on the Lyman-α forest. The high number density of QSOs in this survey and the high signal to noise ratio (SNR) measurement of the Lyman-α spectra allows 3D analysis [353, 401] and powerful investigation of the cosmological dark sector [402, 403].

Large scale numerical simulations indicate that on large cosmological scales both the Lyman-α forest and the 21-cm signal are biased tracers of the underlying dark matter (DM) distribution [91–93, 278, 351]. This has allowed the possibility of studying cross-correlations between Lyman-α and post reionization 21-cm signal [278, 352–355]. We consider the cross correlation of these post-reionization tracers with the weak-lensing convergence field to constrain dark energy models. The cross-correlation of 21-cm signal and the Lyman-α forest with weak-lensing has been studied earlier [357, 358]. We perform an improved analysis of the angular cross power spectrum for correlations of the CMBR weak lensing convergence field with the Lyman-α forest and 21-cm signal for constraining different dark energy parametrizations. We use a visibility based realistic formalism for this purpose. The entire redshift range probed by the Lyman-α and the 21-cm signal is exploited in the present analysis whereby the signal is averaged over redshift bins. Cross-correlating the integrated Lyman-α absorption with weak-lensing convergence has been stud-

[*] http://gmrt.ncra.tifr.res.in/
[†] https://arxiv.org/abs/1703.00621
[‡] http://www.ska.ac.za/meerkat/
[§] https://www.mwatelescope.org/
[¶] http://chime.phas.ubc.ca/
[||] https://www.skatelescope.org/

ied [358]. We extend this idea to the post-reionization signal whereby we consider the signal stacked up over the redshift slices in the observed bandwidth. This is expected to yield greater SNR in detection and more stringent constraints on the dark energy parameters.

The chapter is divided as follows. We first consider the dark energy models. We look at the auto correlation convergence power spectrum for CMBR weak-lensing. We finally make signal to noise predictions with a Fisher matrix parameter estimation using a visibility based formulation of the cross-correlation of the Lyman-α forest flux and 21-cm signal with the convergence field.

4.2 Dark energy models

The evolution of the Hubble parameter $H(a)$ for a spatially flat FRW Universe is given by

$$\frac{H(a)}{H_0} = \sqrt{\Omega_{m_0} a^{-3} + (1 - \Omega_{m_0}) \exp\left[-3 \int_1^a da' \frac{1 + w(a')}{a'}\right]} \tag{4.1}$$

where H_0 and Ω_{m_0} denote the Hubble parameter and the matter density parameter respectively, at the present epoch and the Universe is assumed to be comprised of non-relativistic matter and a dark energy component with an evolving EoS $w(a)$. We have used the cosmological parameters Planck18 results

$$(\Omega_{m_0}, \Omega_{b_0}, H_0, n_s, \sigma_8, \Omega_K) = (0.315,\ 0.0496,\ 67.4,\ 0.965,\ 0.811,\ 0)$$

from [36] in this work.

Our ignorance about the dynamics of Dark energy is modeled using the EoS parametrization $w(z)$ with $a = 1/(1 + z)$. There are innumerable possible choices for $w(z)$. However it has been shown that at most a two-parameter model can be optimally constrained from observations [205].

The model proposed by Chevallier Polarski [206] and Linder [150] gave a phenomenological model-free parametrization to incorporate several features of dark energy. This model has been extensively used by the Dark Energy Task

force [23] as the standard two parameter description of dark energy dynamics. The EoS is given by $w_{_{CPL}}(z) = w_0^{CPL} + w_a^{CPL}\frac{z}{1+z}$. This model gives a smooth variation of $w(z) = w_0 + w_a$ at $z \to \infty$ to $w(z) = w_0$ at $z = 0$. It has also been shown that a wide class of quintessence scalar field models can be mapped into the CPL parametrization [208] . However a better fit to both tracking and thawing class of models require a generalization of the CPL parametrization [388]. We use the following parametrizations in this work.

$$w_{_{CPL}}(z) = w_0^{CPL} + w_a^{CPL}\left(\tfrac{z}{1+z}\right) \quad \text{(CPL)} \tag{4.2}$$

$$w_{_{7CPL}}(z) = w_0^{7CPL} + w_a^{7CPL}\left(\tfrac{z}{1+z}\right)^7 \quad \text{(7CPL)} \tag{4.3}$$

$$w_{_{BA}}(z) = w_0^{BA} + w_a^{BA}\left(\tfrac{z(1+z)}{1+z^2}\right) \quad \text{(BA)} \tag{4.4}$$

Each model is characterized by two constant parameters (w_0, w_a) with w_a quantifying the evolution of dark energy from its present value set by w_0.

Background Evolution

Baryon acoustic oscillation (BAO) observations [127] aim to constrain the angular diameter distance $d_A(z)$ and the Hubble parameter $H(z)$ through the imprint of the oscillatory feature of the matter power spectrum in the transverse (angular) and longitudinal directions respectively. Due to low SNR in BAO measurements, it is often convenient to measure an effective distance defined as [25]

$$D_V(z) = \left[(1+z)^2 d_A(z)^2 \frac{cz}{H(z)}\right]^{1/3} \tag{4.5}$$

This effective distance is a direct quantifier of the background cosmological model (density parameters) and is thereby sensitive to the dynamical evolution of dark energy. We use a dimensionless quantifier of cosmological distances [1]

$$r_{_{BAO}}(z) = \frac{r_s}{D_V(z)} \tag{4.6}$$

where r_s denotes the sound horizon at the recombination epoch. Figure (4.1) shows the departure of $r_{_{BAO}}$ as a function of z from the ΛCDM model prediction. A redshift dependent difference of a few percent from the ΛCDM is seen for the different parametrizations. The behaviour is very similar for the CPL

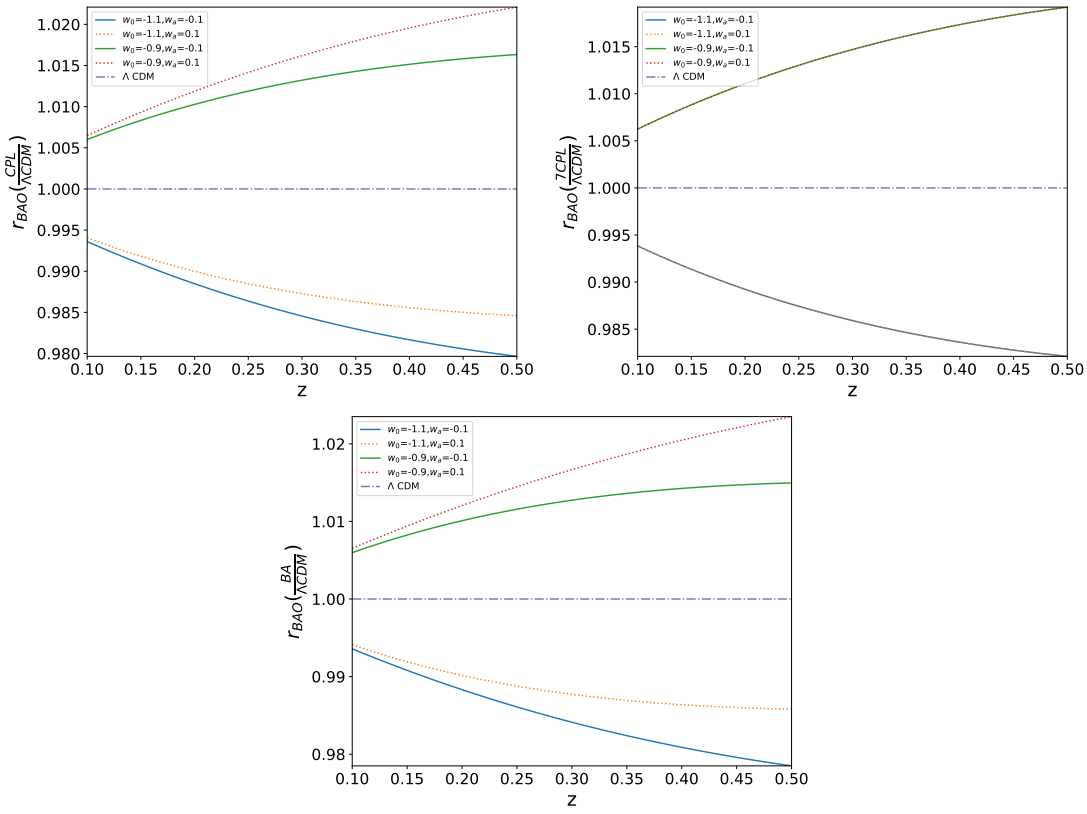

Figure 4.1: The BAO distance ratio $r_{BAO}(z)$ versus redshift z for different dark energy models (CPL, 7CPL, BA) in a spatially flat Universe scaled by $r_{BAO}^{\Lambda\mathrm{CDM}}(z)$ for the ΛCDM model.

and BA parametrizations which are known to mimic the thawing class of dark energy models. The 7CPL parametrization which represents the tracking class shows identical behaviour for some sets of model parameters (see figure (4.1)). Observations from the 2df galaxy redshift survey gives the bounds on r_{BAO} as $r_{BAO}(z = 0.2) = 0.1980 \pm 0.0058$ and $r_{BAO}(z = 0.35) = 0.1094 \pm 0.0033$ [3]. All the models with a redshift dependent $w(z)$ seems to be in better agreement with this data. The analysis of BOSS (SDSS III) CMASS sample along with Luminous red galaxy sample [4] from SDSS-II gives $r_{BAO}(z = 0.57) = 0.07315 \pm 0.002$. Figure (4.2) shows the model predictions as compared to the data at different redshifts.

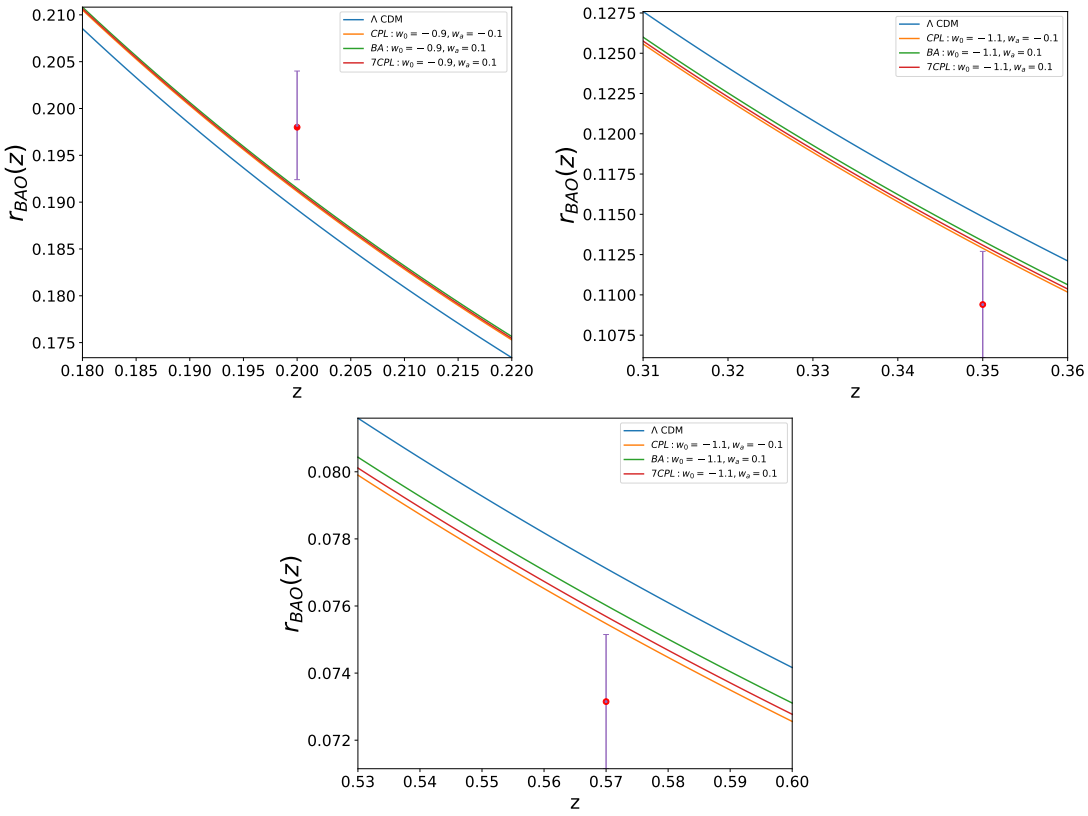

Figure 4.2: The first two figures in the panel shows the data points from the 2df galaxy survey at redshifts $z = 0.2$ and $z = 0.35$ respectively and the third figure shows the high redshift data at $z = 0.57$ from BOSS SDSS-III survey.

Growth of Perturbations

At sufficiently early times and on large spatial scales the matter density fluctuations are much less than unity ($|\delta| << 1$, in linear regime). Under these conditions the matter density contrast $\delta = \frac{\delta\rho_m}{\bar{\rho}_m}$ evolves independently for different Fourier modes k. Separating the time dependent part of the matter overdensity as $\delta(a) = D_+(a)\delta_m(a = 1)$. The growth of density fluctuations on sub horizon scales can be obtained by solving the second order differential equation

$$\frac{d^2D_+}{da^2} + \left(\frac{1}{H}\frac{dH}{da} + \frac{3}{a}\right)\frac{dD_+}{da} - \frac{3}{2}\frac{\Omega_{m_0}H_0^2}{a^5H^2}D_+ = 0 \tag{4.7}$$

In order to solve the above equation we choose the initial conditions in the matter-dominated epoch ($a_i = 10^{-3}$), where the growth function grows linearly with the scale factor ($D_+ \propto a$). Dark energy affects the growth of cosmo-

logical structure formation directly through the role of the expansion history on the gravitational instability in an expanding background. This leads to the appearance of the background evolution $H(z)$ in the equation for the growing mode of density perturbations D_+ (Eq: 4.7). We use the growth rate $f(z)$ defined as

$$f(z) = \frac{d\ln D_+}{d\ln a} \tag{4.8}$$

to quantify the growth rate of perturbations. The observationally measurable function $f(z)$ imprints the dynamics of dark energy and is sensitive to any departure from the ΛCDM.

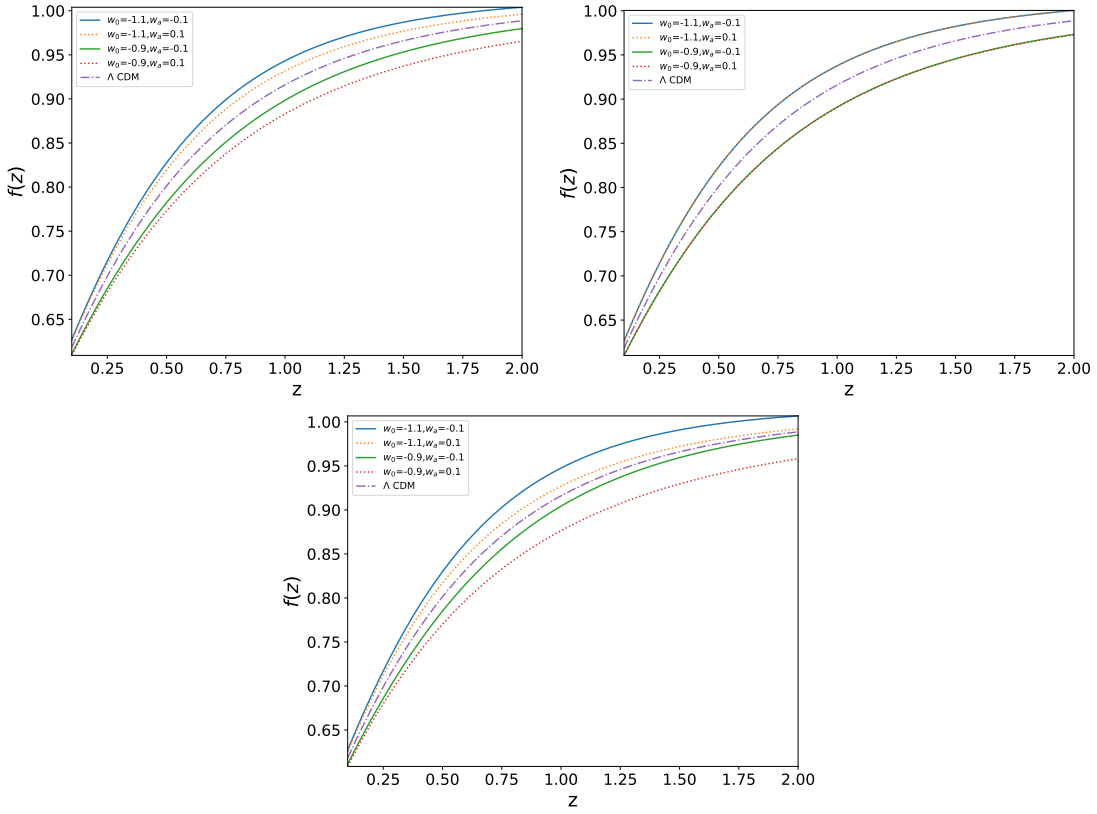

Figure 4.3: The growth rate of density fluctuations $f(z)$ for different dark energy EoS parametrizations. The ΛCDM model is shown in each subfigure for comparison.

Figure (4.3), shows the linear growth rate of density perturbations for CPL, 7CPL and BA parametrizations. At higher redshifts, the all models approach $f \sim 1$ indicating that the growth of perturbation is dominated by non-relativistic matter. Further, for 7CPL model, there is no dependence of the parameter w_a.

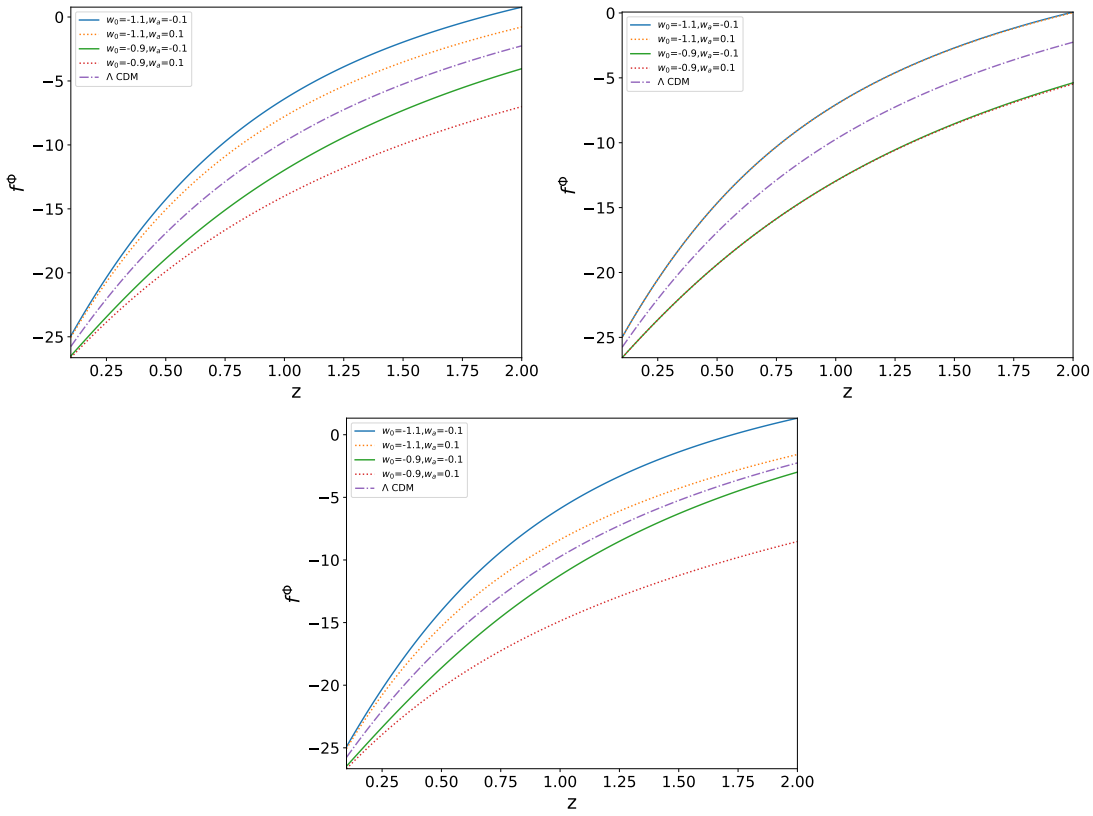

Figure 4.4: The ISW parameter $f^\Phi = \frac{\dot{\Phi}}{\Phi}$ for different dark energy EoS parametrizations. The ΛCDM model is shown in each subfigure for comparison.

Therefore, one does not expect to constrain the parameter w_a for 7CPL model using any observation related to matter clustering. Dark energy also has an implicit observational effect. It causes a decay of the gravitational potential (the scalar perturbation in the Newtonian conformal gauge), when the Universe evolves from the matter dominated to the the dark energy dominated era. This is known to generate a weak anisotropy in the CMB temperature fluctuation, through the Integrated Sachs Wolfe (henceforth ISW) effect [247, 404]. A curved spatial geometry also similarly contributes to this anisotropy. However, the spatial curvature of our Universe is constrained to be zero from CMBR observations [130] whereby the effect of spatial curvature can be ignored in the first approximation. The gravitational potential is expected to remain constant in a purely matter dominated cosmology. Thus, any late-time evolution of the gravitational potential is sensitive to the dark energy model [405–408]. The

ISW anisotropy is a line of sight integral [409, 410]

$$\Delta T(\hat{\mathbf{n}})^{\rm ISW} = 2T \int_{\eta_{\rm LSS}}^{\eta_0} d\eta\ \Phi'(r\hat{\mathbf{n}}, \eta) \tag{4.9}$$

where T is the present CMBR temperature, $\eta_{\rm LSS}$ and η_0 are the conformal times at the last scattering surface and the present epoch respectively and $\Phi' = d\Phi/d\eta$. To quantify this effect we define a diagnostic for dark energy

$$f^{\Phi}(z) = \frac{d}{d\eta}{\rm ln}\Phi = (f-1)\mathcal{H} \tag{4.10}$$

where $\mathcal{H} = \frac{1}{a}da/d\eta$. It is known that $f \sim 1$ in pure matter dominated epoch and any departure from $f = 1$ indicates the action of dark energy. Noting that the role of dark energy is imprinted in $f-1$, the function $f^{\Phi}(z)$ is a sensitive probe of dark energy. It quantifies the interplay of two time scales - the background expansion rate (contained in $H(z)$) and the growth rate of cosmological structure (contained in $f(z)$). Figure (4.4) shows the redshift dependence of $f^{\Phi}(z)$ for different dark energy EoS parametrizations. The 7CPL model shows insensitivity to the parameter w_a, however, both CPL and BA parametrizations show significant $\sim\ 2-4\%$ departure from the ΛCDM behaviour. This may be crucial in the improvement of detection sensitivities for ISW measurements [408].

4.3 Weak-lensing convergence power spectrum

We consider the weak lensing of the Cosmic microwave background radiation (CMBR). Gravitational lensing deflects the photons which are free streaming from the last scattering surface (epoch of recombination $z \sim 1000$) and manifests as a secondary anisotropy in the CMBR temperature maps. The effect of gravitational lensing can be extracted from these maps by constructing various estimators for the convergence field κ through quadratic combination of the (T, E, B) fields [390, 391]. Defining convergence κ as $\kappa = -\frac{1}{2}\nabla \cdot \alpha$ where, α is the total deflection, the convergence power spectrum for the CMBR weak lensing is given by

$$C^{\ell}_{\kappa_{CMB}} = \frac{9}{4}\left(\frac{H_0}{c}\right)^4 \Omega^2_{m0} \int_0^{\chi_{rec}} \frac{g(\chi)^2}{a^2(\chi)} P\left(\frac{\ell}{\chi}, \chi\right) d\chi. \tag{4.11}$$

If $\chi_{rec} = \chi(z_{rec})$ is the comoving distance to the last scattering surface then the weak lensing geometric kernel $g(\chi)$ is given by

$$g(\chi) = \left(\frac{\chi_{rec} - \chi}{\chi_{rec}}\right) \tag{4.12}$$

We have incorporated the Limber approximation in the above expression. The Fisher matrix is diagonal for a full sky survey and the noise for the CMBR convergence power spectrum is given by

$$\Delta C^{\ell}_{\kappa_{CMB}} = \sqrt{\frac{2}{(2\ell+1)}}\left(C^{\ell}_{\kappa_{CMB}} + w^{-1} e^{\ell^2 \sigma_b^2}\right) \tag{4.13}$$

where the first term comes from cosmic variance and the instrumental noise is encapsulated in the weight w and a smoothing determined by the beam width σ_b. We may write $w = (\sigma^2_{pix}\Omega_{pix})^{-1}$. Here σ^2_{pix} is the error in each pixel which depends on the sensitivity s and observation time for each pixel t_{pix} as $\sigma_{pix} = s/\sqrt{t_{pix}}$. If the FWHM (full width at half maximum) is denoted by θ_{fwhm} then $\Omega_{pix} = K\theta_{fwhm} \times \theta_{fwhm}$ and $\sigma_b^2 = \theta^2_{fwhm}/8\ln 2$. The conversion factor $K^{-1} = \frac{1}{(2\pi)^2}\int d^2\vec{\ell}\, \ell^2 C_\ell$, where C_ℓ denotes the CMB angular power spectrum converts noise in CMBR temperature angular power spectrum to that of convergence angular power spectrum. The factor $(2\ell+1)$ in the denominator counts the number of samples of $C^{\ell}_{\kappa_{CMB}}$ for a given ℓ. Figure (4.5) shows the SNR for the CMBR weak-lensing angular power spectrum. We have assumed a CMBPol like experiment with pixel noise of $\sigma^2_{pix} \approx 1\mu K$ and $\theta_{fwhm} = 3\text{arcmin}$ and $w^{-1} = 7.5\mu K^{-2} deg^{-2}$ for our analysis [411].

Figure (4.5) shows the SNR for CMBR weak-lensing convergence angular power spectrum. The sensitivities for different dark energy EoS parameterizations differ by a few percent from the ΛCDM predictions. However, the sensitivities SNR ~ 20 is good enough to rule out some of the parametrizations at 3σ. But most EoS models remains degenerate to ΛCDM at these sensitivity levels since the difference of the angular power spectrum is $\sim 1\%$.

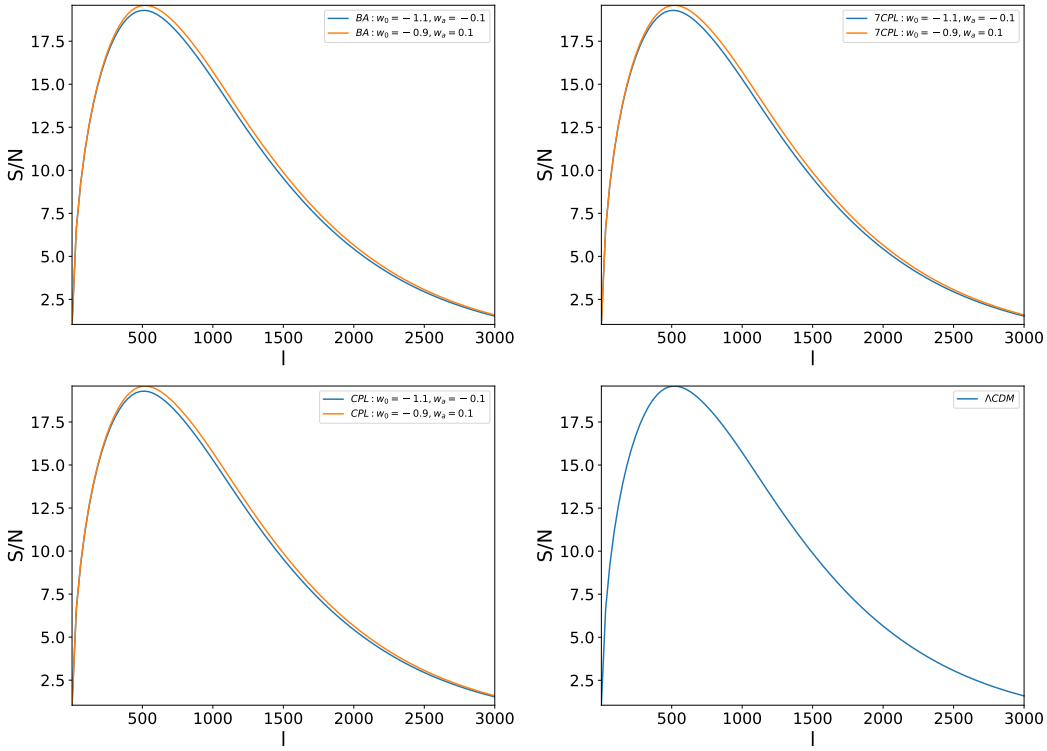

Figure 4.5: SNR for the CMBR convergence power spectrum for different fiducial dark energy parametrizations.

4.4 Cross correlation signal

The angular power spectrum for two redshifts separated by Δ is known to decorrelate very fast in the radial direction [88]. In this work we consider the summation in Eq (3.47) to extend over redshift slices whose separation is more than the typical decorrelation length. This ensures that in the computation of noise, each term in the summation may be thought of as an independent random variable and the mutual covariances between the slices may be ignored. This gives us the errors in the measurement of $C^{F_i\kappa}(U)$ as

$$\sigma_{_{\mathcal{F}_i\kappa}} = \frac{C^{\mathcal{F}_i\kappa}\sqrt{2\ell+1}\sqrt{N_c}}{\sqrt{(C^{\kappa\kappa}+\langle N^{\kappa}\rangle)(C^{F_iF_i}+\langle N^{F_i}\rangle)}} \tag{4.14}$$

where N_c is the number of redshift slices over which the average in Eq (3.47) is taken and $\langle N^{F_i}\rangle$ and $\langle N^{\kappa}\rangle$ denotes the average of the noise power spectrum for F_i and κ respectively. This variance is used in the Fisher matrix analysis for

constraining various dark energy EoS parameters.

The parameters $\mathcal{A}_{\mathcal{F}}$, $\beta_{\mathcal{F}}$, b_T and $\bar{x}_{HI}$ along with the cosmological parameters model the cross-correlation signal. However the parameters $\mathcal{A}_{\mathcal{F}}$, $\beta_{\mathcal{F}}$, b_T and $\bar{x}_{HI}$ are largely uncertain. We perform the Fisher matrix analysis assuming $\mathcal{A}_{\mathcal{F}}$, $\beta_{\mathcal{F}}$, $\mathcal{A}_T$ (related to $\bar{x}_{HI}$) and β_T (related to b_T) along with the DE EoS parameters w_0 and w_a to be the free parameters. The Fisher matrix is given by

$$\mathbf{F}_{ab} = \sum_{\ell} \frac{1}{\sigma^2_{F_i\kappa}} \frac{\partial C_\ell^{F_i\kappa}}{\partial q_a} \frac{\partial C_\ell^{F_i\kappa}}{\partial q_b} \tag{4.15}$$

where we have $q_a = (w_0, w_a, \mathcal{A}_{\mathcal{F}}, \beta_{\mathcal{F}}, \mathcal{A}_T, \beta_T)$. The parameters (w_0, w_a) are different for different models. The Cramer Rao bound gives the errors on the a^{th} parameter $\delta q_a = \sqrt{\mathbf{F}^{-1}_{aa}}$. The error projections on (w_0, w_a) are obtained for different dark energy models by marginalizing over the other parameters.

4.5 Cross-correlation of CMBR weak-lensing with Lyman-α forest

The redshift distribution of quasars is known to peak in the redshift range $1.5 \leq z \leq 3$ [412]. In our work we consider quasars in these redshifts only and also consider that the Lyman-α forest spectrum for these quasars are measured at a high SNR. We note that for any quasar the region $10,000$ km sec^{-1} blue-wards of the quasar's emission line is contaminated by the quasar's proximity effect and the Stromgen sphere. We exclude this from the Lyman-α forest spectra. We also note that pixels at least $1,000$ km sec^{-1} red-ward of the quasar's needs to be excluded from the spectra to avoid contamination from Lyman-β forest and O-VI lines. Thus, for a quasar at the fiducial redshift $z_Q = 2.5$, the Lyman-α forest can be measured in the redshift range $1.96 \leq z \leq 2.39$ covering a band $z_2 - z_1 = 0.43$.

We note that for the Lyman-α forest at a redshift z the noise is given by

$$N^{\mathcal{F}} = \frac{1}{\bar{n}_Q} \left(\sigma^2_{\mathcal{F}L} + \sigma^2_{\mathcal{F}\mathrm{N}} \right) \tag{4.16}$$

where

$$\sigma^2_{\mathcal{F}L} = \int d^2\mathbf{U}\ C^{\mathcal{F}\mathcal{F}}(U)$$

and $\bar{n}_Q$ is the angular number density of quasars. The quantity $\sigma^2_{\mathcal{F}\mathcal{N}}$ is a pixel noise contribution. The observations of Lyman-α forest [413, 414] shows that for the Lyman-α forest smoothed over $\sim 50\mathrm{Kms}^{-1}$, the variance of the flux fluctuations has a value $\sigma^2_{\mathcal{F}L} \approx 0.02$. We adopt this value by choosing the corresponding smoothing scale. We also assume an average $S/N = 5$ for every pixel in the spectra used for cross-correlation. This gives us $\sigma^2_{\mathcal{F}\mathcal{N}} = 0.04\bar{\mathcal{F}}(z)^{-2}\left(\frac{4.6\times10^{-4}}{\Delta z}\right)$. The mean flux $\bar{\mathcal{F}}(z) \sim 1$. The variation of $\bar{\mathcal{F}}(z)$ is however noted [261] The averaging over $N_c = \frac{z_2-z_2}{\Delta z}$ different slices of redshift gives $\langle N^{\mathcal{F}}\rangle$. The smoothing scale Δz is chosen by noting that at a given redshift z the signal decorrelates over $\Delta z \sim 10^{-3}(1+z)^2\left(\frac{\ell}{100}\right)^{-.0.7}$ [88].

Figure (4.6) shows the difference of the Lyman-α CMBR convergence cross angular power spectrum for different dark energy EoS parametrizations from the cross angular power spectrum for the ΛCDM model. We consider Planck sensitivies for the cross-correlation with $\sigma_{pix}\Omega^{1/2}_{pix} = 0.7\mu K.deg$. For Lyman-$\alpha$ forest we have considered a BOSS like experiment with $\bar{n}_Q = 8, 16, \text{ and } 64\mathrm{deg}^{-2}$ for our analysis.

We find that for $\bar{n}_Q = 16\mathrm{deg}^{-2}$ with ΛCDM fiducial model a peak SNR of ~ 50 (see Fig (4.7)) is obtained at $\ell \sim 300$. This allows CPL and 7CPL models to be differentiable from the ΛCDM model at $> 3\sigma$ sensitivity for $\ell > 1000$. The BA model however remains at 1σ from the ΛCDM and can not be differentiated at these sensitivities. However its variance of the cross-correlation signal is very sensitive to the quasar sampling and dense sampling is expected to improve the sensitivity level for the cross-correlation. A Lyman-α survey with $\bar{n}_Q = 64\mathrm{deg}^{-2}$ the cross correlation has a peak SNR of ~ 80 at $\ell \sim 1200$ [see Fig (4.7)] . For such sensitivities CPL and 7CPL models can be differentiated at $> 5\sigma$ for $\ell > 1500$. The best-case scenario is shown in the last figure, which is at $\bar{n}_Q \sim 100\mathrm{deg}^{-2}$. The Fisher matrix in Eq (5.4) is used to put constraints on the dark energy parameters. We have assumed that other cosmological parameters are well constrained from CMBR observations and focus only on the dark energy EoS parameters. Fig (4.9) shows the constraints on the parameters in the $w_0 - w_a$ plane. The contours correspond to also show the 68% and 95% marginalized

Table 4.1: The the 68% $(1-\sigma)$ Constraints of DE parameters (w_0, w_a) from Lyman-α and convergence cross power spectrum

Model	$\bar{n}_Q = 8\text{deg}^{-2}$	$\bar{n}_Q = 16\text{deg}^{-2}$	$\bar{n}_Q = 100\text{deg}^{-2}$
BA	$\Delta w_0 = 0.17$ $\Delta w_a = 0.27$	$\Delta w_0 = 0.15$ $\Delta w_a = 0.243$	$\Delta w_0 = 0.141$ $\Delta w_a = 0.192$
CPL	$\Delta w_0 = 0.191$ $\Delta w_a = 0.57$	$\Delta w_0 = 0.168$ $\Delta w_a = 0.51$	$\Delta w_0 = 0.121$ $\Delta w_a = 0.42$
7CPL	$\Delta w_0 = 0.081$ $\Delta w_a = --$	$\Delta w_0 = 0.079$ $\Delta w_a = --$	$\Delta w_0 = 0.068$ $\Delta w_a = --$

confidence intervals for the parameters w_0 and w_a.

The table (4.1) shows the $1-\sigma$ errors on EoS parameters. We find that if dark energy is described by CPL parametrization, the constraint in $w_0 - w_a$ space is competitive with the Planck+Bao+Supernova+HST for CPL parametrization [415]. We also find that for the 7CPL parametrization, the parameter w_a can not be constrained. However, for 7CPL parametrization we can constrain w_0 much better than CPL or BA. Thus we note that for the measurement of the present day value of the dark energy equation of state, 7CPL is definitely favourable than CPL or BA and the generally popular CPL parametrization may not be the best choice. It is also seen that the parameter space regions corresponding to $(w_0 > -1, w_a > 0)$ and $(w_0 < -1, w_a < 0)$ is constrained much better than the regions corresponding to $(w_0 > -1, w_a < 0)$ and $(w_0 < -1, w_a > 0)$. Thus regions which correspond to dark energy being modeled by only phantom or only non-phantom scalar fields are very strongly constrained.

4.6 Cross-correlation of CMBR weak-lensing with redshifted 21-cm signal

In a radio-interferometric observation the noise *rms*. in the real part in each visibility for single polarization measurement is given by

$$V_{rms} = \frac{T_{sys}}{K\sqrt{2\Delta\nu\Delta t}} \frac{\lambda^2}{2k_B} \tag{4.17}$$

Here k_B is the Boltzmann constant, $\Delta\nu$ is the width of the frequency channels and Δt is the integration time of the correlator. The total system temperature T_{sys} maybe decomposed as $T_{sys} = T_a + T_{sky}$, where T_a is an instrumental contribution and T_{sky} is a sky contribution which is usually subdominant and is given by [79]

$$T_{sky} = 60\mathrm{K}\left(\frac{\nu}{300\mathrm{MHz}}\right)^{-2.55}. \tag{4.18}$$

The quantity K denotes the antenna sensitivity and maybe written as $K = A_{eff}/2\,k_B$ where A_{eff} denotes the effective collecting area of each antenna. The factor $\frac{\lambda^2}{2k_B}$ intensity to temperature units in the Raleigh Jeans limit.

The noise variance in the visibility correlation is written as [88]

$$\sigma^2_{VV} = \frac{8\,V^4_{rms}}{\mathcal{N}_p} \tag{4.19}$$

where $\mathcal{N}_p$ is the number of visibility pairs in a particular visibility bin U to $U + \Delta U$. This is given by [88, 93]

$$\mathcal{N}_p = \frac{1}{2}\left[\frac{N_{ant}(N_{ant}-1)}{2}\frac{T}{\Delta t}\Delta U^2\rho(U,\nu)\right]^2\frac{2\pi U\Delta U}{\Delta U^2} \tag{4.20}$$

where N_{ant} is the total number of antennas is the array, and T is the total observation time. The normalized baseline distribution function $\rho(U,\nu)$ is given by a convolution of the antenna distribution function with itself [416].

$$\rho(U,\nu) = \frac{c}{B}\int_0^\infty \rho_{ant}(\mathbf{r})\rho_{ant}(\mathbf{r}-\lambda\mathbf{U}) \tag{4.21}$$

where B is the band width and c is fixed by the normalization $\int d^2\mathbf{U}\rho(\mathbf{U}) = 1$.

Table 4.2: uGMRT specifications

Observation time T	Freq. range(MHz)	T_{sys}(K)	N_{ant}	ΔU	$A_{eff}(m^2)$
400	550-850	70	60, 100	32	1590

We consider Planck sensitivities for the cross-correlation. For the redshifted 21-cm observation we first consider the upgraded version of GMRT called uGMRT [417], with antenna distribution roughly behaving as $\rho_{ant}(r) \propto 1/r^2$ distributed over a $2 \times 2\mathrm{Km}^2$ region. Each antenna is assumed to be of 45

m in diameter, with a field of view of 1.3° (FWHM). The frequency separation ν over which the 21-cm signal remains correlated scales approximately as $\nu = 1\mathrm{MHz}(\ell/100)^{-0.7}$ [88]. We assume that the signal is averaged over frequency bins of this width to increase the signal-to-noise ratio (S/N). The different telescope parameters used for our analysis is summarized in table (4.2).

Figure (4.8) shows the SNR for a ΛCDM fiducial model. We find that for a uGMRT with $N_{ant} = 60$ with ΛCDM fiducial model a peak SNR of ~ 40 is obtained at $\ell \sim 600$. If the number of antennas in the interferometer is $N_{ant} = 100$ a peak SNR of ~ 54 is achieved at $\ell \sim 1500$. In the limit of negligible instrumental noise a peak SNR of 70 is possible.

Figure (4.10) shows the difference of the 21-cm and CMBR convergence cross angular power spectrum for different dark energy EoS parametrizations from the cross angular power spectrum for the ΛCDM model. We find that BA, CPL and 7CPL models to be differentiable from the ΛCDM model at $> 3\sigma$ sensitivity.

For making error projections on $(w_0 - w_a)$, we also consider the radio interferometer MeerKAT [418]. This telescope has dishes of 13.5m diameter and a wider field of view. We consider the UHF-band of this telescope for our analysis. The telescope parameters for MeerKAT are summarized in the table (4.3).

Table 4.3: MeerKAT specifications

Observation time T (Hrs)	Freq. range (MHz)	T_{sys} (K)	N_{ant}	ΔU	A_{eff}/T_{sys} (m^2/K)
400	580-1015	30	64	12	320

The Fisher matrix in Eq (5.4) is used to make error projections for the dark energy parameters. Fig (4.11) shows the constraints on the parameters in the $w_0 - w_a$ plane for cross-correlation with uGMRT. The contours correspond to the 68% and 95% marginalized confidence intervals for the parameters w_0 and w_a. A summary of the errors obtained in the parameters (w_0, w_a) is given in the table(4.4). We find that the constraints on the EoS parameters are much better than the ones obtained from the cross-correlation with Lyman-α forest. This is due to the large bandwidth of the 21 cm observation over which the signal is

Table 4.4: The the 68% $(1-\sigma)$ Constraints of DE parameters (w_0, w_a) from HI 21-cm and convergence cross power spectrum

Model	Cosmic variance limit	uGMRT	MeerKAT
BA	$\Delta w_0 = 0.079$ $\Delta w_a = 0.121$	$\Delta w_0 = 0.098$ $\Delta w_a = 0.20$	$\Delta w_0 = 0.122$ $\Delta w_a = 0.22$
CPL	$\Delta w_0 = 0.092$ $\Delta w_a = 0.168$	$\Delta w_0 = 0.115$ $\Delta w_a = 0.40$	$\Delta w_0 = 0.138$ $\Delta w_a = 0.434$
7CPL	$\Delta w_0 = 0.04$ $\Delta w_a = --$	$\Delta w_0 = 0.05$ $\Delta w_a = --$	$\Delta w_0 = 0.053$ $\Delta w_a = --$

averaged.

The results from cross-correlation with a more realistic MeerKAT is shown in the figure (4.12). The marginalized 1-σ errors obtained in the parameters (w_0, w_a) for MeerKAT is also given in the table(4.4). The constraints show reasonable degradation as compared to the uGMRT predictions.

The projected constraints on the dark energy equation of state indicate that for a broadband 21-cm survey with uGMRT-like telescope with 100 or more antennas the cross-correlation may constrain dark energy evolution at a level which is better the projections for auto-correlation results with a SKA1 type experiment [396] or a joint Planck+SN+BAO+HST [415]. The 7CPL parametrization is also seen to constrain the present value of dark energy EoS much better than CPL and BA parametrization which is also the conclusion drawn in earlier works [396]. We also find that BA model constrains (w_0, w_a) much better than CPL model. Since CPL parametrization is the widely use parametrization to model dark energy evolution, we note that it may not be suitable to constrain dark energy evolution.

The projection of (w_0, w_a) for CPL model has been studied extensively using eBOSS and DESI cosmological data [419, 420]. The limits of the error contours corresponding to the CPL model are $w_0 = (-1.5, -0.5)$, $w_a = (-1, 1)$ for the eBOSS survey which is similar to our projections. The PLANCK+DESI data limits for w_0 and w_a are $w_0 = (-1.13, -0.86)$ and $w_a = (-0.4, 0.4)$ respectively, which has better figure of merit. A comparison of dark energy EoS parameter error projections for different models are studied in an earlier work using Sne Ia JLA and BAO datasets [421]. Their projected error limits for the CPL

model parameters are $\approx w_0 = (-1.6, -0.75)$ and $w_a = (-2.5, -1.5)$. Thus, we note that the cross-correlations between the weak lensing convergence with HI-21cm and Ly-α forest found better or reasonably close constraints on the w_0, w_a parameter space when compared with some other probes.

4.7 Conclusion

There are several observational aspects that we have not considered in this work. Foreground subtraction issues, is a major concern for the 21-cm signal. Large astrophysical foregrounds from galactic and extra galactic sources pose a serious threat towards achieving desired detection sensitivities [359]. Though the problem of foreground subtraction is less for the cross correlation, a significant amount of foreground subtraction is required to obtain good SNR since the foregrounds appear as noise in the cross-correlation. For the Lyman-α forest observations, continuum subtraction and avoiding metal line contamination, though less serious, needs to carried out with high precision. Further, man made radio frequency interferences (RFIs), calibration errors and other systematics also needs to be tackled for a detection of the HI 21-cm signal. We emphasize that some of the fundamental problems posed by 21-cm foregrounds can be avoided by considering cross correlations.

We also note that we have restricted our study of dark energy evolution to a very small set of commonly used parametrizations. There are a large number of possible 2-parameter descriptions which may suit some specific dark energy dynamics [388]. Though the CPL model and its variants fits a reasonable stretch of dark energy dynamics they do not describe all kinds of dynamics [52, 422]. We also note that the error projections obtained in this work from a Fisher matrix analysis gives a good idea about the efficacy of the cross-correlation in constraining the (w_0, w_a) parameter space. However, a more sophisticated Bayesian analysis is needed for more robust statistical predictions.

We conclude by noting that the cross-correlation power spectrum of the HI tracers from the post reionization epoch with weak-lensing fields is a direct probe of cosmological structure formation which can be detected to a high level of statistical sensitivity with upcoming QSO surveys and radiointerfer-

ometers. This has the potential to provide new insights on dark energy evolution. This probe may be combined with other cosmological observations like CMB, BAO, SNIa etc and a joint analysis shall be able to give us a clearer picture of the nature of dark energy and its cosmic evolution.

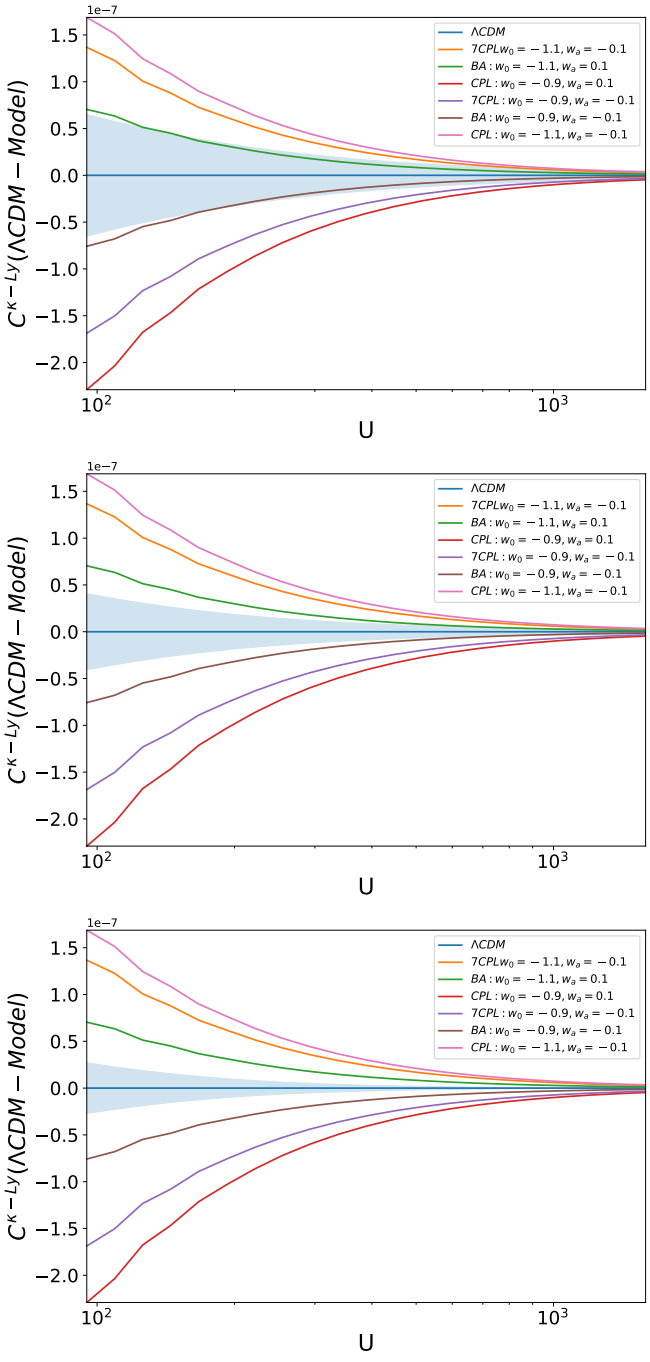

Figure 4.6: The difference of the Lyman-α forest - CMBR convergence cross power spectrum for different fiducial dark energy parametrizations from the ΛCDM model. The $1-\sigma$ error is shown by the shaded region. The first and the second figure corresponds to a quasar number density of $\bar{n}_Q = 16\text{deg}^{-2}$ and $\bar{n}_Q = 64\text{deg}^{-2}$ respectively. The last figure shows the best case scenario in the cosmic variance limit of no observational noise.

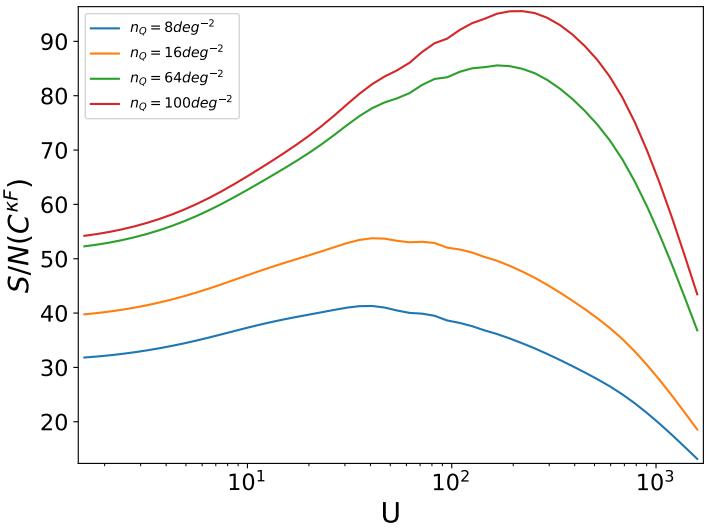

Figure 4.7: Signal to Noise ratio for the Convergence-Lyman-α angular power spectrum for the fiducial ΛCDM model for $\bar{n}_Q = 8, 16, 64, 100$ deg^{-2} respectively.

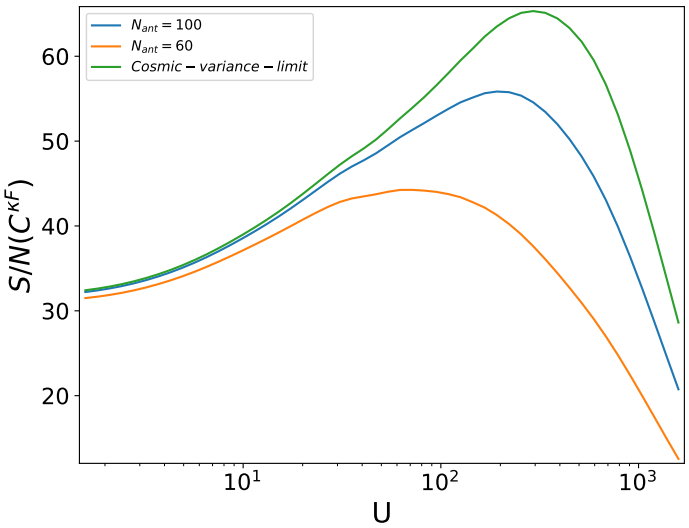

Figure 4.8: Signal to Noise ratio for the Convergence-21 cm cross angular power spectrum for the fiducial ΛCDM model for uGMRT with $N_{ant} = 60, 100$ respectively. We also show the cosmic variance limit.

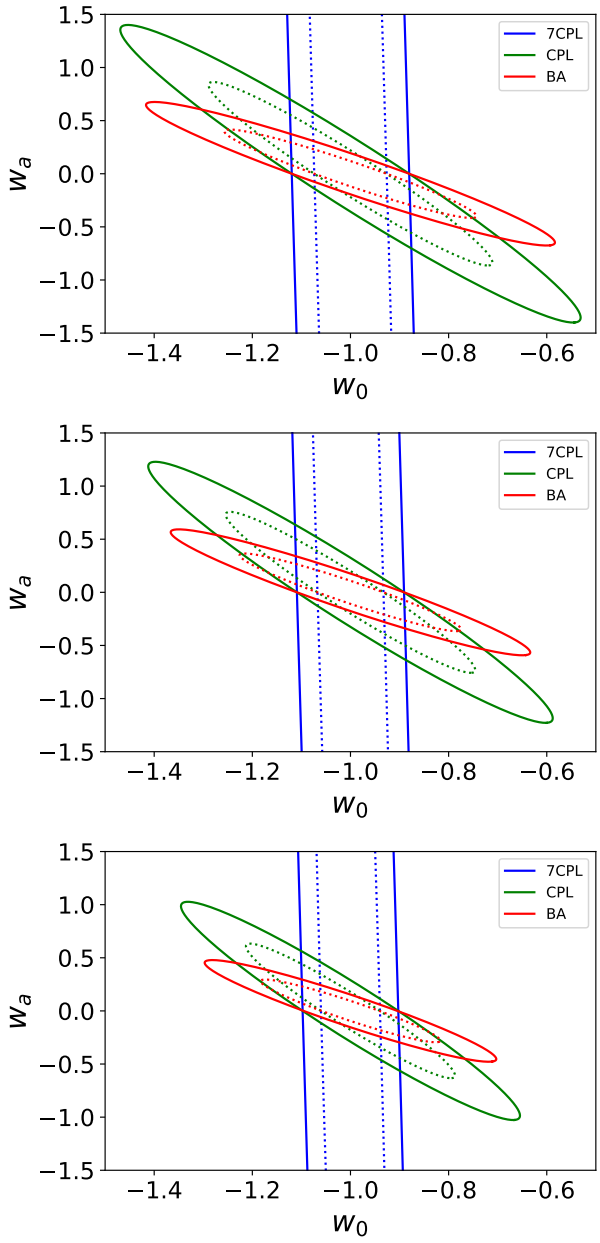

Figure 4.9: The 68% and 95% marginalized confidence intervals for the parameters w_0 and w_a from the Lyman-α convergence cross correlation for different dark energy EoS parametrizations. The fiducial model is chosen as the ΛCDM model with $(w_0, w_a) = (-1, 0)$. The three figures correspond to $\bar{n}_Q = 8\text{deg}^{-2}$, $\bar{n}_Q = 16\text{deg}^{-2}$ and $\bar{n}_Q = 100\text{deg}^{-2}$ respectively.

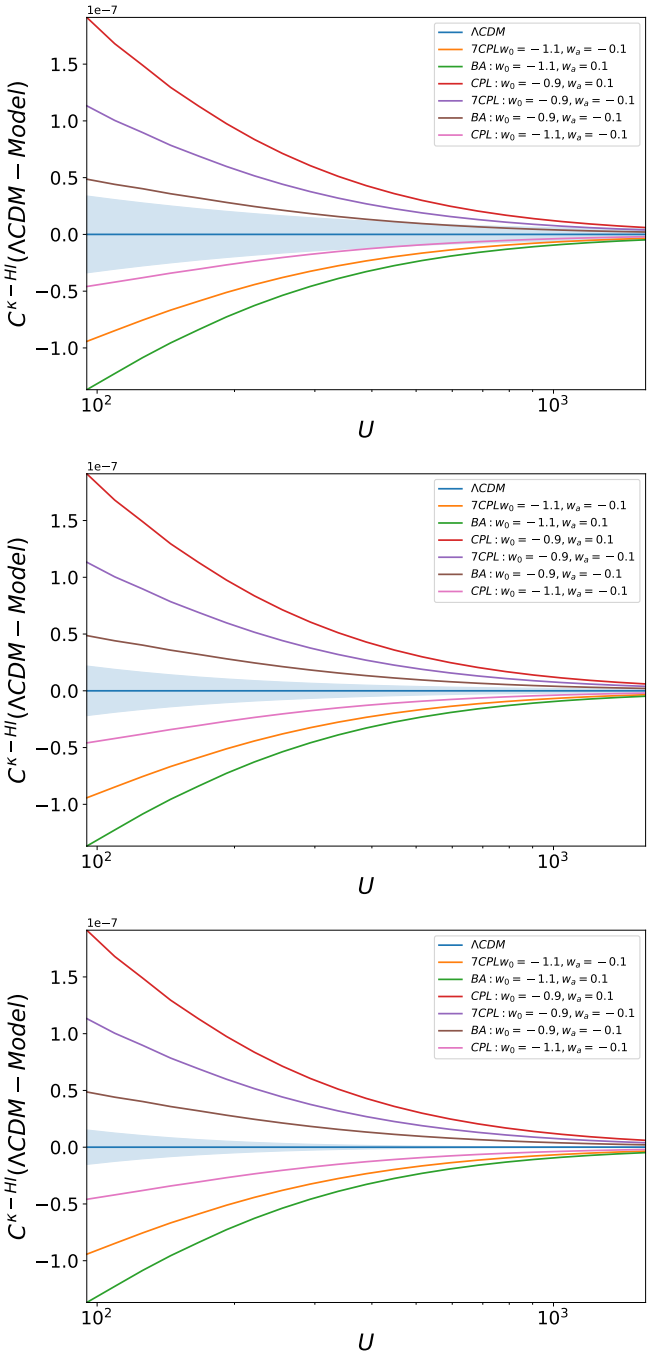
1e−7
ΛCDM
7CPL $w_0 = -1.1, w_a = -0.1$
BA : $w_0 = -1.1, w_a = 0.1$
CPL : $w_0 = -0.9, w_a = 0.1$
7CPL : $w_0 = -0.9, w_a = -0.1$
BA : $w_0 = -0.9, w_a = -0.1$
CPL : $w_0 = -1.1, w_a = -0.1$
$C^{\kappa-HI}(\Lambda CDM - Model)$
1.5
1.0
0.5
0.0
−0.5
−1.0
10^2
10^3
U

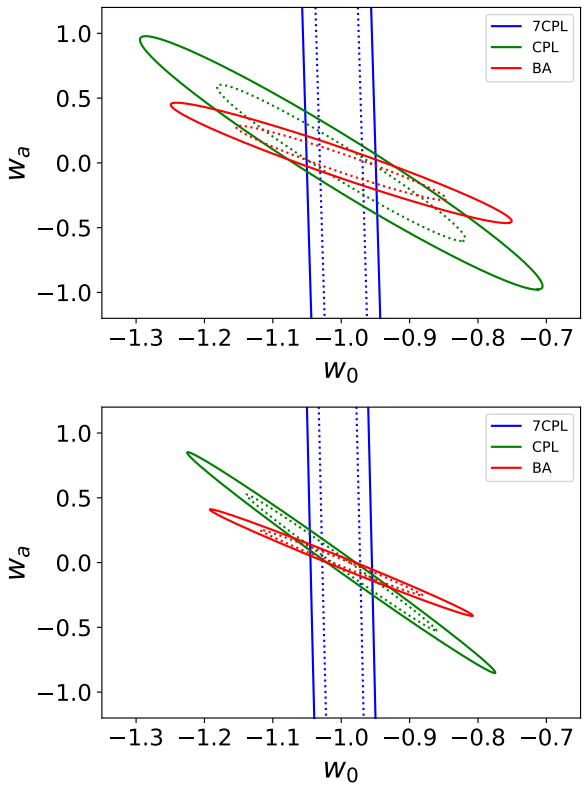

Figure 4.11: The 68% and 95% marginalized confidence intervals for the parameters w_0 and w_a from the 21-cm convergence cross correlation for different dark energy EoS parametrizations for uGMRT. The fiducial model is chosen as the ΛCDM model with $(w_0, w_a) = (-1, 0)$. The second figure shows the best case scenario of a cosmic variance dominated experiment.

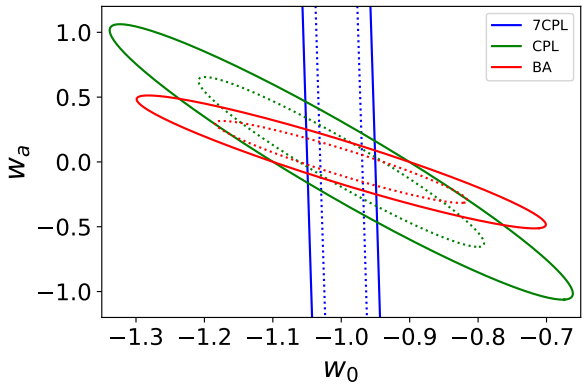

Figure 4.12: The 68% and 95% marginalized confidence intervals for w_0 and w_a from the 21-cm convergence cross correlation for different dark energy EoS parametrizations. The fiducial model is chosen as the ΛCDM model with $(w_0, w_a) = (-1, 0)$. The figure correspond to MeerKAT observations.

CHAPTER 5

Intensity mapping of post-reionization 21-cm signal and its cross-correlations as a probe of $f(R)$ gravity [§]

5.1 Introduction

Einstein's general theory of relativity (GR) has endured a complete century of intensive scrutiny, and has emerged as the most successful theory of gravitation. Several tests on solar system scales have proved its consistency on small scales [423]. However, modifications to the theory of gravity have often been proposed as a way to explain the observed cosmic acceleration [62]. Several observational evidences like Galaxy redshift surveys, Cosmic Microwave Background Radiation (CMBR) observations and supernovae surveys strongly indicate that the energy budget of our universe is dominated by dark energy- a fluid with energy-momentum tensor that violates the strong energy condition [15, 16, 27, 375]. We have seen earlier that though the cosmological constant (Λ) treated as a fluid with an equation of state $p = -\rho$ is the most popular candidate for dark energy in the framework of classical general relativity [19] the ΛCDM, model suffers from several theoretical and observational difficulties [20, 27–29]. In the matter sector, scalar fields have often been used to model various properties of dynamical and clustering dark energy [21, 24, 64, 377–380, 382]. Extensive literature is available on the diversity of such models and their general treatment using model-independent parametrizations [150, 206, 207]. In the last chapter we looked at such scalar field parametrizations.

Alternatively, a modification of Einstein's theory can mimic dark energy without requiring an exotic fluid [25]. In $f(R)$ theory, the Ricci scalar R appearing in the Einstein-Hilbert action, is replaced by a general function of R

[§]The chapter is adapted from *Chandrachud B.V. Dash, Tapomoy Guha Sarkar, Journal of Astronomy & Astrophysics, (2022) on the special issue on Indian participation in SKA*

[61, 183, 424, 425] as

$$S = \frac{1}{2\kappa}\int d^4x\sqrt{-g}f(R) + S_m \tag{5.1}$$

where $\kappa = \frac{8\pi G_N}{c^4}$ and S_m is the action for matter. The $f(R)$ modification naturally has its imprint on the background comsological evolution and growth of structures. The $f(R)$ modification to gravity will affect the 21-cm power spectrum through its signature on cosmic distances, the Hubble parameter and the growth rate of density perturbations. We consider a Hu-Sawicki form of $f(R)$, and investigate the possibility of differentiating such a modification from the standard ΛCDM model.

In this chapter our objective is to make error projections on parameters of a $f(R)$ gravity theory using the post-reionization 21-cm power spectrum in auto and cross-correlations. For cross-correlation of the 21-cm signal we have considered two dark matter tracers: (a) galaxy weak lensing and (b) the Lyman-α forest. We investigate observational strategies with the upcoming SKA towards constraining $f(R)$ theories at precision levels competitive if not significantly better than the next generation of supernova Ia observations, galaxy surveys, and CMB experiments.

5.2 Cosmology with $f(R)$ gravity

We consider a spatially flat Universe comprising of radiation (density ρ_γ) and non-relativistic matter (density ρ_m). In a $f(R)$ gravity theory, the Einstein's field equation and its trace for a Friedman-Lemitre-Robertson-Walker metric (FLRW) with a scale factor $a(t)$ and Hubble parameter $H = \frac{\dot{a}(t)}{a(t)}$ reduces to [194]

$$3H^2 f_{,R} - \frac{1}{2}\left(Rf_{,R} - f\right) + 3H\dot{f}_{,R} = \kappa^2(\rho_m + \rho_\gamma) \tag{5.2}$$

$$Hf_{,R} - 2f_{,R}\dot{H} - \ddot{f}_{,R} = \kappa^2\left(\rho_m + \frac{4}{3}\rho_\gamma\right) \tag{5.3}$$

where $f_{,R} = \partial f(R)/\partial R$ and the "." denotes a differentiation with respect to the cosmic time t. The Ricci scalar R is given by $R = 6(2H^2 + \dot{H})$. It is convenient

to express the above equations in terms of the following set of dimensionless variables $x_1 \equiv -\frac{\dot{f}_{,R}}{Hf_{,R}}$, $x_2 \equiv -\frac{f}{6H^2 f_{,R}}$, $x_3 \equiv \frac{R}{6H^2}$, $x_4 \equiv \frac{\kappa^2\rho_\gamma}{3H^2 f_{,R}}$. In terms of these quantities the dynamical evolution of the density parameters can obtained by solving the following set of autonomous first order differential equations [194]

$$x_1' = -1 - x_3 - 3x_2 + x_1^2 - x_1x_3 + x_4 \tag{5.4}$$

$$x_2' = \frac{x_1x_3}{m} - x_2(2x_3 - 4 - x_1) \tag{5.5}$$

$$x_3' = -\frac{x_1x_3}{m} - 2x_3(x_3 - 2) \tag{5.6}$$

$$x_4' = -2x_3x_4 + x_1x_4 \tag{5.7}$$

where $' = d/d\ln(a)$ and m measures the deviation from ΛCDM model defined as $m \equiv \frac{d\ln f_{,R}}{d\ln R} = \frac{Rf_{,RR}}{f_{,R}}$. These equations form a 4-dimensional coupled dynamical system which can be integrated numerically for a given $f(R)$ and with suitable initial conditions. Solution to the above coupled ODEs can be used to determine the dynamics of the density parameters and map a $f(R)$ gravity theory to a dark energy with an effective equation of state (EoS) $w_{eff}(z)$ as

$$\Omega_m \equiv \frac{\kappa^2\rho_m}{3H^2 f_{,R}} = 1 - (x_1 + x_2 + x_3 + x_4) \tag{5.8}$$

$$\Omega_\gamma \equiv x_4 \tag{5.9}$$

$$\Omega_{DE} \equiv x_1 + x_2 + x_3 \tag{5.10}$$

$$w_{eff} \equiv -\frac{1}{3}(2x_3 - 1) \tag{5.11}$$

A wide variety of $f(R)$ models have been proposed [154, 156, 182, 183]. The functional form of $f(R)$ is chosen so that the model is phenomenologically satisfactory. We expect the $f(R)$ cosmology to be indistinguishable from the ΛCDM at high redshifts where the latter is well constrained from CMBR observations. At low redshifts the accelerated expansion history should be close to the ΛCDM predictions and on Solar system scales the proposed $f(R)$ model should be consistent with the ΛCDM model as a limiting case.

We consider the $f(R)$ gravity model proposed by Hu-Sawicki (HS), where the functional form of $f(R)$ is given by [25, 182]

$$f(R) = R - \mu R_c \frac{(R/R_c)^2}{(R/R_c)^2 + 1} \tag{5.12}$$

Here μ and R_c are two non-negative parameters in the model where R_c is the present day value of the Ricci scalar. The expansion rate H for a viable $f(R)$ gravity theories is expected to be close to the concordance ΛCDM [426] predictions. The quantity $f_{,R}$ plays a crucial role to quantify the deviation of $f(R)$ gravity models from GR whereby $f_{,R}$ behaves like an extra degrees of freedom that acts similar to a scalar field. We may write

$$f_{,R} = -2f_0 \frac{R}{H_0^2} \left[1 + \left(\frac{R}{R_c}\right)^2\right]^{-2} \tag{5.13}$$

with $|f_0| \equiv (\mu H_0^2)/R_c$ as the only free parameter.

To recover standard GR results in Solar system tests, the present day value of $f_{,R}$ is restricted to $\log_{10}|f_{,R0}| < -6$ [182]. Further, the second derivative $f_{,RR} = d^2 f(R)/dR^2 > 0$ in order to avoid ghost and tachyonic solutions [184]. Weak Lensing peak abundance studies have provided strong constraints on $\log_{10}|f_{,R0}| < -4.82$ and < -5.16 with WMAP9 and Planck15 priors, respectively. Tight constraints are also obtained from weak lensing peak statistics study with $\log_{10}|f_{,R0}| < -4.73$ (WMAP9) and $\log_{10}|f_{,R0}| < -4.79$ (Planck2013) ([427]). In our work we adopt the fiducial value $\log_{10}|f_{,R0}| = -5$ from observations [427, 428].

Growth of large scale structure (LSS) offers a unique possibility to constrain cosmological models. The quantity of interest is the growth rate of matter density perturbations $f_g(k,z) \equiv \frac{d\ \ln\ \delta_m(k,z)}{d\ \ln\ a}$ which is sensitive to the expansion history of the Universe. In the linear perturbation theory, and on sub-horizon scales ($k/a >> H$) the evolution of matter density perturbations $\delta_m(k,z)$ is dictated by the differential equation [161, 194–196].

$$\ddot{\delta}_m + 2H\dot{\delta}_m - 4\pi G_{eff}(a,k)\rho_m\delta_m \simeq 0 \tag{5.14}$$

where G_{eff} is an effective gravitational constant which is related to standard Newtonian gravitational constant (G_N) as

$$G_{eff}(a,k) = \frac{G_N}{f_{,R}} \left[1 + \frac{(k^2/a^2)(f_{,RR}/f_{,R})}{1 + 3(k^2/a^2)(f_{,RR}/f_{,R})}\right] \tag{5.15}$$

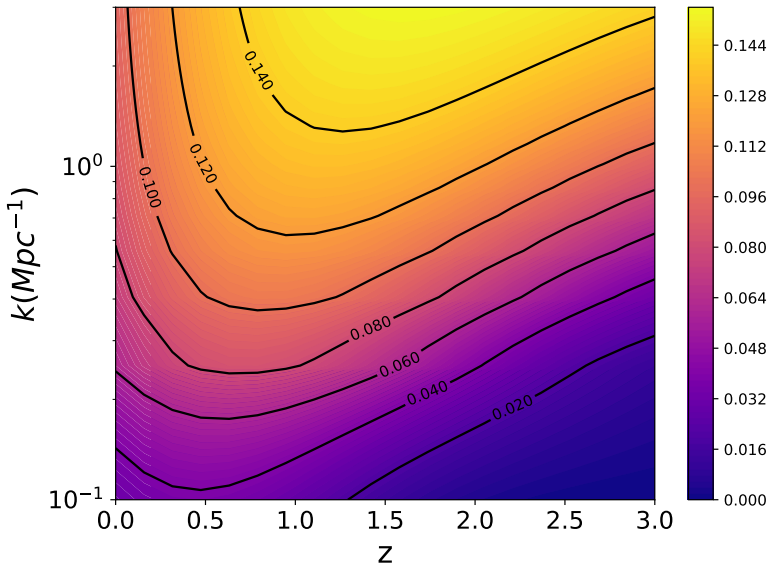

Figure 5.1: The figure shows the departure of the growth rate $f_g(z,k)$ for the $f(R)$ theory with $\log_{10}|f_{,R0}| = -5$ from the ΛCDM prediction. We plot the quantity $|\frac{f_g - f_g^{\Lambda CDM}}{f_g^{\Lambda CDM}}|$ in the (z,k) plane.

In $f(R)$ theories G_{eff} is a scale dependent function [197]. The scale dependence of the growing mode of density fluctuations is widely exploited to differentiate the structure formation beyond standard model of cosmology. In obtaining the approximate equation (5.14) we have incorporated the assumption that oscillating modes are negligible compared to the modes induced by matter perturbations and also $\dot{f_{,R}} \approx 0$ on sub-horizon scales of interest [194].

Figure (5.1) shows the departure of the the growth rate $f_g(z,k)$ for the $f(R)$ theory with $\log_{10}|f_{,R0}| = -5$ from the ΛCDM prediction. We know that the growth rate is scale independent and depends only on redshift for the ΛCDM model. Thus the $k-$dependence seen in the figure arises purely from the $f(R)$ modification to gravity. Since different modes grow differently, the evolution has an additional contribution towards changing the shape of the cosmological power spectrum. The departure is small at very low redshifts and also very high redshifts and increases monotonically with k for a given redshift. We find that a departure of $> 12\%$ is seen in the redshift window $0.5 < z < 1.5$ for $k > 0.5 Mpc^{-1}$.

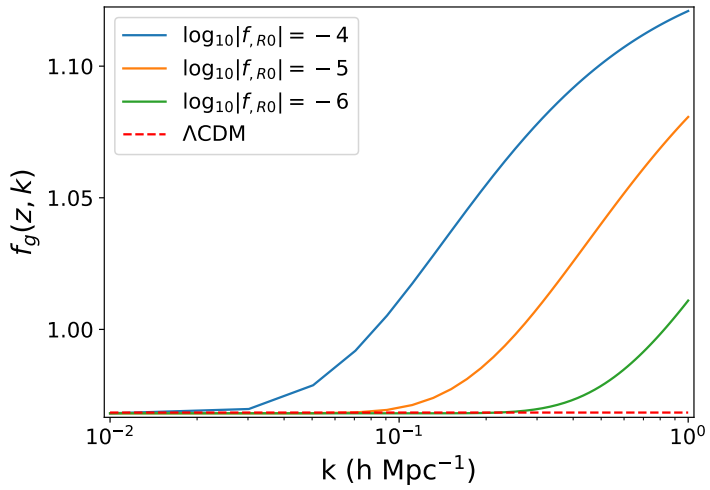

Figure 5.2: The figure shows the growth rate $f_g(z,k)$ for the $f(R)$ theory of $\log_{10}|f_{,R0}| = -5$ model. We also shown the results for $\log_{10}|f_{,R0}| = -4$ and $\log_{10}|f_{,R0}| = -6$ model for comparison purpose. The dotted bottom shows scale independent ΛCDM prediction. The fiducial redshift chosen to be $z = 2.3$.

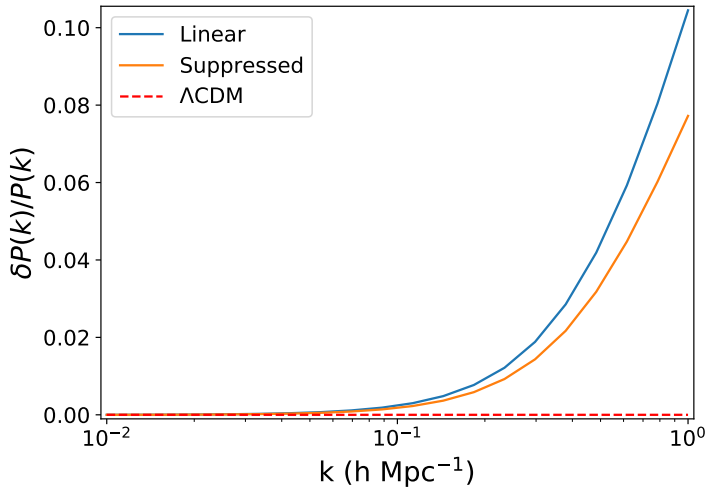

Figure 5.3: The figure shows the departure of the matter power spectrum $P(z,k)$ for the $f(R)$ theory with $\log_{10}|f_{,R0}| = -5$ from the ΛCDM prediction. We plot the quantity $\frac{P_{f(R)}(k,z)-P_{\Lambda CDM}(k,z)}{P_{\Lambda CDM}(k,z)}$ at redshift $z = 2.3$.

In Figure (5.2) we have shown the linear growth rate $f_g(z,k)$ for ΛCDM and $f(R)$ with $\log_{10}|f_{,R0}| = -5$ at a redshift $z = 2.3$. At smaller scales (large k modes) the scale dependent growth become more prominent and larger scales (small k modes) $f(R)$ gravity coincide with ΛCDM. We have also shown the $f_g(k,z)$ for $\log_{10}|f_{,R0}| = -4$ and $\log_{10}|f_{,R0}| = -6$ gravity model for comparison purpose only.

Matter power spectrum

$f(R)$ gravity has a significant impact on structure formation in low density regions through a scale dependent growth factor because of enhancement of gravitational forces. The modification to the force law in modified gravity theories is highly constrained from local tests [429]. It is also well studied that $f(R)$ modification to gravity will induce non-linearities in the power spectrum through mechanisms like chameleon [430], dilaton effect [431] etc. The shape of the matter power spectrum is sensitive to the choice of cosmological model and as such it is sensitive probe of the underlying theory of gravity or dark energy. We model the power spectrum in $f(R)$ gravity models as

$$P_{f(R)}(k) = \frac{P_{Lin}}{(1 + k^2/k^2_{trunc})^2}\, e^{-(k/k_s)^2} \tag{5.16}$$

where P_{Lin} is the linear matter power spectrum. In our analysis we have used the analytic fitting function by Hu-Eisenstein for P_{Lin} [126]. We have used the fitting parameters (k_{trunc}, k_s) for the suppressed matter power spectrum from [432] for $f(R)$ gravity models. $P(k,z)$ is obtained by multiplying the square of the growing mode with this. We remind ourselves that the growing mode is scale dependent for $f(R)$ models and is scale independent for ΛCDM model.

Figure (5.3) shows the relative deviation of matter power spectrum of $f(R)$ gravity theory from ΛCDM at a fiducial redshift $z = 2.3$. The topmost curve corresponds to linear theory prediction and the one below shows the suppressed matter power spectrum due to the additional factor introduced in Eq(5.16). The relative deviation of $P_{Lin}(k)$ from its ΛCDM counterpart grows at smaller scales, because the mass of the scalar field yields a characteristic scale dependence for the linear growing mode. Moreover, on linear scales there is

no additional chameleon screening mechanism.

Many simulation result shows that the deviation is significantly suppressed due to screening mechanism [433, 434]. The additional prefactor in equation (5.16) is fitted for mildly nonlinear behavior and reproduces the suppressed matter power spectrum with sub percent accuracy without requiring the full non linear simulations (refer Fig:5 in [433]).

5.3 The 21-cm signal from the post-reionization era

Bulk of the low density hydrogen gets completely ionized by the end of the reionization epoch around $z \sim 6$ [329]. A small fraction of HI that survives the process of reionization is believed to remain confined in the over-dense regions of the IGM. These clumped, dense damped Lyman-α systems (DLAs) [266] remain neutral as they are self shielded from the background ionizing radiation. They store $\sim 80\%$ of the HI at $z < 4$ [267] with HI column density greater than $2 \times 10^{20}\mathrm{atoms/cm^2}$ [268–270] and are the dominant source of the 21-cm radiation in the post-reionization epoch. The clustering properties of these DLA clouds suggest that they are associated with galaxies and located in regions of highly non-linear matter over densities [271–273]. The 21-cm signal from the post-reionization epoch has been extensively studied [81–83, 87–89, 435]. The emitted flux from individual clouds is extremely weak ($< 10\mu\mathrm{Jy}$). These individual DLA clouds are unlikely to be detected in radio observations, even with futuristic telescopes. However, in an intensity mapping experiment one does not aim to resolve the individual sources. The collective emission forms a diffused background in all radio-observations at the observation frequencies less than $1420\mathrm{MHz}$. Fluctuations of this signal on the sky plane and across redshift, maps out the three dimensional tomographic image of the Universe.

Several assumptions simplify the modeling of the post-reionization HI signal. These are either motivated from implicit observations or from numerical simulations. Adopting all the assumptions discussed above, the power spectrum of post-reionization HI 21-cm brightness temperature fluctuations from

redshift z is given by ([256, 283])

$$P_{\rm HI}(\mathbf{k},z)=\bar{T}(z)^2\bar{x}_{\rm HI}^2 b_T(k,z)^2(1+\beta_T(k,z)\mu^2)^2P(k,z) \tag{5.17}$$

where $\mu=\hat{\mathbf{k}}\cdot\hat{\mathbf{n}}$, $\beta_T(k,z)=f_g(k,z)/b_T(k,z)$, and

$$\bar{T}(z)=4.0\,{\rm mK}\;(1+z)^2\left(\frac{\Omega_{b0}h^2}{0.02}\right)\left(\frac{0.7}{h}\right)\frac{H_0}{H(z)} \tag{5.18}$$

The term $f_g(z,k)\mu^2$ has its origin in the HI peculiar velocities [83, 256] which, as we mentioned, is also sourced by the dark matter fluctuations. The critical density for collapse is smaller in $f(R)$ gravity models which leads to a significant suppression of bias i.e $b_T^{f(R)}<b_T^{GR}$. This has been seen in numerical simulations [434, 436]. Though the fitting function for b_T (6.7) is obtained from ΛCDM simuation, we used the same form for $f(R)$ gravity assuming the bias is not significantly different in the redshifts of our interest. However we have kept the bias as free parameter which we have eventually marginalized over. We kept the third order component of polynomial bias as the free parameter because we know on large scale the bias is completely indistinguishable from ΛCDM and suppression shows up only on small scales. For $\log_{10}|f_{,R0}|=-5$ model our used bias fitting function is well within the error bars and can be used safely [436].

The $f(R)$ modification affects the 21-cm power spectrum through the change in the redshift space distortion parameter $\beta_T(k,z)$, and $P(k,z)$. Figure (5.4) shows the 21-cm power spectrum at $z=1$ in the $(k_\parallel,k_\perp)$ space. The asymmetry in the signal is indicative of redshift space distortion and is sensitive to $\beta_T(k,z)$. We emphasize that $(\bar{x}_{HI},\beta_T(k,z))$ along with the cosmological parameters completely model the post-reionization 21-cm signal. We note that the product $b_T^2\bar{x}_{\rm HI}$ which appears in the overall amplitude of the 21-cm signal is a largely unknown parameter and depends largely on the HI modeling. We shall, therefore be interested in constraining the function $\beta_T(k,z)$ from some radio-interferometric observation of the signal. We shall marginalize our Fisher matrix projections over the overall amplitude to make error projections.

We shall now investigate the possibility of constraining the function $\beta_T(k,z)$ and thereby put observational bounds on $|f_{,R0}|$ from a radio-interferometric

observation of the signal.

Observed 21-cm power spectrum

The quantity of interest in radio-interferometric observation is the complex visibility $\mathcal{V}(\mathbf{U},\nu)$ measured as function of baseline $\mathbf{U} = (u,v)$ and observing frequency ν. Considering an observation frequency bandwidth and defining $\Delta\nu$ as the difference from the central observing frequency, a further Fourier transform in $\Delta\nu$ gives us the visibility $v(\mathbf{U},\tau)$ as a function of delay channel τ. The measured visibility can be written as a sum of signal $s(\mathbf{U},\tau)$ and noise $n(\mathbf{U},\tau)$ as $v(\mathbf{U},\tau) = s(\mathbf{U},\tau) + n(\mathbf{U},\tau)$. The signal $s(\mathbf{U},\tau)$ can be written as

$$s(\mathbf{U}_a,\tau_m) = \frac{2k_B}{\lambda^2}\int \frac{d^3\mathbf{k}}{(2\pi)^3}\, G(\mathbf{k},\mathbf{U}_a,\tau_m)\, \widetilde{\delta T_b}(\mathbf{k}) \tag{5.19}$$

where $\widetilde{\delta T_b}(\mathbf{k})$ denotes the fluctuations of the 21-cm brightness temperature in Fourier space. The transformation kernel G is given by

$$G(\mathbf{k}_\perp, k_\parallel, \mathbf{U}_a, \tau_m) = \widetilde{\mathcal{A}}\left(\frac{\mathbf{k}_\perp r}{2\pi} - \mathbf{U}_a\right)\widetilde{\mathcal{B}}\left(\frac{k_\parallel r'}{2\pi} - \tau_m\right)$$

where $\widetilde{\mathcal{A}}(\mathbf{U})$ and $\widetilde{\mathcal{B}}(\tau)$ denote the Fourier transform of the telescope beam $A(\vec{\theta})$ and the frequency response window function $B(\Delta\nu)$ respectively. We use r to denote comoving distance to the observing redshift $z = (1420\ \mathrm{MHz}/\nu) - 1$ and $r' = dr(\nu)/d\nu$. The signal covariance matrix is defined as

$$\langle s(\mathbf{U}_a,\tau_m)s^*(\mathbf{U}_b,\tau_n)\rangle = C^S_{(a,m),(b,n)}$$

and is given by

$$C^S = \left(\frac{2k_B}{\lambda^2}\right)^2 \frac{1}{r^2 r'}\int d^2\mathbf{U}d\tau\, G(\mathbf{k},\mathbf{U}_a,\tau_m)G^*(\mathbf{k},\mathbf{U}_b,\tau_n)\times P_{HI}(\mathbf{k}) \tag{5.20}$$

where $\mathbf{k} = (\frac{2\pi\mathbf{U}}{r}, \frac{2\pi\tau}{r'})$. The noise in the visibilities measured at different baselines and frequency channels are uncorrelated. If we define the noise covari-

ance matrix as $C^N = \langle n(\mathbf{U}_a, \tau_m)\, n^*(\mathbf{U}_b, \tau_n)\rangle$, we have

$$C^N = \left(\frac{2k_B}{\lambda^2}\right)^2 \left(\frac{\lambda^2 T_{sys}}{A_e}\right)^2 \frac{B}{t}\delta_{m,n}\delta_{a,b} \tag{5.21}$$

where t is the correlator integration time and B is the observing bandwidth. The system temperature T_{sys} can be written as a contribution from the instrument and the sky as $T_{sys} = T_{inst} + T_{sky}$, where $T_{sky} = 60\mathrm{K}\left(\frac{\nu}{300\ \mathrm{MHz}}\right)^{-2.5}$. We first investigate the possibility of constraining the scale dependent function $\beta_T(k, z_{fid})$. We divide the observational range k_{min} to k_{max} into N_{bin} bins and constrain the values of $\beta_T(k_i)$ at the middle of the bin k_i using a Fisher matrix analysis. The departure from the ΛCDM model for the fiducial $\log_{10}|f_{,R0}| < -5$ model for a range of k values, peaks around $z \sim 1$. We choose the observational central frequency to be $710MHz$ corresponding to this redshift. We first consider an OWFA [437–439] like array which is the upgraded version of the Ooty radio telescope and is expected to operate as an linear radio-interferometric array. The OWFA is a 530 m long and 30 m wide parabolic cylindrical reflector that is placed along the north-south direction on a hill that has the same slope ($\sim 11°$) as the latitude of the place. This makes it possible to track a given patch of sky by rotating the cylinder about the long axis of the telescope. The OWFA has 1056 dipoles in total that are equally placed at $\sim 0.5\,\mathrm{m}$ apart from each other along the long axis of the telescope. OWFA is capable of operating in two independent simultaneous radio-interferometric modes - PI and PII. The OWFA PII has 264 antennas in total, the radio signals from 4 consecutive dipoles have been combined to form a single antenna element. The OWFA PII has the smallest baseline length, $d = 1.92\,\mathrm{m}$ that corresponds to the distance between the two consecutive antennas in the array. The OWFA PII has an operating bandwidth, $B = 39\,\mathrm{MHz}$ (for detailed specifications [439]). The full covariance matrix is given by

$$C_{ab} = C^S + \frac{C^N}{N_r} \tag{5.22}$$

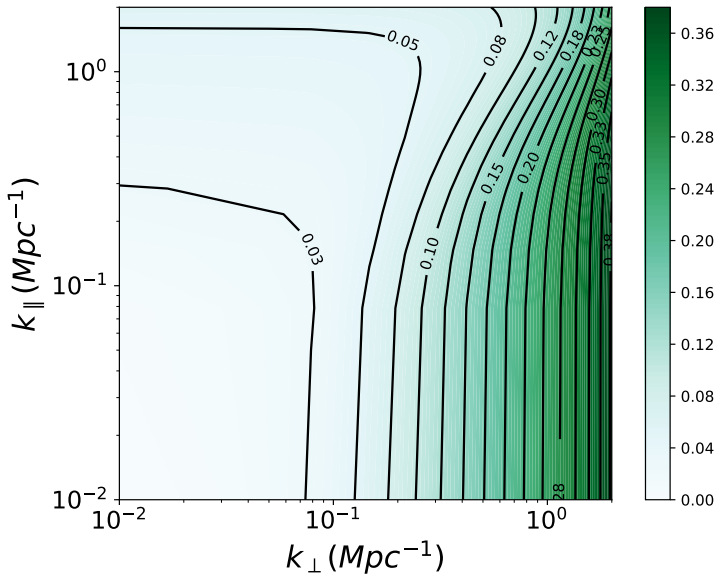

Figure 5.4: The figure shows the 21-cm power spectrum in the $(k_\parallel, k_\perp)$ space at the observing frequency $\nu_0 = 710$MHz.

where $N_r = 264 - a$ is the redundancy of the baselines. The Fisher matrix is given by

$$F_{ij} = \frac{1}{2}\sum_m C^{-1}(m)_{ab}C(m)_{bc,i}C^{-1}(m)_{cd}C(m)_{bc,j} \tag{5.23}$$

where i and j runs over the parameters $\beta_T(k_1), \beta_T(k_2), \ldots \beta_T(k_{N_{bin}})$. The error on the i^{th} parameter is obtained from the Cramer Rao bound as $\sqrt{F_{ii}^{-1}}$. We find that in the $k-$range $0.06 < k < 1.32$ $\beta_T(k)$ can be measured in 4 bins at $> 9\%$ for 500×50hrs observation with 50 independent pointings. Since the maximum departure of $\beta_T(k)$ from the ΛCDM is $\sim 11\%$ in the $k-$range of interest, such an observation will at its best be able to distinguish between a $\log_{10}|f_{,R0}| = -5$ at a $\sim 1-\sigma$ level and $\log_{10}|f_{,R0}| = -4$ at $\sim 2-\sigma$ level.

For stronger constraints, we now consider a SKA1-mid type of radio array. We consider a binning in visibility $\Delta\mathbf{U}$, and a total observing time T_0 causing a reduction of noise variance by a factor N_p where N_p is the number of visibility pairs in the bin given by $N_p = N_{vis}(N_{vis}-1)/2 \approx N_{vis}^2/2$ where N_{vis} is the

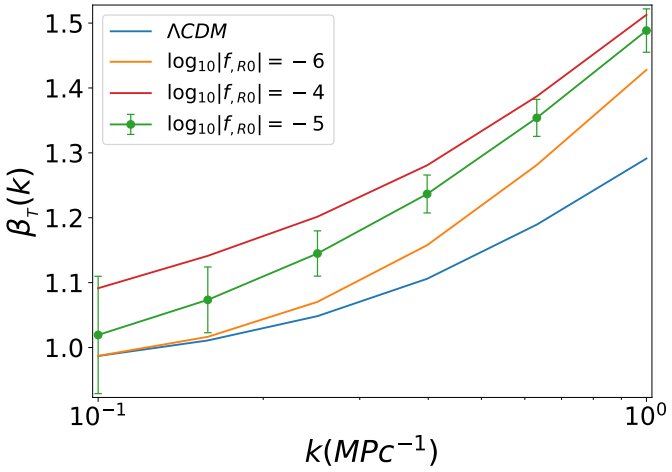

Figure 5.5: The figure shows the variation of $\beta_T(k, z_{fid})$ at the fiducial redshift $z_{fid} = 1$ for various Hu-Sawcki $f(R)$ models. The ΛCDM prediction is also shown. We also show the $1-\sigma$ error bars on β_T at 6 logarithmically spaced $k-$ bins in the observed range of scales for the fiducial model with $\log_{10}|f_{,R0}| = -5$.

number of visibilities in the bin measured in time T_0. We may write

$$N_{vis} = \frac{N_{ant}(N_{ant}-1)}{2}\frac{T_o}{t}\rho(\mathbf{U})\delta^2 U \tag{5.24}$$

where N_{ant} is the total number of antennas in the array and $\rho(\mathbf{U})$ is the baseline distribution function. In general, the baseline distribution function is given by a convolution

$$\rho(\mathbf{U}) = c\int d^2\mathbf{r}\rho_{ant}(\mathbf{r})\rho_{ant}(\mathbf{r}-\lambda\mathbf{U}) \tag{5.25}$$

Where c is fixed by normalization of $\rho(\mathbf{U})$ and ρ_{ant} is the distribution of antennas. Further, if we assume a uniform frequency response over the entire observation bandwidth B and a Gaussian beam for the telescope

$$\int d\tau\ \widetilde{\mathcal{B}}(\tau-\tau_m)\widetilde{\mathcal{B}}^*(\tau-\tau_n) = B\delta_{mn}, \text{ and} \tag{5.26}$$

$$\int d^2\mathbf{U}\mathcal{A}(\mathbf{U}-\mathbf{U}_a)\mathcal{A}^*(\mathbf{U}-\mathbf{U}_b) \approx \frac{\lambda^2}{A_e}\delta_{a,b} \tag{5.27}$$

where, A_e is the effective area of the antenna dishes. With these simplifications

we may then write

$$C^S \approx \left(\frac{2k_B}{\lambda^2}\right)^2 \frac{B\lambda^2}{r^2 r' A_e} P_{HI}\left(\frac{2\pi \mathbf{U}_a}{r}, \frac{2\pi\tau_m}{r'}\right)\delta_{m,n}\delta_{a,b}$$

The 21-cm power spectrum is not spherically symmetric, due to redshift space distortion but is symmetric around the polar angle ϕ. Using this symmetry, we would want to sum all the Fourier cells in an annulus of constant $(k,\ \mu = \cos\theta = k_\parallel/k)$ with radial width Δk and angular width $\Delta\theta$ for a statistical detection with improved SNR. The number of independent cells in such an annulus is

$$N_c = 2\pi k^2 \Delta k \Delta\mu \frac{Vol}{(2\pi)^3} \tag{5.28}$$

where the volume Vol of the intensity mapping survey is given by $Vol = \frac{r^2\lambda^2 r' B}{A_e}$. Thus, the full covariance matrix may be written as

$$C^{Tot} = \frac{1}{\sqrt{N_c}}\left[C^S + \frac{C^N}{N_p}\right] \tag{5.29}$$

The covariance matrix is diagonal owing to the binning in U since different baselines which get correlated due to the telescope beam are now uncorrelated. Further, to increase the sensitivity we consider the angle averaged power spectrum by averaging over μ. Thus we have

$$P_{\rm HI}(k) = \bar{T}(z)^2 \bar{x}_{\rm HI}^2 b_T^2 \left(1 + \frac{2}{3}\beta_T + \frac{1}{5}\beta_T^2\right) P(k,z) \tag{5.30}$$

and the corresponding variance is obtained by summing

$$\delta P_{HI}(k) = \left[\sum_\mu \frac{1}{\delta P_{HI}(k,\mu)^2}\right]^{-1/2} \tag{5.31}$$

where $\delta P_{HI}(k,\mu) = \frac{A_e r^2 r'}{\lambda^2 B} C^{Tot}$.

The fisher matrix for parameters λ_i may be written as

$$F_{ij} = \sum_k \frac{1}{\delta P_{HI}^2(k)} \frac{\partial P_{HI}(k)}{\partial\lambda_i} \frac{\partial P_{HI}(k)}{\partial\lambda_j} \tag{5.32}$$

We consider a radio telescope with an operational frequency range of 350MHz to 14GHz. We consider 250 dish antennae each of diameter $15m$ and efficiency 0.7. To calculate the normalized baseline distribution function We assume that baselines are distributed such that the antenna distribution falls off as $1/r^2$. We also assume that there is no baseline coverage below 30m. We assume $T_{sys} = 60K$ and an observation bandwidth of $128MHz$. We assume $\Delta U = U_{min} = 50$ over which the signal is averaged.

Figure (5.5) shows the variation of $\beta_T(k, z_{fid})$ at the fiducial redshift $z = 1$ corresponding to the observing central frequency of $710MHz$. The monotonic rise of $\beta_T(k, z_{fid} = 1.0)$ owes its origin to both the monotonic growth of $f_g(k)$ and also a slow decrease of $b_T(k, z_{fid} = 1.0)$ in the $k-$ range of interest. The behaviour is similar for different values of $\log_{10}|f_{,R0}|$. The ΛCDM result is seen to coincide with the $f(R)$ prediction on large scales. We note that the $\log_{10}|f_{,R0}| = -6$ matches with the ΛCDM model for $k < 0.15Mpc^{-1}$. We consider a fiducial $\log_{10}|f_{,R0}| = -5$ for our analysis. The $k-$range between the smallest and largest baselines in binned as $\Delta k = \alpha k$ where $\alpha = \frac{1}{N_{bin}} \ln(U_{max}/U_{min})$, with $(U_{min}, U_{max}) = (50,\ 550)$. We consider 400×50 hrs observation in 50 independent pointings. The $1-\sigma$ errors on $\beta_T(k_i)$ are obtained from the Fisher matrix analysis where the overall normalization of the power-spectrum is marginalized over. We find that for $k > 0.4Mpc^{-1}$, the $\log_{10}|f_{,R0}| = -5$ can be differentiated from the ΛCDM model at a sensitivity of $> 5\sigma$ if we consider 6 $k-$bins. On larger scales $k < 0.4Mpc^{-1}$ the $f(R)$ models with $-6 < \log_{10}|f_{,R0}| < -4$ remain statistically indistinguishable from the ΛCDM model. Thus, it appears that 21-cm observations of the post-reionization epoch may only be able to constrain $f(R)$ theories on relatively small scales.

Instead of constraining the binned function $\beta_T(k)$, we investigate the possibility of putting bounds on $\log_{10}|f_{,R0}|$ from the given observation. Marginalizing over the overall amplitude of the power spectrum, we are thus interested in two parameters $(\Omega_{m0},\ \log_{10}|f_{,R0}|)$. The $1-\sigma$ bounds on $\log_{10}|f_{,R0}|$ obtained from the marginalized Fisher matrix is given in the table below. Our error projection maybe compared with constraints obtained from other observational probes. We find that our projected constraints are competitive with constraints obtained from diverse probes.

Table 5.1: The 68% $(1-\sigma)$ marginalized errors on $\log_{10}|f_{,R0}|$ and Ω_{m0}

Model	$\log_{10}\|f_{R0}\|$	Ω_{m0}
$f(R)$	-5 ± 0.62	0.315 ± 0.005

Table 5.2: Bounds on $p = \log_{10}|f_{,R0}|$ from other probes

Probe of $f(R)$ gravity	Bound on $\log_{10}\|f_{,R0}\|$
GW Merger GW170817	$p < -2.52$ [440]
Suyaev Zeldovich clusters PLANCK	$-5.81 < p < -4.40$ [441]
Weak lensing Peak Statistics	$-5.16 < p < -4.82$ [427]
CMB + Cluster + SN + H_0 + BAO	$p < -3.89$ [442]

The radio-interferometric observation of the post-reionization HI 21-cm signal, thus holds the potential of providing robust constraints on $f(R)$ models.

5.4 Cross-correlation of 21-cm signal with galaxy weak lensing

Weak-lensing [67, 68] of background source galaxies by large scale structure (cosmic shear) has been extensively studied as a powerful cosmological probe [69–77]. The quantity of interest to us is the amplification matrix [67, 68] which quantifies the distortions due to gravitational lensing. These distortions allow to analyze large scale structures and map the matter distribution, on a broad range of scales. Noting that scalar perturbations can not induce any rotation, one only has shear (γ) and convergence (κ) effects in the lensed distorted image of a galaxy. This weak shear/convergence signal is superposed on the intrinsic ellipticities and irregularities of background galaxy images [216]. We are interested in the statistical properties of these distortion fields. The angular power spectrum of the shear field is identical to that of the convergence field whereby we shall only be looking at the convergence field. The Weak-lensing convergence field on the sky is given by a weighted line of sight integral [67] of the overdensity field δ

$$\kappa(\vec{\theta}) = \int_0^{\chi_s} \mathcal{A}_\kappa(\chi)\delta(\chi\vec{\theta},\chi)d\chi \tag{5.33}$$

where χ denotes the comoving distance and

$$\mathcal{A}_\kappa(\chi) = \frac{3}{2}\left(\frac{H_0}{c}\right)^2 \Omega_{m_0} \frac{g(\chi)\,\chi}{a(\chi)}, \quad \text{with} \quad g(\chi) = \int_\chi^{\chi_s} n(z)\frac{dz}{d\chi'}\frac{\chi'-\chi}{\chi'}d\chi' \tag{5.34}$$

The weight function appearing in the kernel incorporates the all the sources distributed according to a distribution function $n(\chi)$ upto χ_s. We have assumed that the source galaxies are distributed as [443]

$$n(z) = n_0\left(\frac{z}{z_0}\right)^\alpha exp\left[-(z/z_0)\right]^\beta \tag{5.35}$$

In this work, we have considered a weak-lensing survey where $z_0 = 0.5$, $\alpha = 2$ and $\beta = 1$ [77]. On small angular scales (typically for $\ell > 10$) where "flat sky " approximation is reasonable we can use the Limber approximation [218] in Fourier space and write the weak-lensing convergence angular power spectrum as

$$C_\kappa^\ell = \frac{9}{4}\left(\frac{H_0}{c}\right)^4 \Omega_{m0}^2 \int_0^{\chi_s} \frac{g^2(\chi)}{a^2(\chi)} P\left(\frac{\ell}{\chi}, \chi\right) d\chi \tag{5.36}$$

where P denotes the matter power spectrum. The noise for the convergence angular power spectrum is given by ΔC_κ^ℓ where

$$\Delta C_\kappa^\ell = \sqrt{\frac{2}{(2\ell+1)f_{sky}}}\left(C_\kappa^\ell + \frac{\sigma_\epsilon^2}{n_g}\right) \tag{5.37}$$

Here, the Poisson noise is dictated by the total galaxy count

$$n_g = \int_0^{\chi_s} n(z)\frac{dz}{d\chi'}d\chi' \tag{5.38}$$

The fraction of the sky observed in the weak lensing survey is assumed to be $f_{sky} = 0.5$ and we adopt $\sigma_\epsilon = 0.4$ as the galaxy-intrinsic rms shear [70]. The factor $(2\ell + 1)$ in the denominator counts the number of samples of C_κ^ℓ for a given ℓ.

On large scales the redshifted HI 21-cm signal from post reionization epoch known to be biased tracers of the underlying dark matter distribution. Assuming HI perturbations are generated by a Gaussian random process, and incor-

porating the effect of redshift space distortion the fluctuations of the 21-cm brightness temperature, the cross-correlation signal in a flat sky approximation can be written as,

$$C^{T\kappa}(U) = \frac{1}{\pi(\chi_s - \chi_0)} \sum_{\chi_o}^{\chi_s} \frac{\Delta\chi}{\chi^2} \mathcal{A}_T \mathcal{A}_\kappa \int_0^\infty dk_\parallel \left[1 + \beta_T \frac{k_\parallel^2}{k^2}\right] P(k, \chi) \tag{5.39}$$

with $k = \sqrt{k_\parallel^2 + \left(\frac{2\pi \vec{\mathbf{U}}}{\chi}\right)^2}$.

The auto-correlation angular power spectra may be similarly written as [360]

$$C^{TT}(U) = \frac{1}{\pi(\chi_2 - \chi_1)^2} \sum_{\chi_1}^{\chi_2} \frac{\Delta\chi}{\chi^2} \mathcal{A}_T^2 \int_0^\infty dk_\parallel \left[1 + \beta_T \frac{k_\parallel^2}{k^2}\right]^2 P(k, \chi) \tag{5.40}$$

$$C^{\kappa\kappa}(U) = \frac{1}{\pi} \int_0^{\chi_s} \frac{d\chi}{\chi^2} \mathcal{A}_\kappa^2 \int_0^\infty dk_\parallel P(k, \chi) \tag{5.41}$$

We follow the formalism in [360] and considered the cross-correlation with the 21-cm signal averaged over the signals from redshift slices to improve the signal to noise ratio. As a note of caution we point out that working in the Fourier basis in the flat sky approximation necessarily makes the signal non-ergodic when we consider correlation between two time slices (due to time evolution of all the relevant cosmological quantities). Further, one also notes the complications arising from the inseparability of the baseline $\mathbf{U}$ (transverse) from the frequency (radial) in this formalism [90].

The angular power spectrum for two redshifts separated by Δz is known to decorrelate very fast in the radial direction [88]. In this work we consider the summation in Eq: (6.6) over redshift slices each of whose width is larger than the typical decorrelation length. Each term in the sum can thus be thought of as an independent observation of the signal. Thus the noise in each term in the summation may be thought of as an independent random variable and the mutual noise covaraiances between the slices may be ignored. Thus the errors in $C^{T\kappa}(U)$ is given by

$$\sigma_{_{T\kappa}} = \sqrt{\frac{(C^{\kappa\kappa} + \langle N^\kappa \rangle)(C^{TT} + \langle N^T \rangle)}{(2\ell + 1) N_c}} \tag{5.42}$$

where N_c is the number of redshift slices over which tthe signal is averaged in Eq: (6.6) and $\langle N^{F_{HI}} \rangle$ and $\langle N^{\kappa} \rangle$ corresponds to the average of the noise power spectrum for F_{HI} and κ respectively.

We compute the expected bounds on HS $f(R)$ gravity free parameter which measures the deviation from ΛCDM models. We have considered telescope specifications of the upcoming SKA1-mid radio interfeoremeter. We have used the cosmological parameters from Planck-2018 results $(\Omega_{m_0}, \Omega_{b_0}, H_0, n_s, \sigma_8, \Omega_K) = (0.315,\ 0.0496,\ 67.4,\ 0.965,\ 0.811,\ 0)$ from [36] for our subsequent analysis. The model galaxy distribution function ($n(z, z_0)$) is adopted from [443, 444]. The cross-correlation can only be computed in an overlapping volume for the weak lensing and 21-cm intensity mapping survey. We choose the frequency band $400 - 950\ MHz$ of SKA1-mid since it corresponds to a redshift range that overlaps with the redshift range of the weak lensing survey. SKA1-mid has 250 antennaes. The diameter of each antenna is taken to be 13.5m and system temperature (T_{sys}) assumed to be 40 K for the entire redshift range. We also assume that full frequency band will be sub-divided into smaller frequency bands of 32 MHz. The details of the SKA1-mid telescope specifications including the baseline distribution can be found in the SKA website https://www.skatelescope.org.

Cross-correlation of CMBR weak lensing and HI 21-cm power spectrum has been studied earlier [357, 360]. Here we shall address the cross-correlation with galaxy weak lensing. A typical galaxy weak lensing survey is different from CMBR weak lensing survey for the following reason. The CMBR temperatures are drawn from a Gaussian distribution, where the galaxies are the tracers of the underlying matter distribution, which at least small scales completely non-linear. However we have not incorporated the effects of non-linearity in our analysis as we are working in the regime of the linear perturbation theory. Secondly, the galaxy surveys are purely 3D while CMB anisotropies are in general a function of angular position ℓ on sky. The Figure:(5.6) shows theoretically expected convergence auto-correlation angular power spectrum signal for ΛCDM and HS model with free parameter $\log_{10}|f_{,R0}| = -5$ for reference. The source redshift of galaxy assumed to be $z_s = 1$. It can be seen that on larger scales the $f(R)$ model predictions agree with ΛCDM. A significant de-

viation from classical GR is only found beyond a scale $\ell > 200$ because of the scale dependent growing mode. Similar results are obtained from simulations in [445, 446]. We also note that the deviation from ΛCDM in a range of scale $200 < \ell < 3000$ is typically around $10 - 15\%$.

We are interested in the cross-correlation signal of HI 21-cm and galaxy lensing. The cross-correlation signal takes the same shape as of convergence auto-correlation signal. We have computed the cross-correlation signal using the equation (6.6). The Figure (5.7) shows the difference of the HI 21-cm and galaxy weak lensing angular cross-correlation power spectrum for HS parametrization with $\log_{10}|f_{,R0}| = -5$ from ΛCDM. The 1-σ error bars on ΛCDM shows the HS model with $\log_{10}|f_{,R0}| = -5$ can be differentiate from ΛCDM at a level of $> 2\sigma$ sensitivity using galaxy density $n_g = 60\mathrm{arcmin}^{-2}$ and radio interferometric observation time $T_{obs} = 600hrs$.

Table 5.3: The 68% $(1-\sigma)$ Constraints of $\log_{10}|f_{,R0}|$ and Ω_{m0} from HI21-cm and galaxy lensing cross power spectrum

Model	$\log_{10}\lvert f_{R0}\rvert$	Ω_{m0}
HS-$f(R)$	-5 ± 0.59	0.315 ± 0.10

The Fisher analysis is used to put bound on the parameter $\log_{10}|f_{,R0}|$ using the cross-correlation signal. Assuming the fiducial value of $\log_{10}|f_{,R0}| = -5$ and marginalizing over the overall amplitude, redshift distortion parameter (β_T) we found the $1-\sigma$ bounds on $\log_{10}|f_{,R0}|$ as shown in the above table.

5.5 Crosscorrelation of 21-cm signal with Lyman-α forest

Lyman-α forest power spectrum

Lyman-α forest traces out the small fluctuations in the HIdensity in the IGM along the line of sight (LoS) to distant background quasars and shows an absorption features in the quasar spectra. The quantity of interest is the transmitted QSO flux through the Lyman-α. The fluctuating Gunn-Peterson effect

allows us to write

$$\mathcal{F} = \bar{\mathcal{F}} e^{-A(1+\delta)^{\Gamma}} \tag{5.43}$$

where $\bar{\mathcal{F}}$ denotes the mean transmitted flux, Γ depend on the slope of the temperature-density power spectrum and the factor A depends on the HIphotoionization rate, which is difficult to measure independently and assumed to be nearly ~ 1. Several simulation works of Lyman-α forest shows the transmitted flux $\delta_{\mathcal{F}} = (\bar{\mathcal{F}} - F)/\bar{F} \propto \delta$ [278].

The influence of $f(R)$ gravity theory in the Lyman-α forest power spectrum has been studied extensively [432, 447]. Fitting formulas for Lyman-α forest power spectrum $(P_{\mathcal{F}\mathcal{F}}(k))$ are usually written in terms of the matter power spectrum $P(k)$ with several prefactors to match numerical simulations. We follow [432] to model the Lyman-α power spectrum in $f(R)$ gravity theory. The Lyman-α power spectrum can be written in terms of matter power spectrum as follows

$$P_{\mathcal{F}\mathcal{F}}(k,z) = \frac{(1+\beta_{\mathcal{F}}\mu^2)^2}{(1+f_g k_{\parallel}/k_{NL})} P(k,z) e^{-(k_{\parallel}/k_{th})^2} \tag{5.44}$$

where μ is the cosine of the angle between LoS $(\hat{n})$ and the wave vector $(\vec{k})$ so that $\mu = \hat{k}.\hat{n} = k_{\parallel}/k$. Here $\beta_{\mathcal{F}}$ is the large scale aniosotropy parameter or so called the redshift distortion factor and k_{th} is the thermal brodening cutoff wave number. We will use Eq : 5.44 to compute the 3D and 1D Lyman-α auto correlation power spectrum. The Eq : 5.44 gives the 3D Lyman-α power spectrum in the redshift space. The observed 1D power spectrum along LoS is given by the standard integral

$$P^{1D}_{\mathcal{F}\mathcal{F}}(k_{\parallel}) = \frac{1}{(2\pi)^2} \int dk_{\perp} P_{\mathcal{F}\mathcal{F}}(k) \tag{5.45}$$

Both Lyman-α and the HI 21-cm signal from the post reionization epoch are extremely useful tools to probe underlying theory of gravity and put stringent constraints on cosmological parameters individually. However on large scale both trace the dark matter density field motivating us to investigate their cross-correlation signal [352]. The cross-correlation of the Lyman-α and HI 21-cm signal has been studied for the ΛCDM model extensively [278, 352–355]. In this work we shall extend it to $f(R)$ gravity models. The Lyman-α and HI 21-

cm signal can be written using the formalism in [353] and equation (5.44). We choose a fiducial redshift $z = 2.3$ for this analysis. Figure (5.8) shows the 3D cross correlation power spectrum in $(k_\perp, k_\parallel)$ plane for $\log_{10}|f_{,R0}| = -5$. The asymmetry in cross signal arises because of Kaiser effect in the redshift space. However the deviation of asymmetry is much enhanced than the auto correlation signal. The Figure (5.8) shows the 3D Lyman-α and HI 21-cm cross correlation power spectrum at a fiducial redshift $z = 2.3$. The fiducial redshift chosen to be $z = 2.3$ as the QSO distribution is known to peaks at $z = 2.25$ and falls off as we move away from peak [448]. The deviation of spherical symmetry in power spectrum arises because of the linear redshift space distortion parameter $\beta_{\mathcal{F}}$ and β_T. We next use the cross correlation signal to put constraints on the parameter $\beta_T(k, z)$. We have used the cosmological parameters from Planck-2018 results $(\Omega_{m_0}, \Omega_{b_0}, H_0, n_s, \sigma_8, \Omega_K) = (0.315,\ 0.0496,\ 67.4,\ 0.965,\ 0.811,\ 0)$ from [36] for our subsequent analysis. We consider a radio interferometric array for the 21-cm observations mimicking the SKA1-mid. The SKA1-mid is one of the three different instruments that will be built as a part of the SKA telescope. SKA1-mid has 250 antennaes. The diameter of each antenna is taken to be 13.5m and system temperature (T_{sys}) assumed to be 40 K for the redshift $z = 2.3$. We also assume that full frequency band will be sub-divided into smaller frequency bands of 32 MHz. For Lyman-α forest observation we have used the quasar number of distribution from DR14 of SDSS [448]. It has a total angular coverage of 14,555 deg^2 and we assumed the of QSO number density $\bar{n} = 60 deg^{-2}$. Each spectra is assumed to have been measured at $> 3\sigma$. sensitivity.

We have divided the $k-$range from $0.1 < k < 1$ into 4 $k-$bins. We perform Fisher matrix analysis for the following parameters -the binned values of β_T, the overall normalization factor $(\bar{\mathcal{N}})$, distortion factor $(\beta_{\mathcal{F}})$, third order component of polynomial bias b_T. We have marginalized over all the parameters except the four values of β_T.

Fig:(5.9) shows the $\beta_T(k, z)$ for $f(R)$ gravity models. The shaded region corresponds to the $1-\sigma$ error projection for the fiducial $\log_{10}|f_{,R0}| = -5$ gravity model. At large scale all $f(R)$ gravity theories matches with standard ΛCDM model. However we find that on small scales beyond $(k > 0.5)$, the

$\log_{10}|f_{,R0}| = -5$ model can be distinguished from ΛCDM model at a level of $3-\sigma$ sensitivity if we consider 2 $k-$bins for 500×60hrs observation with 60 independent pointings. But other $f(R)$ gravity models are not very much distinguishable $(< 3-\sigma)$ throughout the k range. This is because where at very higher redshifts we expect all the modified gravity theories matches to our standard concordance ΛCDM model and deviation from it is much smaller. Instead of constraining the binned function $\beta_T(k)$, we investigate the possibility of putting bounds on $\log_{10}|f_{,R0}|$ from the given observation. Marginalizing over the overall amplitude of the power spectrum, we are thus interested in two parameters $(\Omega_{m0}, \log_{10}|f_{,R0}|)$. The error projections given below.

Table 5.4: The 68% $(1-\sigma)$ marginalized errors on $\log_{10}|f_{,R0}|$ and Ω_{m0} from the 21-cm and Lyman-α cross-correlation.

Model	$\log_{10}\lvert f_{R0}\rvert$	Ω_{m0}
$f(R)$	-5 ± 0.29	0.315 ± 0.012

5.6 Conclusion

Einstein's relativity has been extremely well tested on solar system scales [171, 449, 450]. The $f(R)$ modification often confronts the strong agreement of general relativity on such small scales. Einstein's relativity can be recovered and solar system tests be evaded by the chameleon mechanism [172, 451, 452]. Effectively, this implies that $f(R)$ differs very little from R on solar system scales. It has been shown that Hu-Sawicki $f(R)$ gravity models agree well with the late time cosmic acceleration without invoking a cosmological constant and satisfies both cosmological and solar-system tests in the weak field limit [59]. However, solar-system tests alone put only weak bounds on these models [182] and there is a great variability of model parameters. We have shown that the 21 cm intensity mapping instruments like SKA1 will be capable of constraining the a field value $\log_{10}|f_{,R0}| = -5 \pm 0.62$ of 68% confidence. This is an order of magnitude tighter than constraints currently available from galaxy cluster abundance [453]. Further [454] showed that marginalized 95.4% the upper limit on $\log_{10}|f_{,R0}| = -4.79$ using the Cluster+Planck+WMAP+Lensing+ACT+SPT+

SN+BAO data. Joint analysis of 21-cm intensity mapping with the above observation probe shall be able to narrow down the current constraints. We note that the low redshift departure of $f(R)$ gravity from GR predictions is small and better modeling is needed to invoke non-linear chameleon suppression for tighter constraints on $f(R)$ models.

The radio-interferometric observation of the post-reionization HI 21-cm signal, thus holds the potential of providing robust constraints on $f(R)$ models. We have seen that the error projections from both the auto-correlation and cross-correlation signals provide competitive bounds on $f(R)$ models. Several observational aspects, however, plague the detection of the 21-cm signal. We have evaded the key observational challenge arising from large astrophysical foregrounds that plague the signal. Astrophysical foregrounds from both galactic and extra galactic sources plague the signal and significant amount of foreground subtraction is required before one may detect the signal. Several methods of subtracting foregrounds have been suggested (see [295] and citations in this work) Cross-correlation of the 21-cm signal has also been proposed as a way to mitigate the issue of large foregrounds [352, 353]. The cosmological origin of the 21-cm signal may only be ascertained in a cross-correlation. The foregrounds appear as noise in the cross-correlation and may be tackled by considering larger survey volumes. Further, man made radio frequency interferences (RFIs), calibration errors and other observational systematics inhibits the sensitive detection of the HI 21-cm signal. A detailed study of these observational aspects shall be studied in a future work. We conclude by noting that future observation of the redshifted HI 21-cm signal shall be an important addition to the different cosmological probes aimed towards measuring possible modifications to Einstein's gravity. This shall enhance our understanding of late time cosmological evolution and structure formation.

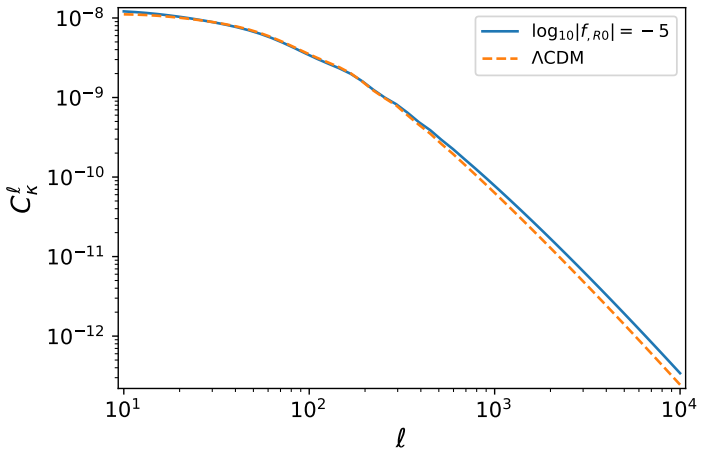

Figure 5.6: The figure shows auto-correlation signal as a function of multiples for modified $f(R)$ model.The dotted line shows the ΛCDM prediction. The source redshift of a galaxy assumed to be $z_s = 1.0$

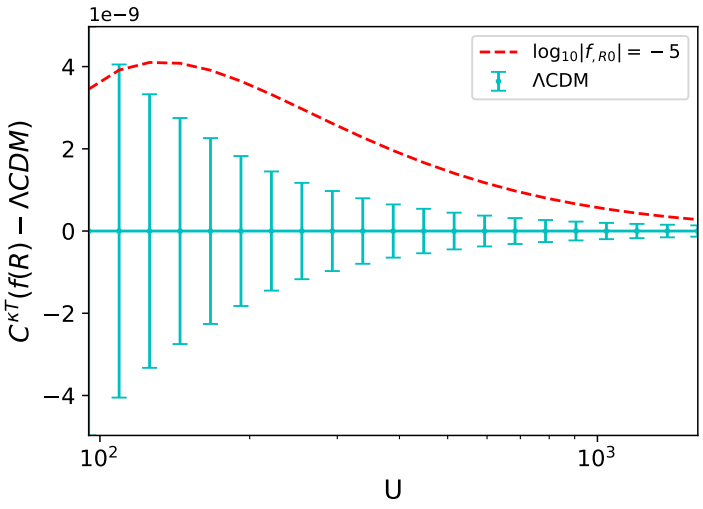

[b]

Figure 5.7: The figure shows difference of HI 21-cm - galaxy weak lensing cross-correlation power spectrum for the HS model with free parameter $\log_{10}|f_{,R0}| = -5$ from the standard ΛCDM. The 1-σ error bars on ΛCDM shown assuming the galaxy density $n_g = 60 arcmin^{-2}$ and observation time $T_{obs} = 600 hrs$.

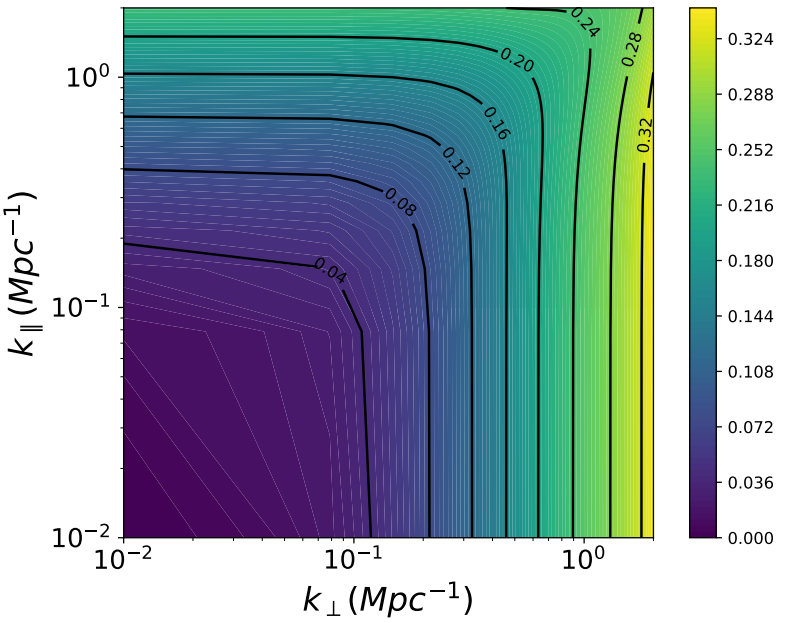

Figure 5.8: Figure shows the 3D cross-correlation power spectrum power spectrum in redshift space for $f(R)$ gravity at a fiducial redshift $z = 2.3$. The asymmetry in the signal is indicative of redshift space distortion.

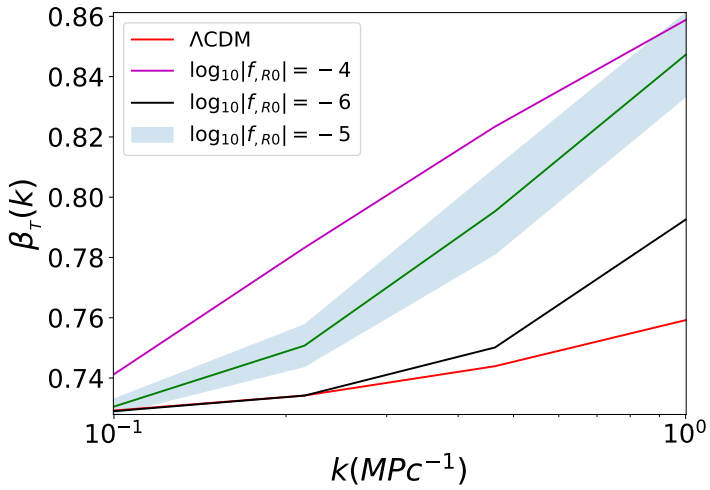

Figure 5.9: The figure shows the redshift distortion parameter β_T at a fiducial redshift $z = 2.3$.The $1-\sigma$ marginalized error is shown by the shaded region on the top of fiducial $f(R)$ gravity $\log_{10}|f_{,R0}| = -5$ model. We also shown the different parameterized $f(R)$ gravity models and ΛCDM for comparison.

CHAPTER 6

Probing Quintessence using BAO imprints on the cross-correlation of weak lensing and post-reionization HI 21-cm signal [§]

6.1 Introduction

The problem of cosmic acceleration [26, 102, 375] can be broadly tackled in two ways. One approach involves modifying the gravity theory itself on large scales [25]. $f(R)$ modification to the Einstein action [182, 183, 452, 455] belongs to this approach of modeling cosmic acceleration. In a second approach the matter sector of Einstein's field equation is modified by considering a dark energy fluid The cause of such cosmic acceleration is attributed to the so called "Dark energy", [25, 32, 456, 457] a fluid that violates the strong energy condition with some nontrivial dynamics. In both the approaches one may find an effective dark energy EoS which dynamically varies as a function of redshift and in principle can be distinguished from the cosmological constant (Λ). There are many models for dark energy that predict a dynamical equation of state. For example, in the quintessence models, dark energy arises from a time dependent scalar field, ϕ [21, 24, 198, 458, 459]. However these models still require fine tuning for consistency with observations. A wide variety of phenomenological potentials have been explored for quintessence field to achieve $w \approx -1$. In all these models, the minimally coupled scalar field is expected to slowly roll in the present epoch. However, other than a few restricted class of potentials, it is difficult to prevent corrections from various symmetry breaking mechanisms which tends to spoil the slow roll condition [460].

[§]The chapter is adapted from *Probing Quintessence using BAO imprints on the cross-correlation of weak lensing and post-reionization HI 21-cm signal, Chandrachud B.V Dash, Tapomoy Guha Sarkar, Monthly Notices on Royal Astronomical Society, 256 , (2022).*

We consider the cross-correlation of HI 21-cm signal with the galaxy weak lensing convergence field. It is known that [461] cross-correlations of individual tracers of IGM often offer crucial advantages over auto-correlations. The systematic noise that arises in the individual surveys is pose less threat in the cross-correlation signal as they appear in the variance. Further, the foregrounds and contaminants of individual surveys are, in most cases, uncorrelated and hence do not bias the cross-correlation signal [357, 358]. The acoustic waves in the primordial baryon-photon plasma are frozen once recombination takes place at $z \sim 1000$. The sound horizon at the epoch of recombination provides a standard ruler which can be then used to calibrate cosmological distances. Baryons imprint the cosmological power spectrum through a distinctive oscillatory signature [126, 127]. The BAO imprint on the 21-cm signal has been studied [462, 463]. The baryon acoustic oscillation (BAO) is an important probe of cosmology [1, 3, 4, 128, 462] as it allows us to measure the angular diameter distance $D_A(z)$ and the Hubble parameter $H(z)$ using the the transverse and the longitudinal oscillatory features respectively thereby allowing us to put stringent constraints on dark energy models. We propose the BAO imprint on the cross-correlation of 21-cm signal and weak lensing convergence as a probe of Quintessence dark energy. The chapter is organized as follows. In Section-2 we discuss the cross-correlation of weak lensing shear/convergence and HI excess brightness temperature. We also discuss the BAO imprint and estimation of errors on the BAO parameters namely the expansion rate $H(z)$, angular diameter distance $D_A(z)$ and the dilation factor $D_V(z)$ from the tomographic measurement of cross-correlation power spectrum using Fisher formalism. In Section-3 we discuss the background and structure formation in quintessence dark energy models and constrain the model parameters using Markov Chain Monte Carlo (MCMC) simulation. We discuss our results and other pertinent observational issues in the concluding section.

6.2 The cross-correlation signal

Weak gravitational lensing [215] by intervening large scale structure distorts the images of distant background galaxies. This is caused by the deflection

of light by the fluctuating gravitational field created by the intervening mass distribution [444]. Weak lensing is a powerful cosmological probe as galaxy shear is sensitive to both spacetime geometry and growth of structures. The Weak-lensing convergence field on the sky is given by a weighted line of sight integral [67] of the matter overdensity field δ as

$$\kappa(\vec{\theta}) = \int_0^{\chi_s} \mathcal{A}_\kappa(\chi)\delta(\chi\vec{\theta},\chi)d\chi \tag{6.1}$$

where χ_s is the maximum distance to which the sources are distributed and the cosmology-dependent function $\mathcal{A}_\kappa(\chi)$ is given by

$$\mathcal{A}_\kappa(\chi) = \frac{3}{2}\Omega_{m0}H_0^2\frac{\chi}{a(\chi)}\int_0^{\chi_s} n_s(z)\frac{dz}{d\chi'}\frac{\chi'-\chi}{\chi'}d\chi' \tag{6.2}$$

where χ denotes the comoving distance and $a(\chi)$, the cosmological scale factor. The redshift selection function of source galaxies, $n_s(z)$ tends to zero at both low and high redshifts. It is typically modeled as a peaked function [444], parametrized by (α, β, z_0) of the from

$$n_s(z) = N_0 z^\alpha e^{-\left(\frac{z}{z_0}\right)^\beta} \tag{6.3}$$

and satisfies the normalization condition

$$\int_0^\infty dz\, n_s(z)dz = \bar{n}_g \tag{6.4}$$

where $\bar{n}_g$ is the the average number density of galaxies per unit steradian.

On large scales the redshifted HI 21-cm signal from post reionization epoch ($z < 6$) known to be biased tracers of the underlying dark matter distribution [91–93]. We use δ_T to denote the redshifted 21-cm brightness temperature fluctuations. The post reionization HI signal has been studied extensively [81–85, 87–89, 464]. We follow the general formalism for the cross-correlation of the 21-cm signal with other cosmological fields given in ([360]). Usually for the investigations involving the 21-cm signal the the radial information is retained for tomographic study. The weak-lensing signal, on the contrary consists of a line of sight integral whereby the redshift information is lost. We

consider an average over the 21-cm signals from redshift slices and thus lose the individual redshift information but improve the signal to noise ratio when cross-correlating with the weak-lensing field.

We define a brightness temperature field on the sky by integrating $\delta_T(\chi\hat{\mathbf{n}}, \chi)$ along the radial direction as

$$T(\hat{n}) = \frac{1}{\chi_2 - \chi_1} \sum_{\chi_1}^{\chi_2} \delta_T(\chi\hat{\mathbf{n}}, \chi)\Delta\chi \tag{6.5}$$

where χ_1 and χ_2 are the comoving distances corresponding to the redshift slices of the 21-cm observation over which the signal is averaged.

Radio interferometric observations of the redshifted 21-cm signal directly measures the complex Visibilities which are the Fourier components of the intensity distribution on the sky. The radio telescope typically has a finite beam which allows us to use the 'flat-sky' approximation. Ideally the fields κ and δ_T are expanded in the basis of spherical harmonics. For convenience, we use a simplified expression for the angular power spectrum by considering the flat sky approximation whereby we can use the Fourier basis. Using this simplifying assumption, we may approximately write the cross-correlation angular power spectrum as [360]

$$C_\ell^{T\kappa} = \frac{1}{\pi(\chi_2 - \chi_1)} \sum_{\chi_1}^{\chi_2} \frac{\Delta\chi}{\chi^2} \mathcal{A}_T(\chi)\mathcal{A}_\kappa(\chi) D_+^2(\chi) \int_0^\infty dk_\parallel \left[1 + \beta_T(\chi)\frac{k_\parallel^2}{k^2}\right] P(k)$$

where $k = \sqrt{k_\parallel^2 + \left(\frac{\ell}{\chi}\right)^2}$, D_+ is the growing mode of density fluctuations, and $\beta_T = f/b_T$ is the redshift distortion factor - the ratio of the logarithmic growth rate f and the bias function and $b_T(k, z)$. The redshift dependent function $\mathcal{A}_T$ is given by [92, 253, 301]

$$\mathcal{A}_T = 4.0\,\mathrm{mK}\, b_T\, \bar{x}_{\mathrm{HI}}(1+z)^2 \left(\frac{\Omega_{b0}h^2}{0.02}\right)\left(\frac{0.7}{h}\right)\left(\frac{H_0}{H(z)}\right) \tag{6.6}$$

The quantity $b_T(k, z)$ is the bias function defined as ratio of HI-21cm power spectrum to dark matter power spectrum $b_T^2 = P_{HI}(z)/P(z)$. In the post-reionization epoch $z < 6$, the neutral hydrogen fraction remains with a value

$\bar{x}_{\rm HI} = 2.45\times10^{-2}$ (adopted from [362, 363]). The clustering of the post-reionization HI is quantified using b_T. On sub-Jean's length, the bias is scale dependent [277]. However, on large scales the bias is known to be scale-independent. The scales above which the bias is linear, is however sensitive to the redshift. Post-reionization HI bias is studied extensively using N-body simulations [91–93, 278]. These simulations demonstrate that the large scale linear bias increases with redshift for $1 < z < 4$ [279]. We have adopted the fitting formula for the bias $b_T(k, z)$ as a function of both redshift z and scale k [91, 92] of the post-reionization signal as

$$b_T(k, z) = \sum_{m=0}^{4}\sum_{n=0}^{2} c(m, n)k^m z^n \tag{6.7}$$

The coefficients $c(m, n)$ in the fit function are adopted from [91].

The angular power spectrum for two redshifts is known to decorrelate very fast in the radial direction [88]. We consider the summation in Eq (6.5) to extend over redshift slices whose separation is more than the typical decorrelation length. This ensures that in the computation of noise for each term in the summation may be thought of as an independent measurement and the mutual covariances between the slices may be ignored.

6.2.1 The Baryon acoustic oscillation in the angular power spectrum

The sound horizon at the epoch of recombination is given by

$$s(z_d) = \int_0^{a_r} \frac{c_s da}{a^2 H(a)} \tag{6.8}$$

where a_r is the scale factor at the epoch of recombination (redshift z_d) and c_s is the sound speed given by $c_s(a) = c/\sqrt{3(1 + 3\rho_b/4\rho_\gamma)}$ where ρ_b and ρ_γ denotes the baryonic and photon densities respectively. The WMAP 5-year data constrains the value of z_d and $s(z_d)$ to be $z_d = 1020.5 \pm 1.6$ and $s(z_d) = 153.3 \pm 2.0$Mpc [130]. We shall use these as the fiducial values in our subsequent analysis. The standard ruler 's' defines a transverse angular scale and a

redshift interval in the radial direction as

$$\theta_s(z) = \frac{s(z_d)}{(1+z)D_A(z)} \qquad \delta z_s = \frac{s(z_d)H(z)}{c} \tag{6.9}$$

Measurement of θ_s and δz_s, allows the independent determination of $D_A(z)$ and $H(z)$. The BAO feature comes from the baryonic part of $P(k)$. Hence we isolate the BAO power spectrum from cold dark matter power spectrum through $P_b(k) = P(k) - P_c(k)$. The baryonic power spectrum can be written as [465, 466]

$$P_b(k) = A\frac{\sin x}{x} e^{-(k\sum_s)^{1.4}} e^{-k^2\sum_{nl}^2/2} \tag{6.10}$$

where A is a normalization, $\sum_s = 1/k_{silk}$ and $\sum_s = 1/k_{nl}$ denotes the inverse scale of 'Silk-damping' and 'non-linearity' respectively. In our analysis we have used $k_{nl} = (3.07h^{-1}Mpc)^{-1}$and $k_{silk} = (8.38h^{-1}Mpc)^{-1}$ from [466] and $x = \sqrt{k_\perp^2 s_\perp^2 + k_\parallel^2 s_\parallel^2}$. We also use the combined effective distance $D_V(z)$ defined as [1]

$$D_V(z) \equiv \left[(1+z)^2 D_A^2(z)\frac{cz}{H(z)}\right]^{1/3} \tag{6.11}$$

The changes in D_A and $H(z)$ are reflected as changes in the values of $s_\perp$ and $s_\parallel$ respectively, and the errors in $s_\perp$ and $s_\parallel$ corresponds to fractional errors in D_A and $H(z)$ respectively. We use $p_1 = \ln(s_\perp^{-1})$ and $p_2 = \ln(s_\parallel)$ as parameters in our analysis. The Fisher matrix is given by

$$F_{ij} = \sum_\ell \frac{1}{\sigma_{T\kappa}^2}\frac{1}{\pi(\chi_2-\chi_1)}\sum_{\chi_1}^{\chi_2}\frac{\Delta\chi}{\chi^2}\mathcal{A}_T(\chi)\mathcal{A}_\chi(\chi)D_+^2(\chi)\int_0^\infty dk_\parallel\left[1+\beta_T(\chi)\frac{k_\parallel^2}{k^2}\right] \times\frac{\partial P_b(k)}{\partial p_i}\frac{\partial P_b(k)}{\partial p_j}$$

$$= \sum_\ell \frac{1}{\sigma_{T\kappa}^2}\frac{\mathcal{A}_T(\chi)\mathcal{A}_\chi(\chi)}{\pi(\chi_2-\chi_1)}\frac{\Delta\chi}{\chi^2}D_+^2(\chi)\int_0^\infty dk_\parallel\left[1+\beta_T\frac{k_\parallel^2}{k^2}\right]\left(\cos x - \frac{\sin x}{x}\right) f_i f_j$$
$$Ae^{-(k\sum_s)^{1.4}}e^{-k^2\sum_{nl}^2/2} \tag{6.12}$$

where $f_1 = k_\parallel^2/k^2 - 1$, $f_2 = k_\parallel^2/k^2$ and $k^2 = k_\parallel^2 + \ell^2/\chi^2$. The variance $\sigma_{T\kappa}$ is given by

$$\sigma_{T\kappa} = \sqrt{\frac{(C_\ell^\kappa + N_\ell^\kappa)(C_\ell^T + N_\ell^T)}{(2\ell+1)f_{sky}}} \tag{6.13}$$

where C_ℓ^κ and C_ℓ^T are the convergence and 21-cm auto-correlation angular power spectra respectively and N_ℓ^κ and N_ℓ^T are the corresponding noise power spectra.

The auto-correlation power spectra are given by ([360])

$$C_\ell^T = \frac{1}{\pi(\chi_2 - \chi_1)^2} \sum_{\chi_1}^{\chi_2} \frac{\Delta\chi}{\chi^2} \mathcal{A}_T(\chi)^2 D_+^2(\chi) \int_0^\infty dk_\parallel \left[1 + \beta_T(\chi)\frac{k_\parallel^2}{k^2}\right]^2 P(k) \tag{6.14}$$

$$C_\ell^\kappa = \frac{1}{\pi} \int_0^{\chi_s} \frac{d\chi}{\chi^2} \mathcal{A}_\kappa(\chi)^2 D_+^2(\chi) \int_0^\infty dk_\parallel P(k) \tag{6.15}$$

The noise in the convergence power spectrum is dominated by Poisson noise. Thus $N^\kappa = \sigma_\epsilon^2/\bar{n_g}$ where σ_ϵ is the galaxy-intrinsic rms shear [70]. The source galaxy distribution is modeled using $(\alpha, \beta, z_0) = (1.28,\ 0.97,\ 0.41)$ which we have adopted from [467]. For the survey under consideration, we have taken $\sigma_\epsilon = 0.4$ [444]. We use a visibility correlation approach to estimate the noise power spectrum N_ℓ^T for the 21-cm signal [353, 468, 469].

$$N_\ell^T = \left(\frac{T_{sys}^2 \lambda^2}{A_e}\right)^2 \frac{B}{T_o N_b(U,\nu)} \tag{6.16}$$

where T_{sys} is the system temperature, B is the total frequency bandwidth, $U = \ell/2\pi$, T_o is the total observation time, and λ is the observed wavelength corresponding to the observed frequency ν of the 21 cm signal. The quantity A_e is the effective collecting area of an individual antenna which can be written $A_e = \epsilon\pi(D_d/2)^2$, where ϵ is the antenna efficiency and D_d is the diameter of the dish. The $N_b(U,\nu)$ is the number density of baseline U and can be expressed as

$$N_b(U,\nu) = \frac{N_{ant}(N_{ant}-1)}{2} \rho_{2D}(U,\nu)\Delta U \tag{6.17}$$

where N_{ant} is the total number of antennae in the radio array and $\rho_{2D}(U,\nu)$ is

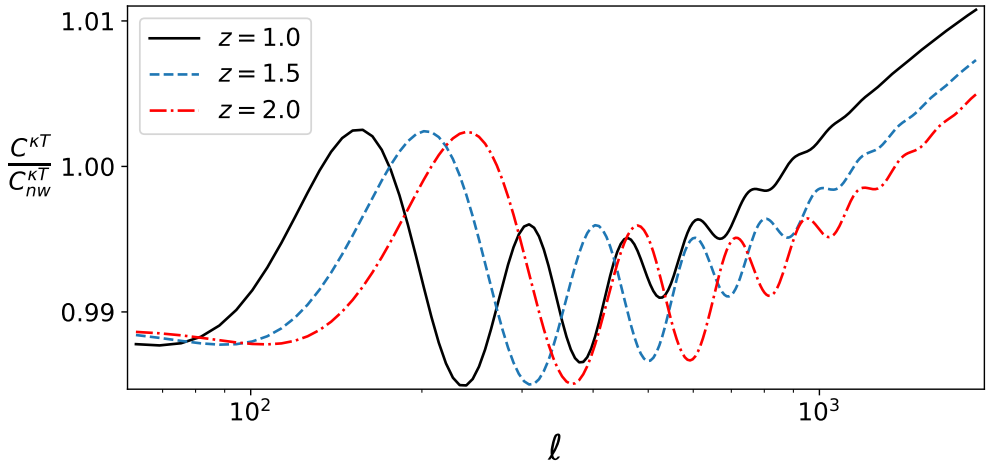

Figure 6.1: This shows the BAO imprint on the transverse cross-correlation angular power spectrum $C_\ell^{T\kappa}$. To highlight the BAO we have divided by the no-wiggles power spectrum $C_{nw}^{T\kappa}$ which corresponds to the power spectrum without the baryonic feature. This is shown for three redshifts $z = 1.0,\ 1.5,\ 2.0$.

the normalized baseline distribution function which follows the normalization condition $\int d^2U \rho_{_{2D}}(U,\nu) = 1$. The system temperature T_{sys} can be written as a sum of contributions from sky and the instrument as

$$T_{sys} = T_{inst} + T_{sky} \tag{6.18}$$

where

$$T_{sky} = 60K \left(\frac{\nu}{300\text{MHz}}\right)^{-2.5} \tag{6.19}$$

We consider a radio telescope with an operational frequency range of $400 - 950$ MHz. We consider 200 dish antennae in a radio interferometer roughly mimicking SKA1-Mid. The telescope parameters are summarized in table (7.1). The full frequency range is divided into 4 bins centered on 916 MHz, 650 MHz, 520 MHz and 430MHz and 32 MHz bandwidth each. To calculate the normalized baseline distribution function we have assumed that baselines are distributed such that the antenna distribution falls off as $1/r^2$. We also assume that there is no baseline coverage below 30m. We have also assumed $\Delta U = A_e/\lambda^2$.

The BAO feature manifests itself as oscillations in the linear matter power spectrum [126]. The first BAO peak has the largest amplitude and is a $\sim 10\%$ feature in the matter power spectrum $P(k)$ at $k \approx 0.045\text{Mpc}^{-1}$. Figure (6.1)

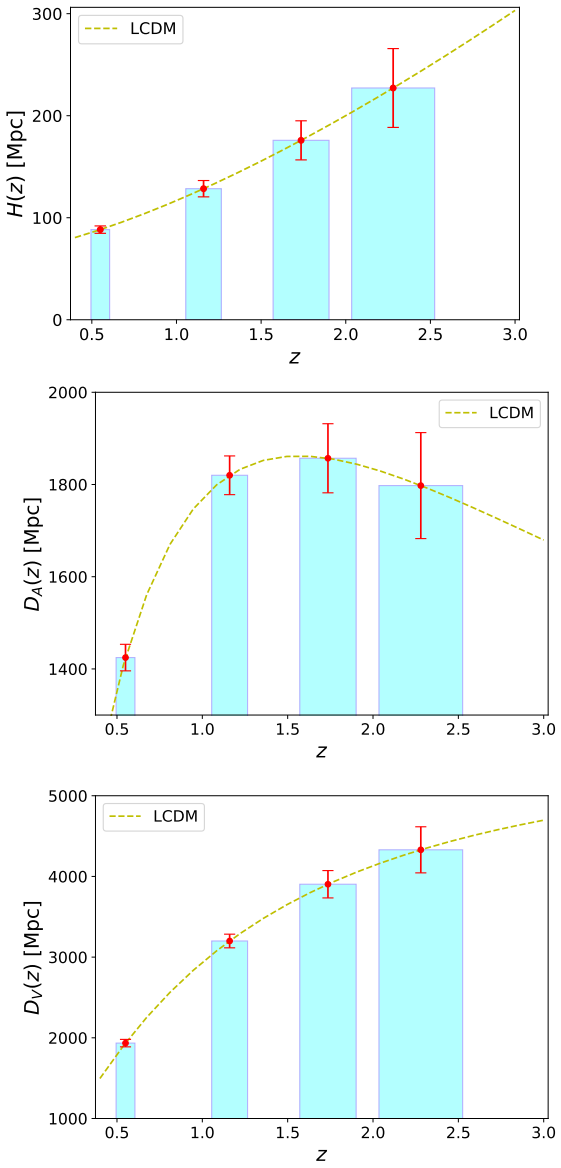

Figure 6.2: The figure shows the projected $1-\sigma$ error bars on $H(z)$, $D_A(z)$ and $D_v(z)$ at 4 redshift bins where the galaxy lensing and HI-21cm cross correlation signal is being observed. The fiducial cosmology is chosen to be ΛCDM.

N_{ant}	Freq. range	Efficiency	D_d	T_o
200	$400-950$ MHz	0.7	15m	600hrs

Table 6.1: Table showing the parameters of the radio interferometer used for making error projections

Redshift(z)	$(\delta H/H)\%$	$(\delta D_A/D_A)\%$	$(\delta D_V/D_V)\%$
0.55	4.09	2.02	2.24
1.16	6.23	2.30	2.79
1.74	10.90	4.035	4.62
2.28	17.00	6.40	6.97

Table 6.2: Percentage $1-\sigma$ errors on D_A, $H(z)$ and D_V.

shows the BAO feature in the cross-correlation angular power spectrum $C_\ell^{T\kappa}$. The BAO, here, seen projected onto a plane appears as a series of oscillations in $C_\ell^{T\kappa}$, The positions of the peaks scales as $\ell \sim k/\chi$. The amplitude of the first oscillation in $C_\ell^{T\kappa}$ is the maximum as is about 1% in contrast to the $\sim 10\%$ feature seen in $P(k)$. This reduction in amplitude arises due to the projection to a plane whereby several $3D$ Fourier modes which do not have the BAO feature also contribute to the ℓ where the BAO peak is seen. For $z = 1.0$ the first peak occurs at $\ell \sim 170$ and it has a full width of $\Delta\ell \sim 75$. If the redshift is changed, the position ℓ and width $\Delta\ell$ of the peak both scale as χ.

We have made error estimates by considering four redshift bins, corresponding to four $32\mathrm{MHz}$ bandwidth radio observations of the 21 cm signal at four observing central frequencies. The total observing time of 2400 hrs is divided into four 600 hrs observations at each frequency.

Figure (6.2) shows the projected errors on $H(z)$ and $D_A(z)$ for the fiducial ΛCDM cosmology. We find that $D_A(z)$ can be measured at a higher level of precision compared to $D_V(z)$ and $H(z)$. This is because the weak lensing kernel is sensitive to $D_A(z)$ and the integration over $\chi(z)$ in the lensing signal leads to stronger constraints on it. The percentage $1-\sigma$ errors are summarized in table (6.2). We find that $H(z)$ is quite poorly constrained especially at higher redshifts.

6.3 Quintessence cosmology

We investigate spatially flat, homogeneous, and isotropic cosmological models filled with three non-interacting components: dark matter, baryobs and a scalar field ϕ, minimally coupled with gravity. The Lagrangian density for the

quintessence field is given by

$$\mathcal{L}_\phi = \frac{1}{2}(\partial^\mu\phi\partial_\nu\phi) - V(\phi) \tag{6.20}$$

where $V(\phi)$ is the quintessence potential. The KG equation for quintessence field obtained by varying action w.r.t the ϕ is

$$\ddot{\phi} + 3H\phi + V_{,\phi} = 0 \tag{6.21}$$

where $V_{,\phi}$ differentiation w.r.t ϕ and the Friedmann equation for H is given by

$$H^2 = \frac{1}{3}(\rho_m + \rho_b + \rho_\phi) \tag{6.22}$$

In order to study the dynamics of background quintessence model, let us define the following dimensionless quantities [25, 459]

$$x = \frac{\phi'}{\sqrt{6}},\;\; y = \frac{\sqrt{V}}{\sqrt{3}H},\;\; \lambda = -\frac{V_{,\phi}}{V},\;\; \Gamma = V\frac{V_{,\phi\phi}}{V_{,\phi}^2},\;\; b = \frac{\sqrt{\rho}_b}{\sqrt{3}H} \tag{6.23}$$

where we use units $8\pi G = c = 1$ and the prime ($'$) denotes the derivative w.r.t the number of e-folding $N = \log(a)$. Using the above quantities we can define the density parameter (Ω_ϕ) and the EoS ($w_\phi = p_\phi/\rho_\phi$) to the scalar field as follows

$$\Omega_\phi = x^2 + y^2, \quad \gamma = 1 + w_\phi = \frac{2x^2}{x^2 + y^2} \tag{6.24}$$

The dynamics of background cosmological evolution is obtained by solving a autonomous system of first order equations [25, 459].

$$\begin{aligned}
\gamma' &= 3\gamma(\gamma - 2) + \sqrt{3\gamma\Omega_\phi}(2 - \gamma)\lambda, \\
\Omega'_\phi &= 3(1 - \gamma)\Omega_\phi(1 - \Omega_\phi), \\
\lambda' &= \sqrt{3\gamma\Omega_\phi}\lambda^2(1 - \Gamma), \\
b' &= -\frac{3}{2}b\Omega_\phi(1 - \gamma)
\end{aligned} \tag{6.25}$$

In order to solve the above set of 1st order ODEs numerically, we fix the initial conditions for γ, Ω_ϕ, λ at the decoupling epoch. For thawing models, the scalar field is initially frozen due to large Hubble damping, and this fixes the initial

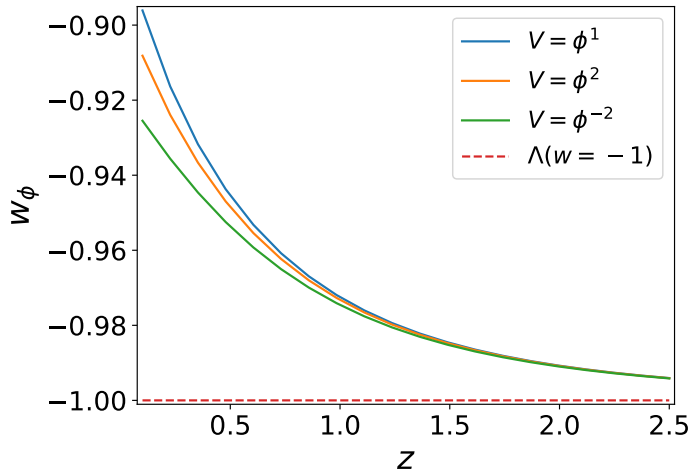

Figure 6.3: The figure shows the EoS (w_ϕ) as a function of redshift z for different quintessence field models after solving the autonomous ODE in (6.25). We kept the initial slope of the field $\lambda_i = 0.7$ in all the cases.

condition $\gamma_i \approx 0$. The quantity Γ which quantifies the shape of the potential is a constant for power law potentials. The parameter λ_i is the initial slope of scalar field and measures the deviation of ΛCDM model. For smaller λ_i the EoS (w_ϕ) of scalar field remain close to cosmological constant, whereas larger values of λ_i lead to a significant deviation from ΛCDM. Assuming the contribution of scalar field to the total energy density is negligibly small in the early universe, we fix the present value of Ω_ϕ. Similarly, we fix the initial value of b (related to the density parameter for baryons) so that one gets right value of the $\Omega_{b0} = 0.049$ [36] at the present epoch. Figure (6.3) shows the dynamical evolution of the EoS of quintessence field for three models. We note that there is no departure from the ΛCDM at large redshifts but a prominent model sensitive departure for small redshifts. At $z \sim 0.5$ there is almost a $\sim 5\%$ departure of the EoS parameter w_ϕ from that of the non-dynamical cosmological constant. The departure of w_ϕ from its ΛCDM value of -1, imprints on the growing mode of density perturbations by virtue of the changes that it brings to the Hubble parameter $H(z)$.

Growth of matter fluctuations in the linear regime provides a powerful complementary observation to put tighter constrains on cosmological parameters, and also break the possible degeneracy in diverse dark energy models. We have assumed spatially flat cosmology in our entire analysis and not

constrained radiation density, as only dark matter and dark energy are dominant in the late universe. The full relativistic treatment of perturbations for Quintessence dark energy has been studied [395]. Ignoring super-horizon effects, we note that on sub-horizon scales, ignoring the clustering of Quintessence field, the linearized equations governing the growth of matter fluctuations is given by the ODE [470, 471]

$$D''_+ + \left(1 + \frac{\mathcal{H}'(a)}{\mathcal{H}(a)}\right) D'_+ - \frac{3}{2}\Omega_m(a) D_+ = 0. \tag{6.26}$$

Here, the prime denotes differentiation w.r.t to '$\log a$', $\mathcal{H}$ is the conformal Hubble parameter defined as $\mathcal{H} = aH$ and δ_m is the linear density contrast for the dark matter. In order to solve the above ODE, we fix the initial conditions D_+ grows linearly with a and the first derivative of $\frac{dD_+}{da} = 1$ at early matter dominated epoch ($a = 0.001$). We now consider the BAO imprint on the cross-correlation angular power spectrum to make error predictions on Quintessence dark energy parameters which affects both background evolution and structure formation.

6.3.1 Statistical analysis and constraints on model parameters

Markov Chain Monte Carlo (MCMC) sampling provides an elegant way to assess the parameters of a model, even if the corresponding posterior distribution is not accessible analytically. Monte Carlo approaches aim at approximating a target probability density $p(x), x \in X$ (with X being a high-dimensional space) by generating an independent and identically distributed set of samples ${x^{(i)}}_{i=1}^{N}$. MCMC sampling combines the Monte Carlo principle of approximating a distribution by drawing random samples with the principle of Markov chains, which offers a mathematical framework to ensure that the derived sample has the desired properties.

In this method, the unknown parameters are the states of a Markov chain, and a proposal function that suggests a new set of parameters (based on the current) one replaces the transition matrix at each step. One popular method is the Metropolis-Hastings algorithm, which we introduce in our work [472, 473]. The method allows to approximate the posterior distribution even if it is not

possible to sample from it directly.

Let θ be the set of unknown parameters, $q(\theta_n \rightarrow \theta_{n+1})$ the proposal function, $L(\theta) = P(D|\theta)$ the likelihood function, and $\pi(\theta)$ a predefined prior. The Markov chain is created by starting with an initial set of parameters, and then repeatedly suggesting a new one and either accepting or rejecting it by turns. The proposal/acceptance steps are repeated until the chain has converged, and a sufficiently large sample has been obtained. This procedure is delineated as follows:

1. Initialize θ_0

2. Proposal step: Given θ_n, draw a candidate θ_0 from the proposal distribution $q(\theta_n \rightarrow \theta_0)$

3. Calculate the quantity $A = \frac{L(\theta_0)}{L(\theta_n)} \cdot \frac{\pi(\theta_0)}{\pi(\theta_n)} \cdot \frac{q(\theta_0 \rightarrow \theta_n)}{q(\theta_n \rightarrow \theta_0)}$

4. Acceptance step: With probability $\min(A, 1)$, let $\theta_{n+1} = \theta_0$ (accept). Otherwise, let $\theta_{n+1} = \theta_n$ (reject)

5. Increment n by one and repeat steps 2 and 3 or 4 until convergence.

In step 3 and 4 allows deciding upon acception / rejection of the newly suggested parameter set based on the true posterior distribution. We have modified and used the publicly available * for our analysis.

We choose the following parameters $(h, \Gamma, \lambda_i, \Omega_{\phi 0})$ to quantify the Quintessence dark energy. We have use uniform priors for these parameters in the Quintessence model. The Hubble parameter at present (z = 0) in our subsequent calculations is assumed to be $H_0 = 100hKm/s/Mpc$, thus define the dimensionless parameter h. We perform a Markov Chain Monte Carlo (MCMC) analysis using the observational data to constraint the model parameters and evolution of cosmological quantities. The analysis is carried out using the Python implementation of MCMC sampler introduced by [474]. We take flat priors for these parameters with ranges of $h \in [0.5, 0.9]$, $\Gamma \in [-1.5, 1.5]$, $\lambda_i \in [0.5, 0.8], \Omega_{\phi 0} \in [0.5, 0.8]$.

*https://github.com/dfm/emcee

Parameters	$\Omega_{\phi 0}$	Γ	λ_i	h
Constraints (BAO only)	$0.660^{0.064}_{-0.049}$	$0.091^{0.784}_{-1.080}$	$0.575^{0.067}_{-0.050}$	$0.723^{0.038}_{-0.036}$
Constraints (BAO+CC+$f\sigma_8$+SN)	$0.616^{0.034}_{-0.020}$	$0.157^{0.895}_{-0.956}$	$0.548^{0.049}_{-0.036}$	$0.701^{0.016}_{-0.015}$

Table 6.3: The parameter values, obtained in the MCMC analysis combining all the data sets are tabulated along the $1-\sigma$ uncertainty.

We first perform the MCMC analysis for the using the error bars obtained on the binned $H(z)$ and D_A from the proposed 21-cm weak lensing cross-correlation. The figure (7.6) shows the marginalized posterior distribution of the set of parameters and $(h, \Gamma, \lambda_i, \Omega_{\phi 0})$ the corresponding 2D confidence contours are obtained for the model $V(\phi) \sim \phi$. The results are summarized in table(7.2).

For a joint analysis, we employ three mainstream cosmological probes, namely cosmic chronometers (CC), Supernovae Ia (SN) and $f\sigma_8$. We have used the observational measurements of Hubble expansion rate as a function of redshift using cosmic chronometers (CC) as compiled by [475]. The distance modulus measurement of type Ia supernovae (SN), is adopted from the Joint Light-cone Analysis sample from [476]. We also incorporated the linear growth rate data, namely the $f\sigma_8(z)(\equiv f(z)\sigma_8 D_m(z))$ from the measurements by various galaxy surveys as compiled by [477]. The posterior probability distributions of the parameters and the corresponding 2D confidence contours are shown in figure (7.6). The constraint obtained for different parameters are shown in table (7.2). The joint analysis gives improved constraints compared to the constraints obtained from the analysis of only our projected BAO results. These constraints are also competitive with other probes [478–480].

6.4 Conclusion

In this work, we have explored the cross-correlation signal of weak galaxy lensing and HI 21-cm. From the tomographic study we estimated the projected errors on the $H(z)$, $D_A(z)$ and $D_V(z)$ over a redshift range $z \sim 0-3$. The quantities of interest namely $H(z)$ and $D_A(z)$ explicitly appears in the lensing

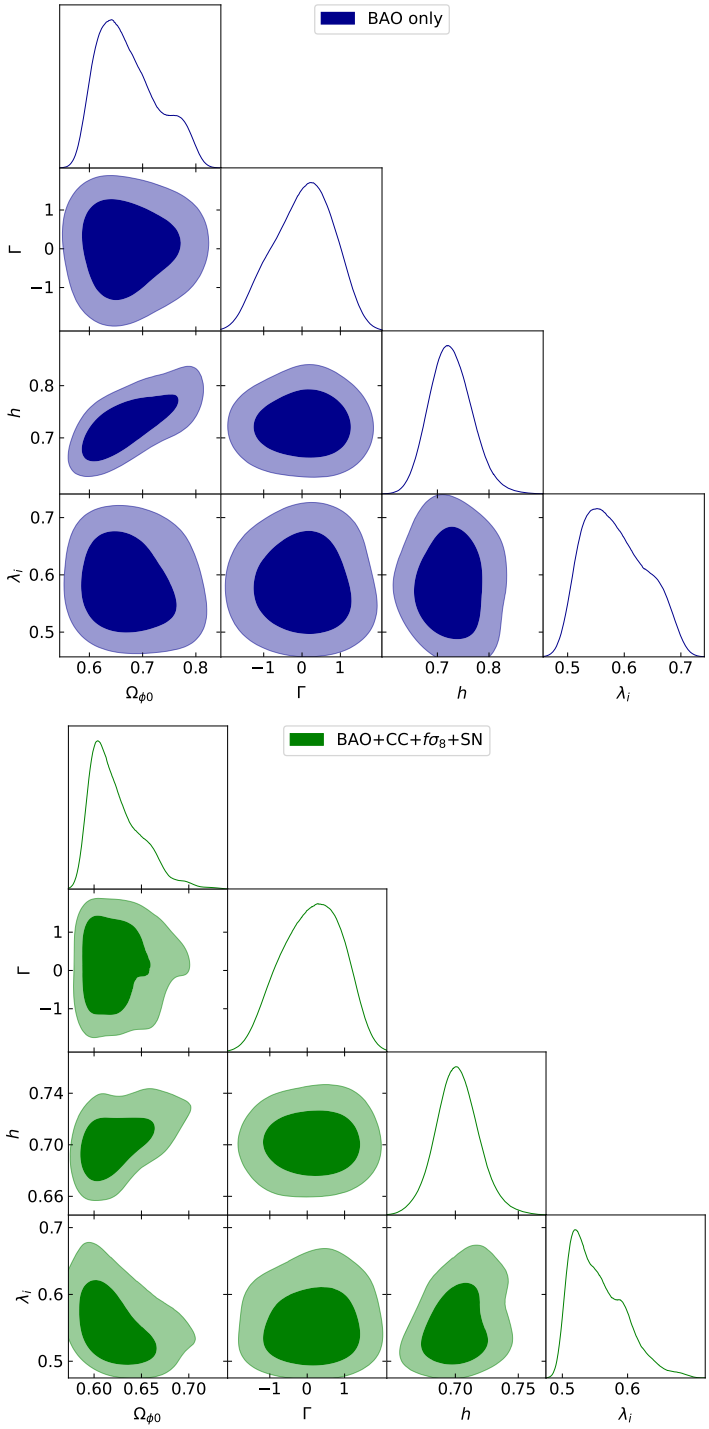

Figure 6.4: Marginalized posterior distribution of the set of parameters and $(\Omega_{\phi 0}, \Gamma, \lambda_i, h)$ corresponding 2D confidence contours obtained from the MCMC analysis for the model $V(\phi) \sim \phi$. Left panel: utilizing the information from the fisher matrix only. Right panel: utilizing all the data sets mentioned in the discussion on the top of the fisher information.

kernel and also in the BAO feature of the power spectrum. The cross-angular spectrum involve a radial integral and hence loses the redshift information. We have obtained tomographic information by locating the 21-cm slice at different redshift bins before cross-correlating.

Several observational challenges come in the way of measuring the cosmological 21-cm signal. The 21-cm signal is buried deep under galactic and extra-galactic foregrounds [295]. We have assumed that this key challenge is addressed. Even after significant foreground removal, the cosmological origin of the 21 cm signal can only be ascertained only through a cross-correlation [278, 352, 355]. The foregrounds for the two individual probes are expected to be significantly uncorrelated and hence leads to negligible effects in the observing cross-correlation power spectrum. We have not considered systematic error which arises from photometric redshift (or so called photo-z) errors which may significantly degrade the cosmological information in the context of lensing auto-correlation [77].

The BAO estimates of $H(z)$, $D_A(z)$ allows us to probe dark energy models. We have considered the quintessence scalar field as a potential dark energy candidate and studied the background dynamics as well as the growth perturbation in linear regime in such a paradigm. A Baysean parameter estimation using our BAO estimates indicate the possibility of good constraints on scalar field models. The constraints also improve when joint analysis with other probes is undertaken and reaches precision levels competitive with the existing literature.

CHAPTER 7

Post-reionization HI 21-cm signal: A probe of negative cosmological constant [§]

7.1 Introduction

We have seen that the ΛCDM model [20, 21, 481] provides a good description towards explaining most properties of a wide range of astrophysical and cosmological data, including distance measurements at high redshifts [9, 102, 113], the cosmic microwave background (CMB) anisotropies power spectrum [12], the statistical properties of large scale structures of the Universe [482] and the observed abundances of different types of light nuclei [483–485]. All these observations point towards an accelerated expansion history of the Universe.

Despite the overwhelming success of the ΛCDM model as a standard model explaining these diverse observations, it still leaves significant uncertainties and is plagued with difficulties [29, 30, 32, 33, 458, 486–489]. We have indicated some of the observational anomalies with the ΛCDM model at a $> 2-3\sigma$ level, like the Hubble tension [138, 490–493]/ growth tension [40, 140, 494] CMBR anomalies [42, 142], BAO discrepancy [43, 44, 144] and many others [137].

A positive cosmological constant is sometimes interpreted as a scalar field at the positive minimum of its potential by moving the term $\Lambda g_{\mu\nu}$ to the right-hand side of the Einstein's equation to include it in the energy momentum tensor $T_{\mu\nu}$. A Quintessence [55, 199, 201, 202] scalar field, on the contrary, slowly rolls towards the minimum in the positive part of the potential giving rise to a dynamical dark energy with a time dependent equation of state $w(a) = P_{DE}/\rho_{DE}$. Several reports of the Hubble tension [141, 486, 489, 495–499] has led to the proposal of a wide range of dark energy models. There are certain

[§]The chapter is adapted from *Post-reionization HI 21-cm signal: A probe of negative cosmological constant, Chandrachud B.V Dash, Tapomoy Guha Sarkar, Anjan A. Sen* , Monthly Notices of the Royal Astronomical Society, (527), February 2024

proposed quintessence models with an AdS vacuum [65, 500–504] which do not rule out the possibility of a negative Λ. We have considered Quintessence models, with a non zero vacuum, which can be effectively seen as as a rolling scalar field ϕ on top of a cosmological constant $\Lambda \neq 0$. The combination $\rho_{_{DE}} = \rho_\phi + \Lambda$ satisfying the energy condition $\rho_{DE} > 0$ drives an accelerated expansion [8].

We consider the post-reionization HI 21 cm brightness temperature maps as a tracer of the underlying dark matter distribution and thereby a viable probe of structure formation. The intensity mapping [78] of the post-reionization HI 21 cm signal [256] is a promising observational tool to measure cosmological evolution and structure formation tomographically [255, 256, 397].

In this work, we have made projections of uncertainties on the dark energy parameters in Quintessence models, with a non zero vacuum, using a proposed future observation of the power spectrum of the post-reionization 21 cm signal. We have used a Fisher/Monte-carlo analysis to indicate how the error projection on the binned power spectrum allow us to constrain dark energy models with a negative Λ.

The chapter is organized as follows: In Section-2 we discuss the dark energy models and constraints of observable quantities like the Hubble parameter and growth rate of density perturbations from diverse observations. In Section-3 we discuss the 21-cm signal from the post reionization epoch and noise projections using the futuristic SKA1-mid observations. We also constrain dark energy model parameters using Markov Chain Monte Carlo (MCMC) simulation. We finally look at the anisotropic 21-cm power spectrum in redshift space using a new quantifier of the AP effect and show how we can constrain dark energy models using this probe of dark energy. We discuss our results and other pertinent observational issues in the concluding section.

7.2 Quintessence dark energy with non-zero vacuum

We consider a Universe where the Quintessence field (ϕ) and cosmological constant Λ both contribute to the overall dark energy density i.e. $\rho_{DE} = \rho_\phi + \Lambda$ with the constraint that $\rho_{DE} > 0$ to ensure the late time cosmic acceleration

[8]. Instead of working with a specific form of the Quintessence potential we chose to use a broad equation of state (EoS) parametrization $w_\phi(z)$. It has been shown that at most a two-parameter model can be optimally constrained from observations [205]. We use the CPL model proposed by CHEVALLIER and POLARSKI [206] and Linder [150] which gave a phenomenological model-free parametrization and incorporate several features of dark energy. This model has been extensively used by the Dark Energy Task force [23] as the standard two parameter description of dark energy dynamics. It has also been shown that a wide class of quintessence scalar field models can be mapped into the CPL parametrization [388]. The equation of state (EoS) is given by

$$w_\phi(z) = w_0 + w_a \left(\frac{z}{1+z}\right).$$

This model gives a smooth variation of $w_\phi(z) = w_0 + w_a$ as $z \to \infty$ to $w_\phi(z) = w_0$ for $z = 0$ and the corresponding density of the quintessence field varies with redshift as $\rho_\phi(a) \propto a^{-3(1+w_0+w_a)} \exp^{3w_a a}$. In a spatially flat Universe, evolution of the Hubble parameter $H(a)$ is given by

$$\frac{H(a)}{H_0} = \sqrt{\Omega_{m_0} a^{-3} + \Omega_{\phi 0} \exp\left[-3\int_1^a da' \frac{1+w_\phi(a')}{a'}\right] + \Omega_{\Lambda 0}} \tag{7.1}$$

with $\Omega_{m0} + \Omega_{\phi 0} + \Omega_\Lambda = 1$. We shall henceforth call this model with Λ along with a scalar field as the CPL-ΛCDM model.

We consider two important cosmological observables. Firstly we consider a dimensionless quantifier of cosmological distances [1]

$$r_{_{BAO}}(z) = \frac{r_s}{D_{_V}(z)} \tag{7.2}$$

where r_s denotes the sound horizon at the drag epoch and $D_{_V}(z)$ is the BAO effective distance D_V [25] is defined as

$$D_{_V}(z) = \left[(1+z)^2 D_A^2(z) \frac{cz}{H(z)}\right]^{1/3} \tag{7.3}$$

This dimension-less distance $r_{_{BAO}}$ is a quantifier of the background cosmological model (density parameters) and is thereby sensitive to the dynamical

evolution of dark energy.

Secondly, we use the growth rate of density fluctuations as a quantifier of cosmological structure formation. Clustering of galaxies in spectroscopic surveys [7], counts of galaxy clusters [505, 506] aim to measure the quantity called the growth rate of matter density perturbations and the root mean square normalization of the matter power spectrum σ_8 given by:

$$f(a) \equiv \frac{d \ \log \ D_+(a)}{d \ \log \ a} \ \text{ and } \ \sigma_8(a) \equiv \sigma_{8,0} \frac{D_+(a)}{D_+(a=1)} \tag{7.4}$$

A more robust and reliable quantity $f\sigma_8(a)$ that is measured by redshift surveys is the combination of the growth rate $f(a)$ and $\sigma_8(a)$. Figure (7.1) shows variation of r_{BAO} in the (Ω_Λ, w_0) plane for the CPL-ΛCDM model with $H_0 = 72$ Km/s/Mpc. We have chosen $w_a = 0$ for simplicity. Further, we have kept the r_s fixed to the value computed for the fixed Ω_m and Ω_b from ΛCDM model [36]. We note that r_s does not change much with Ω_ϕ Ω_Λ.

We note that Ω_Λ is negative in the second and third quadrant. The red contour line corresponds to the observational data and the blue shaded region depicts the 1σ errors. The first figure in the panel corresponds to $z = 0.2$ and the red contour corresponds to observations from the 2df galaxy redshift survey gives the bounds on $r_{_{BAO}}$ as $r_{_{BAO}}(z = 0.2) = 0.1980 \pm 0.0058$ [3]. The second figure in the panel corresponds to $z = 0.35$ with measured $r_{_{BAO}}(z = 0.35) = 0.1094 \pm 0.0033$ [3]. The analysis of BOSS (SDSS III) CMASS sample along with Luminous red galaxy sample [4] from SDSS-II gives $r_{_{BAO}}(z = 0.57) = 0.07315 \pm 0.002$, as is shown in the third figure of the panel. We also show the contour for r_{BAO} at the corresponding to that redshift for a pure ΛCDM cosmology with cosmological parameters [36] results $(\Omega_{m_0}, \Omega_{b_0}, H_0, n_s, \sigma_8, \Omega_K) = (0.315,\ 0.0496,\ 67.4,\ 0.965,\ 0.811,\ 0)$. All these observations are consistent with the possibility of models with negative Λ with varying uncertainties. It is clear from the observations that there are two separate regions consistent with data: The third quadrant corresponds to Phantom models with negative Λ and the first quadrant which corresponds to non-phantom models with positive Λ. It is also clear that in spatially flat cosmologies with conditions $\rho_m > 0$ and $\rho_\phi > 0$ implies that $\Omega_\Lambda < 1$ which is not supported by data. The addition of a neg-

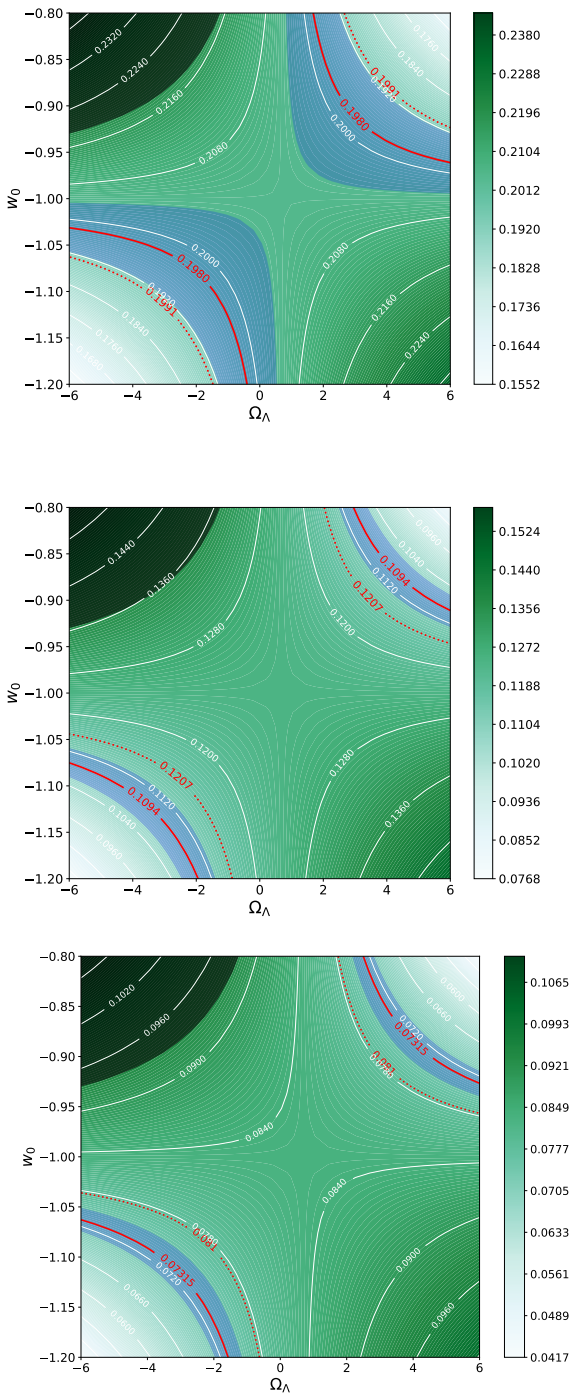

Figure 7.1: shows r_{BAO} in the (Ω_Λ, w_0) plane. The red contour line corresponds to the observational data point and the blue shaded region depicts the 1σ errors. The data points in the left two figures come from the 2df galaxy survey at redshifts of $z = 0.2$ and $z = 0.35$ respectively [3] and the third figure shows the high redshift data at $z = 0.57$ from BOSS SDSS-III survey [4]. The red dotted contour correspond to r_{BAO} computed for a ΛCDM model. The grey sectors correspond to the models for which the Universe did not ever go through an accelerated phase till that redshift.

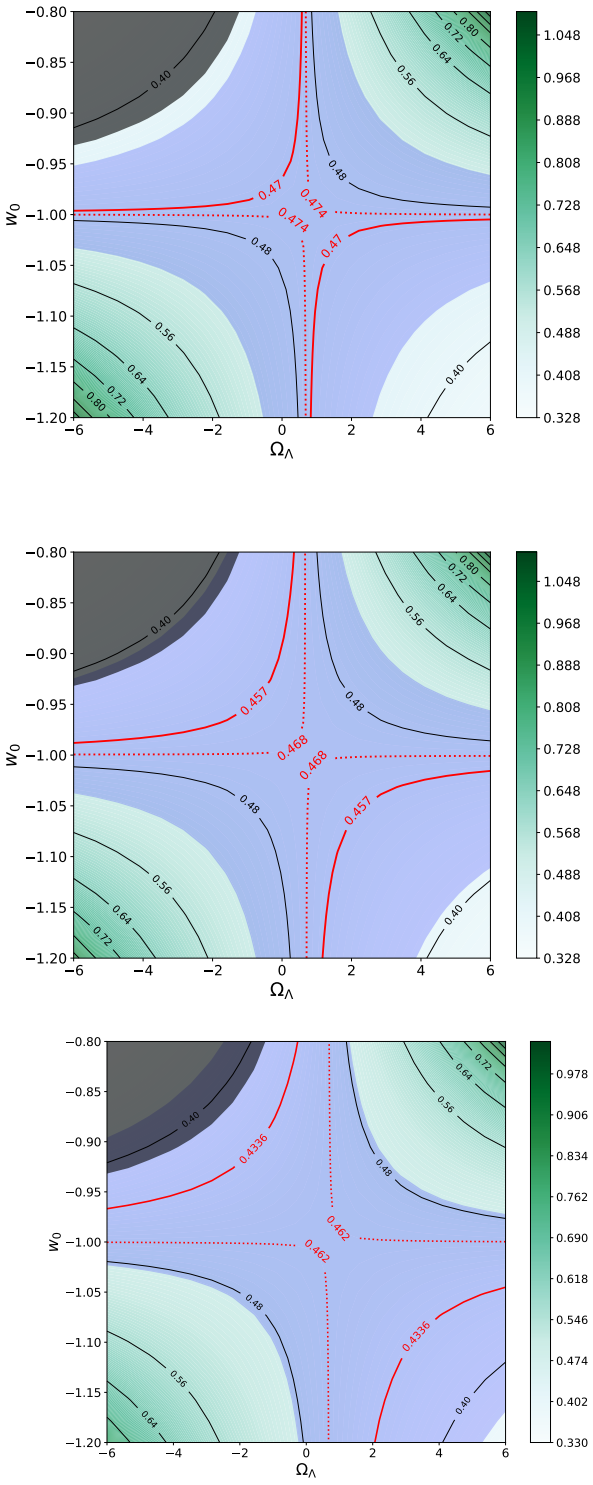

Figure 7.2: shows variation of $f\sigma_8(z)$ in the (Ω_Λ, w_0) plane. The solid red line corresponds to the observational data points from SDSS-III BOSS $f\sigma_8(z = 0.51) = 0.470 \pm 0.041$ [5], $f\sigma_8(z = 0.61) = 0.457 \pm 0.052$ [6] and eBOSS DR16 LRGxELG data $f\sigma_8(z = 0.7) = 0.4336 \pm 0.05003$ [7]. The red dotted contour corresponds to $f\sigma_8(z)$ computed for a ΛCDM model. The grey sectors correspond to the models for which the Universe did not ever go through an accelerated phase till that redshift.

ative cosmological constant to a phantom dark energy model seems viable from the data. We find that the CPL-Λ CDM with a phantom field and negative Λ and $H_0 = 72$ Km/s/Mpc, the observational data as also ΛCDM with $H_0 = 67.4$Km/s/Mpc are all qualitatively consistent. We note that while computing r_{BAO}, the sound horizon distance r_s is fixed to the value computed for Ω_m and Ω_b from [36] since r_s does not change much with Ω_ϕ Ω_Λ.

Figure (7.2) shows variation of $f\sigma_8(z)$ in the (Ω_Λ, w_0) plane. The solid red line corresponds to the observational data from SDSS-III BOSS $f\sigma_8(z = 0.51) = 0.470 \pm 0.041$ [5], $f\sigma_8(z = 0.61) = 0.457 \pm 0.052$ [6] and eBOSS DR16 LRGxELG data $f\sigma_8(z = 0.7) = 0.4336 \pm 0.05003$ [7] respectively. While the mean observational $f\sigma_8$ data falls in the non-phantom sector with negative Λ, the error bars are quite large and again, the ΛCDM predictions (with $H_0 = 67.4$Km/s/Mpc), observed data and CPL-ΛCDM with phantom field and negative Λ for $H_0 = 72$ Km/s/Mpc are all consistent within $1 - \sigma$ errors. The addition of a negative Λ to a phantom dark energy model seems to also push H_0 to a higher value.

In models with negative cosmological constants there are regions in the $(w_0 - \Omega_\Lambda)$ which corresponds to cosmologies which never had an accelerated phase in the past or had a transient accelerated phase or $H^2(z) < 0$. These regions are studied in an earlier work [65]. In the range of $(w_0 - \Omega_\Lambda)$ shown in the above figures we have shaded these regions where the acceleration parameter became negative, corresponding to the fact that in these models, the universe did not ever accelerate upto that redshift.

7.2.1 The post-reionization 21cm power spectrum: The Alcock-Paczyski anisotropy in redshift space

The power spectrum of post-reionization HI 21-cm excess brightness temperature field δT_b from redshift z [78, 241, 256, 283] is given by

$$P_{21}(k, z, \mu) = \mathcal{A}_T^2 (b_T + f\mu^2)^2 P_m(k, z) \tag{7.5}$$

where

$$\mathcal{A}_T = 4.0\,\mathrm{mK}\, b_T\, \bar{x}_{\mathrm{HI}} (1+z)^2 \left(\frac{\Omega_{b0}h^2}{0.02}\right)\left(\frac{0.7}{h}\right)\left(\frac{H_0}{H(z)}\right) \tag{7.6}$$

The term $f(z)\mu^2$ has its origin in the HI peculiar velocities [83, 256] which, is also assumed to be sourced by the dark matter fluctuations. Since our cosmological model is significantly different from the fiducial one (i.e., ΛCDM), the difference will introduce additional anisotropies in the correlation function through the Alcock-Paczynski effect [507–509]. In the presence of the Alcock-Paczynski effect, the redshift-space HI 21-cm power spectrum is given by: [78, 241]

$$P_{21}(k,z,\mu) = \frac{\mathcal{A}_T^2}{\alpha_\parallel \alpha_\perp^2}\left[b_T + \frac{f(z)\mu^2}{F^2+\mu^2(1-F^2)}\right]^2 P_m\left(\frac{k}{\alpha_\perp}\sqrt{1+\mu^2(F^{-2}-1)}, z\right) \tag{7.7}$$

where $F = \alpha_\parallel/\alpha_\perp$, with $\alpha_\parallel$ and $\alpha_\perp$ being the ratios of angular and radial distances between fiducial and real cosmologies, $\alpha_\parallel = H^f/H^r$, $\alpha_\perp = D_A^r/D_A^f$. The overall factor $\alpha_\parallel\alpha_\perp^2$ is due to the scaling of the survey's physical volume. As the real geometry of the Universe differs from the one predicted by the fiducial cosmology, we introduce additional distortion in the redshift space. The AP test is sensitive to the isotropy of the Universe and can help differentiate between different cosmological models. We note that the geometric factors shall also imprint in the BAO feature of the power spectrum. Since $0 \leq \mu 1$ the redshift space 21cm power spectrum can be decomposed in the basis of Legendre polynomials $\mathscr{P}_\ell(\mu)$ as [510]

$$P_{21}(k,\mu,z) = \sum_\ell P_\ell(z,k)\mathscr{P}_\ell(\mu) \tag{7.8}$$

The odd harmonics vanish by pair exchange symmetry and non-zero azimuthal harmonics. (as $Y_{\ell,m}$'s with $m \neq 0$ vanish by symmetry about the line of sight). Using the standard normalization

$$\int_{-1}^{+1} \mathscr{P}_\ell(\mu)\mathscr{P}_r(\mu)d\mu = \frac{2}{2\ell+1}\delta_{\ell,r}$$

the first few Legendre polynomials are given by

$$\mathscr{P}_0(\mu) = 1, \quad \mathscr{P}_2(\mu) = \frac{1}{2}\left(3\mu^2-1\right), \quad \mathscr{P}_4(\mu) = \frac{1}{8}(35\mu^4 - 30\mu^2 + 3) \tag{7.9}$$

The coefficients of the expansion of the 21cm power spectrum, can be found by inverting the equation (7.8). Thus, we have

$$P_\ell(z,k) = \frac{(2\ell+1)}{2}\int_{-1}^{+1} d\mu\ \mathscr{P}_\ell(\mu)P_{21}(z,k,\mu) \tag{7.10}$$

While full information is contained in an infinite set of functions $\{P_\ell(z,k)\}$, we shall be interested in the first few of these function which has the dominant information.

7.2.2 The BAO feature in the multipoles of 21-cm power spectrum

The sound horizon at the drag epoch ($z \sim 1000$) provides a standard ruler, which can be used to calibrate cosmological distances. Baryons imprint the cosmological power spectrum through a distinct oscillatory signature [126, 127]. The BAO imprint on the 21-cm signal has been studied extensively [462, 463]. The baryon acoustic oscillation (BAO) is an important probe of cosmology [1, 3, 4, 128, 462] as it allows us to measure the angular diameter distance $D_A(z)$ and the Hubble parameter $H(z)$ using the transverse and the longitudinal oscillatory features respectively [120].

The sound horizon at the drag epoch is given by

$$s(z_d) = \int_0^{a_{drag}} \frac{c_s da}{a^2 H(a)} \tag{7.11}$$

where a_{drag} is the scale factor at the drag epoch redshift z_d and c_s is the sound speed given by $c_s(a) = c/\sqrt{3(1+3\rho_b/4\rho_\gamma)}$ where ρ_b and ρ_γ denotes the baryonic and photon densities, respectively. The Planck 2018 constrains the value of z_d and $s(z_d)$ to be $z_d = 1060.01 \pm 0.29$ and $s(z_d) = 147.21 \pm 0.23$Mpc [36]. We shall use these as the fiducial values in our subsequent analysis. The standard ruler 's' defines a transverse angular scale and a redshift interval in the radial direction as

$$\theta_s(z) = \frac{s(z_d)}{(1+z)D_A(z)} \qquad \delta z_s = \frac{s(z_d)H(z)}{c} \tag{7.12}$$

Measurement of θ_s and δz_s, allows the independent determination of $D_A(z)$

and $H(z)$. The BAO feature comes from the baryonic part of $P(k)$. In order to isolate the BAO feature, we subtract the cold dark matter power spectrum from total $P(k)$ as $P_b(k) = P(k) - P_c(k)$. Owing to significant deviations between the assumed cosmology and the fiducial cosmology, our longitudinal and tangential coordinates are rescaled by $\alpha_\parallel$ and $\alpha_\perp$ respectively, the true power spectrum scaled as $k' = k\sqrt{1+\mu^2(F^{-2}-1)}/\alpha_\perp$ from the apparent one [507, 511, 512]. Incorporating the Alcock-Paczynski corrections explicitly in the BAO power spectrum can be written as [465, 466]

$$P_b(k') = A\frac{\sin x}{x}e^{-(k'\sum_s)^{1.4}}e^{-k'^2\sum_{nl}^2/2} \tag{7.13}$$

where A is a normalization, $\sum_s = 1/k_{silk}$ and $\sum_s = 1/k_{nl}$ denotes the inverse scale of 'Silk-damping' and 'non-linearity' respectively. In our analysis we have used $k_{nl} = (3.07h^{-1}Mpc)^{-1}$and $k_{silk} = (8.38h^{-1}Mpc)^{-1}$ from Seo and Eisenstein [466] and $x = \sqrt{k^2(1-\mu^2)s_\perp^2 + k^2\mu^2 s_\parallel^2}$. The changes in $D_A(z)$ and $H(z)$ are reflected as changes in the values of $s_\perp$ and $s_\parallel$ respectively, and the errors in $s_\perp$ and $s_\parallel$ corresponds to fractional errors in D_A and $H(z)$ respectively. We use $p_1 = \ln(s_\perp^{-1})$ and $p_2 = \ln(s_\parallel)$ as parameters in our analysis. The Fisher matrix is given by

$$F_{ij} = \left(\frac{2\ell+1}{2}\right)\int dk' \int_{-1}^{+1} d\mu \frac{A_T^2}{\alpha_\parallel\alpha_\perp^2}\left[b_T + \frac{f(z)\mu^2}{F^2+\mu^2(1-F^2)}\right]^2 \frac{\mathscr{P}_\ell(\mu)}{\delta P_{21}^2(k,z,\mu)}\frac{\partial P_b(k')}{\partial p_i}\frac{\partial P_b(k')}{\partial p_j} \tag{7.14}$$

$$= \left(\frac{2\ell+1}{2}\right)\int dk' \int_{-1}^{+1} d\mu \frac{A_T^2}{\alpha_\parallel\alpha_\perp^2}\left[b_T + \frac{f(z)\mu^2}{F^2+\mu^2(1-F^2)}\right]^2 \frac{\mathscr{P}_\ell(\mu)}{\delta P_{21}^2(k,z,\mu)} \left(\cos x - \frac{\sin x}{x}\right)^2 f_i f_j A^2 e^{-2(k'\sum_s)^{1.4}} e^{-k'^2\sum_{nl}^2} \tag{7.15}$$

where $f_1 = \mu^2 - 1$ and $f_2 = \mu^2$.

We choose SKA's a Medium-Deep Band-2 survey that covers a sky area of 5,000 $\deg^2$ in the frequency range $0.95 - 1.75$GHz ($z = [0-0.5]$) and a Wide Band-1 survey that covers a sky area of 20,000 $\deg^2$ in the frequency range $0.35-1.05$GHz ($z = [0.35-3]$) [513]. We calculate the expected error projections

on $D_A(z)$ and $H(z)$ in five evenly spaced, non-overlapping redshift bins, in the redshift range [z=0-3] with $\Delta z = 0.5$. Each of the six bins is taken to be independent and is centered at redshifts of $z = [0.25, 0.75, 1.25, 1.75, 2.25]$.

7.2.3 Visibility correlation

We use a visibility correlation approach to estimate the noise power spectrum for the 21-cm signal [82, 253, 291, 353, 468, 469]. A radio interferometric observation measures the complex visibility. The measured visibility written as a function of baseline $\mathbf{U} = (u, v)$ and frequency ν is a sum of signal and noise

$$\mathcal{V}(\mathbf{U}, \nu) = \mathcal{S}(\mathbf{U}, \nu) + \mathcal{N}(\mathbf{U}, \nu) \tag{7.16}$$

$$\mathcal{S}(\mathbf{U}, \nu) = \frac{2k_B}{\lambda^2} \int d\vec{\theta}\, A(\vec{\theta}) e^{2\pi i \mathbf{U}\cdot\vec{\theta}}\, \delta T_b(\vec{\theta}, \nu) \tag{7.17}$$

where, $\delta T_b(\vec{\theta}, \nu)$ is the fluctuations of the 21-cm brightness temperature and $A(\vec{\theta})$ is the telescope beam. The factor $\left(\frac{2k_B}{\lambda^2}\right)^2$ converts brightness temperature to intensity (Raleigh Jeans limit). Defining $\Delta\nu$ as the difference from the central frequency, a further Fourier transform in frequency $\Delta\nu$ gives us

$$s(\mathbf{U}, \tau) = \frac{2k_B}{\lambda^2} \int d\vec{\theta}\, d\nu\, A(\vec{\theta}) B(\Delta\nu)\, e^{2\pi i(\mathbf{U}\cdot\vec{\theta} + \tau\Delta\nu)}\, \delta T_b(\vec{\theta}, \nu) \tag{7.18}$$

where $B(\Delta\nu)$ is the frequency response function of the radio telescope.

$$\begin{aligned} s(\mathbf{U}_a, \tau_m) = \frac{2k_B}{\lambda^2} \int d\vec{\theta}\, d\Delta\nu \int \frac{d^3\mathbf{k}}{(2\pi)^3}\, e^{-i(\mathbf{k}_\perp \cdot \vec{\theta} + k_\parallel r' \Delta\nu)}\, A(\vec{\theta}) B(\Delta\nu) \\ e^{2\pi i(\mathbf{U}_a\cdot\vec{\theta} + \tau_m\Delta\nu)}\, \widetilde{\delta T_b}(\mathbf{k}_\perp, k_\parallel) \end{aligned} \tag{7.19}$$

where the tilde denotes a Fourier transform and $r' = dr(\nu)/d\nu$.

$$\begin{aligned} s(\mathbf{U}_a, \tau_m) = \frac{2k_B}{\lambda^2} \int d\vec{\theta}\, d\Delta\nu \int \frac{d^3\mathbf{k}}{(2\pi)^3}\, e^{-i(\mathbf{k}_\perp r - 2\pi\mathbf{U}_a)\cdot\vec{\theta}} e^{-i(k_\parallel r' - 2\pi\tau_m)\Delta\nu} \\ A(\vec{\theta}) B(\Delta\nu)\, \widetilde{\delta T_b}(\mathbf{k}_\perp, k_\parallel) \end{aligned} \tag{7.20}$$

Performing the $\vec{\theta}$ and $\Delta\nu$ integral we have

$$s(\mathbf{U}_a,\tau_m)=\frac{2k_B}{\lambda^2}\int\frac{d^3\mathbf{k}}{(2\pi)^3}\,\widetilde{A}\left(\frac{\mathbf{k}_\perp r}{2\pi}-\mathbf{U}_a\right)\widetilde{B}\left(\frac{k_\parallel r'}{2\pi}-\tau_m\right)\,\widetilde{\delta T_b}(\mathbf{k}_\perp,k_\parallel) \quad (7.21)$$

Defining new integration variables as $\mathbf{U}=\frac{\mathbf{k}_\perp r}{2\pi}$ and $\tau=\frac{k_\parallel r'}{2\pi}$ we have

$$\langle s(\mathbf{U}_a,\tau_m)s^*(\mathbf{U}_b,\tau_n)\rangle=\left(\frac{2k_B}{\lambda^2}\right)^2\frac{1}{r^2r'}\int d\mathbf{U}\,d\tau\widetilde{A}\left(\mathbf{U}-\mathbf{U}_a\right)\widetilde{A}^*\left(\mathbf{U}-\mathbf{U}_b\right)$$
$$\widetilde{B}\left(\tau-\tau_m\right)\widetilde{B}^*\left(\tau-\tau_n\right)P_{21}\left(\frac{2\pi\mathbf{U}}{r},\frac{2\pi\tau}{r'}\right) \quad (7.22)$$

Approximately, we may write

$$\int\widetilde{B}\left(\tau-\tau_m\right)\widetilde{B}^*\left(\tau-\tau_n\right)\approx B\delta_{m,n}\quad\text{and}\quad\int d\mathbf{U}\,\widetilde{A}\left(\mathbf{U}-\mathbf{U}_a\right)\widetilde{A}^*\left(\mathbf{U}-\mathbf{U}_b\right)\approx\frac{\lambda^2}{A_e}\delta_{a,b} \quad (7.23)$$

where B is the bandwidth of the telescope and where A_e is the effective area of each dish. Hence

$$\langle s(\mathbf{U}_a,\tau_m)s^*(\mathbf{U}_b,\tau_n)\rangle\approx\left(\frac{2k_B}{\lambda^2}\right)^2\frac{B\lambda^2}{r^2r'A_e}\;P_{21}\left(\frac{2\pi\mathbf{U}_a}{r},\frac{2\pi\tau}{r'}\right)\delta_{m,n}\delta_{a,b} \quad (7.24)$$

The noise in the visibilities measured at different baselines and frequency channels are uncorrelated. We then have

$$\langle\mathcal{N}(\mathbf{U}_a,\nu_m)\,\mathcal{N}^*(\mathbf{U}_b,\nu_n)\rangle=\delta_{a,b}\delta_{m,n}2\sigma^2 \quad (7.25)$$

where

$$\sigma=\frac{\sqrt{2}k_BT_{sys}}{A_e\sqrt{\Delta\nu t}} \quad (7.26)$$

where A_e is the effective area of the dishes, t is the correlator integration time and $\Delta\nu$ is the channel width. If B is the observing bandwidth, there would be $B/\Delta\nu$ channels. The system temperature T_{sys} can be written as

$$T_{sys}=T_{inst}+T_{sky} \quad (7.27)$$

where

$$T_{sky}=60\mathrm{K}\left(\frac{\nu}{300\ \mathrm{MHz}}\right)^{-2.5} \quad (7.28)$$

Under a Fourier transform

$$n(\mathbf{U},\tau) = \sum_{i=1}^{B/\Delta\nu} \mathcal{N}(\mathbf{U},\nu_i)\Delta\nu \;\; e^{2\pi i\nu_i\tau} \tag{7.29}$$

$$\langle n(\mathbf{U}_a,\tau)\; n^*(\mathbf{U}_b,\tau)\rangle = 2\sigma^2\delta_{a,b}\Delta\nu^2\frac{B}{\Delta\nu} = 2\sigma^2\delta_{a,b}\Delta\nu B \tag{7.30}$$

$$\langle n(\mathbf{U}_a,\tau)\; n^*(\mathbf{U}_b,\tau)\rangle = \frac{4k_B^2T_{sys}^2B}{A_e^2t} = \left(\frac{2k_B}{\lambda^2}\right)^2\left(\frac{\lambda^2T_{sys}}{A_e}\right)^2\frac{B}{t} \tag{7.31}$$

Now cosidering a total observation time T_o and a bin $\Delta\mathbf{U}$, there is a reduction of noise by a factor $\sqrt{N_p}$ where N_p is the number of visibility pairs in the bin

$$N_p = N_{vis}(N_{vis}-1)/2 \approx N_{vis}^2/2 \tag{7.32}$$

where N_{vis} is the number of visibilities in the bin. We may write

$$N_{vis} = \frac{N_{ant}(N_{ant}-1)}{2}\frac{T_o}{t}\rho(\mathbf{U})\delta^2U \tag{7.33}$$

where N_{ant} is the total number of antennas and $\rho(\mathbf{U})$ is the baseline distribution function.

$$\langle n(\mathbf{U}_a,\tau)\; n^*(\mathbf{U}_b,\tau)\rangle = \left(\frac{2k_B}{\lambda^2}\right)^2\left(\frac{\lambda^2T_{sys}B}{A_e}\right)^2\frac{2\delta_{a,b}}{N_{ant}(N_{ant}-1)B\;T_o\;\rho(\mathbf{U})\delta^2U} \tag{7.34}$$

where an additional reduction by $\sqrt{2}$ is incorporated by considering visibilities in half plane. The 21 cm power spectrum is not spherically symmetric, due to redshift space distortion but is symmetric around the polar angle ϕ. Because of this symmetry, we want to sum all the Fourier cells in an annulus of constant $(k,\; \mu = \cos\theta = k_\parallel/k)$ with radial width Δk and angular width $\Delta\theta$ for a statistical detection. The number of independent cells in such an annulus is

$$N_c = 2\pi k^2\sin(\theta)\Delta k\Delta\theta\frac{Vol}{(2\pi)^3} = 2\pi k^2\Delta k\Delta\mu\frac{Vol}{(2\pi)^3} \tag{7.35}$$

where

$$Vol = \frac{r^2\lambda^2 r' B}{A_e} \tag{7.36}$$

Thus the full covariance matrix for visibility correlation is [291, 353, 468, 469]

$$C_{a,b} = \frac{1}{\sqrt{N_c}}\left(\frac{2k_B}{\lambda^2}\right)^2\left[\frac{B\lambda^2}{r^2 r' A_e}\ P_{21}\left(\frac{2\pi \mathbf{U}_a}{r}, \frac{2\pi\tau}{r'}\right) + \left(\frac{\lambda^2 T_{sys} B}{A_e}\right)^2 \frac{2}{N_{ant}(N_{ant}-1)B\ T_o\ \rho(\mathbf{U})\delta^2 U}\right]\delta_{a,b}$$

We choose $\delta^2 U = A_e/\lambda^2$, $\Delta k = k/10$, $\Delta\mu = \mu/10$.

The baseline distribution function $\rho(\mathbf{U})$ is normalized as

$$\int d\mathbf{U}\rho(\mathbf{U}) = 1 \tag{7.37}$$

For uniform baseline distribution

$$\rho(\mathbf{U}) = \frac{1}{\pi(U_{max}^2 - U_{min}^2)} \tag{7.38}$$

Generally

$$\rho(\mathbf{U}) = c\int d^2\mathbf{r}\rho_{ant}(\mathbf{r})\rho_{ant}(\mathbf{r} - \lambda\mathbf{U}) \tag{7.39}$$

Where c is fixed by normalization of $\rho(\mathbf{U})$ and ρ_{ant} is the distribution of antennae. The covariance matrix in Eq (7.37) is used in our analysis to make noise projections on the 21-cm power spectrum and its multipoles. Observations with total time time exceeding a limiting value will make the instrumental noise insignificant and the Signal to Noise Ratio is primarily influenced by cosmic variance for such observations. Therefore, by introducing N_{point} as the number of independent pointings, the covariance is further reduced by a factor of $1/\sqrt{N_{point}}$.

7.3 Results and discussion

In this section we discuss the results of our investigation. The figure (7.3) shows the dimensionless 3D 21-cm power spectrum ($\Delta_{21}^2 = k^3 P_{21}(\mathbf{k}, z)/(2\pi^2)$) in redshift space at the fiducial redshift $z = 1$. In the plane of $k_\parallel$ and $k_\perp$, the

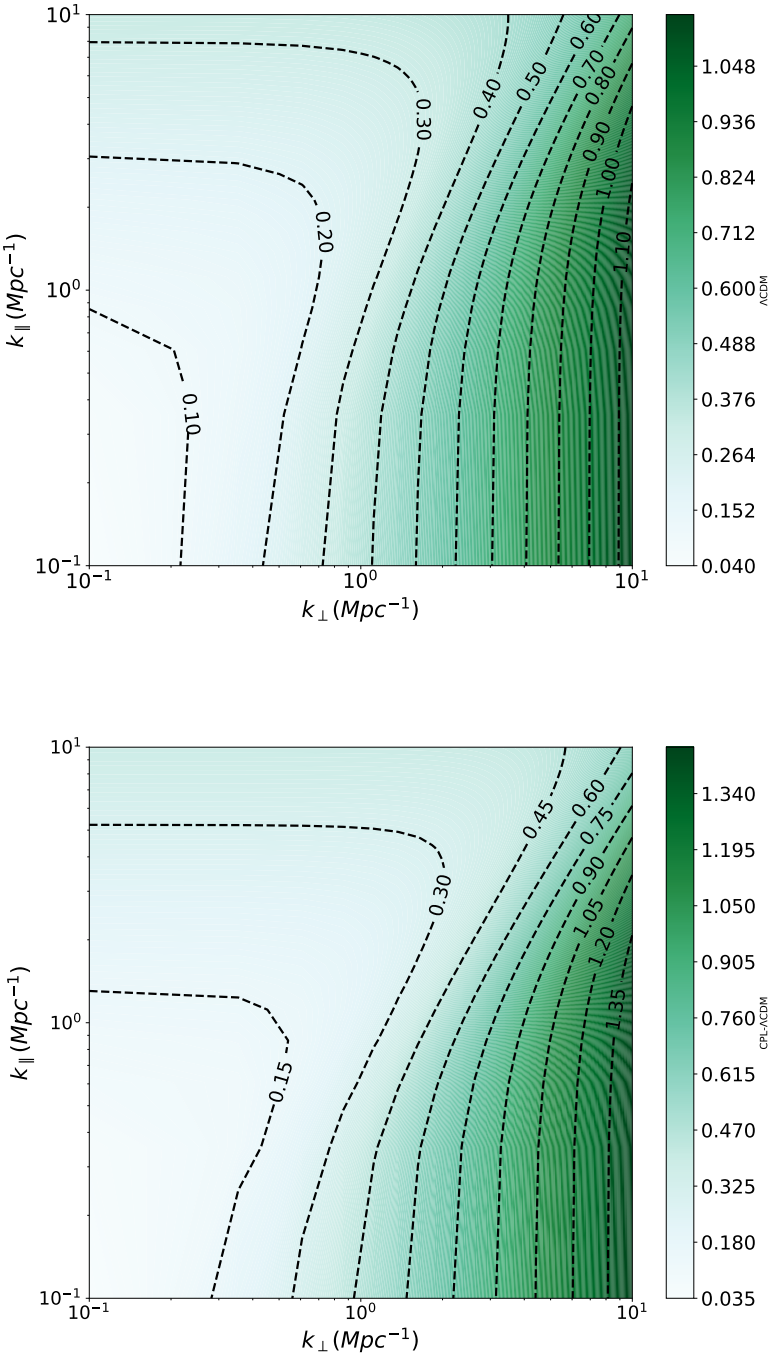

Figure 7.3: shows the 3D HI 21-cm power spectrum at $z = 1$ in the $(k_\perp, k_\parallel)$ space. The asymmetry in the signal is indicative of redshift space distortion: the left figure corresponds to the ΛCDM. In contrast, the right figure represents the CPL-ΛCDM model, where the Alcock-Paczynski effect enhanced the distortions. The colorbar shows the value of the dimensionless quantity $\Delta^2_{21} = k^3 P_{21}(\mathbf{k})/(2\pi^2)$ in mK^2.

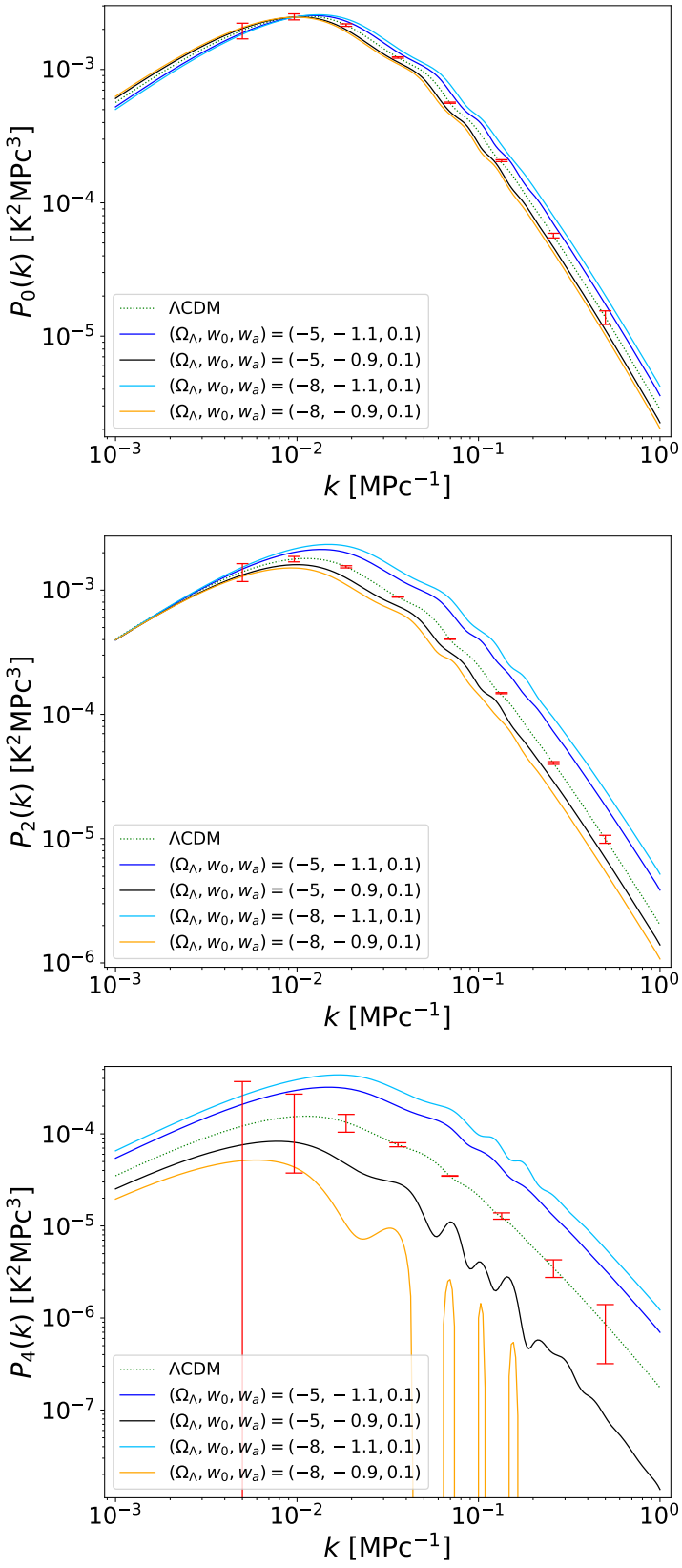

Figure 7.4: shows the 21-cm linear power spectrum monopole (top), quadrupole (middle) and hexadecapole (bottom) at redshift $z = 0.2$. The dotted line corresponds to ΛCDM.

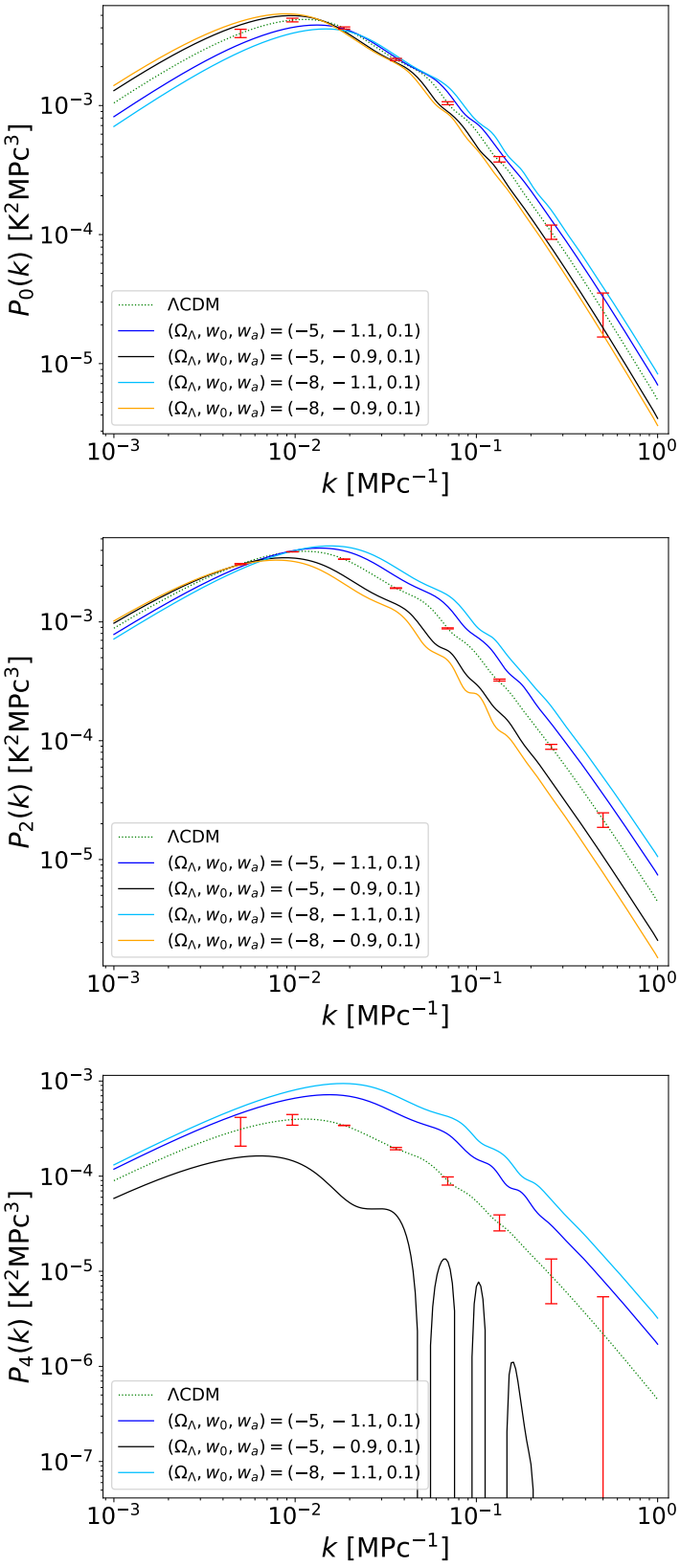

Figure 7.5: shows the 21-cm linear power spectrum monopole (top), quadrupole (middle) and hexadecapole (bottom) at redshift $z = 0.57$. The dotted line corresponds to ΛCDM.

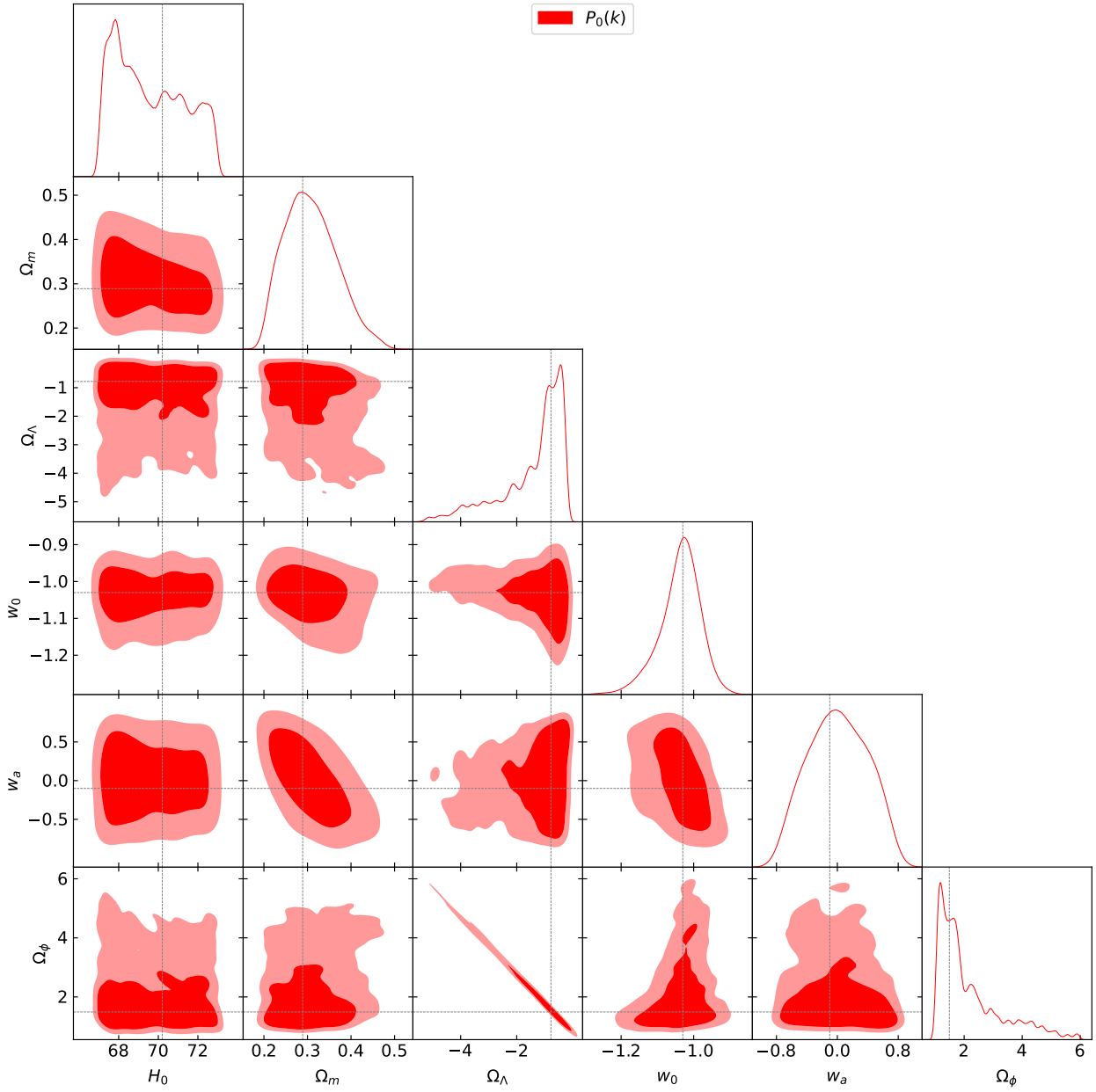

Figure 7.6: Marginalized posterior distribution of the set of parameters and $(H_0, \Omega_m, \Omega_\Lambda, w_0, w_a, \omega_\phi)$ corresponding 2D confidence contours obtained from the MCMC analysis. The fiducial model parameters are taken from Sen *et al.* [8]

N_{ant}	Antennae Efficiency	D_{dis}	T_o	T_{sys}	B
250	0.7	15m	500hrs	60K	200MHz

Table 7.1: Table showing the telescope parameters used in our analysis.

power spectrum shows the anisotropy of the redshift space power spectrum. The contours colored in blue correspond to the fiducial ΛCDM model, while those in red pertain to the CPL-ΛCDM model. We choose the best-fit value on CPL-ΛCDM model parameters ($\Omega_m = 0.289, \Omega_\Lambda = -0.781, w_0 = -1.03, w_a = -0.10$) obtained from the combined data CMB+BAO+Pantheon+R21 [8]. The Alcock-Paczynski effect makes a notable contribution, intensifying the anisotropy observed in the power spectrum. The significant departure of the CPL-ΛCDM model $\sim 5\%$ at $k \sim 1 Mpc^{-1}$ indicates that a closer investigation of the possibility of discerning such models from the ΛCDM model is justified.

For the measurement of the 21-cm power spectrum, we consider a radio-interferometric observation using a futuristic SKA1-Mid like experiment. The typical telescope parameters used are summarized in the table below. We also assume that the antenna distribution falls off as $1/r^2$, whereby the baseline coverage on small scales is suppressed.

We consider 250 dish antennae each of diameter 15m and efficiency 0.7. We assume $T_{sys} = 60K$ and an observation bandwidth of 128MHz. The k-range between the smallest and largest baselines is binned as $\Delta k = \alpha k$ where $\alpha = 1/N_{bin} \ln(U_{max}/U_{min})$. The minimum value of k is taken to be 0.005Mpc^{-1} the maximum value of k is taken to be 0.5Mpc^{-1} with logarithmically number of bins $N_{bin} = 8$. We consider a total observation time of 500×150hrs with 150 independent pointings, we obtain the $1-\sigma$ errors on $P_\ell(k, z)$. The fiducial model is chosen to be the ΛCDM. Figure (7.5) shows the multiples of $P_{21}(k, z)$ for selective parameter values of CPL-ΛCDM model. The central dotted line corresponds to ΛCDM. The fiducial redshift is chosen to be 0.2 (top) and 0.57 (bottom). We found that in the k range 0.01Mpc$^{-1} < k < 0.1$Mpc^{-1} phantom models are distinguishable from ΛCDM at a sensitivity of $> 3\sigma$. For higher multipoles, they are even more differentiable from fiducial ΛCDM. On the contrary, non-phantom models remain statistically indistinguishable from the ΛCDM model while considering monopole only. They are only distinguish-

Parameters	H_0	Ω_m	Ω_Λ	w_0	w_a	Ω_ϕ
Constraints	$69.276^{2.465}_{-1.600}$	$0.303^{0.067}_{-0.060}$	$-0.968^{0.539}_{-1.611}$	$-1.031^{0.046}_{-0.061}$	$-0.005^{0.442}_{-0.537}$	$1.750^{1.546}_{-0.537}$

Table 7.2: The parameter values, obtained in the MCMC analysis are tabulated along the $1-\sigma$ uncertainty.

able in higher multipoles.

We see a strong effect of Ω_Λ on the multipole components of the power spectrum. A non-trivial Ω_Λ introduces additional enhancement of anisotropy in the 21-cm power spectrum through the redshift space distortion factor $f\mu^2$. Additionally the power spectrum gets further modified through the departure of the factor $F = \alpha_\parallel/\alpha_\perp$ from unity and through the matter power spectrum $P(k,\mu)$ though the scalings of $k_\perp$ and $k_\parallel$. This explains the significant deviation of the 21-cm power spectrum for the CPL-ΛCDM model from its standard ΛCDM counterpart. This is become more prominent in the quadrupole and hexadecapole components cause of the terms with the anisotropy are enhanced by integrals of higher powers of μ in the Legendre polynomials.

The BAO imprint on the monopole $P_0(z,k)$ allows us to constrain $D_A(z)$ and $H(z)$. We perform a Markov Chain Monte Carlo (MCMC) analysis to constrain the model parameters using the projected error constraints obtained on the binned $H(z)$ and $D_A(z)$ from the $P_0(z,k)$. The analysis uses the Python implementation of the MCMC sampler introduced by Foreman-Mackey *et al.* [474]. We take flat priors for CPL-ΛCDM model parameters with ranges of $H_0 \in [67,73], \Omega_m \in [0.2,0.6], \Omega_\Lambda \in [-7,2], w_0 \in [-1.5,1.5], w_a \in [-0.7,0.7]$. The figure (7.6) shows the marginalized posterior distribution of the set of parameters $(H_0, \Omega_m, \Omega_\Lambda, w_0, w_a)$, and the corresponding 2D confidence contours are obtained. The fiducial value of the model parameters are taken from the best fit values of $H_0, \Omega_m, \Omega_\Lambda, w_0, w_a$ obtained from the combined data CMB+BAO+Pantheon+R21 [8]. Constraints on model parameters are tabulated in Table (7.2). While comparing with the projected error limits for the parameters of the CPL-ΛCDM as obtained in Sen *et al.* [8], we find that 21-cm alone doesn't impose stringent constraints on the values of Ω_Λ and w_a. However, it does exhibit a reasonably good ability to constrain the parameter w_0. To attain more robust constraints on these model parameters, a more comprehensive approach is re-

quired. This involves combining the 21-cm power spectrum data with other cosmological observations such as the CMB, BAO, SNIa, galaxy surveys etc. Through the joint analysis, it becomes possible to significantly improve the precision of parameter estimation.

Alcock-Paczynski anisotropy in redshift space: a dark energy marker

We explore a more straightforward and robust measure of anisotropy that doesn't necessitate the fitting of the power spectrum to a specific form. The 'anisotropy ratio' is defined as [514]

$$r(k,z) \equiv \frac{\int_{-1}^{0.5} P_{21}(k,z,\mu)\, d\mu + \int_{0.5}^{1} P_{21}(k,z,\mu)\, d\mu}{\int_{-0.5}^{0.5} P_{21}(k,z,\mu)\, d\mu} - 1 \tag{7.40}$$

This quantity was proposed originally to study reionization power spectrum [514] where the anisotropy arises even in a Λ CDM cosmology due to different coefficients to different powers of μ in the reionization power spectrum. Here, we use the same quantifier but the anisotropy is now rooted in the AP effect. The quantity $r(k,z)$ is usually studied at a fixed z. We have looked at its behavior in the entire (k,z) plane. The idea behind this to use the tomographic power spectrum measurement of the 21-cm power spectrum and find the optimal (k,z) range for detection with high SNR. We can see that for the ΛCDM model there is no $k-$dependence of $r(k,z)$ due to the cancellation of the k dependent quantities from the numerator and the denominator, and what survives depends only on the growth rate f which has redshift dependence at low redshifts. At high redshifts $f \sim 1$ and $r(k,z)$ becomes a constant.

Introducing a CPL model for dark energy shows z dependence from the growth rate and a k dependence from the AP effect. The BAO oscillations also imprint due to the AP effect. The departure from Λ CDM is quite significant when we consider the CPL-ΛCDM model. This implies that the quantity $r(k,z)$ is a potential probe of dark energy.

Figure 7.7 shows the behaviour of $r(k,z)$ in the (k,z) plane. As discussed earlier r has no $k-$ dependence in the ΛCDM model (for a constant linear bias).

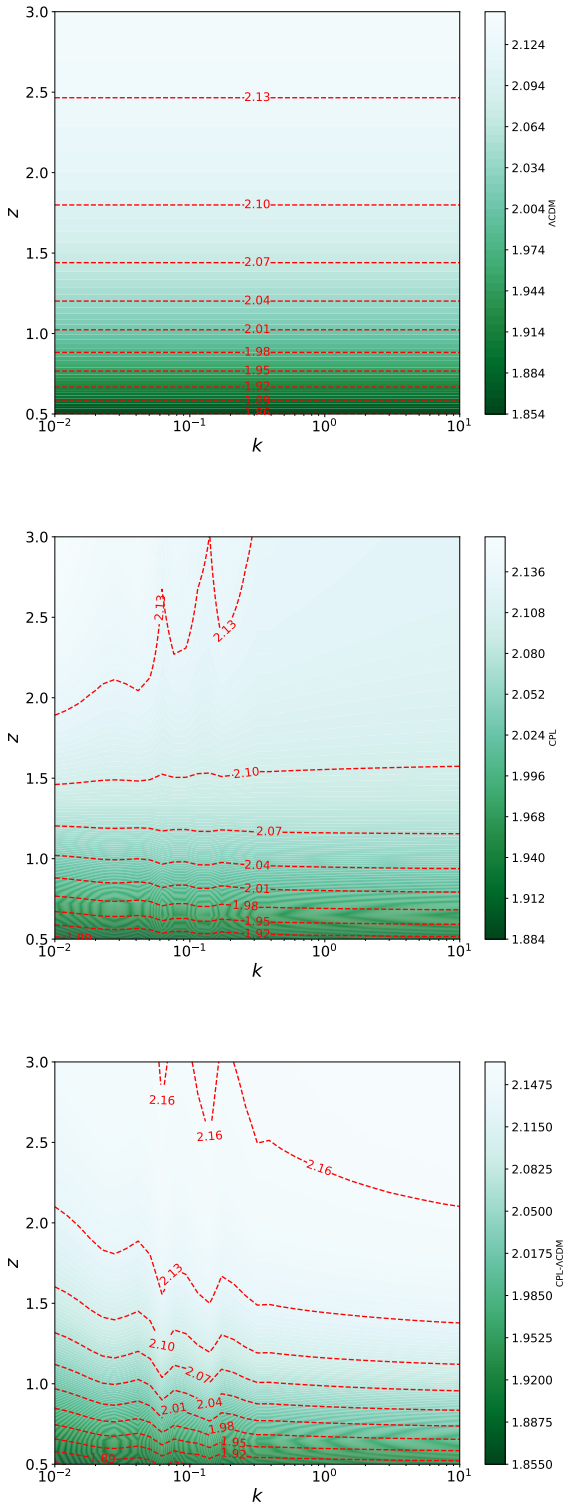

Figure 7.7: shows the $r(k, z)$ from 3D HI 21-cm power spectrum in the (k, z) space. The upper one corresponds to ΛCDM, whereas the middle one corresponds to CPL model with $(w_0, w_a = -1.1, -0.1)$ and the bottom one for the best fit values of CPL-ΛCDM parameters.

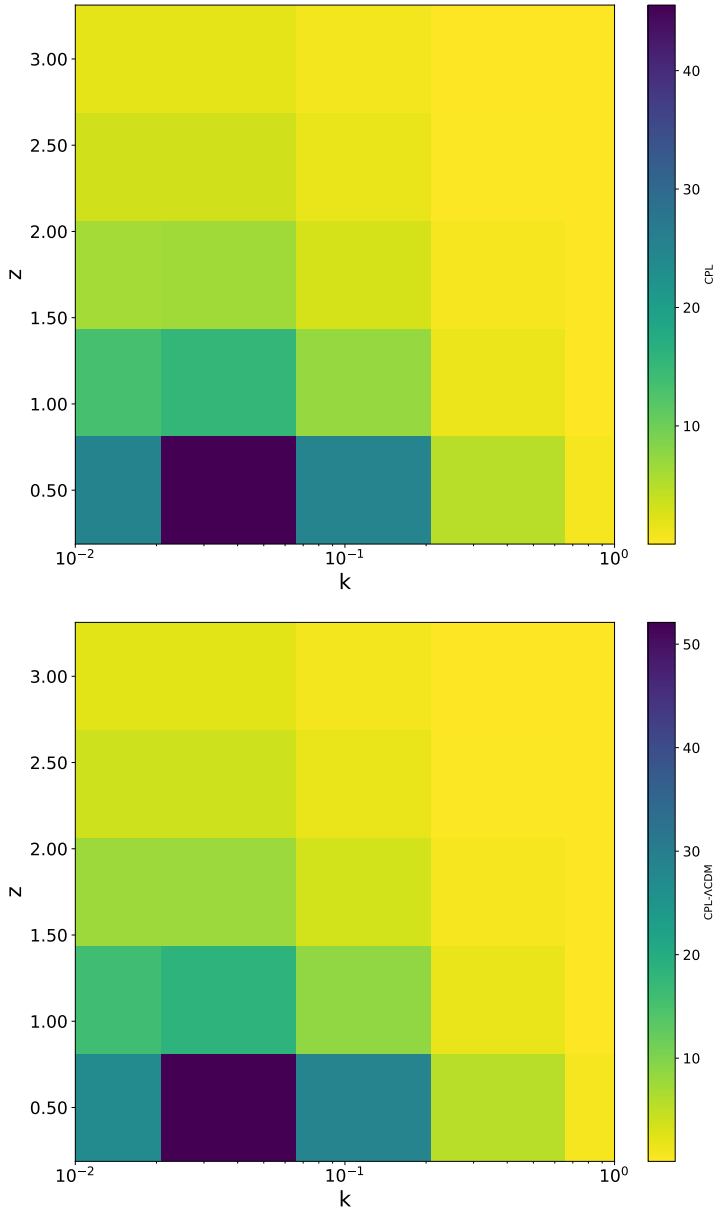

Figure 7.8: shows the SNR for $r(k, z)$ from 3D HI 21-cm power spectrum in the (k, z) bins. The upper figure one corresponds to the CPL model with $(w_0, w_a = -1.1, -0.1)$ and the lower one is for the best fit values of CPL-ΛCDM parameters [8].

We see some redshift dependence at small redshift due to the variation of $\beta(z)$ with redshift at low redshifts. For the CPL model, we see that $r(k.z)$ shows additional anisotropy in the $k-$range ($k < 10^{-1}Mpc^{-1}$) at redshifts $z \sim 2.5$ The anisotropy is more pronounced for a model with negative cosmological constant. The oscillatory feature indicates the BAO feature which does not cancel in $r(k,z)$ (as in the case of ΛCDM model) due to Alcock-Pacyzinski anisotropy.

We consider the possibility of measuring the quantity r in 5 $k-$ bands at 5 observing frequencies. These 5 k-bins corresponds to different baseline U bins at the different observing frequencies. The $1-\sigma$ SNR is calculated using

$$\delta r(k,z) = \left[\frac{\delta P_{21}^{N}(k,z)}{P^{N}(k,z)} + \frac{\delta P_{21}^{D}(k,z)}{P^{D}(k,z)}\right] r(k,z) \tag{7.41}$$

where $\delta P_{21}^{N}(k,z)$ and $\delta P_{21}^{D}(k,z)$ are the variances of the numerator and denominator parts of the Eq: 7.40.

The figure 7.8 shows the SNR for (i) CPL and (ii) CPL-ΛCDM fiducial cosmologies. We find that a peak SNR of ~ 40 is possible at $z \sim 0.5$ in the k-bin centered at $0.03MPc^{-1}$ for the CPL model. The peak SNR in this bin is ~ 50 for a CPL-ΛCDM fiducial model. This allows us to use $r(k,z)$ as a cosmological probe of dark energy.

Model	CPL	CPL-ΛCDM
Constraints	$\Delta w_0 = 0.067, \Delta w_a = 0.152$	$\Delta w_0 = 0.0181$

Table 7.3: Table showing 68% error projection on different dark energy models.

Figure 7.9 shows the confidence ellipses obtained from the Fisher matrix

$$F_{ij} = \sum \frac{1}{\delta r^2} \frac{\partial r}{\partial \lambda_i} \frac{\partial r}{\partial \lambda_j} \tag{7.42}$$

where $\lambda_i = w_0, w_a$ The $1-\sigma$ (68%) errors are summarized in the table 7.3.

7.4 Conclusion

In this work, we study the possibility of constraining negative Λ using the post-reionization HI 21-cm power spectrum. We specifically investigate the

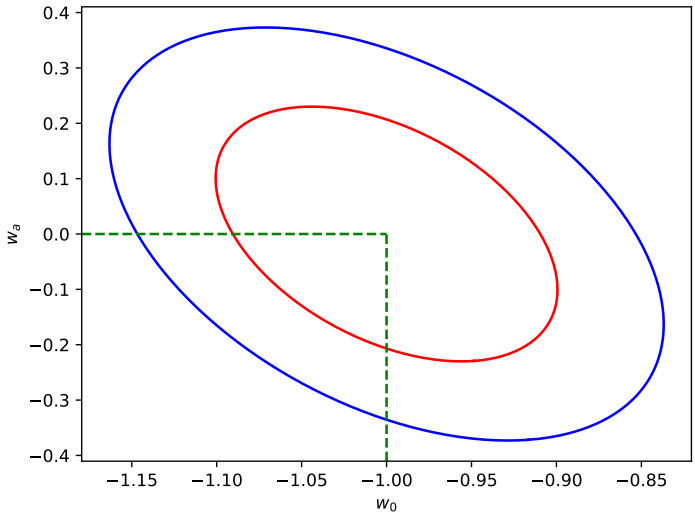

Figure 7.9: shows 68% and 95% marginalized confidence intervals for the parameters (w_0, w_a) from the 21-cm anisotropy ratio for the CPL model. The fiducial model is chosen as the ΛCDM model with $(w_0, w_a) = (-1, 0)$.

quintessence models with the most widely used dark energy EoS parameterization and add a non-zero vacua (in terms of a $\pm\Lambda$).

By the analysis of BOSS (SDSS) data we find that addition of a negative cosmological constant to a phantom dark energy model seems viable. We see that the CPL-ΛCDM with a phantom field and negative Λ and $H_0 = 72$ Km/s/Mpc qualitatively consistent with the data.

Further, we study the non-trivial CPL-ΛCDM model with the $f\sigma_8$ data from the galaxy surveys. We find that the mean observational $f\sigma_8$ falls in the non-phantom sector with negative Λ. Since the error bars are quite large, both ΛCDM predictions (with $H_0 = 67.4$Km/s/Mpc), and CPL-ΛCDM with phantom field and negative Λ for $H_0 = 72$ Km/s/Mpc are consistent within $1 - \sigma$ errors. The addition of a negative Λ to a phantom dark energy model also seems to push H_0 to a higher value.

Subsequently, we look into the influence of the Alcock-Packzynski effect on 3D HI 21-cm power spectrum. Using ΛCDM as a fiducial cosmology, we explore the implications of the first few multipoles of the redshift-space 21-cm power spectrum for the upcoming SKA intensity mapping experiments.

We find that the multipoles specially the quadrupole and hexadecapole components show significant departure from their standard ΛCDM counterparts. We focus on the BAO feature on the monopole component, and estimate the projected errors on the $H(z)$ and $D_A(z)$ over a redshift range $z \sim 0 - 3$.

Further, we perform a MCMC analysis to constrain the CPL-ΛCDM model parameters using the projected error constraints obtained on the binned $H(z)$ and $D_A(z)$ from the $P_0(z, k)$. We find that 21-cm alone doesn't impose stringent constraints on the model parameters. Combining the 21-cm power spectrum data with other cosmological observations such as the CMB, BAO, SNIa, galaxy surveys, etc can significantly improve the precision of parameter estimation.

In the end, we have considered an alternative quantifier $r(k, z)$ to measure the anisotropy in the power spectrum and made error projections on dark energy model parameters.

While we have not factored in several observational challenges towards detecting the 21-cm signal. Proper mitigation of large galactic and extra-galactic foregrounds and minimizing calibration errors are imperative for the any cosmological investigation. In a largely observationally idealized scenario, we have obtained error projections on the model parameters from the BAO imprint on the post-reionization 21-cm intensity maps. We employ a Bayesian analysis techniques to put constraints on the model parameters. Precision measurement of these parameters shall enhance our understanding of the underlying cosmological dynamics and potential implications of negative Λ values. We would like to factor in some of the key observational issues in future.

CHAPTER 8

Conclusion and Future Scope

This thesis investigates the possibility of using the probes of the post-reionization matter density field to improve our understanding of various dark energy models. The dark energy models we have studied are

- Dark energy EoS parameterized in a model-independent manner
- $f(R)$ modification to Einstein's gravity
- Quintessence scalar fields

We have used the statistics of three tracers of the dark matter distribution. Weak lensing and Lyman-alpha forest sample the large-scale matter distribution along one-dimensional line of sight skewers. The redshifted 21-cm signal from the post-reionization Hi gives a three-dimensional map of the Universe. We have studied these tomographic probes in auto and cross-correlation.

We have focused on the possibility of differentiating these models from the ΛCDM model with a high statistical significance in upcoming experiments. We have also used simulated futuristic data to make error projections on diverse model parameters.

Future Scope

The following topics will be the focus of ongoing and future research.

- Recently, many authors suggested that the presence of the negative Λ along with Quintessence dark energy can alleviate the H_0 tension and lift the $f\sigma_8$ degeneracy. In our elementary study, we saw that negative Ω_Λ can be constrained using the HI 21cm observation. Further, the ramifications and details of such scenarios need to be explored using other probes as well in a multi-probe study.

- We investigated the BAO oscillatory signature in the cross-power spectrum. BAO features in highly anisotropic 21-cm power spectrum in redshift space due to AP effect is an exciting area of investigation, especially in models where exotic dark energy causes significant departure from ΛCDM predictions of expansion rates and distances.

- While using different cosmological model/modified gravity theories, we have not taken account of the Alcock-Panczyski effect in our calculation, which severely impacts the power spectrum in redshift space and show more anisotropies in the $(k_{\parallel}, k_{\perp})$ plane.

- Foreground subtraction is crucial to cosmological HI observations. We would like to find out if cross-correlation actually gets around the foreground problem. Finding the optimal window function to remove foreground seepage in the weak lensing signal is to be investigated.

- An accurate determination of the cosmic HI signal will probably be possible by detecting the cross-correlation power spectrum. For more accurate projections/constraints, it is necessary to investigate the best observational techniques and telescope designs.

- Angular HI 21-cm bispectrum in the redshift space needs to be explored. Similarly, it is essential to look into cross-bispectrum taking different cosmological probes of IGM.

- The physics involved behind the observed Lyman-α forest and 21-cm signal involves non-linear effects on small scales. Our linear theory analysis needs to be justified using non-linear theories like the Halo model or through simulations.

- We have not explicitly modeled the effects of the galaxy photo-z errors in our analysis with weak lensing. Since fairly broad redshift bins are used, the effect of these errors may be largely mitigated in the case of the galaxy autocorrelation lensing power spectrum.

- Extending our approaches towards intensity mapping with other emission lines (CO, CII) would enable us to form a comprehensive picture.

Exploiting the synergy of CMB, HI, Lyman-α forest, and galaxy surveys, the methodology would be a powerful tool to explore more parameters in cosmological models such as e.g., testing higher order gravity theories, k-essence models etc.

The field of cosmology may rapidly change with an improved understanding of the dark sector from observations and fundamental theoretical physics. New avenues of theoretical investigations and observation strategies shall be envisaged in sync with these developments.

APPENDIX A

Field equations for Quintessence and $f(R)$ gravity

A.1 Derivation of the Klein-Gordon Equation

The action of scalar field:

$$S_\phi = \int \sqrt{-g} L_\phi(\phi, \partial_a \phi) d^4x \tag{A.1}$$

where L_ϕ is the Lagrangian density. For a region Ω, we consider variation of the field. $\phi(x) \Rightarrow \phi(x) + \delta(x)$ which vanishes on the surface $\Gamma(\Omega)$, i.e $\delta\phi(x) = 0$. Hence

$$\delta S(\Omega) = \delta\left(\int_\Omega \sqrt{-g} L_\phi(\phi, \partial_a \phi) d^4x\right) = \int_\Omega \left[\frac{\partial(\sqrt{-g}L_\phi)}{\partial\phi}\delta\phi + \frac{\partial(\sqrt{-g}L_\phi)}{\partial(\partial_a\phi)}\delta(\partial_a\phi)\right] \tag{A.2}$$

The second term in the above expression:

$$\frac{\partial(\sqrt{-g}L_\phi)}{\partial(\partial_a\phi)}\delta(\partial_a\phi) = \frac{\partial}{\partial x^a}\left[\frac{\partial(\sqrt{-g}L_\phi)}{\partial(\partial_a\phi)}\delta\phi\right] - \frac{\partial}{\partial x^a}\left[\frac{\partial(\sqrt{-g}L_\phi)}{\partial(\partial_a\phi)}\right]\delta\phi \tag{A.3}$$

$$\delta S(\Omega) = \int_\Omega \left[\frac{\partial(\sqrt{-g}L_\phi)}{\partial\phi}\delta\phi - \frac{\partial}{\partial x^a}\left(\frac{\partial(\sqrt{-g}L_\phi)}{\partial(\partial_a\phi)}\right)\right]\delta\phi d^4x + \int_\Omega \left[\frac{\partial}{\partial x^a}\left(\frac{\partial(\sqrt{-g}L_\phi)}{\partial(\partial_a\phi)}\right)\delta\phi\right] d^4x \tag{A.4}$$

Using the divergence theorem, the last term of the above expression goes off as $\delta\phi = 0$ an $S = \Gamma(\Omega)$:

$$\int_\Omega \left[\frac{\partial}{\partial x^a}\left(\frac{\partial(\sqrt{-g}L_\phi)}{\partial(\partial_a\phi)}\right)\delta\phi\right] d^4x = \int_{S=\Gamma(\Omega)} \left(\frac{\partial(\sqrt{-g}L_\phi)}{\partial(\partial_a\phi)}\right)\delta\phi.ndS = 0 \tag{A.5}$$

As $\delta S(\Omega) = 0$, we obtain the Euler-Lagrange equation:

$$\int_\Omega \left[\frac{\partial(\sqrt{-g}L_\phi)}{\partial\phi}\delta\phi - \frac{\partial}{\partial x^a}\left(\frac{\partial(\sqrt{-g}L_\phi)}{\partial(\partial_a\phi)}\right)\right]\delta\phi d^4x = 0$$
$$\frac{\partial(\sqrt{-g}L_\phi)}{\partial\phi}\delta\phi - \frac{\partial}{\partial x^a}\left(\frac{\partial(\sqrt{-g}L_\phi)}{\partial(\partial_a\phi)}\right) = 0$$

Evaluating the first term of the above,

$$\frac{\partial}{\partial\phi}(\sqrt{-g}L_\phi) = \sqrt{-g}\frac{\partial}{\partial\phi}L_\phi = \sqrt{-g}\frac{\partial}{\partial\phi}\left(\frac{1}{2}g^{\mu\nu}\partial_\mu\phi\partial_\nu\phi - V(\phi)\right) = -\sqrt{-g}\frac{\partial V}{\partial\phi} \tag{A.6}$$

and the second term,

$$\begin{aligned}\partial_a\left[\frac{\partial(\sqrt{-g}L_\phi)}{\partial(\partial_a\phi)}\right] &= \partial_a\left[\frac{\partial}{\partial(\partial_a\phi)}\left(\sqrt{-g}\frac{1}{2}g^{\mu\nu}\partial_\mu\phi\partial_\nu\phi - \sqrt{-g}V(\phi)\right)\right]\\ &= \partial_a\left[\sqrt{-g}\frac{1}{2}g^{\mu\nu}(\partial_\mu\phi\delta_{\mu a} + \partial_\nu\phi\delta_{\nu a})\right] = \partial_\mu(\sqrt{-g}g^{\mu\nu}\partial_\nu\phi)\\ &= \partial_\mu(\sqrt{-g})g^{\mu\nu}\partial_\nu\phi + \partial_\mu(g^{\mu\nu})\sqrt{-g}\partial_\nu\phi + g^{\mu\nu}\sqrt{-g}\partial_\mu\partial_\nu\phi\\ &= \sqrt{-g}\left(\frac{1}{2g}\partial_\mu(g)g^{\mu\nu}\partial_\nu\phi + \partial_\mu(g^{\mu\nu})\partial_\nu\phi + g^{\mu\nu}\partial_\mu\partial_\nu\phi\right)\end{aligned} \tag{A.7}$$

For FLRW metric $g_{\mu\nu}$ = dig$(1 - a^2(t) - a^2(t) - a^2(t))$, with determinant $g = det(g_{\mu\nu}) = -a^6(t)$. Since metric is diagonal, we can read out the following quantities:

$$\partial_0 g = -6a^5\dot{a} \quad , \quad \partial_i g = 0 \quad , \quad \partial_\mu g^{\mu\nu} = \partial_\mu g^{\mu\mu} = 0 \tag{A.8}$$

Further we have $\partial_0\phi = \dot{\phi}$ and $\partial_i\phi = 0$. Hence the term,

$$\begin{aligned}\partial_a\left[\frac{\partial(\sqrt{-g}L_\phi)}{\partial(\partial_a\phi)}\right] &= \sqrt{a^6}\left(-\frac{1}{2a^6}\partial_0 g g^{0\nu}\partial_\nu\phi + g^{\mu 0}\partial_\mu\partial_0\phi\right)\\ &= a^3\left(-\frac{1}{2a^6}\partial_0 g g^{00}\partial_0\phi + g^{00}\partial_0\partial_0\phi\right)\\ &= a^3\left(-\frac{1}{2a^6}(-6a^5\dot{a})\dot{\phi} + \ddot{\phi}\right) = a^3\left(3\left(\frac{\dot{a}}{a}\right)\dot{\phi} + \ddot{\phi}\right)\end{aligned} \tag{A.9}$$

Remaining term:

$$-\sqrt{-g}\frac{\partial V}{\partial\phi} - a^3\left(a\frac{\dot{a}}{a}\dot{\phi} + \ddot{\phi}\right) = -a^3\left(\frac{\partial V}{\partial\phi} + 3\left(\frac{\dot{a}}{a}\right)\dot{\phi} + \ddot{\phi}\right) = 0 \tag{A.10}$$

finally we have reached the Klein-Gordon equation:

$$\ddot{\phi} + 3\left(\frac{\dot{a}}{a}\right)\dot{\phi} + \frac{\partial V}{\partial \phi} = 0 \tag{A.11}$$

A.2 Deriving field equation in $f(R)$ gravity theory

The action in case of $f(R)$ gravity can be written as

$$A = \frac{1}{2\kappa^2}\int d^4x\sqrt{-g}f(R) + \int d^4x\sqrt{-g}L_m(g_{\mu\nu},\phi) \tag{A.12}$$

where $\kappa^2 = \frac{8\pi G}{c^2}$ and L_m is the Lagrangian matter density which is a function of metric $g_{\mu\nu}$ and matter field ϕ. Now let's vary the action w.r.t metric $g_{\mu\nu}$ to get the modified field equation.

$$^{*}\delta A = \int d^4x\delta(\sqrt{-g}f(R)) = \int d^4x\sqrt{-g}\delta(f(R)) + \int d^4x\delta(\sqrt{-g})f(R) \tag{A.13}$$

Above we have not considered the variation of matter action which will eventually give the standard Einstein's stress-energy-momentum tensor $T_{\mu\nu}$. The variation of $\sqrt{-g}$ can be work out as

$$\delta\sqrt{-g} = \delta\left[(-g^{-1})^{-1/2}\right] = -\frac{1}{2}(-g^{-1})^{-3/2}\delta(-g) = -\frac{1}{2}\sqrt{-g}g_{\mu\nu}\delta g^{\mu\nu} \tag{A.14}$$

where the last expression we used the cyclic property of the trace i.e $\delta(g^{-1}) = \frac{1}{g}g_{\mu\nu}\delta g^{\mu\nu}$ (using $Trace(N^{-1}\delta N) = \frac{1}{detN}\delta(detN)$ where $N = g_{\mu\nu}$ and $detN = detg^{\mu\nu} = 1/g$). The variation of $f(R)$ is expressed as

$$\delta f(R) = \frac{\partial f}{\partial R} = \frac{\partial f}{\partial R}(\delta g^{\mu\nu})R_{\mu\nu} + \frac{\partial f}{\partial R}g^{\mu\nu}\delta R_{\mu\nu} \tag{A.15}$$

From now onward we will use the short hand notation of $\frac{\partial f}{\partial R} \equiv f_{,R}$ and $\frac{\partial^2 f}{\partial R^2} \equiv f_{,RR}$. So the total action has three parts as follows

$$\delta A = \int d^4x\sqrt{-g}(f_{,R}R_{\mu\nu})\delta g^{\mu\nu} + \int d^4x\sqrt{-g}(f_{,R}g^{\mu\nu})\delta R_{\mu\nu} + \int d^4x\sqrt{-g}\left(-\frac{1}{2}g_{\mu\nu}f\right)\delta g^{\mu\nu} \tag{A.16}$$

*dropped the κ^2 term for a while

The first and third term of the action are already in a designed form which is multiplied by $\delta g^{\mu\nu}$. So in order to organize the second term we need the variation of $R_{\mu\nu}$ using the Palatini equation

$$\delta R_{\mu\nu} = \nabla_\lambda \delta\Gamma^\lambda_{\mu\nu} - \nabla_\nu \delta\Gamma^\lambda_{\mu\lambda} \tag{A.17}$$

Hence the second term (δA_2) now can be expressed as

$$\begin{aligned}
(\delta A_2) &= \int d^4x\sqrt{-g} f_{,R} g^{\mu\nu}\left[\nabla_\lambda \delta\Gamma^\lambda_{\mu\nu} - \nabla_\nu \delta\Gamma^\lambda_{\mu\lambda}\right] \\
&= \int d^4x\sqrt{-g} f_{,R} g^{\mu\nu}\left[\nabla_\lambda g^{\mu\nu}\delta\Gamma^\lambda_{\mu\nu} - \nabla_\nu g^{\mu\nu}\delta\Gamma^\lambda_{\mu\lambda}\right] \\
&= \int d^4x\sqrt{-g} f_{,R} g^{\mu\nu}\left[\nabla_\sigma g^{\mu\nu}\delta\Gamma^\sigma_{\mu\nu} - \nabla_\sigma g^{\mu\sigma}\delta\Gamma^\lambda_{\mu\lambda}\right] \\
&= \int d^4x\sqrt{-g} f_{,R} g^{\mu\nu}\nabla_\sigma\left[g^{\mu\nu}\delta\Gamma^\sigma_{\mu\nu} - g^{\mu\sigma}\delta\Gamma^\lambda_{\mu\lambda}\right]
\end{aligned} \tag{A.18}$$

Inserting the variation $\delta\Gamma^\sigma_{\mu\nu}$ in terms of $\delta g_{\mu\nu}$ using the following expression

$$\delta\Gamma^\sigma_{\mu\nu} = -\frac{1}{2}\left[g_{\lambda\mu}\nabla_\nu(\delta g^{\lambda\sigma}) + g_{\lambda\mu}\nabla_\mu(\delta g^{\lambda\sigma} - g_{\mu\alpha}g_{\nu\beta}\nabla^\sigma(\delta g^{\alpha\beta})\right] \tag{A.19}$$

we now have the variation of action in the form

$$\begin{aligned}
(\delta A_2) &= \int d^4x\sqrt{-g}(-\frac{1}{2}f_{,R})\nabla_\sigma\Big[\delta^\lambda_\nu\nabla_\nu(\delta g^{\lambda\sigma}) + \delta^\lambda_\nu\nabla_\mu(\delta g^{\lambda\sigma}) - g_{\alpha\beta}\nabla_\sigma(\delta g^{\alpha\beta}) \\
&\quad - \delta^\sigma_\rho\nabla_\nu(\delta g^{\lambda\rho}) - g^{\mu\sigma}g_{\rho\lambda}\nabla_\nu(\delta g^{\lambda\rho}) + \delta^\sigma_\beta\nabla^\lambda(\delta g^{\alpha\beta})\Big] \\
&= \int d^4x\sqrt{-g}(-\frac{1}{2}f_{,R})\nabla_\sigma\Big[\nabla_\lambda(\delta g^{\lambda\sigma}) - \nabla_\lambda(\delta g^{\lambda\sigma}) + \nabla_\mu(\delta g^{\mu\sigma}) \\
&\quad - g_{\alpha\beta}\nabla^\sigma(\delta g^{\alpha\beta}) - g^{\mu\sigma}g_{\rho\lambda}\nabla_\mu(\delta g^{\lambda\rho}) + g_{\lambda\alpha}\nabla^\lambda(\delta g^{\alpha\sigma})\Big] \\
&= \int d^4x\sqrt{-g}(-\frac{1}{2}f_{,R})\nabla_\sigma\Big[\nabla_\mu(\delta g^{\mu\sigma}) + \nabla_\alpha(\delta g^{\alpha\sigma}) - g_{\alpha\beta}\nabla^\sigma(\delta g^{\alpha\beta}) - g_{\rho\lambda}\nabla^\sigma(\delta g^{\lambda\rho})\Big] \\
&= \int d^4x\sqrt{-g}(-\frac{1}{2}f_{,R})\nabla_\sigma\Big[\nabla_\mu(\delta g^{\mu\sigma}) + \nabla_\mu(\delta g^{\mu\sigma}) - g_{\mu\nu\beta}\nabla^\sigma(\delta g^{\mu\nu}) - g_{\mu\nu}\nabla^\sigma(\delta g^{\mu\nu})\Big] \\
&= \int d^4x\sqrt{-g}(-\frac{1}{2}f_{,R})\nabla_\sigma\Big[g_{\mu\nu}\nabla^\sigma(\delta g^{\mu\nu}) - \nabla_\mu(\delta g^{\mu\sigma})\Big]
\end{aligned} \tag{A.20}$$

Now the total variation of the action turn out as follows

$$\delta A = \frac{1}{2\kappa^2}\int d^4x\sqrt{-g}\left[f_{,R}R_{\mu\nu}\delta g^{\mu\nu} + (-\frac{1}{2}f_{,R})\nabla_\sigma\left[g_{\mu\nu}\nabla^\sigma(\delta g^{\mu\nu}) - \nabla_\mu(\delta g^{\mu\sigma})\right] + (-\frac{1}{2}g_{\mu\nu}f\delta g^{\mu\nu}\right] \tag{A.21}$$

Now vary the action (A.21) with respect to the metric gives the field equation

$$\frac{\delta A}{\delta g_{\mu\nu}} = f_{,R}R_{\mu\nu} - \frac{1}{2}f(R)g_{\mu\nu} - \nabla_\mu\nabla_\nu f_{,R} + g_{\mu\nu} + g_{\mu\nu}\Box f_{,R} = \kappa^2 T_{\mu\nu} \tag{A.22}$$

Where $\Box = \frac{1}{\sqrt{-g}}\partial_\mu(\sqrt{-g}g^{\mu\nu}\partial_\mu)$ and the energy momentum stress tensor of matter is defined as

$$T_{\mu\nu} = -\frac{2}{\sqrt{-g}}\frac{\delta A_m}{\delta g^{\mu\nu}} \tag{A.23}$$

which satisfy the continuity equation $\nabla^\mu T_{\mu\nu} = 0$. While varying the field equation we have incorporated the fact that $f_{,R}$ is a scalar quantity and we can safely compute covariant derivative. Multiplying $g_{\mu\nu}$ in eqn (A.22) leads to

$$f_{,R}R^\mu_\mu - \frac{1}{2}f(R)\delta^\mu_\mu - \nabla^\mu\nabla_\mu f_{,R} + \delta^\mu_\mu\Box f_{,R} = \kappa^2 T^\nu_\mu \tag{A.24}$$

Using $\delta^\nu_\mu = 4$ and $\nabla^\mu\nabla_\mu \equiv \Box$, the trace of the field equation is

$$f_{,R}R + 3\Box f_{,R} - 2f(R) = \kappa^2 T \tag{A.25}$$

For $f(R) = R - 2\Lambda$ where $f_{,R} = 1$ we retrieve the standard Einstein's field equations. Comparing $f(R)$ gravity to GR, the extra term $\Box f_{,R}$ in $f(R)$ gravity does not vanish and act like an extra propagating degrees of freedom $\phi \equiv f_{,R}$ called 'Scalaron', whose dynamics can be determined by the eqn (A.25). Looking at the (00) component of A.24 i.e,

$$f_{,R}R_{00} - \frac{1}{2}f(R)g_{00} - \nabla_0\nabla_0 f_{,R} + g_{00}\Box f_{,R} = \kappa^2 g_{00}T^0_0 \tag{A.26}$$

The fourth term:

$$\begin{aligned} g_{00}\Box f_{,R} &= -1\frac{1}{\sqrt{-g}}\partial_0(\sqrt{-g}g^{00}\partial_0 f_{,R}) \\ &= -\frac{1}{a^3}\frac{\partial}{\partial t}\left(-a^3\frac{\partial}{\partial t}f_{,R}\right) \\ &= \frac{1}{a^3}3a^2\dot{a}\dot{f}_{,R} + \frac{a^3}{a^3}\ddot{f}_{,R} \\ &= 3H\dot{f}_{,R} + \ddot{f}_{,R} \end{aligned} \tag{A.27}$$

The third term of A.24, the covariant derivative will be simply partial derivative as $f_{,R}$ is a scalar quantity and thus it will cancel the $\ddot{f}_{,R}$ term coming from the last expression. So the remaining terms are,

$$f_{,R}(3H^2 - \frac{1}{2}R) + \frac{1}{2}f(R) + 3H\dot{f}_{,R} = \kappa^2\rho \tag{A.28}$$

Rearranging we reached the first modified Friedmann equation,

$$3f_{,R}H^2 = (f_{,R}R - f(R))/2 - 3R\dot{f}_{,R} + \kappa^2\rho \tag{A.29}$$

For the second Friedmann equation, let us consider the (ii) term of (A.24):

$$f_{,R}R_{ii} - \frac{1}{2}f(R)g_{ii} - \nabla_i\nabla_i f_{,R} + g_{ii}\Box f_{,R} = \kappa^2 g_{ii}T^i_i \tag{A.30}$$

Again considering the last term of LHS,

$$\begin{aligned} g_{ii}R_{ii} &= a^2\frac{1}{\sqrt{-g}}\partial_\mu(\sqrt{-g}g^{\mu\nu}\partial_\nu f_{,R}) \\ &= a^2\frac{1}{\sqrt{-g}}\left[\partial_0(\sqrt{-g}g^{00}\partial_0 f_{,R}) + \partial_i(\sqrt{-g}g^{ii}\partial_i f_{,R})\right] \\ &= a^2\frac{1}{a^3}\left[\partial_0\left(a^3(-1)\dot{f}_{,R}\right)\partial_i\left(a^3\frac{1}{a^2}\partial_i f_{,R}\right)\right] \\ &= \frac{1}{a}\left[-3a^2\dot{a}\dot{f}_{,R} - a^3\ddot{f}_{,R} + \partial_i a\partial_i f_{,R} + a\partial_i\partial_i f_{,R}\right] \\ &= -3a^2H\dot{f}_{,R} - a^2\ddot{f}_{,R} + a^2H\dot{f}_{,R} + \partial_i\partial_i f_{,R} \\ &= -2a^2H\dot{f}_{,R} - a^2\ddot{f}_{,R} + \partial_i\partial_i f_{,R} \end{aligned} \tag{A.31}$$

Now the last term of the above expression cancels with the $\nabla_i\nabla_i$ term in field equation. Plugging the result and the Ricci tensor, R_{ii} for FRLW metric we

have,

$$\begin{aligned}(2\dot{a}^2 + a\ddot{a})f_{,R} - \frac{a^2}{2}f(R) - 2a^2H\dot{f}_{,R} - a^2\ddot{f}_{,R} &= \kappa^2 a^2 P \\ \left(\frac{2\dot{a}^2 + a\ddot{a}}{a^2}\right)f_{,R} - \frac{1}{2}f(R) - 2H\dot{f}_{,R} - \ddot{f}_{,R} &= \kappa^2 P \\ \left(\frac{a\ddot{a} - \dot{a}^2}{a^2} + 3\frac{\dot{a^2}}{a^2}\right)f_{,R} - \frac{1}{2}f(R) - 2H\dot{f}_{,R} - \ddot{f}_{,R} &= \kappa^2 P\end{aligned} \tag{A.32}$$

Replacing the $f(R)/2$ term from the expresssion A.24,

$$-\frac{1}{2}f(R) = 2H^2 f_{,R}f_{,R} - \frac{1}{2}f_{,R}R + 3H\dot{f}_{,R} - \ddot{f}_{,R} - \kappa^2\rho \tag{A.33}$$

we have the following,

$$\begin{aligned}\dot{H}f_{,R} + 3H^2 f_{,R} + 3H^2 f_{,R} - \frac{1}{2}f_{,R}f_{,R} + 3H\dot{f}_{,R} - 2H\dot{f}_{,R} - \ddot{f}_{,R} &= \kappa^2(\rho + P) \\ \dot{H}f_{,R} + 6H^2 f_{,R} - 3(2H^2 + \dot{H})f_{,R} + H\dot{f}_{,R} - \ddot{f}_{,R} &= \kappa^2(\rho + P)\end{aligned}$$

Rearranging we get the second modified Friedmann equation:

$$H\dot{f}_{,R} - 2\dot{H}f_{,R} - \ddot{f}_{,R} = \kappa^2(\rho + P) \tag{A.34}$$

Along with

$$3H^2 f_{,R} - \frac{1}{2}(Rf_{,R} - f(R)) + 3H\dot{f}_{,R} = \kappa^2\rho \tag{A.35}$$

governs the background dynamics of a flat FLRW universe in $f(R)$ gravity theory.

APPENDIX B

Weak Gravitaional Lensing

B.1 Deriving weak gravitaional lensing convergence power spectrum

Convergence $\kappa(\vec{\theta})$, in the direction of $\vec{\theta}$ integrated along the LoS,

$$\kappa(\vec{\theta}) = \frac{3}{2}\left(\frac{H_0}{c}\right)^2 \Omega_{m0} \int_0^{\chi_s} d\chi\, g(\chi)\, \chi \frac{\delta(\chi\vec{\theta},\chi)}{a(\chi)} \quad : \quad g(\chi) = \int_0^{\chi_s} d\chi' n_s(\chi') \frac{\chi' - \chi}{\chi'} \tag{B.1}$$

Similar to the mass density power spectrum, we can define the convergence power spectrum,

$$\langle \tilde{\kappa}(\vec{l})\tilde{\kappa}(\vec{l'})\rangle = (2\pi)^2 \delta_D(\vec{l} - \vec{l'}) P_\kappa(\vec{l}) \tag{B.2}$$

Assume $\kappa(\vec{\theta}) = \int d\chi W(\chi)\delta(\chi\vec{\theta},\chi)$ and the correlation function,

$$\begin{aligned} \xi_\kappa(\Delta\vec{\theta}) &= \langle \kappa(\vec{\theta})\kappa(\vec{\theta} + \Delta\vec{\theta})\rangle \\ &= \int d\chi W(\chi) \int d\chi' W(\chi') \langle \delta(\chi\vec{\theta},\chi)\delta(\chi'(\vec{\theta} + \Delta\vec{\theta}),\chi')\rangle \end{aligned} \tag{B.3}$$

Now we have $P_\kappa(\vec{l}) = \int d\vec{\theta}\xi_\kappa(\vec{\theta})e^{-il.\vec{\theta}}$ and the density contrast $\delta(\chi\vec{\theta},\chi) = \delta(\vec{r})$ can be expressed in Fourier space:

$$\begin{aligned} \delta(\vec{r}) &= \int \frac{d\vec{k}}{(2\pi)^3} e^{-i(\vec{k}.\vec{r})} \tilde{\delta}(\vec{k},\chi) \\ &= \int \frac{d\vec{k}}{(2\pi)^3} e^{-i\vec{k}_\perp.\theta\chi} e^{-ik_\parallel \chi} D_+(\chi)\tilde{\delta}(\vec{k}) \qquad (\vec{k} = (\vec{k}_\perp, k_\parallel)) \end{aligned} \tag{B.4}$$

Now

$$\langle \delta(\vec{r})\delta^*(\vec{r})\rangle = \int d\vec{k} e^{-i\vec{k}_\perp.\theta\chi} e^{-i\vec{k}_\perp.(\theta+\Delta\vec{\theta})\chi'} e^{-ik_\parallel(\chi-\chi')} D_+(\chi)D_+(\chi')P_{3D}(k) \tag{B.5}$$

For small angle approximation ($\Delta\vec{\theta} \leq 1 - 2\,\mathrm{deg}$), $\vec{k}_\perp$ carries most of the power at $|\vec{k}|$ i.e. $P_{3D}(k) = P_{3D}(k_\perp)$. Moving to Eq: (B.3);

$$\begin{aligned}\xi_\kappa(\Delta\vec{\theta}) &= \int d\chi W(\chi) \int d\chi' W(\chi') \int \frac{d^2\vec{k}_\perp}{(2\pi)^2} P_{3D}(|\vec{k}_\perp|, \chi) e^{i\chi\vec{k}_\perp(\vec{\theta}-\vec{\theta}')} e^{ik_\parallel \chi} \int d\chi' e^{ik_\parallel \chi'} \\ &= \int d\chi W^2(\chi) \int \frac{d^2\vec{k}_\perp}{(2\pi)^2} P_{3D}(|\vec{k}_\perp|, \chi) e^{-i\chi\vec{k}_\perp.\vec{\theta}}\end{aligned} \tag{B.6}$$

Where in the above expression we have assumed that the window function $(W(\chi))$ does not vary significantly over a redshift range. Putting the above result in the $P_\kappa(\vec{l})$ expression,

$$\begin{aligned}P_\kappa(\vec{l}) &= \int d^2\vec{\theta} \int d\chi W(\chi) \int \frac{d^2\vec{k}_\perp}{(2\pi)^2} P_{3D}(|\vec{k}_\perp|, \chi) e^{-i\chi\vec{k}_\perp.\vec{\theta}} . e^{i\vec{l}.\vec{\theta}} \\ &= \int d\chi W^2(\chi) \int \frac{d^2\vec{k}_\perp}{(2\pi)^2} P_{3D}(|\vec{k}_\perp|, \chi) . (2\pi)^2 \delta_D(\vec{l} - \chi\vec{k}_\perp)\end{aligned} \tag{B.7}$$

Changing variable $\vec{k}_\perp\chi = \vec{l}$ we have

$$P_\kappa(\vec{l}) = \int d\chi \frac{W^2(\chi)}{\chi^3} P_{3D}\left(\frac{\vec{l}}{\chi}, \chi\right) \tag{B.8}$$

Coming back to our original notation; the convergence power spectrum takes the form

$$P_\kappa(\vec{l}) = \frac{9}{4}\left(\frac{H_0}{c}\right)^4 \Omega_{m0}^2 \int_0^{\chi_s} d\chi \, \frac{g^2(\chi)}{a^2(\chi)} \, D_+^2(\chi) P_{3D}\left(\frac{\vec{l}}{\chi}\right) \tag{B.9}$$

Spherical harmonic approach: The spherical harmonic moment of convergence $\kappa(\hat{n})$ are defined as

$$\begin{aligned}a_{lm}^\kappa &= \int d\Omega_{\hat{n}} \, \kappa(\hat{n}) \, Y_{lm}^*(\hat{n}) \\ &= \int dz W(z) \int_{S^2} d\Omega \int \frac{d^3\vec{k}}{(2\pi)^3} \tilde{\delta}(\vec{k}, z) e^{i\vec{k}.\vec{r}} Y_{lm}^*(\hat{n})\end{aligned} \tag{B.10}$$

Using the plane wave expansion,

$$e^{i\vec{k},\vec{\chi}} = e^{ik\chi(\hat{k}.\hat{n})} = 4\pi \sum_{l=0}^{\infty} \sum_{m=-l}^{l} i^l j_l(k\chi) Y^*_{lm}(\hat{k}) Y^*_{lm}(\hat{n}) \tag{B.11}$$

with orthogonalization condition $\int_{S^2} d\Omega Y^*_{lm}(\hat{n}) Y_{l'm'}(\hat{n}) = \delta^{l'}_{l} \delta^{m'}_{m}$.

Define angular power spectrum, $P_\kappa(\vec{l}) \equiv \langle a_{l_1 m_1} a^*_{l_2 m_2} \rangle$,

$$\begin{aligned} &= (4\pi)^2 i^{(l_1 - l_2)} \int dz_1 dz_2 W(z_1) W(z_2) \int \frac{d^3\vec{k}_1}{(2\pi)^3} \frac{d^3\vec{k}'_2}{(2\pi)^3} \langle \tilde{\delta}(\vec{k}_1, z_1) \tilde{\delta}(\vec{k}_2, z_2) \rangle \\ &\quad j_{l_1}(k_1\chi_1) j_{l_2}(k_2\chi_2) Y^*_{l_1 m_1}(\hat{k}_1) Y_{l_2 m_2}(\hat{k}_2) \end{aligned} \tag{B.12}$$

Using the properties of the δ_D in spherical system; $\delta_D(\vec{k}_1 + \vec{k}_2) = \frac{1}{k_1^2} \delta_D(k_1 + k_2) \delta_D(\hat{k}_1 + \hat{k}_2)$,

$$\begin{aligned} P_\kappa(\vec{l}) &= (4\pi)^2 i^{(l_1 - l_2)} \int dz_1 dz_2 W(z_1) W(z_2) \int \frac{d^3\vec{k}_1}{(2\pi)^3} \frac{d^3\vec{k}'_2}{(2\pi)^3} (2\pi)^3 P_{3D}(k_1, z_1, z_2) \\ &\quad \delta_D(\vec{k}_1 + \vec{k}_2) j_{l_1}(k_1\chi_1) j_{l_2}(k_2\chi_2) Y^*_{l_1 m_1}(\hat{k}_1) Y_{l_2 m_2}(\hat{k}_2) \\ &= \frac{(4\pi)^2}{(2\pi)^3} i^{(l_1 - l_2)} \int dz_1 dz_2 W(z_1) W(z_2) \int d^3\vec{k}_1 P_{3D}(k_1, z_1, z_2) j_{l_1}(k_1\chi_1) \\ &\quad j_{l_2}(-k_1\chi_2) Y^*_{l_1 m_1}(\hat{k}_1) Y_{l_2 m_2}(-\hat{k}_2) \end{aligned} \tag{B.13}$$

Using the parity symmetry of Bessel function, spherical harmonics and orthogonality condition, i.e. $j_l(-x) = (-i)^l j_l(x)$ and $Y_{lm}(-x) = (-i)^l Y_{lm}(x)$,

$$\begin{aligned} P_\kappa(\vec{l}) &= \delta^{l_2}_{l_1} \delta^{m_2}_{m_1} (4\pi)^2 i^{(l_1 - l_2)} \int dz_1 dz_2 W(z_1) W(z_2) \int \frac{d\vec{k}_1}{(2\pi)^3} k_1^2 P_{3D}(k_1, z_1, z_2) j_{l_1}(k_1\chi_1) j_{l_2}(k_2\chi_2) \\ &= \frac{2}{\pi} \int dk\ k^2 \int dz_1\ dz_2 W(z_1) W(z_2) j_l(k\chi_1) j_l(k\chi_2) P_{3D}(k, z_1, z_2) \\ &\approx \frac{2}{\pi} \int dk\ k^2 \int dz W^2(z) j_l(k\chi_1) j_l(k\chi_2) P_{3D}(k, z_1, z_2) \end{aligned} \tag{B.14}$$

Using small scale approximation or so called Limber approximation,

$$\int\ dk\ k^2\ j_l(k\chi_1) j_l(k\chi_2) f(k) \approx \frac{\pi}{2} \frac{\delta_D(\chi_1 - \chi_2)}{\chi_1^2} f\left(\frac{l}{\chi_1}\right) \tag{B.15}$$

Hence the final expression for the convergence power spectrum,

$$C_\kappa(\vec{l}) = \int dz \frac{W^2(z)}{\chi^2(z)} P_{3D}\left(\frac{l}{\chi}, \chi\right) \tag{B.16}$$

APPENDIX C

Multifrequency Angular Power Spectrum of 21cm signal

C.1 Deriving 21cm power spectrum

The '21 cm radiation efficiency in redshift space'.

$$\eta_{HI}(\mathbf{n}, z) = \frac{\rho_{HI}}{\bar{\rho}_H}\left(1 - \frac{T_\gamma}{T_s}\right)\left[1 - \frac{(1+z)}{H(z)}\frac{\partial v}{\partial z}\right] \tag{C.1}$$

which varies with position and redshift, and it incorporates the details of the HI evolution and the effects of the growth of large scale structures. We also introduce $\tilde{\eta}_{HI}(\mathbf{k}, z)$, the Fourier transform of $\eta_{HI}(\mathbf{x}, z)$, defined through

$$\eta_{HI}(\mathbf{n}, z) = \int \frac{d^3k}{(2\pi)^3} e^{i\mathbf{k}.\chi_\nu \mathbf{n}} \tilde{\eta}_{HI}(\mathbf{k}, z) \tag{C.2}$$

where

$$\tilde{\eta}_{HI} = \bar{x}_{HI}\left[\Delta_{HI}(z, \mathbf{k}) + f(z)(\hat{\mathbf{k}}.\hat{\mathbf{n}})^2 \Delta(z, \mathbf{k})\right] \tag{C.3}$$

where $\Delta_{HI}(z, \mathbf{k})$, $\Delta(z, \mathbf{k})$ are the Fourier transform of the fluctuations in the HI and dark matter densities. The redshift space distortion factor $f(z)$ relates the peculiar velocities to the dark matter. Now define the three dimensional power spectrum $P_{HI}(\mathbf{k}, z)$,

$$\langle \tilde{\eta}_{HI}(\mathbf{k}, z) \tilde{\eta}^*_{HI}(\mathbf{k}', z) \rangle = (2\pi)^2 \delta^3_D(\mathbf{k} - \mathbf{k}') P_{HI}(\mathbf{k}, z) \tag{C.4}$$

Harmonic approach to MAPS

The spherical harmonic moment of $T(z, \hat{\mathbf{n}})$ are defined as

$$a_{lm}^{21}(z) = \int d\Omega Y_{lm}^{*}(\hat{\mathbf{n}}) T(z, \hat{\mathbf{n}}) \tag{C.5}$$

$$= \bar{T} \int d\Omega Y_{lm}^{*}(\hat{\mathbf{n}}) \int \frac{d^3k}{(2\pi)^3} \tilde{\eta}_{HI}(\mathbf{k}) e^{-ik\chi_\nu(\hat{\mathbf{k}}.\hat{\mathbf{n}})} \tag{C.6}$$

Using the expression (C.3) for $\tilde{\eta}_{HI}(\mathbf{k})$ in equation (C.5), the expression for $a_{lm}^{21}(z)$ can be written as

$$a_{lm}^{21}(z) = \bar{T}\bar{x}_{HI} \int d\Omega Y_{lm}^{*}(\hat{\mathbf{n}}) \int \frac{d^3k}{(2\pi)^3} \left[\Delta_{HI}(z, \mathbf{k}) + f(z)(\hat{\mathbf{k}}.\hat{\mathbf{n}})^2 \Delta(z, \mathbf{k})\right] e^{-ik\chi_\nu(\hat{\mathbf{k}}.\hat{\mathbf{n}})} \tag{C.7}$$

Expanding the term $e^{-ik\chi_\nu(\hat{\mathbf{k}}.\hat{\mathbf{n}})}$ in terms of spherical Bessel function $j_l(k\chi_\nu)$, one can show that

$$\int d\Omega Y_{lm}^{*}(\hat{\mathbf{n}}) e^{-ik\chi_\nu(\hat{\mathbf{k}}.\hat{\mathbf{n}})} = 4\pi(-i)^l j_l(k\chi_\nu) Y_{lm}^{*}(\hat{\mathbf{k}}) \tag{C.8}$$

Differentiating the above equation w.r.t $k\chi_\nu$ twice, we have

$$\int d\Omega (\hat{\mathbf{k}}.\hat{\mathbf{n}})^2 Y_{lm}^{*}(\hat{\mathbf{n}}) e^{-ik\chi_\nu(\hat{\mathbf{k}}.\hat{\mathbf{n}})} = -4\pi(-i)^l j_l''(k\chi_\nu) Y_{lm}^{*}(\hat{\mathbf{k}}) \tag{C.9}$$

where $j_l''(x)$ is the second derivative of $j_l(x)$ with respect to the argument, and can be obtained through the recursion relation

$$j_l''(x) = \frac{l(l-1) - x^2}{x^2} j_l(x) + \frac{2}{x} j_{l+1}(x) \tag{C.10}$$

So the final expression of a_{lm}^{21} is given by

$$a_{lm}^{21}(z) = 4\pi\bar{T}\bar{x}_{HI}(-i)^l \int \frac{d^3k}{(2\pi)^3} Y_{lm}^{*}(\hat{\mathbf{k}}) \left[\Delta_{HI}(z, \mathbf{k}) j_l(k\chi_\nu) - f(z)\Delta(z, \mathbf{k}) j_l''(k\chi_\nu)\right] \tag{C.11}$$

On large scales the redshifted HI 21-cm signal from post reionization epoch $(z < 6)$ known to be biased tracers of the underlying dark matter distribution [91–93]. The bias function b quantifies the nature of HI clustering in the post-reionization epoch. On large scales the bias is known to be scale-independent, though the scales above which the bias is linear. Hence we impose $\Delta_{HI}(z, \mathbf{k}) =$

$b\Delta(z,\mathbf{k})$ in the subsequent expressions. As $f(z)$ is a slowly varying function, we have neglected the difference between z_1 and z_2. Next we will calculate the power spectrum $C_l(z_1,z_2) \equiv \langle a_{lm}^{21}(z_1) a_{lm}^{21*}(z_2)\rangle$. Writing C_l

$$\begin{aligned} C_l(z_1,z_2) = (4\pi)^2 \bar{T}(z_1)\bar{T}(z_2)\bar{x}_{HI}^2 \int \frac{d^3k_1}{(2\pi)^3}\int \frac{d^3k_2}{(2\pi)^3} Y_{lm}^*(\hat{\mathbf{k}}_\mathbf{1}) Y_{lm}(\hat{\mathbf{k}}_\mathbf{2}) \\ \times \langle [b\Delta(z_1,\mathbf{k}_1) j_l(k_1\chi_{\nu_1}) - f(z)\Delta(z_1,\mathbf{k}_1) j_l''(k_1\chi_{\nu_1})]\rangle \\ \times \langle [b\Delta^*(z_2,\mathbf{k}_2) j_l(k_2\chi_{\nu_2}) - f(z)\Delta^*(z_2,\mathbf{k}_2) j_l''(k_2\chi_{\nu_2})]\rangle \end{aligned}$$

The terms involving the ensemble average of the form $\langle \Delta(z_1,\mathbf{k}_1)\Delta^*(z_2,\mathbf{k}_2)\rangle \approx (2\pi)^3\delta_D(\mathbf{k}_1-\mathbf{k}_2)P(z_1,z_2,k_1)$. We can then use the Dirac delta function $\delta_D(\mathbf{k}_1 - \mathbf{k}_2)$ to compute the $\mathbf{k}_2$ integral and thus can write the angular power spectrum as

$$\begin{aligned} C_l(z_1,z_2) = (4\pi)^2 \bar{T}(z_1)\bar{T}(z_2)\bar{x}_{HI}^2 \int \frac{d^3k}{(2\pi)^3} Y_{lm}^*(\hat{\mathbf{k}}_\mathbf{1}) Y_{lm}(\hat{\mathbf{k}}_\mathbf{2}) P(z_1,z_2,k) \\ \times \left[b^2 j_l(k\chi_{\nu_1}) j_l(k\chi_{\nu_2}) - bf(z)(j_l(k\chi_{\nu_1}) j_l''(k\chi_{\nu_2}) + j_l(k\chi_{\nu_2}) j_l''(k\chi_{\nu_1}))\right] \\ + \left[f^2(z) j_l''(k\chi_{\nu_1}) j_l''(k\chi_{\nu_2})\right] \end{aligned}$$

Using the normalzation property of the spherical harmonics $\int d\hat{\mathbf{n}} |Y_{lm}(\hat{\mathbf{n}})|^2 = 1$, one can carry out the angular integration and hence obtain,

$$\begin{aligned} C_l(z_1,z_2) = \frac{2\bar{T}(z_1)\bar{T}(z_2)\bar{x}_{HI}^2}{\pi} \int_0^\infty k^2 dk P(z_1,z_2,k) \\ \times \left[b^2 j_l(k\chi_{\nu_1}) j_l(k\chi_{\nu_2}) - bf(z)(j_l(k\chi_{\nu_1}) j_l''(k\chi_{\nu_2}) + j_l(k\chi_{\nu_2}) j_l''(k\chi_{\nu_1}))\right] \\ + \left[f^2(z) j_l''(k\chi_{\nu_1}) j_l''(k\chi_{\nu_2})\right] \end{aligned} \tag{C.12}$$

Typically $\chi \sim 5 - 10,000$Mpc and $k \sim 0.1$Mpc^{-1} so the spherical Bessel functions $j_l(x)$ are typically evaluated in the limit of $l < x < l^2$. In practice integrals over the product of two spherical Bessel functions are numerically challenging due to their oscillatory behavior, so we will look for a scheme to approximate this integral obtained using the method of steepest descent (this method is also used, for example, to derive Stirling's approximation to $\log n!$ for large n). Starting with the integral representation of the spherical Bessel functions, the integration contour is deformed slightly to pass through saddle points of

the integrand, approaching along paths of steepest descent. This allows the integral to be approximated as a Gaussian integral, which can be analytically evaluated to

$$j_l(x) \approx \frac{1}{x}\sin\left(x_\parallel + \Phi(l) - \frac{l\pi}{2}\right)\sqrt{\frac{x}{x_\parallel}} \tag{C.13}$$

where we have suggestively defined $x_\parallel = \sqrt{x^2 - l^2}$ and $\Phi(l) = (l{+}1/2)\arctan(l/x_\parallel)$ tends to zero for nearby frequency channels. Using the Bessel approximation in (C.13) and the recursion for $j''(x)$ in (C.10) we will evaluate the integral for 'flat sky approximation' of MAPS. Consider the first term in (C.12)

$$\begin{aligned}
C_l^{(1)} &= \int_0^\infty k^2 dk\; P(z_1, z_2, k)\; b^2 j_l(k\chi_{\nu_1}) j_l(k\chi_{\nu_2}) \\
&= \int_0^\infty \cancel{k^2} dk\; P(z_1, z_2, k)\; b^2 \frac{\sin(k_\parallel\chi_{\nu_1} + \Phi_1)}{\cancel{k}\chi_{\nu_1}}\sqrt{\frac{k}{k_\parallel}}\frac{\sin(k_\parallel\chi_{\nu_2} + \Phi_2)}{\cancel{k}\chi_{\nu_2}}\sqrt{\frac{k}{k_\parallel}} \\
&= \int_0^\infty \frac{\cancel{k_\parallel}}{\cancel{k}} dk_\parallel\; P(z_1, z_2, k)\; b^2 \frac{\sin(k_\parallel\chi_{\nu_1} + \Phi_1)}{\chi_{\nu_1}}\sqrt{\frac{\cancel{k}}{\cancel{k_\parallel}}}\frac{\sin(k_\parallel\chi_{\nu_2} + \Phi_2)}{\chi_{\nu_2}}\sqrt{\frac{\cancel{k}}{\cancel{k_\parallel}}} \\
&= \int_0^\infty dk_\parallel \frac{\cos(k_\parallel(\chi_{\nu_1} - \chi_{\nu_2}) + (\Phi_1 - \Phi_2)l)}{2\chi_{\nu_1}\chi_{\nu_2}} b^2 P(z_1, z_2, k)
\end{aligned}$$

Ignoring the second term in the above expression, we have the final expression (for the 1st term only)

$$C_l^{(1)} = \frac{\bar{T}(z_1)\bar{T}(z_2)\bar{x}_{HI}^2 b^2}{\pi\chi_{\nu_1}\chi_{\nu_2}}\int_0^\infty dk_\parallel \cos(k_\parallel\Delta\chi) P(z_1, z_2, k) \tag{C.14}$$

Moving to the second term of (C.12), and using the recursion relation for $j_l''(x)$ we have

$$\begin{aligned}
C_l^{(2)} &= \int_0^\infty k^2 dk\; P(z_1, z_2, k)\; b f(z) j_l(k\chi_{\nu_1}) j_l''(k\chi_{\nu_2}) \\
&= \int_0^\infty k^2 dk\; P(z_1, z_2, k)\; b f(z) j_l(k\chi_{\nu_1})\left(\frac{l^2}{k^2\chi_{\nu_2}^2} - 1\right) j_l(k\chi_{\nu_2})
\end{aligned}$$

where in the $j''(kx)$ recursion we ignored the $j_{l+1}(x)$ term and for for large scale

we approximate, $l(l-1) \approx l^2$. Proceeding further

$$
\begin{aligned}
C_l^{(2)} &= \int_0^\infty \cancel{k^2} dk\ P(z_1, z_2, k)\ bf(z) \frac{\sin(k_\parallel \chi_{\nu_1} + \Phi_1)}{\cancel{k}\chi_{\nu_1}} \sqrt{\frac{k}{k_\parallel}} \left(\frac{l^2}{k^2 \chi_{\nu_2}^2} - 1 \right) \frac{\sin(k_\parallel \chi_{\nu_2} + \Phi_2)}{\cancel{k}\chi_{\nu_2}} \sqrt{\frac{k}{k_\parallel}} \\
&= \int_0^\infty \frac{\cancel{k_\parallel}}{\cancel{k}} dk_\parallel\ P(z_1, z_2, k)\ bf(z) \frac{\sin(k_\parallel \chi_{\nu_1} + \Phi_1)}{\cancel{k}\chi_{\nu_1}} \sqrt{\frac{\cancel{k}}{\cancel{k_\parallel}}} \left(\frac{k_\perp^2}{k^2} - 1 \right) \frac{\sin(k_\parallel \chi_{\nu_2} + \Phi_2)}{\cancel{k}\chi_{\nu_2}} \sqrt{\frac{\cancel{k}}{\cancel{k_\parallel}}} \\
&= -\int_0^\infty dk_\parallel \frac{\cos(k_\parallel(\chi_{\nu_1} - \chi_{\nu_2}) + (\Phi_1 - \Phi_2)l)}{2\chi_{\nu_1}\chi_{\nu_2}} bf(z)\mu^2 P(z_1, z_2, k)
\end{aligned}
$$

where in the last expression we have used $\mu^2 = 1 - (k_\perp^2/k^2) = k_\parallel^2/k^2$, which is the cosine of the angle between line of sight and the wave vector. Hence the final expression

$$
C_l^{(2)} = -\frac{\bar{T}(z_1)\bar{T}(z_2)\bar{x}_{HI}^2}{\pi \chi_{\nu_1}\chi_{\nu_2}} \int_0^\infty dk_\parallel \cos(k_\parallel \Delta\chi) bf(z)\mu^2 P(z_1, z_2, k) \tag{C.15}
$$

Third term of (C.12) takes the same form as above. So we will not calculate it explicitly. Moving towards the last expression of (C.12),

$$
\begin{aligned}
C_l^{(4)} &= \int_0^\infty k^2 dk\ P(z_1, z_2, k)\ f^2(z) j_l''(k\chi_{\nu_1}) j_l''(k\chi_{\nu_2}) \\
&= \int_0^\infty k^2 dk\ P(z_1, z_2, k)\ f^2(z) \left(\frac{l^2}{k^2\chi_{\nu_1}^2} - 1 \right) j_l(k\chi_{\nu_1}) \left(\frac{l^2}{k^2\chi_{\nu_2}^2} - 1 \right) j_l(k\chi_{\nu_2}) \\
&= \int_0^\infty \cancel{k^2} dk\ P(z_1, z_2, k)\ f^2(z) \left(\frac{l^2}{k^2\chi_{\nu_1}^2} - 1 \right) \frac{\sin(k_\parallel \chi_{\nu_1} + \Phi_1)}{\cancel{k}\chi_{\nu_1}} \sqrt{\frac{k}{k_\parallel}} \left(\frac{l^2}{k^2\chi_{\nu_2}^2} - 1 \right) \\
&\quad \frac{\sin(k_\parallel \chi_{\nu_2} + \Phi_2)}{\cancel{k}\chi_{\nu_2}} \sqrt{\frac{k}{k_\parallel}} \\
&= \int_0^\infty \frac{\cancel{k_\parallel}}{\cancel{k}} dk_\parallel\ P(z_1, z_2, k)\ f^2(z) \left(\frac{k_\perp^2}{k^2} - 1 \right) \frac{\sin(k_\parallel \chi_{\nu_1} + \Phi_1)}{\cancel{k}\chi_{\nu_1}} \sqrt{\frac{\cancel{k}}{\cancel{k_\parallel}}} \left(\frac{k_\perp^2}{k^2} - 1 \right) \\
&\quad \frac{\sin(k_\parallel \chi_{\nu_2} + \Phi_2)}{\cancel{k}\chi_{\nu_2}} \sqrt{\frac{\cancel{k}}{\cancel{k_\parallel}}} \\
&= \int_0^\infty dk_\parallel \frac{\cos(k_\parallel(\chi_{\nu_1} - \chi_{\nu_2}) + (\Phi_1 - \Phi_2)l)}{2\chi_{\nu_1}\chi_{\nu_2}} f^2(z)\mu^4 P(z_1, z_2, k)
\end{aligned}
$$

Returning to the final expression,

$$
C_l^{(4)} = \frac{\bar{T}(z_1)\bar{T}(z_2)\bar{x}_{HI}^2}{\pi \chi_{\nu_1}\chi_{\nu_2}} \int_0^\infty dk_\parallel \cos(k_\parallel \Delta\chi) f^2(z)\mu^4 P(z_1, z_2, k) \tag{C.16}
$$

Using the above results the final expression of MAPS in "Flat sky approximation",

$$C_l(z_1,z_2) = \frac{\bar{T}(z_1)\bar{T}(z_2)\bar{x}_{HI}^2}{\pi\chi_{\nu_1}\chi_{\nu_2}} \int_0^\infty dk_\parallel \cos(k_\parallel \Delta\chi)[b^2 + 2bf(z)\mu^2 + f^2(z)\mu^4]P(z_1,z_2,k)$$
$$C_l(z_1,z_2) = \frac{\bar{T}(z_1)\bar{T}(z_2)\bar{x}_{HI}^2}{\pi\chi_{\nu_1}\chi_{\nu_2}} \int_0^\infty dk_\parallel \cos(k_\parallel \Delta\chi)[b + f(z)\mu^2]^2P(z_1,z_2,k) \tag{C.17}$$

Consequently we arrive at the "flat sky approximation" used by [253] and [301].

C.2 Noise estimation

We use a visibility correlation approach to estimate the noise power spectrum for the 21-cm signal [82, 253, 291, 353, 468, 469]. A radiointerferometric observation measures the complex visibility. The measured visibility written as a function of baseline $\mathbf{U} = (u, v)$ and frequency ν is a sum of signal and noise

$$\mathcal{V}(\mathbf{U},\nu) = \mathcal{S}(\mathbf{U},\nu) + \mathcal{N}(\mathbf{U},\nu) \tag{C.18}$$

$$\mathcal{S}(\mathbf{U},\nu) = \frac{2k_B}{\lambda^2} \int d\vec{\theta}\, A(\vec{\theta}) e^{2\pi i \mathbf{U}\cdot\vec{\theta}}\, \delta T_b(\vec{\theta},\nu) \tag{C.19}$$

where, $\delta T_b(\vec{\theta},\nu)$ is the fluctuations of the 21-cm brightness temperature and $A(\vec{\theta})$ is the telescope beam. The factor $\left(\frac{2k_B}{\lambda^2}\right)^2$ converts brightness temperature to intensity (Raleigh Jeans limit). Defining $\Delta\nu$ as the difference from the central frequency, a further Fourier transform in frequency $\Delta\nu$ gives us

$$s(\mathbf{U},\tau) = \frac{2k_B}{\lambda^2} \int d\vec{\theta}\, d\nu\, A(\vec{\theta}) B(\Delta\nu)\, e^{2\pi i(\mathbf{U}\cdot\vec{\theta}+\tau\Delta\nu)}\, \delta T_b(\vec{\theta},\nu) \tag{C.20}$$

where $B(\Delta\nu)$ is the frequency response function of the radio telescope.

$$s(\mathbf{U}_a,\tau_m) = \frac{2k_B}{\lambda^2} \int d\vec{\theta}\, d\Delta\nu \int \frac{d^3\mathbf{k}}{(2\pi)^3}\, e^{-i(\mathbf{k}_\perp r\cdot\vec{\theta}+k_\parallel r'\Delta\nu)}\, A(\vec{\theta}) B(\Delta\nu)\, e^{2\pi i(\mathbf{U}_a\cdot\vec{\theta}+\tau_m\Delta\nu)}\, \widetilde{\delta T_b}(\mathbf{k}_\perp,k_\parallel) \tag{C.21}$$

where the tilde denotes a fourier transform and $r' = dr(\nu)/d\nu$.

$$s(\mathbf{U}_a, \tau_m) = \frac{2k_B}{\lambda^2} \int d\vec{\theta}\, d\Delta\nu \int \frac{d^3\mathbf{k}}{(2\pi)^3}\, e^{-i(\mathbf{k}_\perp r - 2\pi\mathbf{U}_a)\cdot\vec{\theta}} e^{-i(k_\parallel r' - 2\pi\tau_m)\Delta\nu}\, A(\vec{\theta}) B(\Delta\nu)\, \widetilde{\delta T_b}(\mathbf{k}_\perp, k_\parallel) \tag{C.22}$$

Performing the $\vec{\theta}$ and $\Delta\nu$ integral we have

$$s(\mathbf{U}_a, \tau_m) = \frac{2k_B}{\lambda^2} \int \frac{d^3\mathbf{k}}{(2\pi)^3}\, \widetilde{A}\left(\frac{\mathbf{k}_\perp r}{2\pi} - \mathbf{U}_a\right) \widetilde{B}\left(\frac{k_\parallel r'}{2\pi} - \tau_m\right)\, \widetilde{\delta T_b}(\mathbf{k}_\perp, k_\parallel) \tag{C.23}$$

$$\begin{aligned}\langle s(\mathbf{U}_a, \tau_m) s^*(\mathbf{U}_b, \tau_n)\rangle = \left(\frac{2k_B}{\lambda^2}\right)^2 \int \frac{d^3\mathbf{k}}{(2\pi)^3} \int \frac{d^3\mathbf{k}'}{(2\pi)^3} \widetilde{A}\left(\frac{\mathbf{k}_\perp r}{2\pi} - \mathbf{U}_a\right) \widetilde{B}\left(\frac{k_\parallel r'}{2\pi} - \tau_m\right) \\ \times \widetilde{A}^*\left(\frac{\mathbf{k}'_\perp r}{2\pi} - \mathbf{U}_b\right) \widetilde{B}^*\left(\frac{k'_\parallel r'}{2\pi} - \tau_n\right) (2\pi)^3 P_{HI}(\mathbf{k}) \delta_D(\mathbf{k} - \mathbf{k}')\end{aligned}$$

$$\begin{aligned}\langle s(\mathbf{U}_a, \tau_m) s^*(\mathbf{U}_b, \tau_n)\rangle = \left(\frac{2k_B}{\lambda^2}\right)^2 \int \frac{d^3\mathbf{k}}{(2\pi)^3} \widetilde{A}\left(\frac{\mathbf{k}_\perp r}{2\pi} - \mathbf{U}_a\right) \widetilde{B}\left(\frac{k_\parallel r'}{2\pi} - \tau_m\right) \\ \times \widetilde{A}^*\left(\frac{\mathbf{k}_\perp r}{2\pi} - \mathbf{U}_b\right) \widetilde{B}^*\left(\frac{k_\parallel r'}{2\pi} - \tau_n\right) P_{HI}(\mathbf{k})\end{aligned}$$

Defining new integration variables as $\mathbf{U} = \frac{\mathbf{k}_\perp r}{2\pi}$ and $\tau = \frac{k_\parallel r'}{2\pi}$ we have

$$\begin{aligned}\langle s(\mathbf{U}_a, \tau_m) s^*(\mathbf{U}_b, \tau_n)\rangle = \left(\frac{2k_B}{\lambda^2}\right)^2 \frac{1}{r^2 r'} \int d\mathbf{U}\, d\tau \widetilde{A}\left(\mathbf{U} - \mathbf{U}_a\right) \widetilde{A}^*\left(\mathbf{U} - \mathbf{U}_b\right) \\ \widetilde{B}\left(\tau - \tau_m\right) \widetilde{B}^*\left(\tau - \tau_n\right) P_{HI}\left(\frac{2\pi\mathbf{U}}{r}, \frac{2\pi\tau}{r'}\right)\end{aligned} \tag{C.24}$$

Approximately, we may write

$$\int \widetilde{B}\left(\tau - \tau_m\right) \widetilde{B}^*\left(\tau - \tau_n\right) \approx B\delta_{m,n} \quad \text{and} \quad \int d\mathbf{U}\, \widetilde{A}\left(\mathbf{U} - \mathbf{U}_a\right) \widetilde{A}^*\left(\mathbf{U} - \mathbf{U}_b\right) \approx \frac{\lambda^2}{A_e}\delta_{a,b} \tag{C.25}$$

where B is the bandwidth of the telescope and

$$\int d\mathbf{U}\, \widetilde{A}\left(\mathbf{U} - \mathbf{U}_a\right) \widetilde{A}^*\left(\mathbf{U} - \mathbf{U}_b\right) \approx \frac{\lambda^2}{A_e}\delta_{a,b} \tag{C.26}$$

where A_e is the effective area of each dish. Hence

$$\langle s(\mathbf{U}_a, \tau_m) s^*(\mathbf{U}_b, \tau_n) \rangle \approx \left(\frac{2k_B}{\lambda^2} \right)^2 \frac{B\lambda^2}{r^2 r' A_e} \; P_{HI} \left(\frac{2\pi \mathbf{U}_a}{r}, \frac{2\pi\tau}{r'} \right) \delta_{m,n} \delta_{a,b} \tag{C.27}$$

where

$$P_{HI}(\mathbf{k}) = \bar{T}^2 b_T^2(z)(1 + \beta_T \mu^2) P_m(k, z) \tag{C.28}$$

The noise in the visibilities measured at different baselines and frequency channels are uncorrelated. We then have

$$\langle \mathcal{N}(\mathbf{U}_a, \nu_m) \; \mathcal{N}^*(\mathbf{U}_b, \nu_n) \rangle = \delta_{a,b} \delta_{m,n} 2\sigma^2 \tag{C.29}$$

where

$$\sigma = \frac{\sqrt{2} k_B T_{sys}}{A_e \sqrt{\Delta\nu t}} \tag{C.30}$$

where A_e is the effective area of the dishes, t is the correlator integration time and $\Delta\nu$ is the channel width. If B is the observing bandwidth, there would be $B/\Delta\nu$ channels. The system temperature T_{sys} can be written as

$$T_{sys} = T_{inst} + T_{sky} \tag{C.31}$$

where

$$T_{sky} = 60\mathrm{K} \left(\frac{\nu}{300 \text{ MHz}} \right)^{-2.5} \tag{C.32}$$

Under a Fourier transform

$$n(\mathbf{U}, \tau) = \sum_{i=1}^{B/\Delta\nu} \mathcal{N}(\mathbf{U}, \nu_i) \Delta\nu \; e^{2\pi i \nu_i \tau} \tag{C.33}$$

$$\langle n(\mathbf{U}_a, \tau) \; n^*(\mathbf{U}_b, \tau) \rangle = 2\sigma^2 \delta_{a,b} \sum_{i=1}^{B/\Delta\nu} \sum_{j=1}^{B/\Delta\nu} \delta_{i,j} e^{2\pi i (\nu_i - \nu_j)\tau} \Delta\nu^2 = 2\sigma^2 \delta_{a,b} \sum_{i=1}^{B/\Delta\nu} \Delta\nu^2$$

$$\langle n(\mathbf{U}_a, \tau) \; n^*(\mathbf{U}_b, \tau) \rangle = 2\sigma^2 \delta_{a,b} \Delta\nu^2 \frac{B}{\Delta\nu} = 2\sigma^2 \delta_{a,b} \Delta\nu B \tag{C.34}$$

$$\langle n(\mathbf{U}_a, \tau) \; n^*(\mathbf{U}_b, \tau) \rangle = \frac{4k_B^2 T_{sys}^2 B}{A_e^2 t} = \left(\frac{2k_B}{\lambda^2} \right)^2 \left(\frac{\lambda^2 T_{sys}}{A_e} \right)^2 \frac{B}{t} \tag{C.35}$$

Now considering a total observation time T_o and a bin $\Delta\mathbf{U}$, there is a reduction of noise by a factor $\sqrt{N_p}$ where N_p is the number of visibility pairs in the bin

$$N_p = N_{vis}(N_{vis}-1)/2 \approx N_{vis}^2/2 \tag{C.36}$$

where N_{vis} is the number of visibilities in the bin. We may write

$$N_{vis} = \frac{N_{ant}(N_{ant}-1)}{2}\frac{T_o}{t}\rho(\mathbf{U})\delta^2 U \tag{C.37}$$

where N_{ant} is the total number of antennas and $\rho(\mathbf{U})$ is the baseline distribution function.

$$\langle n(\mathbf{U}_a,\tau)\, n^*(\mathbf{U}_b,\tau)\rangle = \left(\frac{2k_B}{\lambda^2}\right)^2\left(\frac{\lambda^2 T_{sys}B}{A_e}\right)^2 \frac{2\delta_{a,b}}{N_{ant}(N_{ant}-1)B\; T_o\; \rho(\mathbf{U})\delta^2 U} \tag{C.38}$$

where an additional reduction by $\sqrt{2}$ is incorporated by considering visibilities in half plane. The 21 cm power spectrum is not spherically symmetric, due to redshift space distortion but is symmetric around the polar angle ϕ. Because of this symmetry, we want to sum all the Fourier cells in an annulus of constant $(k,\ \mu = \cos\theta = k_\parallel/k)$ with radial width Δk and angular width $\Delta\theta$ for a statistical detection. The number of independent cells in such an annulus is

$$N_c = 2\pi k^2 \sin(\theta)\Delta k\Delta\theta\frac{Vol}{(2\pi)^3} = 2\pi k^2\Delta k\Delta\mu\frac{Vol}{(2\pi)^3} \tag{C.39}$$

where

$$Vol = \frac{r^2\lambda^2 r' B}{A_e} \tag{C.40}$$

Thus the full covariance matrix for visibility correlation is [291, 353, 468, 469]

$$C_{a,b} = \frac{1}{\sqrt{N_c}}\left(\frac{2k_B}{\lambda^2}\right)^2\left[\frac{B\lambda^2}{r^2 r' A_e}\; P_{HI}\left(\frac{2\pi\mathbf{U}_a}{r},\frac{2\pi\tau}{r'}\right) + \left(\frac{\lambda^2 T_{sys}B}{A_e}\right)^2 \times\frac{2}{N_{ant}(N_{ant}-1)B\; T_o\; \rho(\mathbf{U})\delta^2 U}\right]\delta_{a,b} \tag{C.41}$$

$$C_{a,b} = \frac{1}{\sqrt{N_c}} \left(\frac{2k_B}{\lambda^2}\right)^2 \left[\frac{B\lambda^2}{r^2 r' A_e} P_{HI}\left(\frac{2\pi \mathbf{U}_a}{r}, \frac{2\pi\tau}{r'}\right) + \left(\frac{\lambda^2 T_{sys} B}{A_e}\right)^2 \frac{2}{N_{ant}(N_{ant}-1)BT_o\rho(\mathbf{U})\delta^2 U}\right]\delta_{a,b} \tag{C.42}$$

We choose $\delta^2 U = A_e/\lambda^2$, $\Delta k = k/10$, $\Delta\mu = \mu/10$. The baseline distribution function $\rho(\mathbf{U})$ is normalized as

$$\int d\mathbf{U}\rho(\mathbf{U}) = 1 \tag{C.43}$$

For uniform baseline distribution

$$\rho(\mathbf{U}) = \frac{1}{\pi(U_{max}^2 - U_{min}^2)} \tag{C.44}$$

Generally

$$\rho(\mathbf{U}) = c\int d^2\mathbf{r}\rho_{ant}(\mathbf{r})\rho_{ant}(\mathbf{r} - \lambda\mathbf{U}) \tag{C.45}$$

Where c is fixed by normalization of $\rho(\mathbf{U})$ and ρ_{ant} is the distribution of antennaes. The total noise in the 3D 21-cm power spectrum is given by

$$\delta P_{HI}(k, z, \mu) = \frac{1}{\sqrt{N_c}}\left(P_{HI}(k, z, \mu) + N_{HI}\right) \tag{C.46}$$

Beyond certain hours of observation in a single field of view, Signal to Noise Ratio is primarily influenced by cosmic variance. Therefore, by introducing N_{point} as the number of independent pointings, the covariance is further reduced by a factor of $1/\sqrt{N_{point}}$.

Bibliography

[1] D. J. Eisenstein, I. Zehavi, D. W. Hogg, R. Scoccimarro, M. R. Blanton, R. C. Nichol, R. Scranton, H. Seo, M. Tegmark, Z. Zheng, and et al., "*Detection of the Baryon Acoustic Peak in the Large-Scale Correlation Function of SDSS Luminous Red Galaxies*," The Astrophysical Journal **633**, 560–574 (2005).

[2] R. Narayan and M. Bartelmann, "*Lectures on gravitational lensing*," arXiv preprint astro-ph/9606001 (1996).

[3] W. J. Percival, S. Cole, D. J. Eisenstein, R. C. Nichol, J. A. Peacock, A. C. Pope, and A. S. Szalay, "*Measuring the Baryon Acoustic Oscillation scale using the Sloan Digital Sky Survey and 2dF Galaxy Redshift Survey*," Monthly Notices of the Royal Astronomical Society **381**, 1053–1066 (2007).

[4] L. Anderson, E. Aubourg, S. Bailey, D. Bizyaev, M. Blanton, A. S. Bolton, J. Brinkmann, J. R. Brownstein, A. Burden, A. J. Cuesta, *et al.*, "*The clustering of galaxies in the SDSS-III Baryon Oscillation Spectroscopic Survey: baryon acoustic oscillations in the Data Release 9 spectroscopic galaxy sample*," Monthly Notices of the Royal Astronomical Society **427**, 3435 (2012).

[5] A. G. Sánchez, R. Scoccimarro, M. Crocce, J. N. Grieb, S. Salazar-Albornoz, C. D. Vecchia, M. Lippich, F. Beutler, J. R. Brownstein, C.-H. Chuang, *et al.*, "*The clustering of galaxies in the completed SDSS-III Baryon Oscillation Spectroscopic Survey: cosmological implications of the configuration-space clustering wedges*," Monthly Notices of the Royal Astronomical Society **464**, 1640 (2017).

[6] C.-H. Chuang, M. Pellejero-Ibanez, S. Rodriguez-Torres, A. J. Ross, G.-b. Zhao, Y. Wang, A. J. Cuesta, J. Rubin o Martin, F. Prada, S. Alam, *et al.*, "*The clustering of galaxies in the completed SDSS-III Baryon Oscillation Spec-*

troscopic Survey: Single-probe measurements from DR12 galaxy clustering–towards an accurate model," Monthly Notices of the Royal Astronomical Society **471**, 2370 (2017).

[7] G.-B. Zhao, Y. Wang, A. Taruya, W. Zhang, H. Gil-Marín, A. De Mattia, A. J. Ross, A. Raichoor, C. Zhao, W. J. Percival, *et al.*, "*The completed SDSS-IV extended Baryon Oscillation Spectroscopic Survey: a multitracer analysis in Fourier space for measuring the cosmic structure growth and expansion rate*," Monthly Notices of the Royal Astronomical Society **504**, 33 (2021).

[8] A. A. Sen, S. A. Adil, and S. Sen, "*Do cosmological observations allow a negative Λ?*" Monthly Notices of the Royal Astronomical Society **518**, 1098 (2023).

[9] S. Perlmutter *et al.*, "*Supernovae, dark energy, and the accelerating universe*," Physics today **56**, 53 (2003).

[10] B. P. Schmidt, N. B. Suntzeff, M. Phillips, R. A. Schommer, A. Clocchiatti, R. P. Kirshner, P. Garnavich, P. Challis, B. Leibundgut, J. Spyromilio, *et al.*, "*The high-Z supernova search: measuring cosmic deceleration and global curvature of the universe using type Ia supernovae*," The Astrophysical Journal **507**, 46 (1998).

[11] S. Perlmutter, G. Aldering, M. D. Valle, S. Deustua, R. Ellis, S. Fabbro, A. Fruchter, G. Goldhaber, D. Groom, I. Hook, *et al.*, "*Discovery of a supernova explosion at half the age of the Universe*," Nature **391**, 51 (1998).

[12] D. N. Spergel, R. Bean, O. Doré, M. Nolta, C. Bennett, J. Dunkley, G. Hinshaw, N. e. Jarosik, E. Komatsu, L. Page, *et al.*, "*Three-year Wilkinson Microwave Anisotropy Probe (WMAP) observations: implications for cosmology*," The Astrophysical Journal Supplement Series **170**, 377 (2007).

[13] R. Sachs and A. Wolfe, "*Perturbations of a Cosmological Model and Angular*," Inflationary Cosmology , 377 (1986).

[14] N. Kaiser, "*Clustering in real space and in redshift space*," Monthly Notices of the Royal Astronomical Society **227**, 1 (1987).

[15] D. N. Spergel, L. Verde, H. V. Peiris, E. Komatsu, M. R. Nolta, C. L. Bennett, M. Halpern, G. Hinshaw, N. Jarosik, A. Kogut, and et al., "*First Year*

Wilkinson Microwave Anisotropy Probe (WMAP) Observations: Determination of Cosmological Parameters," The Astrophysical Journal Supplement Series **148**, 175–194 (2003).

[16] G. Hinshaw, D. N. Spergel, L. Verde, R. S. Hill, S. S. Meyer, C. Barnes, C. L. Bennett, M. Halpern, N. Jarosik, A. Kogut, and et al., "*First Year Wilkinson Microwave Anisotropy Probe (WMAP) Observations: The Angular Power Spectrum*," The Astrophysical Journal Supplement Series **148**, 135–159 (2003).

[17] N. Aghanim, Y. Akrami, M. Ashdown, J. Aumont, C. Baccigalupi, M. Ballardini, A. J. Banday, R. Barreiro, N. Bartolo, S. Basak, *et al.*, "*Planck 2018 results-V. CMB power spectra and likelihoods*," Astronomy & Astrophysics **641**, A5 (2020).

[18] K. N. Abazajian, P. Adshead, Z. Ahmed, S. W. Allen, D. Alonso, K. S. Arnold, C. Baccigalupi, J. G. Bartlett, N. Battaglia, B. A. Benson, *et al.*, "*CMB-S4 science book*," arXiv preprint arXiv:1610.02743 (2016).

[19] T. Padmanabhan, "*Cosmological constant—the weight of the vacuum*," Physics Reports **380**, 235–320 (2003).

[20] S. M. Carroll, "*The Cosmological Constant*," Living Reviews in Relativity **4** (2001), 10.12942/lrr-2001-1.

[21] B. Ratra and P. J. E. Peebles, "*Cosmological consequences of a rolling homogeneous scalar field*," Phys. Rev. D **37**, 3406 (1988).

[22] S. Dodelson and F. Schmidt, *Modern cosmology* (Academic Press, 2020).

[23] A. Albrecht, G. Bernstein, R. Cahn, W. L. Freedman, J. Hewitt, W. Hu, J. Huth, M. Kamionkowski, E. W. Kolb, L. Knox, *et al.*, "*Report of the dark energy task force*," arXiv preprint astro-ph/0609591 (2006).

[24] R. R. Caldwell, R. Dave, and P. J. Steinhardt, "*Cosmological Imprint of an Energy Component with General Equation of State*," Phys. Rev. Lett. **80**, 1582 (1998).

[25] L. Amendola and S. Tsujikawa, *Dark Energy: Theory and Observations* (Cambridge University Press, 2010).

[26] K. Bamba, S. Capozziello, S. Nojiri, and S. D. Odintsov, "*Dark energy cosmology: the equivalent description via different theoretical models and cosmography tests*," Astrophysics and Space Science **342**, 155 (2012).

[27] A. G. Riess, L. M. Macri, S. L. Hoffmann, D. Scolnic, S. Casertano, A. V. Filippenko, B. E. Tucker, M. J. Reid, D. O. Jones, J. M. Silverman, and et al., "*A 2.4% DETERMINATION OF THE LOCAL VALUE OF THE HUBBLE CONSTANT*," The Astrophysical Journal **826**, 56 (2016).

[28] G.-B. Zhao, M. Raveri, L. Pogosian, Y. Wang, R. G. Crittenden, W. J. Handley, W. J. Percival, F. Beutler, J. Brinkmann, C.-H. Chuang, and et al., "*Dynamical dark energy in light of the latest observations*," Nature Astronomy **1**, 627–632 (2017).

[29] S. Weinberg, "*The cosmological constant problem*," Reviews of modern physics **61**, 1 (1989).

[30] E. Abdalla, G. F. Abellán, A. Aboubrahim, A. Agnello, Ö. Akarsu, Y. Akrami, G. Alestas, D. Aloni, L. Amendola, L. A. Anchordoqui, *et al.*, "*Cosmology intertwined: A review of the particle physics, astrophysics, and cosmology associated with the cosmological tensions and anomalies*," Journal of High Energy Astrophysics **34**, 49 (2022).

[31] N. Schöneberg, G. F. Abellán, A. P. Sánchez, S. J. Witte, V. Poulin, and J. Lesgourgues, "*The H0 Olympics: A fair ranking of proposed models*," Physics Reports **984**, 1 (2022).

[32] E. J. Copeland, M. Sami, and S. Tsujikawa, "*Dynamics of dark energy*," International Journal of Modern Physics D **15**, 1753 (2006).

[33] C. Burgess, "*The cosmological constant problem: why it's hard to get dark energy from micro-physics*," 100e Ecole d'Ete de Physique: Post-Planck Cosmology , 149 (2015).

[34] P. J. Steinhardt, "*Cosmological challenges for the 21st century*," Critical problems in physics , 123 (1997).

[35] H. E. Velten, R. Vom Marttens, and W. Zimdahl, "*Aspects of the cosmological "coincidence problem"*," The European Physical Journal C **74**, 1 (2014).

[36] N. Aghanim, Y. Akrami, M. Ashdown, J. Aumont, C. Baccigalupi, M. Ballardini, A. J. Banday, R. B. Barreiro, N. Bartolo, and et al., "*Planck 2018 results*," Astronomy and Astrophysics **641**, 6 (2020).

[37] E. Di Valentino, L. A. Anchordoqui, Ö. Akarsu, Y. Ali-Haimoud, L. Amendola, N. Arendse, M. Asgari, M. Ballardini, S. Basilakos, E. Battistelli, *et al.*, "*Cosmology intertwined III: fσ8 and S8*," Astroparticle Physics **131**, 102604 (2021).

[38] A. G. Riess, S. Casertano, W. Yuan, L. M. Macri, and D. Scolnic, "*Large Magellanic Cloud Cepheid standards provide a 1% foundation for the determination of the Hubble constant and stronger evidence for physics beyond ΛCDM*," The Astrophysical Journal **876**, 85 (2019).

[39] K. C. Wong, S. H. Suyu, G. C. Chen, C. E. Rusu, M. Millon, D. Sluse, V. Bonvin, C. D. Fassnacht, S. Taubenberger, M. W. Auger, *et al.*, "*H0LiCOW–XIII. A 2.4 per cent measurement of H 0 from lensed quasars: 5.3 σ tension between early-and late-Universe probes*," Monthly Notices of the Royal Astronomical Society **498**, 1420 (2020).

[40] S. Basilakos and S. Nesseris, "*Conjoined constraints on modified gravity from the expansion history and cosmic growth*," Physical Review D **96** (2017), 10.1103/physrevd.96.063517.

[41] T. Abbott, M. Aguena, A. Alarcon, S. Allam, O. Alves, A. Amon, F. Andrade-Oliveira, J. Annis, S. Avila, D. Bacon, *et al.*, "*Dark Energy Survey Year 3 results: Cosmological constraints from galaxy clustering and weak lensing*," Physical Review D **105**, 023520 (2022).

[42] Y. Akrami, M. Ashdown, J. Aumont, C. Baccigalupi, M. Ballardini, A. J. Banday, R. Barreiro, N. Bartolo, S. Basak, K. Benabed, *et al.*, "*Planck 2018 results-VII. Isotropy and statistics of the CMB*," Astronomy & Astrophysics **641**, A7 (2020).

[43] G. Addison, D. Watts, C. Bennett, M. Halpern, G. Hinshaw, and J. Weiland, "*Elucidating ΛCDM: impact of baryon acoustic oscillation measurements on the Hubble constant discrepancy*," The Astrophysical Journal **853**, 119 (2018).

[44] A. Cuceu, J. Farr, P. Lemos, and A. Font-Ribera, "*Baryon acoustic oscillations and the Hubble constant: past, present and future*," Journal of Cosmology and Astroparticle Physics **2019**, 044 (2019).

[45] L. Verde, P. Protopapas, and R. Jimenez, "*Planck and the local Universe: Quantifying the tension*," Physics of the Dark Universe **2**, 166 (2013).

[46] B. D. Fields, "*The primordial lithium problem*," Annual Review of Nuclear and Particle Science **61**, 47 (2011).

[47] J. D. Bowman, A. E. Rogers, R. A. Monsalve, T. J. Mozdzen, and N. Mahesh, "*An absorption profile centred at 78 megahertz in the sky-averaged spectrum*," Nature **555**, 67 (2018).

[48] C. Deffayet, X. Gao, D. A. Steer, and G. Zahariade, "*From k-essence to generalized Galileons*," Physical Review D **84**, 064039 (2011).

[49] G. W. Horndeski, "*Second-order scalar-tensor field equations in a four-dimensional space*," International Journal of Theoretical Physics **10**, 363 (1974).

[50] R. Kase and S. Tsujikawa, "*Dark energy in Horndeski theories after GW170817: A review*," International Journal of Modern Physics D **28**, 1942005 (2019).

[51] T. Kobayashi, "*Horndeski theory and beyond: a review*," Reports on Progress in Physics **82**, 086901 (2019).

[52] E. V. Linder, "*The dynamics of quintessence, the quintessence of dynamics*," General Relativity and Gravitation **40**, 329 (2008), arXiv:0704.2064 [astro-ph] .

[53] S. Tsujikawa, "*Quintessence: a review*," Classical and Quantum Gravity **30**, 214003 (2013).

[54] V. Sahni, "*The cosmological constant problem and quintessence*," Classical and Quantum Gravity **19**, 3435 (2002).

[55] R. R. Caldwell and E. V. Linder, "*Limits of Quintessence*," Physical Review Letters **95** (2005), 10.1103/physrevlett.95.141301.

[56] C. Martins, "*The status of varying constants: a review of the physics, searches and implications*," Reports on Progress in Physics **80**, 126902 (2017).

[57] J. D. Bekenstein, "*Fine-structure constant: Is it really a constant?*" Physical Review D **25**, 1527 (1982).

[58] J. D. Barrow and A. A. Graham, "*General dynamics of varying-alpha universes*," Physical Review D **88**, 103513 (2013).

[59] A. De Felice and S. Tsujikawa, "*f (R) theories*," Living Reviews in Relativity **13**, 1 (2010).

[60] A. A. Starobinsky, "*Disappearing cosmological constant in f (R) gravity*," JETP letters **86**, 157 (2007).

[61] S. Capozziello and M. Francaviglia, "*Extended theories of gravity and their cosmological and astrophysical applications*," General Relativity and Gravitation **40**, 357 (2008).

[62] V. Faraoni, "*Nine Years of f(R) Gravity and Cosmology*," in *4th International Meeting on Gravitation and Cosmology (MGC 4)* (2009) pp. 19–32.

[63] E. Barausse, T. P. Sotiriou, and J. C. Miller, "*A no-go theorem for polytropic spheres in Palatini f (R) gravity*," Classical and Quantum Gravity **25**, 062001 (2008).

[64] S. Nojiri, S. D. Odintsov, and M. Sami, "*Dark energy cosmology from higher-order, string-inspired gravity, and its reconstruction*," Phys. Rev. D **74**, 046004 (2006).

[65] R. Calderón, R. Gannouji, B. L'Huillier, and D. Polarski, "*Negative cosmological constant in the dark sector?*" Physical Review D **103**, 023526 (2021).

[66] K.-i. Maeda and N. Ohta, "*Cosmic acceleration with a negative cosmological constant in higher dimensions*," Journal of High Energy Physics **2014**, 1 (2014).

[67] L. V. Waerbeke and Y. Mellier, "*Gravitational Lensing by Large Scale Structures: A Review*," (2003), arXiv:astro-ph/0305089 [astro-ph] .

[68] D. Munshi, P. Valageas, L. Van Waerbeke, and A. Heavens, "*Cosmology with weak lensing surveys*," Physics Reports **462**, 67–121 (2008).

[69] B. Jain and U. Seljak, "*Cosmological Model Predictions for Weak Lensing: Linear and Nonlinear Regimes*," The Astrophysical Journal **484**, 560–573 (1997).

[70] W. Hu, "*Power Spectrum Tomography with Weak Lensing*," The Astrophysical Journal **522**, L21–L24 (1999).

[71] D. Huterer and M. White, "*Weak Lensing as a Calibrator of the Cluster Mass-Temperature Relation*," The Astrophysical Journal **578**, L95–L98 (2002).

[72] M. Takada and B. Jain, "*Three-point correlations in weak lensing surveys: model predictions and applications*," Monthly Notices of the Royal Astronomical Society **344**, 857–886 (2003).

[73] A. Heavens, "*3D weak lensing*," Monthly Notices of the Royal Astronomical Society **343**, 1327–1334 (2003).

[74] L. Knox, A. Albrecht, and Y. S. Song, "*Weak Lensing and Supernovae: Complementary Probes of Dark Energy*," (2004), arXiv:astro-ph/0408141 [astro-ph] .

[75] S. Miyazaki, T. Hamana, R. S. Ellis, N. Kashikawa, R. J. Massey, J. Taylor, and A. Refregier, "*A Subaru Weak-Lensing Survey. I. Cluster Candidates and Spectroscopic Verification*," The Astrophysical Journal **669**, 714–728 (2007).

[76] H. Hoekstra and B. Jain, "*Weak Gravitational Lensing and Its Cosmological Applications*," Annual Review of Nuclear and Particle Science **58**, 99–123 (2008).

[77] M. Takada and B. Jain, "*The impact of non-Gaussian errors on weak lensing surveys*," Monthly Notices of the Royal Astronomical Society **395**, 2065–2086 (2009).

[78] P. Bull, P. G. Ferreira, P. Patel, and M. G. Santos, "*LATE-TIME COSMOLOGY WITH 21 cm INTENSITY MAPPING EXPERIMENTS*," The Astrophysical Journal **803**, 21 (2015).

[79] A. Obuljen, E. Castorina, F. Villaescusa-Navarro, and M. Viel, "*High-redshift post-reionization cosmology with 21cm intensity mapping*," Journal of Cosmology and Astroparticle Physics **2018**, 004–004 (2018).

[80] T. Chang, U. Pen, J. B. Peterson, and P. McDonald, "*Baryon Acoustic Oscillation Intensity Mapping of Dark Energy*," Physical Review Letters **100**, 091303 (2008), arXiv:0709.3672 .

[81] J. S. B. Wyithe and A. Loeb, "*The 21-cm power spectrum after reionization*," MNRAS **397**, 1926 (2009).

[82] S. Bharadwaj and S. K. Sethi, "*HI Fluctuations at Large Redshifts: I–Visibility correlation*," Journal of Astrophysics and Astronomy **22**, 293 (2001), arXiv:astro-ph/0203269 .

[83] S. Bharadwaj, B. B. Nath, and S. K. Sethi, "*Using HI to Probe Large Scale Structures at z = 3*," Journal of Astrophysics and Astronomy **22**, 21 (2001), arXiv:astro-ph/0003200 .

[84] S. Wyithe and A. Loeb, "*Fluctuations in 21cm Emission After Reionization*," ArXiv e-prints (2007), arXiv:0708.3392 .

[85] A. Loeb and J. S. B. Wyithe, "*Possibility of Precise Measurement of the Cosmological Power Spectrum with a Dedicated Survey of 21cm Emission after Reionization*," Physical Review Letters **100**, 161301 (2008), arXiv:0801.1677 .

[86] S. Wyithe and A. Loeb, "*The 21cm Power Spectrum After Reionization*," ArXiv e-prints (2008), arXiv:0808.2323 .

[87] E. Visbal, A. Loeb, and S. Wyithe, "*Cosmological constraints from 21cm surveys after reionization*," Journal of Cosmology and Astro-Particle Physics **10**, 30 (2009), arXiv:0812.0419 .

[88] S. Bharadwaj and S. K. Pandey, "*HI Fluctuations at Large Redshifts: II - the Signal Expected for the GMRT*," Journal of Astrophysics and Astronomy **24**, 23 (2003), arXiv:astro-ph/0307303 .

[89] S. Bharadwaj and P. S. Srikant, "*HI Fluctuations at Large Redshifts: III - Simulating the Signal Expected at GMRT*," Journal of Astrophysics and Astronomy **25**, 67 (2004), arXiv:astro-ph/0402262 .

[90] A. K. Sarkar, S. Bharadwaj, and V. R. Marthi, "*An analytical method to simulate the HI 21-cm visibility signal for intensity mapping experiments*," Monthly Notices of the Royal Astronomical Society **473**, 261–270 (2017).

[91] D. Sarkar, S. Bharadwaj, and S. Anathpindika, "*Modelling the post-reionization neutral hydrogen HI bias*," Monthly Notices of the Royal Astronomical Society **460**, 4310–4319 (2016).

[92] T. Guha Sarkar, S. Mitra, S. Majumdar, and T. R. Choudhury, "*Constraining large-scale HI bias using redshifted 21-cm signal from the post-reionization epoch*," Monthly Notices of the Royal Astronomical Society **421**, 3570–3578 (2012).

[93] J. S. Bagla, N. Khandai, and K. K. Datta, "*HI as a probe of the large-scale structure in the post-reionization universe*," Monthly Notices of the Royal Astronomical Society **407**, 567–580 (2010).

[94] N. Y. Gnedin and L. Hui, "*Probing the Universe with the Lyman-alpha Forest: I. Hydrodynamics of the Low Density IGM*," arXiv preprint astro-ph/9706219 (1997).

[95] V. Khaire, M. Walther, J. F. Hennawi, J. Oñorbe, Z. Lukić, J. X. Prochaska, T. M. Tripp, J. N. Burchett, and C. Rodriguez, "*The power spectrum of the Lyman-α Forest at z< 0.5*," Monthly Notices of the Royal Astronomical Society **486**, 769 (2019).

[96] V. IrVsiVc, M. Viel, T. A. Berg, V. D'Odorico, M. G. Haehnelt, S. Cristiani, G. Cupani, T.-S. Kim, S. López, S. Ellison, *et al.*, "*The Lyman α forest power spectrum from the XQ-100 Legacy Survey*," Monthly Notices of the Royal Astronomical Society **466**, 4332 (2017).

[97] P. McDonald, U. Seljak, S. Burles, D. J. Schlegel, D. H. Weinberg, R. Cen, D. Shih, J. Schaye, D. P. Schneider, N. A. Bahcall, *et al.*, "*The Ly-alpha Forest Power Spectrum from the Sloan Digital Sky Survey*," The Astrophysical Journal Supplement Series **163**, 80 (2006).

[98] D. H. Weinberg, R. Dave, N. Katz, and J. A. Kollmeier, "*The Lyman-alpha Forest as a Cosmological Tool*," in *AIP Conference Proceedings*, Vol. 666 (American Institute of Physics, 2003) pp. 157–169.

[99] M. Rauch, "*The Lyman alpha forest in the spectra of quasistellar objects*," Annual Review of Astronomy and Astrophysics **36**, 267 (1998).

[100] R. Mandelbaum, P. McDonald, U. Seljak, and R. Cen, "*Precision cosmology from the Lyman alpha forest: power spectrum and bispectrum*," Monthly Notices of the Royal Astronomical Society **344**, 776–788 (2003).

[101] P. McDonald and D. J. Eisenstein, "*Dark energy and curvature from a future baryonic acoustic oscillation survey using the Lyman alpha forest*," Physical Review D **76** (2007), 10.1103/physrevd.76.063009.

[102] A. G. Riess, A. V. Filippenko, P. Challis, A. Clocchiatti, A. Diercks, P. M. Garnavich, R. L. Gilliland, C. J. Hogan, S. Jha, R. P. Kirshner, *et al.*, "*Observational evidence from supernovae for an accelerating universe and a cosmological constant*," The Astronomical Journal **116**, 1009 (1998).

[103] S. Perlmutter, G. Aldering, G. Goldhaber, R. Knop, P. Nugent, P. G. Castro, S. Deustua, S. Fabbro, A. Goobar, D. E. Groom, *et al.*, "*Measurements*

of Ω and Λ from 42 high-redshift supernovae," The Astrophysical Journal **517**, 565 (1999).

[104] H. Lorentz, A. Einstein, H. Minkowski, and A. Einstein, *Kosmologische Betrachtungen zur allgemeinen Relativitats-theorie* (Springer, 1922).

[105] A. Lewis and S. Bridle, "*Cosmological parameters from CMB and other data: A Monte Carlo approach*," Physical Review D **66**, 103511 (2002).

[106] J. Bartlett, M. Bucher, J. Cardoso, J. Delabrouille, K. Ganga, C. Gauthier, M. Le Jeune, G. Patanchon, M. Piat, M. Remazeilles, *et al.*, "*Planck 2015 results: XI. CMB power spectra, likelihoods, and robustness of parameters*," Astronomy and Astrophysics **594**, A11 (2016).

[107] G. F. Smoot, C. L. Bennett, A. Kogut, E. Wright, J. Aymon, N. Boggess, E. Cheng, G. De Amici, S. Gulkis, M. Hauser, *et al.*, "*Structure in the COBE differential microwave radiometer first-year maps*," Astrophysical Journal, Part 2-Letters (ISSN 0004-637X), vol. 396, no. 1, Sept. 1, 1992, p. L1-L5. Research supported by NASA. **396**, L1 (1992).

[108] P. De Bernardis, P. A. Ade, J. Bock, J. Bond, J. Borrill, A. Boscaleri, K. Coble, B. Crill, G. De Gasperis, G. De Troia, *et al.*, "*First results from the BOOMERanG experiment*," in *AIP Conference Proceedings*, Vol. 555 (American Institute of Physics, 2001) pp. 85–94.

[109] Ø. Elgarøy and T. Multamäki, "*On using the cosmic microwave background shift parameter in tests of models of dark energy*," Astronomy & Astrophysics **471**, 65 (2007).

[110] J. Weller and A. Albrecht, "*Future supernovae observations as a probe of dark energy*," Physical Review D **65**, 103512 (2002).

[111] S. Perlmutter, M. S. Turner, and M. White, "*Constraining dark energy with type Ia supernovae and large-scale structure*," Physical Review Letters **83**, 670 (1999).

[112] Y. Wang and M. Tegmark, "*Uncorrelated measurements of the cosmic expansion history and dark energy from supernovae*," Physical Review D **71**, 103513 (2005).

[113] T. Padmanabhan and T. R. Choudhury, "*A theoretician's analysis of the supernova data and the limitations in determining the nature of dark energy*," Monthly Notices of the Royal Astronomical Society **344**, 823 (2003).

[114] W. Hillebrandt and J. C. Niemeyer, "*Type Ia supernova explosion models*," Annual Review of Astronomy and Astrophysics **38**, 191 (2000).

[115] D. Branch and G. Tammann, "*Type Ia supernovae as standard candles*," Annual review of astronomy and astrophysics **30**, 359 (1992).

[116] K. Nomoto, K. Iwamoto, and N. Kishimoto, "*Type Ia supernovae: their origin and possible applications in cosmology*," science **276**, 1378 (1997).

[117] M. M. Phillips, "*The absolute magnitudes of Type IA supernovae*," The Astrophysical Journal **413**, L105 (1993).

[118] D. J. Adams and D. J. Adams, *An introduction to galaxies and cosmology* (Cambridge University Press, 2004).

[119] D. Camarena and V. Marra, "*Local determination of the Hubble constant and the deceleration parameter*," Physical Review Research **2**, 013028 (2020).

[120] M. Lopez-Corredoira, "*ALCOCK–PACZYNSKI COSMOLOGICAL TEST*," The Astrophysical Journal **781**, 96 (2014).

[121] B. Bassett and R. Hlozek, "*Baryon acoustic oscillations*," Dark energy: observational and theoretical approaches **246** (2010).

[122] F. Beutler, C. Blake, M. Colless, D. H. Jones, L. Staveley-Smith, L. Campbell, Q. Parker, W. Saunders, and F. Watson, "*The 6dF Galaxy Survey: baryon acoustic oscillations and the local Hubble constant*," Monthly Notices of the Royal Astronomical Society **416**, 3017 (2011).

[123] W. J. Percival, B. A. Reid, D. J. Eisenstein, N. A. Bahcall, T. Budavari, J. A. Frieman, M. Fukugita, J. E. Gunn, VZ. Ivezić, G. R. Knapp, *et al.*, "*Baryon acoustic oscillations in the Sloan Digital Sky Survey data release 7 galaxy sample*," Monthly Notices of the Royal Astronomical Society **401**, 2148 (2010).

[124] L. Anderson, É. Aubourg, S. Bailey, F. Beutler, V. Bhardwaj, M. Blanton, A. S. Bolton, J. Brinkmann, J. R. Brownstein, A. Burden, *et al.*, "*The clustering of galaxies in the SDSS-III Baryon Oscillation Spectroscopic Survey: baryon acoustic oscillations in the Data Releases 10 and 11 Galaxy samples*," Monthly Notices of the Royal Astronomical Society **441**, 24 (2014).

[125] V. Sahni, A. Shafieloo, and A. A. Starobinsky, "*Model-independent evidence for dark energy evolution from baryon acoustic oscillations*," The Astrophysical Journal Letters **793**, L40 (2014).

[126] D. J. Eisenstein and W. Hu, "*Baryonic features in the matter transfer function*," The Astrophysical Journal **496**, 605 (1998).

[127] M. White, "*Baryon oscillations*," Astroparticle Physics **24**, 334–344 (2005).

[128] M. Shoji, D. Jeong, and E. Komatsu, "*Extracting angular diameter distance and expansion rate of the universe from two-dimensional galaxy power spectrum at high redshifts: baryon acoustic oscillation fitting versus full modeling*," The Astrophysical Journal **693**, 1404 (2009).

[129] É. Aubourg, S. Bailey, J. E. Bautista, F. Beutler, V. Bhardwaj, D. Bizyaev, M. Blanton, M. Blomqvist, A. S. Bolton, J. Bovy, *et al.*, "*Cosmological implications of baryon acoustic oscillation measurements*," Physical Review D **92**, 123516 (2015).

[130] E. Komatsu, J. Dunkley, M. R. Nolta, C. L. Bennett, B. Gold, G. Hinshaw, N. Jarosik, D. Larson, M. Limon, L. Page, and et al., "*FIVE-YEAR WILKINSON MICROWAVE ANISOTROPY PROBE OBSERVATIONS: COSMOLOGICAL INTERPRETATION*," The Astrophysical Journal Supplement Series **180**, 330–376 (2009).

[131] P. J. E. Peebles, *The large-scale structure of the universe* (Princeton university press, 2020).

[132] V. Springel, C. S. Frenk, and S. D. White, "*The large-scale structure of the Universe*," nature **440**, 1137 (2006).

[133] S. W. Hawking and G. F. Ellis, *The large scale structure of space-time* (Cambridge university press, 2023).

[134] F. Bernardeau, S. Colombi, E. Gaztanaga, and R. Scoccimarro, "*Large-scale structure of the Universe and cosmological perturbation theory*," Physics reports **367**, 1 (2002).

[135] M. Steyvers and J. B. Tenenbaum, "*The large-scale structure of semantic networks: Statistical analyses and a model of semantic growth*," Cognitive science **29**, 41 (2005).

[136] E. Di Valentino, L. A. Anchordoqui, Ö. Akarsu, Y. Ali-Haimoud, L. Amendola, N. Arendse, M. Asgari, M. Ballardini, S. Basilakos, E. Battistelli, *et al.*, "*Snowmass2021-Letter of interest cosmology intertwined II: The hubble constant tension*," Astroparticle Physics **131**, 102605 (2021).

[137] L. Perivolaropoulos and F. Skara, "*Challenges for ΛCDM: An update*," New Astronomy Reviews **95**, 101659 (2022).

[138] A. G. Riess, "*The expansion of the Universe is faster than expected*," Nature Reviews Physics **2**, 10 (2020).

[139] D. Huterer and D. L. Shafer, "*Dark energy two decades after: observables, probes, consistency tests*," Reports on Progress in Physics **81**, 016901 (2017).

[140] S. Joudaki, C. Blake, A. Johnson, A. Amon, M. Asgari, A. Choi, T. Erben, K. Glazebrook, J. Harnois-Déraps, C. Heymans, *et al.*, "*KiDS-450+ 2dFLenS: Cosmological parameter constraints from weak gravitational lensing tomography and overlapping redshift-space galaxy clustering*," Monthly Notices of the Royal Astronomical Society **474**, 4894 (2018).

[141] E. Di Valentino, A. Melchiorri, and J. Silk, "*Reconciling Planck with the local value of H0 in extended parameter space*," Physics Letters B **761**, 242 (2016).

[142] D. J. Schwarz, C. J. Copi, D. Huterer, and G. D. Starkman, "*CMB anomalies after Planck*," Classical and Quantum Gravity **33**, 184001 (2016).

[143] A. Rassat, J.-L. Starck, P. Paykari, F. Sureau, and J. Bobin, "*Planck CMB anomalies: astrophysical and cosmological secondary effects and the curse of masking*," Journal of Cosmology and Astroparticle Physics **2014**, 006 (2014).

[144] J. Evslin, "*Isolating the Lyman alpha forest BAO anomaly*," Journal of Cosmology and Astroparticle Physics **2017**, 024 (2017).

[145] A. Banerjee, E. Ó. Colgáin, M. Sasaki, M. M. Sheikh-Jabbari, and T. Yang, "*On problems with cosmography in cosmic dark ages*," Physics Letters B **818**, 136366 (2021).

[146] E. Lusso, E. Piedipalumbo, G. Risaliti, M. Paolillo, S. Bisogni, E. Nardini, and L. Amati, "*Tension with the flat LCDM model from a high redshift Hubble Diagram of supernovae, quasars and gamma-ray bursts*," arXiv preprint arXiv:1907.07692 (2019).

[147] G. Risaliti and E. Lusso, "*Cosmological constraints from the Hubble diagram of quasars at high redshifts*," Nature Astronomy **3**, 272 (2019).

[148] V. L. Fitch, D. R. Marlow, and M. A. Dementi, *Critical problems in physics*, Vol. 34 (Princeton University Press, 2021).

[149] S. Dodelson, M. Kaplinghat, and E. Stewart, "*Solving the coincidence problem: Tracking oscillating energy*," Physical Review Letters **85**, 5276 (2000).

[150] E. V. Linder, "*Exploring the Expansion History of the Universe*," Phys. Rev. Lett. **90**, 091301 (2003).

[151] S. Hawking, "*The cosmological constant is probably zero*," Physics Letters B **134**, 403 (1984).

[152] J. Yokoyama, "*Cosmological Constant From Degenerate Vacua*," Physical Review Letters **88** (2002), 10.1103/physrevlett.88.151302.

[153] S.-H. Henry Tye and I. Wasserman, "*Brane World Solution to the Cosmological Constant Problem*," Physical Review Letters **86**, 1682–1685 (2001).

[154] S. Capozziello, "*Curvature quintessence*," International Journal of Modern Physics D **11**, 483 (2002).

[155] S. Capozziello, S. Carloni, and A. Troisi, "*Quintessence without scalar fields*," arXiv preprint astro-ph/0303041 (2003).

[156] S. M. Carroll, V. Duvvuri, M. Trodden, and M. S. Turner, "*Is cosmic speed-up due to new gravitational physics?*" Physical Review D **70**, 043528 (2004).

[157] A. D. Dolgov and M. Kawasaki, "*Can modified gravity explain accelerated cosmic expansion?*" Physics Letters B **573**, 1 (2003).

[158] V. Faraoni, "*Matter instability in modified gravity*," Physical Review D **74**, 104017 (2006).

[159] S. M. Carroll, I. Sawicki, A. Silvestri, and M. Trodden, "*Modified-source gravity and cosmological structure formation*," New Journal of Physics **8**, 323 (2006).

[160] R. Bean, D. Bernat, L. Pogosian, A. Silvestri, and M. Trodden, "*Dynamics of linear perturbations in f (R) gravity*," Physical Review D **75**, 064020 (2007).

[161] Y.-S. Song, W. Hu, and I. Sawicki, "*Large scale structure of f (R) gravity*," Physical Review D **75**, 044004 (2007).

[162] I. Sawicki and W. Hu, "*Stability of cosmological solutions in f (R) models of gravity*," Physical Review D **75**, 127502 (2007).

[163] T. Faulkner, M. Tegmark, E. F. Bunn, and Y. Mao, "*Constraining f (R) gravity as a scalar-tensor theory*," Physical Review D **76**, 063505 (2007).

[164] L. Amendola, D. Polarski, and S. Tsujikawa, "*Are f (R) dark energy models cosmologically viable?*" Physical review letters **98**, 131302 (2007).

[165] L. Amendola, D. Polarski, and S. Tsujikawa, "*Power-laws f (R) theories are cosmologically unacceptable*," International Journal of Modern Physics D **16**, 1555 (2007).

[166] P. Astier and R. Pain, "*Observational evidence of the accelerated expansion of the universe*," Comptes Rendus Physique **13**, 521 (2012).

[167] G. J. Olmo, "*The gravity lagrangian according to solar system experiments*," Physical review letters **95**, 261102 (2005).

[168] G. J. Olmo, "*Post-Newtonian constraints on f (R) cosmologies in metric and Palatini formalism*," Physical Review D **72**, 083505 (2005).

[169] V. Faraoni, "*Solar system experiments do not yet veto modified gravity models*," Physical Review D **74**, 023529 (2006).

[170] A. L. Erickcek, T. L. Smith, and M. Kamionkowski, "*Solar system tests do rule out 1/R gravity*," Physical Review D **74**, 121501 (2006).

[171] T. Chiba, T. L. Smith, and A. L. Erickcek, "*Solar System constraints to general f (R) gravity*," Physical Review D **75**, 124014 (2007).

[172] S. Capozziello and S. Tsujikawa, "*Solar system and equivalence principle constraints on f (R) gravity by the chameleon approach*," Physical Review D **77**, 107501 (2008).

[173] T. Clifton and J. D. Barrow, "*The power of general relativity*," Physical Review D **72**, 103005 (2005).

[174] B. Li and J. D. Barrow, "*Cosmology of f (R) gravity in the metric variational approach*," Physical Review D **75**, 084010 (2007).

[175] S. P. Bergliaffa, "*Constraining f (R) theories with the energy conditions*," Physics Letters B **642**, 311 (2006).

[176] L. Amendola and S. Tsujikawa, "*Phantom crossing, equation-of-state singularities, and local gravity constraints in f (R) models*," Physics Letters B **660**, 125 (2008).

[177] J. C. de Souza and V. Faraoni, "*The phase-space view of f (R) gravity*," Classical and Quantum Gravity **24**, 3637 (2007).

[178] D. Bazeia, B. C. da Cunha, R. Menezes, and A. Y. Petrov, "*Perturbative aspects and conformal solutions of F (R) gravity*," Physics Letters B **649**, 445 (2007).

[179] K. Atazadeh and H. Sepangi, "*Accelerated expansion in modified gravity with a Yukawa-like term*," International Journal of Modern Physics D **16**, 687 (2007).

[180] M. Abdelwahab, S. Carloni, and P. Dunsby, "*Cosmological dynamics of 'exponential gravity'*," Classical and Quantum Gravity **25**, 135002 (2008).

[181] B. Paul, P. Debnath, and S. Ghose, "*Accelerating universe in modified theories of gravity*," Physical Review D **79**, 083534 (2009).

[182] W. Hu and I. Sawicki, "*Models off(R)cosmic acceleration that evade solar system tests*," Physical Review D **76** (2007), 10.1103/physrevd.76.064004.

[183] S. Nojiri and S. D. Odintsov, "*Introduction to modified gravity and gravitational alternative for dark energy*," International Journal of Geometric Methods in Modern Physics **4**, 115 (2007).

[184] L. Amendola, R. Gannouji, D. Polarski, and S. Tsujikawa, "*Conditions for the cosmological viability off(R)dark energy models*," Physical Review D **75** (2007), 10.1103/physrevd.75.083504.

[185] W. Hu and I. Sawicki, "*Models of f (R) cosmic acceleration that evade solar system tests*," Physical Review D **76**, 064004 (2007).

[186] S. A. Appleby and R. A. Battye, "*Do consistent F (R) models mimic general relativity plus Λ?*" Physics Letters B **654**, 7 (2007).

[187] S. Tsujikawa, "*Observational signatures of f (R) dark energy models that satisfy cosmological and local gravity constraints*," Physical Review D **77**, 023507 (2008).

[188] G. Cognola, E. Elizalde, S. Nojiri, S. Odintsov, L. Sebastiani, and S. Zerbini, "*Class of viable modified f (R) gravities describing inflation and the onset of accelerated expansion*," Physical Review D **77**, 046009 (2008).

[189] L. Pogosian and A. Silvestri, "*Pattern of growth in viable f (R) cosmologies*," Physical Review D **77**, 023503 (2008).

[190] P. Zhang, "*Testing gravity against the early time integrated Sachs-Wolfe effect*," Physical Review D **73**, 123504 (2006).

[191] Y.-S. Song, H. Peiris, and W. Hu, "*Cosmological constraints on f (R) acceleration models*," Physical Review D **76**, 063517 (2007).

[192] S. Tsujikawa and T. Tatekawa, "*The effect of modified gravity on weak lensing*," Physics Letters B **665**, 325 (2008).

[193] F. Schmidt, "*Weak lensing probes of modified gravity*," Physical Review D **78**, 043002 (2008).

[194] S. Tsujikawa, R. Gannouji, B. Moraes, and D. Polarski, "*Dispersion of growth of matter perturbations in f (R) gravity*," Physical Review D **80**, 084044 (2009).

[195] B. Boisseau, G. Esposito-Farese, D. Polarski, and A. A. Starobinsky, "*Reconstruction of a scalar-tensor theory of gravity in an accelerating universe*," Physical Review Letters **85**, 2236 (2000).

[196] S. Tsujikawa, K. Uddin, S. Mizuno, R. Tavakol, and J. Yokoyama, "*Constraints on scalar-tensor models of dark energy from observational and local gravity tests*," Physical Review D **77**, 103009 (2008).

[197] S. Baghram and S. Rahvar, "*Structure formation in f (R) gravity: A distinguishing probe between the dark energy and modified gravity*," Journal of Cosmology and Astroparticle Physics **2010**, 008 (2010).

[198] P. J. Steinhardt, L. Wang, and I. Zlatev, "*Cosmological tracking solutions*," Phys. Rev. D **59**, 123504 (1999).

[199] S. M. Carroll, "*Quintessence and the Rest of the World: Suppressing Long-Range Interactions*," Phys. Rev. Lett. **81**, 3067 (1998).

[200] C. Kolda and D. H. Lyth, "*Quintessential difficulties*," Physics Letters B **458**, 197 (1999).

[201] P. Brax and J. Martin, "*Quintessence and supergravity*," Physics Letters B **468**, 40 (1999).

[202] Y. Nomura, T. Watari, and T. Yanagida, "*Quintessence axion potential induced by electroweak instanton effects*," Physics Letters B **484**, 103 (2000).

[203] J. E. Kim and H.-P. Nilles, "*A quintessential axion*," Physics Letters B **553**, 1 (2003).

[204] S. Tsujikawa, "*Dark energy: investigation and modeling*," Dark Matter and Dark Energy: A Challenge for Modern Cosmology , 331 (2011).

[205] E. V. Linder and D. Huterer, "*How many dark energy parameters?*" Phys. Rev. D **72**, 043509 (2005).

[206] M. CHEVALLIER and D. POLARSKI, "*ACCELERATING UNIVERSES WITH SCALING DARK MATTER*," International Journal of Modern Physics D **10**, 213–223 (2001).

[207] E. Barboza and J. Alcaniz, "*A parametric model for dark energy*," Physics Letters B **666**, 415–419 (2008).

[208] R. J. Scherrer, "*Mapping the Chevallier-Polarski-Linder parametrization onto physical dark energy models*," Physical Review D **92**, 043001 (2015).

[209] H. Jassal, J. Bagla, and T. Padmanabhan, "*WMAP constraints on low redshift evolution of dark energy*," Monthly Notices of the Royal Astronomical Society: Letters **356**, L11 (2005).

[210] H. K. Jassal, J. Bagla, and T. Padmanabhan, "*Observational constraints on low redshift evolution of dark energy: How consistent are different observations?*" Physical Review D **72**, 103503 (2005).

[211] C. B. V. Dash, T. G. Sarkar, and A. A. Sen, "*Post-reionization HI 21-cm signal: A probe of negative cosmological constant*," (2023), arXiv:2309.01623 [astro-ph.CO] .

[212] A. Einstein, "*Über den Einfluß der Schwerkraft auf die Ausbreitung des Lichtes*," Annalen der Physik **340**, 898 (1911).

[213] A. Einstein, *Über die allgemeine Relativitätstheorie* (Springer, 2009).

[214] M. Bartelmann and M. Maturi, "*Weak gravitational lensing*," arXiv preprint arXiv:1612.06535 (2016).

[215] M. Bartelmann and P. Schneider, "*Weak gravitational lensing*," Physics Reports **340**, 291–472 (2001).

[216] T. Treu, "*Strong lensing by galaxies*," Annual Review of Astronomy and Astrophysics **48**, 87 (2010).

[217] V. Bozza, "*Gravitational lensing in the strong field limit*," Physical Review D **66**, 103001 (2002).

[218] D. N. Limber, "*The Analysis of Counts of the Extragalactic Nebulae in Terms of a Fluctuating Density Field. II.*" Astrophysical Journal **119**, 655 (1954).

[219] C. Heymans, L. Van Waerbeke, L. Miller, T. Erben, H. Hildebrandt, H. Hoekstra, T. D. Kitching, Y. Mellier, P. Simon, C. Bonnett, *et al.*, "*CFHTLenS: the Canada–France–Hawaii telescope lensing survey*," Monthly Notices of the Royal Astronomical Society **427**, 146 (2012).

[220] D. Huterer, "*Weak lensing, dark matter and dark energy*," General Relativity and Gravitation **42**, 2177 (2010).

[221] A. Cooray and W. Hu, "*Weak gravitational lensing bispectrum*," The Astrophysical Journal **548**, 7 (2001).

[222] S. Dodelson and P. Zhang, "*Weak lensing bispectrum*," Physical Review D **72**, 083001 (2005).

[223] D. J. Bacon, A. R. Refregier, and R. S. Ellis, "*Detection of weak gravitational lensing by large-scale structure*," Monthly Notices of the Royal Astronomical Society **318**, 625 (2000).

[224] N. Kaiser, G. Wilson, and G. A. Luppino, "*Large-scale cosmic shear measurements*," arXiv preprint astro-ph/0003338 (2000).

[225] L. Van Waerbeke, Y. Mellier, T. Erben, J. Cuillandre, F. Bernardeau, R. Maoli, E. Bertin, H. Mc Cracken, O. L. Fevre, B. Fort, *et al.*, "*Detection of correlated galaxy ellipticities on CFHT data: first evidence for gravitational lensing by large-scale structures*," Arxiv preprint astro-ph/0002500 (2000).

[226] L. Marian, R. E. Smith, and G. M. Bernstein, "*The impact of correlated projections on weak lensing cluster counts*," The Astrophysical Journal **709**, 286 (2009).

[227] H. Hoekstra, H. K. Yee, and M. D. Gladders, "*Properties of galaxy dark matter halos from weak lensing*," The Astrophysical Journal **606**, 67 (2004).

[228] L. Van Waerbeke, Y. Mellier, and H. Hoekstra, "*Dealing with systematics in cosmic shear studies: New results from the VIRMOS-Descart survey*," Astronomy & Astrophysics **429**, 75 (2005).

[229] H. Hoekstra, Y. Mellier, L. van Waerbeke, E. Semboloni, L. Fu, M. Hudson, L. Parker, I. Tereno, and K. Benabed, "*First cosmic shear results from the canada-france-hawaii telescope wide synoptic legacy survey*," The Astrophysical Journal **647**, 116 (2006).

[230] H. Hildebrandt, T. Erben, M. Schirmer, J. P. Dietrich, and P. Schneider, "*The Garching-Bonn Deep Survey (GaBoDS) Wide-Field-Imaging Reduction Pipeline*," in *The 2007 ESO Instrument Calibration Workshop: Proceedings of the ESO Workshop held in Garching, Germany, 23-26 January 2007* (Springer, 2008) pp. 553–558.

[231] J. Benjamin, C. Heymans, E. Semboloni, L. Van Waerbeke, H. Hoekstra, T. Erben, M. D. Gladders, M. Hetterscheidt, Y. Mellier, and H. Yee, "*Cosmological constraints from the 100-deg2 weak-lensing survey*," Monthly Notices of the Royal Astronomical Society **381**, 702 (2007).

[232] A. Refregier, J. Rhodes, and E. J. Groth, "*Cosmic shear and power spectrum normalization with the hubble space telescope*," The Astrophysical Journal **572**, L131 (2002).

[233] J. Rhodes, A. Refregier, N. R. Collins, J. P. Gardner, E. J. Groth, and R. S. Hill, "*Measurement of cosmic shear with the space telescope imaging spectrograph*," The Astrophysical Journal **605**, 29 (2004).

[234] R. Massey, J. Rhodes, R. Ellis, N. Scoville, A. Leauthaud, A. Finoguenov, P. Capak, D. Bacon, H. Aussel, J.-P. Kneib, *et al.*, "*Dark matter maps reveal cosmic scaffolding*," Nature **445**, 286 (2007).

[235] A. Leauthaud, R. Massey, J.-P. Kneib, J. Rhodes, D. E. Johnston, P. Capak, C. Heymans, R. S. Ellis, A. M. Koekemoer, O. Le Fevre, *et al.*, "*Weak gravitational lensing with COSMOS: Galaxy selection and shape measurements*," The Astrophysical Journal Supplement Series **172**, 219 (2007).

[236] E. Semboloni, Y. Mellier, L. van Waerbeke, H. Hoekstra, I. Tereno, K. Benabed, S. D. Gwyn, L. Fu, M. Hudson, R. Maoli, *et al.*, "*Cosmic shear analysis with CFHTLS deep data*," Astronomy & Astrophysics **452**, 51 (2006).

[237] M. Jarvis, B. Jain, G. Bernstein, and D. Dolney, "*Dark energy constraints from the CTIO lensing survey*," The Astrophysical Journal **644**, 71 (2006).

[238] C. Schimd and I. Tereno, "*Scalar-field quintessence by cosmic shear: CFHT data analysis and forecasts for DUNE*," Journal of Physics A: Mathematical and Theoretical **40**, 7105 (2007).

[239] B. Jain and P. Zhang, "*Observational tests of modified gravity*," Physical Review D **78**, 063503 (2008).

[240] J.-P. Uzan, "*Tests of general relativity on astrophysical scales*," General Relativity and Gravitation **42**, 2219 (2010).

[241] S. R. Furlanetto, S. Peng Oh, and F. H. Briggs, "*Cosmology at low frequencies: The 21cm transition and the high-redshift Universe*," Physics Reports **433**, 181–301 (2006).

[242] R. A. C. Croft, D. H. Weinberg, M. Pettini, L. Hernquist, and N. Katz, "*The Power Spectrum of Mass Fluctuations Measured from the Lyman alpha Forest at z = 2.5*," The Astrophysical Journal **520**, 1–23 (1999).

[243] R. Sunyaev and Y. B. Zel'Dovich, "*Microwave background radiation as a probe of the contemporary structure and history of the universe*," Annual review of astronomy and astrophysics **18**, 537 (1980).

[244] M. Birkinshaw, "*The Sunyaev–Zel'dovich effect*," Physics Reports **310**, 97 (1999).

[245] J. E. Carlstrom, G. P. Holder, and E. D. Reese, "*Cosmology with the Sunyaev-Zel'dovich effect*," Annual Review of Astronomy and Astrophysics **40**, 643 (2002).

[246] A. Refregier, E. Komatsu, D. N. Spergel, and U.-L. Pen, "*Power spectrum of the Sunyaev-Zel'dovich effect*," Physical Review D **61**, 123001 (2000).

[247] S. Boughn and R. Crittenden, "*A detection of the integrated Sachs–Wolfe effect*," New Astronomy Reviews **49**, 75–78 (2005).

[248] S. Ho, C. Hirata, N. Padmanabhan, U. Seljak, and N. Bahcall, "*Correlation of CMB with large-scale structure. I. Integrated Sachs-Wolfe tomography and cosmological implications*," Physical Review D **78** (2008), 10.1103/physrevd.78.043519.

[249] P. Dayal, A. Ferrara, and J. S. Dunlop, "*The physics of the fundamental metallicity relation*," Monthly Notices of the Royal Astronomical Society **430**, 2891 (2013).

[250] J. Schaye, A. Aguirre, T.-S. Kim, T. Theuns, M. Rauch, and W. L. Sargent, "*Metallicity of the intergalactic medium using pixel statistics. II. The distribution of metals as traced by C IV*," The Astrophysical Journal **596**, 768 (2003).

[251] N. Y. Gnedin, "*Metal enrichment of the intergalactic medium*," Monthly Notices of the Royal Astronomical Society **294**, 407 (1998).

[252] S. Saiyad Ali, S. Bharadwaj, and S. K. Pandey, "*Probing the bispectrum at high redshifts using 21-cm HI observations*," Monthly Notices of the Royal Astronomical Society **366**, 213–218 (2006).

[253] S. Bharadwaj and S. S. Ali, "*On using visibility correlations to probe the HI distribution from the dark ages to the present epoch - I. Formalism and the expected signal*," MNRAS **356**, 1519 (2005), arXiv:astro-ph/0406676 .

[254] C. M. Hirata, "*Wouthuysen-Field coupling strength and application to high-redshift 21-cm radiation*," Monthly Notices of the Royal Astronomical Society **367**, 259 (2006).

[255] A. Loeb and M. Zaldarriaga, "*Measuring the Small-Scale Power Spectrum of Cosmic Density Fluctuations through 21cm Tomography Prior to the Epoch of Structure Formation*," Physical Review Letters **92**, 211301 (2004), arXiv:astro-ph/0312134 .

[256] S. Bharadwaj and S. S. Ali, "*The cosmic microwave background radiation fluctuations from HI perturbations prior to reionization*," MNRAS **352**, 142 (2004), arXiv:astro-ph/0401206 .

[257] A. Lewis and A. Challinor, "*21 cm angular-power spectrum from the dark ages*," Physical Review D **76**, 083005 (2007).

[258] Y. Ali-Haimoud, P. D. Meerburg, and S. Yuan, "*New light on 21 cm intensity fluctuations from the dark ages*," Physical Review D **89**, 083506 (2014).

[259] P. R. Shapiro, K. Ahn, M. A. Alvarez, I. T. Iliev, H. Martel, and D. Ryu, "*The 21 cm background from the cosmic dark ages: minihalos and the intergalactic medium before reionization*," The Astrophysical Journal **646**, 681 (2006).

[260] J. E. Gunn and B. A. Peterson, "*On the Density of Neutral Hydrogen in Intergalactic Space.*" Astrophysical Journal, vol. 142, p. 1633-1636 **142**, 1633 (1965).

[261] G. D. Becker, P. C. Hewett, G. Worseck, and J. X. Prochaska, "*A refined measurement of the mean transmitted flux in the Lyman alpha forest using composite quasar spectra*," Monthly Notices of the Royal Astronomical Society **430**, 2067 (2013), https://academic.oup.com/mnras/article-pdf/430/3/2067/13759836/stt031.pdf .

[262] X. Fan, M. A. Strauss, R. H. Becker, R. L. White, J. E. Gunn, G. R. Knapp, G. T. Richards, D. P. Schneider, J. Brinkmann, and M. Fukugita, "*Constraining the evolution of the ionizing background and the epoch of reionization with z 6 quasars. II. A sample of 19 quasars*," The Astronomical Journal **132**, 117 (2006).

[263] B. Ciardi, A. Ferrara, and S. White, "*Early reionization by the first galaxies*," Monthly Notices of the Royal Astronomical Society **344**, L7 (2003).

[264] P. Madau, A. Meiksin, and M. J. Rees, "*21 Centimeter Tomography of the Intergalactic Medium at High Redshift*," Astrophysical Journal **475**, 429 (1997), arXiv:astro-ph/9608010 .

[265] X. Chen and J. Miralda-Escudé, "*The spin-kinetic temperature coupling and the heating rate due to Lyα scattering before reionization: predictions for 21 centimeter emission and absorption*," The Astrophysical Journal **602**, 1 (2004).

[266] A. M. Wolfe, E. Gawiser, and J. X. Prochaska, "*Damped Ly-alpha Systems*," ARAA **43**, 861 (2005), arXiv:astro-ph/0509481 .

[267] J. X. Prochaska, S. Herbert-Fort, and A. M. Wolfe, "*The SDSS Damped Lyα Survey: Data Release 3*," ApJ **635**, 123 (2005), arXiv:astro-ph/0508361 .

[268] K. M. Lanzetta, A. M. Wolfe, and D. A. Turnshek, "*The IUE Survey for Damped Lyman- alpha and Lyman-Limit Absorption Systems: Evolution of the Gaseous Content of the Universe*," Astrophysical Journal **440**, 435 (1995).

[269] L. J. Storrie-Lombardi, R. G. McMahon, and M. J. Irwin, "*Evolution of neutral gas at high redshift: implications for the epoch of galaxy formation*," MNRAS **283**, L79 (1996), arXiv:astro-ph/9608147 .

[270] C. Peroux, R. G. McMahon, L. J. Storrie-Lombardi, and M. J. Irwin, "*The evolution of OmegaHI and the epoch of formation of damped Lyman-alpha absorbers*," MNRAS **346**, 1103 (2003), arXiv:astro-ph/0107045 .

[271] J. Cooke, A. M. Wolfe, E. Gawiser, and J. X. Prochaska, "*Measurement of the Spatial Cross-Correlation Function of Damped Ly-alpha Systems and Lyman Break Galaxies*," Astrophysical Journal Letters **636**, L9 (2006), arXiv:astro-ph/0511509 .

[272] M. A. Zwaan, J. M. van der Hulst, F. H. Briggs, M. A. W. Verheijen, and E. V. Ryan-Weber, "*Reconciling the local galaxy population with damped Lyman alpha cross-sections and metal abundances*," MNRAS **364**, 1467 (2005), arXiv:astro-ph/0510127 .

[273] K. Nagamine, A. M. Wolfe, L. Hernquist, and V. Springel, "*Distribution of Damped Ly-alpha Absorbers in a Lambda Cold Dark Matter Universe*," Astrophysical Journal **660**, 945 (2007), arXiv:astro-ph/0510729 .

[274] A. Dekel and O. Lahav, "*Stochastic Nonlinear Galaxy Biasing*," Astrophysical Journal **520**, 24 (1999), arXiv:astro-ph/9806193 .

[275] H. J. Mo, Y. P. Jing, and S. D. M. White, "*The correlation function of clusters of galaxies and the amplitude of mass fluctuations in the Universe*," MNRAS **282**, 1096 (1996), arXiv:astro-ph/9602052 .

[276] K. Yoshikawa, A. Taruya, Y. P. Jing, and Y. Suto, "*Nonlinear Stochastic Biasing of Galaxies and Dark Halos in Cosmological Hydrodynamic Simulations*," Astrophysical Journal **558**, 520 (2001), arXiv:astro-ph/0104361 .

[277] L. Z. Fang, H. Bi, S. Xiang, and G. Boerner, "*Linear evolution of cosmic baryonic medium on large scales*," The Astrophysical Journal **413**, 477 (1993).

[278] I. P. Carucci, F. Villaescusa-Navarro, and M. Viel, "*The cross-correlation between 21 cm intensity mapping maps and the Ly alpha forest in the post-reionization era*," Journal of Cosmology and Astroparticle Physics **2017**, 001–001 (2017).

[279] F. A. Marín, N. Y. Gnedin, H.-J. Seo, and A. Vallinotto, "*MODELING THE LARGE-SCALE BIAS OF NEUTRAL HYDROGEN*," The Astrophysical Journal **718**, 972–980 (2010).

[280] J. N. Fry, "*The Evolution of Bias*," ApJ letters **461**, L65 (1996).

[281] H. J. Mo, S. Mao, and S. D. M. White, "*The structure and clustering of Lyman-break galaxies*," MNRAS **304**, 175 (1999), arXiv:astro-ph/9807341 .

[282] T. D. Saini, S. Bharadwaj, and S. K. Sethi, "*Using gravitational lensing to study HI Clouds at high redshift*," The Astrophysical Journal **557**, 421 (2001).

[283] S. Bharadwaj, S. K. Sethi, and T. D. Saini, "*Estimation of cosmological parameters from neutral hydrogen observations of the post-reionization epoch*," Physical Rev D **79**, 083538 (2009), arXiv:0809.0363 .

[284] Y. Mao, M. Tegmark, M. McQuinn, M. Zaldarriaga, and O. Zahn, "*How accurately can 21cm tomography constrain cosmology?*" Physical Rev D **78**, 023529 (2008), arXiv:0802.1710 .

[285] R. Barkana and A. Loeb, "*A method for separating the physics from the astrophysics of high-redshift 21 centimeter fluctuations*," The Astrophysical Journal **624**, L65 (2005).

[286] S. Wyithe, A. Loeb, and P. Geil, "*Baryonic Acoustic Oscillations in 21cm Emission: A Probe of Dark Energy out to High Redshifts*," ArXiv e-prints (2007), arXiv:0709.2955 .

[287] T.-C. Chang, U.-L. Pen, K. Bandura, and J. B. Peterson, "*Hydrogen 21-cm Intensity Mapping at redshift 0.8*," arXiv preprint arXiv:1007.3709 (2010).

[288] M. Davis, J. A. Newman, and S. M. F. A. C. Phillips, "*The deep2 redshift survey*," in *Deep Fields: Proceedings of the ESO Workshop Held at Garching, Germany, 9-12 October 2000* (Springer, 2003) pp. 241–246.

[289] K. Masui, E. Switzer, N. Banavar, K. Bandura, C. Blake, L.-M. Calin, T.-C. Chang, X. Chen, Y.-C. Li, Y.-W. Liao, *et al.*, "*Measurement of 21 cm brightness fluctuations at z 0.8 in cross-correlation*," The Astrophysical Journal Letters **763**, L20 (2013).

[290] E. Switzer, K. Masui, K. Bandura, L.-M. Calin, T.-C. Chang, X.-L. Chen, Y.-C. Li, Y.-W. Liao, A. Natarajan, U.-L. Pen, *et al.*, "*Determination of z 0.8 neutral hydrogen fluctuations using the 21 cm intensity mapping autocorrelation*," Monthly Notices of the Royal Astronomical Society: Letters **434**, L46 (2013).

[291] M. McQuinn, O. Zahn, M. Zaldarriaga, L. Hernquist, and S. R. Furlanetto, "*Cosmological parameter estimation using 21 cm radiation from the epoch of reionization*," The Astrophysical Journal **653**, 815 (2006).

[292] M. G. Santos, A. Cooray, and L. Knox, "*Multifrequency analysis of 21 centimeter fluctuations from the era of reionization*," The Astrophysical Journal **625**, 575 (2005).

[293] T. Di Matteo, R. Perna, T. Abel, and M. J. Rees, "*Radio foregrounds for the 21 centimeter tomography of the neutral intergalactic medium at high redshifts*," The Astrophysical Journal **564**, 576 (2002).

[294] P. Shaver, R. Windhorst, P. Madau, and A. De Bruyn, "*Can the reionization epoch be detected as a global signature in the cosmic background?*" arXiv preprint astro-ph/9901320 (1999).

[295] A. Ghosh, S. Bharadwaj, S. S. Ali, and J. N. Chengalur, "*Improved foreground removal in GMRT 610 MHz observations towards redshifted 21-cm tomography*," MNRAS **418**, 2584 (2011), arXiv:1108.3707 [astro-ph.CO] .

[296] G. Paciga, T.-C. Chang, Y. Gupta, R. Nityanada, J. Odegova, U.-L. Pen, J. B. Peterson, J. Roy, and K. Sigurdson, "*The GMRT Epoch of Reionization experiment: a new upper limit on the neutral hydrogen power spectrum at z = 8.6*," Monthly Notices of the Royal Astronomical Society **413**, 1174 (2011).

[297] A. Datta, J. Bowman, and C. Carilli, "*Bright source subtraction requirements for redshifted 21 cm measurements*," The Astrophysical Journal **724**, 526 (2010).

[298] E. Chapman, F. B. Abdalla, G. Harker, V. Jelić, P. Labropoulos, S. Zaroubi, M. A. Brentjens, A. de Bruyn, and L. Koopmans, "*Foreground removal using FASTICA: a showcase of LOFAR-EoR*," Monthly Notices of the Royal Astronomical Society **423**, 2518 (2012).

[299] F. Mertens, A. Ghosh, and L. Koopmans, "*Statistical 21-cm signal separation via Gaussian Process Regression analysis*," Monthly Notices of the Royal Astronomical Society **478**, 3640 (2018).

[300] C. M. Trott, R. Mondal, G. Mellema, S. G. Murray, B. Greig, J. L. Line, N. Barry, and M. F. Morales, "*Multi-frequency angular power spectrum of the 21˜ cm signal from the Epoch of Reionisation using the Murchison Widefield Array*," arXiv preprint arXiv:2208.06082 (2022).

[301] K. K. Datta, T. R. Choudhury, and S. Bharadwaj, "*The multifrequency angular power spectrum of the epoch of reionization 21-cm signal*," Monthly Notices of the Royal Astronomical Society **378**, 119 (2007).

[302] K. M. A. Elahi, S. Bharadwaj, S. Pal, A. Ghosh, S. S. Ali, S. Choudhuri, A. Chakraborty, A. Datta, N. Roy, M. Choudhury, and P. Dutta, "*Towards 21-cm intensity mapping at z = 2.28 with uGMRT using the tapered gridded estimator - III. Foreground removal*," mnras **525**, 3439 (2023), arXiv:2308.08284 [astro-ph.CO] .

[303] J. C. Pober, A. R. Parsons, J. E. Aguirre, Z. Ali, R. F. Bradley, C. L. Carilli, D. DeBoer, M. Dexter, N. E. Gugliucci, D. C. Jacobs, *et al.*, "*Opening the 21 cm epoch of reionization window: Measurements of foreground isolation with paper*," The Astrophysical Journal Letters **768**, L36 (2013).

[304] J. C. Pober, A. Liu, J. S. Dillon, J. E. Aguirre, J. D. Bowman, R. F. Bradley, C. L. Carilli, D. R. DeBoer, J. N. Hewitt, D. C. Jacobs, *et al.*, "*What next-generation 21 cm power spectrum measurements can teach us about the epoch of reionization*," The Astrophysical Journal **782**, 66 (2014).

[305] A. Liu, A. R. Parsons, and C. M. Trott, "*Epoch of reionization window. I. Mathematical formalism*," Physical Review D **90**, 023018 (2014).

[306] J. S. Dillon, A. R. Neben, J. N. Hewitt, M. Tegmark, N. Barry, A. Beardsley, J. Bowman, F. Briggs, P. Carroll, A. de Oliveira-Costa, *et al.*, "*Empirical covariance modeling for 21 cm power spectrum estimation: A method demonstration and new limits from early Murchison Widefield Array 128-tile data*," Physical Review D **91**, 123011 (2015).

[307] S. Pal, S. Bharadwaj, A. Ghosh, and S. Choudhuri, "*Demonstrating the Tapered Gridded Estimator (TGE) for the cosmological H i 21-cm power spectrum using 150-MHz GMRT observations*," Monthly Notices of the Royal Astronomical Society **501**, 3378 (2021).

[308] D. A. Mitchell, L. J. Greenhill, R. B. Wayth, R. J. Sault, C. J. Lonsdale, R. J. Cappallo, M. F. Morales, and S. M. Ord, "*Real-time calibration of the Murchison Widefield Array*," IEEE Journal of Selected Topics in Signal Processing **2**, 707 (2008).

[309] S. Kazemi, S. Yatawatta, S. Zaroubi, P. Lampropoulos, A. De Bruyn, L. Koopmans, and J. Noordam, "*Radio interferometric calibration using the SAGE algorithm*," Monthly Notices of the Royal Astronomical Society **414**, 1656 (2011).

[310] I. S. Sullivan, M. F. Morales, B. J. Hazelton, W. Arcus, D. Barnes, G. Bernardi, F. H. Briggs, J. D. Bowman, J. D. Bunton, R. J. Cappallo, *et al.*, "*Fast holographic deconvolution: A new technique for precision radio interferometry*," The Astrophysical Journal **759**, 17 (2012).

[311] S. Kazemi and S. Yatawatta, "*Robust radio interferometric calibration using the t-distribution*," Monthly Notices of the Royal Astronomical Society **435**, 597 (2013).

[312] J. S. Dillon, M. Lee, Z. S. Ali, A. R. Parsons, N. Orosz, C. D. Nunhokee, P. La Plante, A. P. Beardsley, N. S. Kern, Z. Abdurashidova, *et al.*, "*Redundant-baseline calibration of the hydrogen epoch of reionization array*," Monthly Notices of the Royal Astronomical Society **499**, 5840 (2020).

[313] N. S. Kern, J. S. Dillon, A. R. Parsons, C. L. Carilli, G. Bernardi, Z. Abdurashidova, J. E. Aguirre, P. Alexander, Z. S. Ali, Y. Balfour, *et al.*, "*Absolute calibration strategies for the hydrogen epoch of reionization array and their impact on the 21 cm power spectrum*," The Astrophysical Journal **890**, 122 (2020).

[314] R. Byrne, M. F. Morales, B. J. Hazelton, and M. Wilensky, "*A unified calibration framework for 21 cm cosmology*," Monthly Notices of the Royal Astronomical Society **503**, 2457 (2021).

[315] P. H. Sims, J. C. Pober, and J. L. Sievers, "*A Bayesian approach to high fidelity interferometric calibration- II: demonstration with simulated data*," Monthly Notices of the Royal Astronomical Society **517**, 935 (2022).

[316] A. Ewall-Wice, J. S. Dillon, B. Gehlot, A. Parsons, T. Cox, and D. C. Jacobs, "*Precision Calibration of Radio Interferometers for 21 cm Cosmology with No Redundancy and Little Knowledge of Antenna Beams and the Radio Sky*," The Astrophysical Journal **938**, 151 (2022).

[317] R. Byrne, "*Delay-weighted Calibration: Precision Calibration for 21 cm Cosmology with Resilience to Sky Model Error*," The Astrophysical Journal **943**, 117 (2023).

[318] P. McDonald, "*Toward a Measurement of the Cosmological Geometry at z 2: Predicting Ly alpha Forest Correlation in Three Dimensions and the Potential of Future Data Sets*," The Astrophysical Journal **585**, 34–51 (2003).

[319] R. A. Croft, D. H. Weinberg, M. Bolte, S. Burles, L. Hernquist, N. Katz, D. Kirkman, and D. Tytler, "*Toward a precise measurement of matter clustering: Lyα forest data at redshifts 2-4*," The Astrophysical Journal **581**, 20 (2002).

[320] V. IrVsiVc, M. Viel, M. G. Haehnelt, J. S. Bolton, and G. D. Becker, "*First constraints on fuzzy dark matter from Lyman-α forest data and hydrodynamical simulations*," Physical review letters **119**, 031302 (2017).

[321] J. Baur, N. Palanque-Delabrouille, C. Yeche, A. Boyarsky, O. Ruchayskiy, É. Armengaud, and J. Lesgourgues, "*Constraints from Ly-α forests on non-thermal dark matter including resonantly-produced sterile neutrinos*," Journal of Cosmology and Astroparticle Physics **2017**, 013 (2017).

[322] M. Walther, J. F. Hennawi, H. Hiss, J. Oñorbe, K.-G. Lee, A. Rorai, and J. O'Meara, "*A new precision measurement of the small-scale line-of-sight power spectrum of the Lyα forest*," The Astrophysical Journal **852**, 22 (2017).

[323] D. H. Weinberg, S. Burles, R. A. C. Croft, R. Dave', G. Gomez, L. Hernquist, N. Katz, D. Kirkman, S. Liu, J. Miralda-Escude', M. Pettini, J. Phillips, D. Tytler, and J. Wright, "*Cosmology with the Lyman-alpha Forest*," ArXiv Astrophysics e-prints (1998), astro-ph/9810142 .

[324] R. A. C. Croft, D. H. Weinberg, N. Katz, and L. Hernquist, "*Recovery of the Power Spectrum of Mass Fluctuations from Observations of the Ly alpha Forest*," apj **495**, 44 (1998), arXiv:astro-ph/9708018 .

[325] U. Seljak, A. Slosar, and P. McDonald, "*Cosmological parameters from combining the Lyman-α forest with CMB, galaxy clustering and SN constraints*," Journal of Cosmology and Astro-Particle Physics **10**, 14 (2006), arXiv:astro-ph/0604335 .

[326] S. Gratton, A. Lewis, and G. Efstathiou, "*Prospects for constraining neutrino mass using Planck and Lyman-α forest data*," prd **77**, 083507 (2008), arXiv:0705.3100 .

[327] M. Viel, G. D. Becker, J. S. Bolton, M. G. Haehnelt, M. Rauch, and W. L. W. Sargent, "*How Cold Is Cold Dark Matter? Small-Scales Constraints from the Flux Power Spectrum of the High-Redshift Lyman-α Forest*," Physical Review Letters **100**, 041304 (2008), arXiv:0709.0131 .

[328] L. Hui and N. Y. Gnedin, "*Equation of state of the photoionized intergalactic medium*," Monthly Notices of the Royal Astronomical Society **292**, 27–42 (1997).

[329] S. Gallerani, T. R. Choudhury, and A. Ferrara, "*Constraining the reionization history with QSO absorption spectra*," Monthly Notices of the Royal Astronomical Society **370**, 1401–1421 (2006).

[330] R. Cen, P. McDonald, H. Trac, and A. Loeb, "*Probing the Epoch of Reionization with the Lyα Forest at $z \sim 4-5$*," Astrophysical Journal Letters **706**, L164 (2009), arXiv:0907.0735 .

[331] M. Viel, J. Lesgourgues, M. G. Haehnelt, S. Matarrese, and A. Riotto, "*Constraining warm dark matter candidates including sterile neutrinos and light gravitinos with WMAP and the Lyman-α forest*," Physical Review D **71**, 063534 (2005).

[332] M. McQuinn, "*The evolution of the intergalactic medium*," Annual Review of Astronomy and Astrophysics **54**, 313 (2016).

[333] T. Theuns, A. Leonard, G. Efstathiou, F. Pearce, and P. Thomas, "*P3M-SPH simulations of the Lyα forest*," Monthly Notices of the Royal Astronomical Society **301**, 478 (1998).

[334] L. Hui and N. Y. Gnedin, "*Equation of state of the photoionized intergalactic medium*," Monthly Notices of the Royal Astronomical Society **292**, 27 (1997).

[335] J. R. Bond, A. S. Szalay, and J. Silk, "*Lyman-alpha clouds as a relic of primordial density fluctuations*," apj **324**, 627 (1988).

[336] R. Cen, J. Miralda-Escudé, J. P. Ostriker, and M. Rauch, "*Gravitational collapse of small-scale structure as the origin of the Lyman-alpha forest*," apjl **437**, L9 (1994), arXiv:astro-ph/9409017 .

[337] R. Davee, L. Hernquist, N. Katz, D. Weinberg, and C. Churchill, "*Comparing Simulations and Observations of the Lyalpha Forest*," in *Bulletin of the American Astronomical Society*, Bulletin of the American Astronomical Society, Vol. 28 (1996) pp. 856–860.

[338] R. Davé, L. Hernquist, N. Katz, and D. H. Weinberg, "*The Low-Redshift LYalpha Forest in Cold Dark Matter Cosmologies*," apj **511**, 521 (1999), arXiv:astro-ph/9807177 .

[339] A. G. Doroshkevich and S. F. Shandarin, "*Structure of the intergalactic medium*," mnras **179**, 95P (1977).

[340] C. McGill, "*The redshift projection. II - Caustics and the Lyman alpha forest*," mnras **242**, 544 (1990).

[341] H. Bi, J. Ge, and L. Fang, "*A Simulation of LY alpha Absorption Forests in Linear Approximation of Cold Dark Matter and Cold Plus Hot Dark Matter Models*," apj **452**, 90 (1995), arXiv:astro-ph/9504061 .

[342] L. Hui, N. Y. Gnedin, and Y. Zhang, "*The Statistics of Density Peaks and the Column Density Distribution of the Ly alpha Forest*," apj **486**, 599 (1997), arXiv:astro-ph/9608157 .

[343] H. Bi and A. F. Davidsen, "*Evolution of Structure in the Intergalactic Medium and the Nature of the Lymanf alpha Forest*," The Astrophysical Journal **479**, 523–542 (1997).

[344] T. R. Choudhury, T. Padmanabhan, and R. Srianand, "*Semi-analytic approach to understanding the distribution of neutral hydrogen in the Universe*," mnras **322**, 561 (2001), arXiv:astro-ph/0005252 .

[345] T. R. Choudhury, R. Srianand, and T. Padmanabhan, "*Semianalytic Approach to Understanding the Distribution of Neutral Hydrogen in the Universe: Comparison of Simulations with Observations*," apj **559**, 29 (2001), arXiv:astro-ph/0012498 .

[346] N. Palanque-Delabrouille, C. Yeche, J. Baur, C. Magneville, G. Rossi, J. Lesgourgues, A. Borde, E. Burtin, J.-M. LeGoff, J. Rich, *et al.*, "*Neutrino masses and cosmology with Lyman-alpha forest power spectrum*," Journal of Cosmology and Astroparticle Physics **2015**, 011 (2015).

[347] S. Chabanier, N. Palanque-Delabrouille, C. Yèche, J.-M. Le Goff, E. Armengaud, J. Bautista, M. Blomqvist, K. Dawson, T. Etourneau, A. Font-Ribera, *et al.*, "*The one-dimensional power spectrum from the SDSS DR14 Lyα forests*," Journal of Cosmology and Astroparticle Physics **2019**, 017 (2019).

[348] A. Slosar, A. Font-Ribera, M. M. Pieri, J. Rich, J.-M. L. Goff, E. Aubourg, J. Brinkmann, N. Busca, B. Carithers, R. Charlassier, and et al., "*The Lyman alpha forest in three dimensions: measurements of large scale flux correlations from BOSS 1st-year data*," Journal of Cosmology and Astroparticle Physics **2011**, 001–001 (2011).

[349] T. Delubac, J. E. Bautista, N. G. Busca, J. Rich, D. Kirkby, S. Bailey, A. Font-Ribera, A. Slosar, K.-G. Lee, M. M. Pieri, and et al., "*Baryon acoustic oscillations in the Lyman alpha forest of BOSS DR11 quasars*," Astronomy and Astrophysics **574** (2015), 10.1051/0004-6361/201423969.

[350] A. Font-Ribera, J. Miralda-Escudé, E. Arnau, B. Carithers, K.-G. Lee, P. Noterdaeme, I. Pâris, P. Petitjean, J. Rich, E. Rollinde, and et al., "*The large-scale cross-correlation of Damped Lyman alpha systems with the Lyman alpha forest: first measurements from BOSS*," Journal of Cosmology and Astroparticle Physics **2012** (2012), 10.1088/1475-7516/2012/11/059.

[351] F. Villaescusa-Navarro, S. Genel, E. Castorina, A. Obuljen, D. N. Spergel, L. Hernquist, D. Nelson, I. P. Carucci, A. Pillepich, F. Marinacci, B. Diemer, M. Vogelsberger, R. Weinberger, and R. Pakmor, "*Ingredients for 21 cm Intensity Mapping*," The Astrophysical Journal **866**, 135 (2018).

[352] T. Guha Sarkar, S. Bharadwaj, T. R. Choudhury, and K. K. Datta, "*Cross-correlation of the HI 21-cm signal and Lyman alpha forest: a probe of cosmology*," Monthly Notices of the Royal Astronomical Society **410**, 1130–1134 (2010).

[353] T. G. Sarkar and K. K. Datta, "*On using large scale correlation of the Lyman alpha forest and redshifted 21-cm signal to probe HI distribution during the post reionization era*," Journal of Cosmology and Astroparticle Physics **2015**, 001–001 (2015).

[354] A. K. Sarkar, S. Bharadwaj, and T. G. Sarkar, "*Predictions for measuring the cross power spectrum of the HI 21-cm signal and the Lymana alpha forest using*

OWFA," Journal of Cosmology and Astroparticle Physics **2018**, 051–051 (2018).

[355] A. Sarkar, A. K. Pal, and T. G. Sarkar, "*Constraining warm dark matter power spectrum using the cross-correlation of HI 21 cm signal and the Lyman- Alpha forest*," Journal of Cosmology and Astroparticle Physics **2019**, 058–058 (2019).

[356] M. Amiri, K. Bandura, T. Chen, M. Deng, M. Dobbs, M. Fandino, S. Foreman, M. Halpern, A. S. Hill, G. Hinshaw, *et al.*, "*Detection of cosmological 21 cm emission with the Canadian hydrogen intensity mapping experiment*," The Astrophysical Journal **947**, 16 (2023).

[357] T. G. Sarkar, "*CMBR weak lensing and HI 21-cm cross-correlation angular power spectrum*," Journal of Cosmology and Astroparticle Physics **2010**, 002–002 (2010).

[358] A. Vallinotto, S. Das, D. N. Spergel, and M. Viel, "*Lenses in the Forest: Cross Correlation of the Lyman alpha Flux with Cosmic Microwave Background Lensing*," Physical Review Letters **103** (2009), 10.1103/physrevlett.103.091304.

[359] A. Ghosh, S. Bharadwaj, S. S. Ali, and J. N. Chengalur, "*GMRT observation towards detecting the post-reionization 21-cm signal*," Monthly Notices of the Royal Astronomical Society **411**, 2426–2438 (2010).

[360] C. B. Dash and T. Guha Sarkar, "*Constraining dark energy using the cross correlations of weak lensing with post-reionization probes of neutral hydrogen*," Journal of Cosmology and Astroparticle Physics **2021**, 016 (2021).

[361] C. Péroux, R. G. McMahon, L. J. Storrie-Lombardi, and M. J. Irwin, "*The evolution of omega HI and the epoch of formation of damped Lyman alpha absorbers*," Monthly Notices of the Royal Astronomical Society **346**, 1103–1115 (2003).

[362] P. Noterdaeme, P. Petitjean, C. Ledoux, and R. Srianand, "*Evolution of the cosmological mass density of neutral gas from Sloan Digital Sky Survey II – Data Release 7*," Astronomy and Astrophysics **505**, 1087–1098 (2009).

[363] T. Zafar, C. Péroux, A. Popping, B. Milliard, J.-M. Deharveng, and S. Frank, "*The ESO UVES advanced data products quasar sample*," Astronomy and Astrophysics **556**, A141 (2013).

[364] M. Viel, S. Matarrese, H. Mo, M. Haehnelt, and T. Theuns, "*Probing the intergalactic medium with the Lyman alpha forest along multiple lines of sight to distant QSOs*," Monthly Notices of the Royal Astronomical Society **329**, 848–862 (2002).

[365] A. Slosar, S. Ho, M. White, and T. Louis, "*The acoustic peak in the Lyman alpha forest*," Journal of Cosmology and Astroparticle Physics **2009**, 019–019 (2009).

[366] U. Seljak, "*Bias, redshift space distortions and primordial nongaussianity of nonlinear transformations: application to Ly-alpha forest*," jcap **2012**, 004 (2012), arXiv:1201.0594 [astro-ph.CO] .

[367] A. M. Cieplak and A. Slosar, "*Towards physics responsible for large-scale Lyman-alpha forest bias parameters*," jcap **2016**, 016 (2016), arXiv:1509.07875 [astro-ph.CO] .

[368] M. A. Fernandez, S. Bird, and P. Upton Sanderbeck, "*Effect of Separate Initial Conditions on the Lyman-alpha Forest in Simulations*," arXiv e-prints , arXiv:2009.09119 (2020), arXiv:2009.09119 [astro-ph.CO] .

[369] S. Bird, K. K. Rogers, H. V. Peiris, L. Verde, A. Font-Ribera, and A. Pontzen, "*An emulator for the Lyman-alpha forest*," jcap **2019**, 050 (2019), arXiv:1812.04654 [astro-ph.CO] .

[370] S. Tanaka, S. Yoshiura, K. Kubota, K. Takahashi, A. J. Nishizawa, and N. Sugiyama, "*Detectability of CMB Weak Lensing and HI Cross Correlation and constraints on cosmological parameters*," (2020), arXiv:1904.10363 [astro-ph.CO] .

[371] S. Cunnington, L. Wolz, A. Pourtsidou, and D. Bacon, "*Impact of foregrounds on H i intensity mapping cross-correlations with optical surveys*," Monthly Notices of the Royal Astronomical Society **488**, 5452 (2019).

[372] C. Guandalin, I. P. Carucci, D. Alonso, and K. Moodley, "*Clustering redshifts with the 21cm-galaxy cross-bispectrum*," Monthly Notices of the Royal Astronomical Society **516**, 3029 (2022).

[373] R. Kothari and R. Maartens, "*A geometrical interpretation of foreground filters for HI intensity*," arXiv preprint arXiv:2308.03462 (2023).

[374] R. Durrer and R. Maartens, "*Dark Energy and Modified Gravity*," (2008), arXiv:0811.4132 [astro-ph] .

[375] S. Perlmutter, S. Gabi, G. Goldhaber, A. Goobar, D. E. Groom, I. M. Hook, A. G. Kim, M. Y. Kim, J. C. Lee, and R. e. a. Pain, "*Measurements of the Cosmological Parameters Omega and Lambda from the First Seven Supernovae at z > 0.35*," The Astrophysical Journal **483**, 565–581 (1997).

[376] M. Ata, F. Baumgarten, J. Bautista, F. Beutler, D. Bizyaev, M. R. Blanton, J. A. Blazek, and A. S. e. Bolton, "*The clustering of the SDSS-IV extended Baryon Oscillation Spectroscopic Survey DR14 quasar sample: first measurement of baryon acoustic oscillations between redshift 0.8 and 2.2*," Monthly Notices of the Royal Astronomical Society **473**, 4773 (2017), https://academic.oup.com/mnras/article-pdf/473/4/4773/21941846/stx2630.pdf .

[377] M. S. Turner and M. White, "*CDM models with a smooth component*," Phys. Rev. D **56**, R4439 (1997).

[378] C. Armendariz-Picon, V. Mukhanov, and P. J. Steinhardt, "*Essentials of k-essence*," Phys. Rev. D **63**, 103510 (2001).

[379] M. C. Bento, O. Bertolami, and A. A. Sen, "*Generalized Chaplygin gas, accelerated expansion, and dark-energy-matter unification*," Phys. Rev. D **66**, 043507 (2002).

[380] T. Padmanabhan and T. R. Choudhury, "*Can the clustered dark matter and the smooth dark energy arise from the same scalar field?*" Phys. Rev. D **66**, 081301 (2002).

[381] S. Sen and A. A. Sen, "*Late time acceleration in Brans-Dicke cosmology*," Phys. Rev. D **63**, 124006 (2001).

[382] J. S. Bagla, H. K. Jassal, and T. Padmanabhan, "*Cosmology with tachyon field as dark energy*," Phys. Rev. D **67**, 063504 (2003).

[383] F. Perrotta, C. Baccigalupi, and S. Matarrese, "*Extended quintessence*," Phys. Rev. D **61**, 023507 (1999).

[384] J. Kujat, R. J. Scherrer, and A. A. Sen, "*Phantom dark energy models with negative kinetic term*," Phys. Rev. D **74**, 083501 (2006).

[385] R. Gannouji and M. Sami, "*Galileon gravity and its relevance to late time cosmic acceleration*," Phys. Rev. D **82**, 024011 (2010).

[386] I. Maor, R. Brustein, J. McMahon, and P. J. Steinhardt, "*Measuring the equation of state of the universe: Pitfalls and prospects*," Phys. Rev. D **65**, 123003 (2002).

[387] S. Thakur, A. Nautiyal, A. A. Sen, and T. R. Seshadri, "*Thawing versus tracker behaviour: observational evidence*," Monthly Notices of the Royal Astronomical Society **427**, 988 (2012), https://academic.oup.com/mnras/article-pdf/427/2/988/3006783/427-2-988.pdf .

[388] G. Pantazis, S. Nesseris, and L. Perivolaropoulos, "*Comparison of thawing and freezing dark energy parametrizations*," Phys. Rev. D **93**, 103503 (2016).

[389] A. LEWIS and A. CHALLINOR, "*Weak gravitational lensing of the CMB*," Physics Reports **429**, 1–65 (2006).

[390] W. Hu, "*Mapping the Dark Matter through the Cosmic Microwave Background Damping Tail*," The Astrophysical Journal **557**, L79–L83 (2001).

[391] U. Seljak and M. Zaldarriaga, "*Measuring Dark Matter Power Spectrum from Cosmic Microwave Background*," Physical Review Letters **82**, 2636–2639 (1999).

[392] W. Hu and T. Okamoto, "*Mass Reconstruction with Cosmic Microwave Background Polarization*," The Astrophysical Journal **574**, 566–574 (2002).

[393] M. Kamionkowski and E. D. Kovetz, "*The Quest for B Modes from Inflationary Gravitational Waves*," Annual Review of Astronomy and Astrophysics **54**, 227–269 (2016).

[394] J. R. Pritchard and A. Loeb, "*21 cm cosmology in the 21st century*," Reports on Progress in Physics **75**, 086901 (2012).

[395] A. Hussain, S. Thakur, T. Guha Sarkar, and A. A. Sen, "*Prospects of probing quintessence with H i 21-cm intensity mapping survey*," Monthly Notices of the Royal Astronomical Society **463**, 3492 (2016).

[396] B. R. Dinda, A. A. Sen, and T. R. Choudhury, "*Dark energy constraints from the 21cm intensity mapping surveys with SKA1*," arXiv e-prints , arXiv:1804.11137 (2018), 1804.11137 .

[397] Y. Mao, M. Tegmark, M. McQuinn, M. Zaldarriaga, and O. Zahn, "*How accurately can 21 cm tomography constrain cosmology?*" Physical Review D **78** (2008), 10.1103/physrevd.78.023529.

[398] N. Y. Gnedin and A. J. S. Hamilton, "*Matter power spectrum from the Lyman-alpha forest: myth or reality?*" Monthly Notices of the Royal Astronomical Society **334**, 107–116 (2002).

[399] J. Lesgourgues, M. Viel, M. G. Haehnelt, and R. Massey, "*A combined analysis of 3D weak lensing, Lyman alpha forest and WMAP year three data*," Journal of Cosmology and Astroparticle Physics **2007**, 008–008 (2007).

[400] A. Font-Ribera and SDSS-III Collaboration, "*Cosmology from the BOSS Lyman-Alpha Forest*," in *American Astronomical Society Meeting Abstracts #225*, American Astronomical Society Meeting Abstracts, Vol. 225 (2015) p. 125.03.

[401] M. McQuinn and M. White, "*On estimating Lyman alpha forest correlations between multiple sightlines*," Monthly Notices of the Royal Astronomical Society **415**, 2257–2269 (2011).

[402] A. Garzilli, A. Magalich, T. Theuns, C. S. Frenk, C. Weniger, O. Ruchayskiy, and A. Boyarsky, "*The Lyman alpha forest as a diagnostic of the nature of the dark matter*," Monthly Notices of the Royal Astronomical Society **489**, 3456–3471 (2019).

[403] M. Viel, S. Matarrese, T. Theuns, D. Munshi, and Y. Wang, "*Dark energy effects on the Lyman alpha forest*," Monthly Notices of the Royal Astronomical Society **340**, L47–L51 (2003).

[404] R. K. Sachs and A. M. Wolfe, "*Perturbations of a Cosmological Model and Angular Variations of the Microwave Background*," Astrophysical Journal **147**, 73 (1967).

[405] R. Scranton, A. J. Connolly, R. C. Nichol, A. Stebbins, I. Szapudi, D. J. Eisenstein, N. Afshordi, T. Budavari, I. Csabai, J. A. Frieman, J. E. Gunn, D. Johnston, Y. Loh, R. H. Lupton, C. J. Miller, E. S. Sheldon, R. S. Sheth, A. S. Szalay, M. Tegmark, and Y. Xu, "*Physical Evidence for Dark Energy*," (2003), arXiv:astro-ph/0307335 [astro-ph] .

[406] N. Afshordi, Y.-S. Loh, and M. A. Strauss, "*Cross-correlation of the cosmic microwave background with the 2MASS galaxy survey: Signatures of dark energy, hot gas, and point sources*," Phys. Rev. D **69**, 083524 (2004).

[407] T. Giannantonio, R. Scranton, R. G. Crittenden, R. C. Nichol, S. P. Boughn, A. D. Myers, and G. T. Richards, "*Combined analysis of the integrated Sachs-Wolfe effect and cosmological implications*," Physical Review D **77** (2008), 10.1103/physrevd.77.123520.

[408] T. G. Sarkar, K. K. Datta, and S. Bharadwaj, "*The CMBR ISW and HI 21 cm cross-correlation angular power spectrum*," Journal of Cosmology and Astroparticle Physics **2009**, 019–019 (2009).

[409] W. Hu, "*Lecture Notes on CMB Theory: From Nucleosynthesis to Recombination*," (2008), arXiv:0802.3688 [astro-ph] .

[410] K. Subramanian, "*The Physics of CMBR Anisotropies*," (2004), arXiv:astro-ph/0411049 [astro-ph] .

[411] K. M. Smith, A. Cooray, S. Das, O. Dore, D. Hanson, C. Hirata, M. Kaplinghat, B. Keating, M. LoVerde, N. Miller, and et al., "*Gravitational Lensing*," AIP Conference Proceedings (2009), 10.1063/1.3160886.

[412] D. P. Schneider, P. B. Hall, G. T. Richards, D. E. V. Berk, S. F. Anderson, X. Fan, S. Jester, C. Stoughton, M. A. Strauss, and M. SubbaRao, "*The Sloan Digital Sky Survey Quasar Catalog. III. Third Data Release*," The Astronomical Journal **130**, 367 (2005).

[413] F. Coppolani and P. e. Petitjean, "*Transverse and longitudinal correlation functions in the intergalactic medium from 32 close pairs of high-redshift quasars**," Monthly Notices of the Royal Astronomical Society **370**, 1804 (2006), https://academic.oup.com/mnras/article-pdf/370/4/1804/17316710/mnras0370-1804.pdf .

[414] V. D'Odorico, M. Viel, F. Saitta, S. Cristiani, S. Bianchi, B. Boyle, S. Lopez, J. Maza, and P. Outram, "*Tomography of the intergalactic medium with Ly alpha forests in close QSO pairs*," Monthly Notices of the Royal Astronomical Society **372**, 1333–1344 (2006).

[415] Planck Collaboration, Ade, P. A. R., Aghanim, N., Arnaud, M., and A. et;al, "*Planck 2015 results - XIV. Dark energy and modified gravity*," Astronomy and Astrophysics **594**, A14 (2016).

[416] K. K. Datta, S. Bharadwaj, and T. R. Choudhury, "*Detecting ionized bubbles in redshifted 21-cm maps*," Monthly Notices of the Royal Astronomical Society **382**, 809 (2007), https://academic.oup.com/mnras/article-pdf/382/2/809/3432450/mnras0382-0809.pdf .

[417] Y. Gupta, B. Ajithkumar, H. S. Kale, S. Nayak, S. Sabhapathy, S. Sureshkumar, R. V. Swami, J. N. Chengalur, S. K. Ghosh, C. H. Ishwara-Chandra, B. C. Joshi, N. Kanekar, D. V. Lal, and S. Roy, "*The upgraded GMRT: opening new windows on the radio Universe*," Current Science **113**, 707 (2017).

[418] J. Jonas, "*The MeerKAT Radio Telescope*," (2018) p. 001.

[419] G.-B. Zhao, Y. Wang, A. J. Ross, S. Shandera, W. J. Percival, K. S. Dawson, J.-P. Kneib, A. D. Myers, J. R. Brownstein, J. Comparat, and et al., "*The extended Baryon Oscillation Spectroscopic Survey: a cosmological forecast*," Monthly Notices of the Royal Astronomical Society **457**, 2377–2390 (2016).

[420] M. Vargas-Magana, D. D. Brooks, M. M. Levi, and G. G. Tarle, "*Unraveling the Universe with DESI*," (2019), arXiv:1901.01581 [astro-ph.IM] .

[421] C. Escamilla-Rivera, "*Status on Bidimensional Dark Energy Parameterizations Using SNe Ia JLA and BAO Datasets*," Galaxies **4**, 8 (2016).

[422] Y. Wang and M. Tegmark, "*New Dark Energy Constraints from Supernovae, Microwave Background, and Galaxy Clustering*," Phys. Rev. Lett. **92**, 241302 (2004).

[423] F. D. Marchi and G. Cascioli, "*Testing general relativity in the solar system: present and future perspectives*," Classical and Quantum Gravity **37**, 095007 (2020).

[424] T. P. Sotiriou and S. Liberati, "*Metric-affine f (R) theories of gravity*," Annals of Physics **322**, 935 (2007).

[425] T. P. Sotiriou and V. Faraoni, "*f (R) theories of gravity*," Reviews of Modern Physics **82**, 451 (2010).

[426] W. Hu and I. Sawicki, "*Parametrized post-Friedmann framework for modified gravity*," Physical Review D **76**, 104043 (2007).

[427] X. Liu, B. Li, G.-B. Zhao, M.-C. Chiu, W. Fang, C. Pan, Q. Wang, W. Du, S. Yuan, L. Fu, *et al.*, "*Constraining f (R) gravity theory using weak lensing peak statistics from the Canada-France-Hawaii-Telescope Lensing Survey*," Physical Review Letters **117**, 051101 (2016).

[428] M. Cataneo, D. Rapetti, F. Schmidt, A. B. Mantz, S. W. Allen, D. E. Applegate, P. L. Kelly, A. Von Der Linden, and R. G. Morris, "*New constraints on f (R) gravity from clusters of galaxies*," Physical Review D **92**, 044009 (2015).

[429] C. M. Will, "*The confrontation between general relativity and experiment*," Living reviews in relativity **17**, 1 (2014).

[430] D. F. Mota and D. J. Shaw, "*Evading equivalence principle violations, cosmological, and other experimental constraints in scalar field theories with a strong coupling to matter*," Physical Review D **75**, 063501 (2007).

[431] P. Brax, C. Van De Bruck, S. Clesse, A.-C. Davis, and G. Sculthorpe, "*Early modified gravity: Implications for cosmology*," Physical Review D **89**, 123507 (2014).

[432] P. Brax and P. Valageas, "*Lyman-α power spectrum as a probe of modified gravity*," Journal of Cosmology and Astroparticle Physics **2019**, 049 (2019).

[433] B. Li, W. A. Hellwing, K. Koyama, G.-B. Zhao, E. Jennings, and C. M. Baugh, "*The non-linear matter and velocity power spectra in f (R) gravity*," Monthly Notices of the Royal Astronomical Society **428**, 743 (2013).

[434] C. Arnold, P. Fosalba, V. Springel, E. Puchwein, and L. Blot, "*The modified gravity light-cone simulation project–I. Statistics of matter and halo distributions*," Monthly Notices of the Royal Astronomical Society **483**, 790 (2019).

[435] K. Subramanian and T. Padmanabhan, "*Neutral Hydrogen at High Redshifts as a Probe of Structure Formation - Part One - Post-Cobe Analysis of CDM and HDM Models*," MNRAS **265**, 101 (1993).

[436] A. Aviles, M. A. Rodriguez-Meza, J. De-Santiago, and J. L. Cervantes-Cota, "*Nonlinear evolution of initially biased tracers in modified gravity*," Journal of Cosmology and Astroparticle Physics **2018**, 013 (2018).

[437] A. K. Sarkar, S. Bharadwaj, and T. Guha Sarkar, "*Predictions for measuring the cross power spectrum of the HI 21-cm signal and the Lyman-α forest using OWFA*," Journal of Cosmology and Astroparticle Physics **2018**, 051 (2018).

[438] A. K. Sarkar, S. Bharadwaj, and S. S. Ali, "*Fisher matrix-based predictions for measuring the z= 3.35 binned 21-cm power spectrum using the ooty wide field array (owfa)*," Journal of Astrophysics and Astronomy **38**, 14 (2017).

[439] S. Bharadwaj, A. K. Sarkar, and S. S. Ali, "*Fisher matrix predictions for detecting the cosmological 21-cm signal with the ooty wide field array (owfa)*," Journal of Astrophysics and Astronomy **36**, 385 (2015).

[440] S. Jana and S. Mohanty, "*Constraints on $f(R)$ theories of gravity from GW170817*," Phys. Rev. D **99**, 044056 (2019).

[441] S. Peirone, M. Raveri, M. Viel, S. Borgani, and S. Ansoldi, "*Constraining f (R) gravity with Sunyaev-Zel'dovich clusters detected by the Planck satellite*," prd **95**, 023521 (2017), arXiv:1607.07863 [astro-ph.CO] .

[442] F. Schmidt, A. Vikhlinin, and W. Hu, "*Cluster constraints on f(R) gravity*," prd **80**, 083505 (2009), arXiv:0908.2457 [astro-ph.CO] .

[443] D. Huterer, M. Takada, G. Bernstein, and B. Jain, "*Systematic errors in future weak-lensing surveys: requirements and prospects for self-calibration*," Monthly Notices of the Royal Astronomical Society **366**, 101–114 (2006).

[444] M. Takada and B. Jain, "*Cosmological parameters from lensing power spectrum and bispectrum tomography*," Monthly Notices of the Royal Astronomical Society **348**, 897 (2004).

[445] Y. Higuchi and M. Shirasaki, "*The imprint of f (R) gravity on weak gravitational lensing–I. Connection between observables and large-scale structure*," Monthly Notices of the Royal Astronomical Society **459**, 2762 (2016).

[446] B. Li and M. Shirasaki, "*Galaxy–galaxy weak gravitational lensing in f (R) gravity*," Monthly Notices of the Royal Astronomical Society **474**, 3599 (2018).

[447] C. Arnold, E. Puchwein, and V. Springel, "*The Lyman α forest in f (R) modified gravity*," Monthly Notices of the Royal Astronomical Society **448**, 2275 (2015).

[448] B. Abolfathi, D. Aguado, G. Aguilar, C. A. Prieto, A. Almeida, T. T. Ananna, F. Anders, S. F. Anderson, B. H. Andrews, B. Anguiano, *et al.*, "*The fourteenth data release of the Sloan Digital Sky Survey: First spectroscopic data from the extended Baryon Oscillation Spectroscopic Survey and from the second phase of the Apache Point Observatory Galactic Evolution Experiment*," The Astrophysical Journal Supplement Series **235**, 42 (2018).

[449] S. S. Shapiro, J. L. Davis, D. E. Lebach, and J. Gregory, "*Measurement of the solar gravitational deflection of radio waves using geodetic very-long-baseline interferometry data, 1979–1999*," Physical Review Letters **92**, 121101 (2004).

[450] B. Bertotti, L. Iess, and P. Tortora, "*A test of general relativity using radio links with the Cassini spacecraft*," Nature **425**, 374 (2003).

[451] J.-A. Gu and W.-T. Lin, "*Solar-System Constraints on f (R) Chameleon Gravity*," arXiv preprint arXiv:1108.1782 (2011).

[452] J. Khoury and A. Weltman, "*Chameleon cosmology*," Physical Review D **69** (2004), 10.1103/physrevd.69.044026.

[453] S. Ferraro, F. Schmidt, and W. Hu, "*Cluster abundance in f (R) gravity models*," Physical Review D **83**, 063503 (2011).

[454] M. Cataneo, D. Rapetti, F. Schmidt, A. B. Mantz, S. W. Allen, D. E. Applegate, P. L. Kelly, A. von der Linden, and R. G. Morris, "*New constraints onf(R)gravity from clusters of galaxies*," Physical Review D **92** (2015), 10.1103/physrevd.92.044009.

[455] A. A. Starobinsky, "*Disappearing cosmological constant in f(R) gravity*," JETP Letters **86**, 157–163 (2007).

[456] V. Sahni and A. Starobinsky, "*The case for a positive cosmological Λ-term*," International Journal of Modern Physics D **9**, 373 (2000).

[457] P. J. E. Peebles and B. Ratra, "*The cosmological constant and dark energy*," Rev. Mod. Phys. **75**, 559 (2003).

[458] I. Zlatev, L. Wang, and P. J. Steinhardt, "*Quintessence, Cosmic Coincidence, and the Cosmological Constant*," Phys. Rev. Lett. **82**, 896 (1999).

[459] R. J. Scherrer and A. Sen, "*Thawing quintessence with a nearly flat potential*," Physical Review D **77**, 083515 (2008).

[460] S. Panda, Y. Sumitomo, and S. P. Trivedi, "*Axions as quintessence in string theory*," Physical Review D **83**, 083506 (2011).

[461] J. Fonseca, R. Maartens, and M. G. Santos, "*Probing the primordial Universe with MeerKAT and DES*," Monthly Notices of the Royal Astronomical Society **466**, 2780 (2017).

[462] T. G. Sarkar and S. Bharadwaj, "*Predictions for BAO distance estimates from the cross-correlation of the Lyman-α forest and redshifted 21-cm emission*," Journal of Cosmology and Astroparticle Physics **2013**, 023 (2013).

[463] T. G. Sarkar and S. Bharadwaj, "*The Imprint of the Baryon Acoustic Oscillations (BAO) in the Cross-correlation of the Redshifted HI 21-cm Signal and the Ly-alpha Forest*," arXiv preprint arXiv:1112.0745 (2011).

[464] H. Padmanabhan, T. R. Choudhury, and A. Refregier, "*Theoretical and observational constraints on the Hi intensity power spectrum*," Monthly Notices of the Royal Astronomical Society **447**, 3745 (2015).

[465] W. Hu and N. Sugiyama, "*Small-scale cosmological perturbations: an analytic approach*," The Astrophysical Journal **471**, 542 (1996).

[466] H.-J. Seo and D. J. Eisenstein, "*Improved forecasts for the baryon acoustic oscillations and cosmological distance scale*," The Astrophysical Journal **665**, 14 (2007).

[467] C. Chang, M. Jarvis, B. Jain, S. Kahn, D. Kirkby, A. Connolly, S. Krughoff, E.-H. Peng, and J. Peterson, "*The effective number density of galaxies for weak lensing measurements in the LSST project*," Monthly Notices of the Royal Astronomical Society **434**, 2121 (2013).

[468] P. M. Geil, B. Gaensler, and J. S. B. Wyithe, "*Polarized foreground removal at low radio frequencies using rotation measure synthesis: uncovering the signature of hydrogen reionization*," Monthly Notices of the Royal Astronomical Society **418**, 516 (2011).

[469] F. Villaescusa-Navarro, M. Viel, K. K. Datta, and T. R. Choudhury, "*Modeling the neutral hydrogen distribution in the post-reionization Universe: intensity mapping*," Journal of Cosmology and Astroparticle Physics **2014**, 050 (2014).

[470] L. Amendola, "*Coupled quintessence*," Physical Review D **62**, 043511 (2000).

[471] L. Amendola, "*Linear and nonlinear perturbations in dark energy models*," Physical Review D **69**, 103524 (2004).

[472] N. Metropolis, A. W. Rosenbluth, M. N. Rosenbluth, A. H. Teller, and E. Teller, "*Equation of state calculations by fast computing machines*," The journal of chemical physics **21**, 1087 (1953).

[473] W. K. Hastings, "*Monte Carlo sampling methods using Markov chains and their applications*," (1970).

[474] D. Foreman-Mackey, D. W. Hogg, D. Lang, and J. Goodman, "*emcee: the MCMC hammer*," Publications of the Astronomical Society of the Pacific **125**, 306 (2013).

[475] A. Gómez-Valent and L. Amendola, "*H0 from cosmic chronometers and Type Ia supernovae, with Gaussian Processes and the novel Weighted Polynomial Regression method*," Journal of Cosmology and Astroparticle Physics **2018**, 051 (2018).

[476] M. Betoule, R. Kessler, J. Guy, J. Mosher, D. Hardin, R. Biswas, P. Astier, P. El-Hage, M. Konig, S. Kuhlmann, *et al.*, "*Improved cosmological constraints from a joint analysis of the SDSS-II and SNLS supernova samples*," Astronomy & Astrophysics **568**, A22 (2014).

[477] S. Nesseris, G. Pantazis, and L. Perivolaropoulos, "*Tension and constraints on modified gravity parametrizations of Geff(z) from growth rate and Planck data*," Physical Review D **96** (2017), 10.1103/physrevd.96.023542.

[478] G. Gupta, S. Majumdar, and A. A. Sen, "*Constraining thawing quintessence*," Monthly Notices of the Royal Astronomical Society **420**, 1309 (2012).

[479] A. Sangwan, A. Tripathi, and H. Jassal, "*Observational constraints on quintessence models of dark energy*," arXiv preprint arXiv:1804.09350 (2018).

[480] W. Yang, M. Shahalam, B. Pal, S. Pan, and A. Wang, "*Constraints on quintessence scalar field models using cosmological observations*," Physical Review D **100**, 023522 (2019).

[481] P. e. Bull, "*Beyond LCDM: Problems, solutions, and the road ahead*," Physics of the Dark Universe **12**, 56 (2016), arXiv:1512.05356 [astro-ph.CO] .

[482] P. Bull, "*Extending cosmological tests of general relativity with the square kilometre array*," The Astrophysical Journal **817**, 26 (2016).

[483] D. N. Schramm and M. S. Turner, "*Big-bang nucleosynthesis enters the precision era*," Reviews of Modern Physics **70**, 303 (1998).

[484] G. Steigman, "*Primordial nucleosynthesis in the precision cosmology era*," Annu. Rev. Nucl. Part. Sci. **57**, 463 (2007).

[485] R. H. Cyburt, B. D. Fields, K. A. Olive, and T.-H. Yeh, "*Big bang nucleosynthesis: Present status*," Reviews of Modern Physics **88**, 015004 (2016).

[486] E. Di Valentino, O. Mena, S. Pan, L. Visinelli, W. Yang, A. Melchiorri, D. F. Mota, A. G. Riess, and J. Silk, "*In the realm of the Hubble tension—a review of solutions*," Classical and Quantum Gravity **38**, 153001 (2021).

[487] B. et.al, "*Observational challenges for the standard FLRW model*," International Journal of Modern Physics D **25**, 1630007-244 (2016), arXiv:1512.03313 [astro-ph.CO] .

[488] L. A. e. Anchordoqui, "*Dissecting the H0 and S8 tensions with Planck + BAO + supernova type Ia in multi-parameter cosmologies*," Journal of High Energy Astrophysics **32**, 28 (2021), arXiv:2107.13932 [astro-ph.CO] .

[489] S. N. et.al., "*The H0 Olympics: A fair ranking of proposed models*," Physics Reports **984**, 1 (2022), arXiv:2107.10291 [astro-ph.CO] .

[490] E. Di Valentino, "*A combined analysis of the H 0 late time direct measurements and the impact on the Dark Energy sector*," Monthly Notices of the Royal Astronomical Society **502**, 2065 (2021).

[491] E. N. Saridakis, R. Lazkoz, V. Salzano, P. V. Moniz, S. Capozziello, J. B. Jiménez, M. De Laurentis, and G. J. Olmo, *Modified gravity and cosmology* (Springer, 2021).

[492] M. G. Dainotti, B. De Simone, T. Schiavone, G. Montani, E. Rinaldi, and G. Lambiase, "*On the Hubble constant tension in the SNe Ia Pantheon sample*," The Astrophysical Journal **912**, 150 (2021).

[493] G. Bargiacchi, M. Dainotti, and S. Capozziello, "*Tensions with the flat LCDM model from high-redshift cosmography*," arXiv preprint arXiv:2307.15359 (2023).

[494] T. M. Abbott, F. B. Abdalla, A. Alarcon, J. Aleksić, S. Allam, S. Allen, A. Amara, J. Annis, J. Asorey, S. Avila, *et al.*, "*Dark Energy Survey year 1 results: Cosmological constraints from galaxy clustering and weak lensing*," Physical Review D **98**, 043526 (2018).

[495] E. Di Valentino, A. Melchiorri, O. Mena, and S. Vagnozzi, "*Nonminimal dark sector physics and cosmological tensions*," Physical Review D **101**, 063502 (2020).

[496] S. Vagnozzi, "*New physics in light of the H 0 tension: an alternative view*," Physical Review D **102**, 023518 (2020).

[497] G. Alestas, L. Kazantzidis, and L. Perivolaropoulos, "*H 0 tension, phantom dark energy, and cosmological parameter degeneracies*," Physical Review D **101**, 123516 (2020).

[498] L. A. Anchordoqui, I. Antoniadis, D. Lüst, J. F. Soriano, and T. R. Taylor, "*H 0 tension and the string swampland*," Physical Review D **101**, 083532 (2020).

[499] A. Banerjee, H. Cai, L. Heisenberg, E. Ó. Colgáin, M. M. Sheikh-Jabbari, and T. Yang, "*Hubble sinks in the low-redshift swampland*," Physical Review D **103**, L081305 (2021).

[500] K. Dutta, A. Roy, Ruchika, A. A. Sen, and M. Sheikh-Jabbari, "*Beyond Λ CDM with low and high redshift data: Implications for dark energy*," General Relativity and Gravitation **52**, 15 (2020).

[501] Ö. Akarsu, J. D. Barrow, L. A. Escamilla, and J. A. Vazquez, "*Graduated dark energy: Observational hints of a spontaneous sign switch in the cosmological constant*," Physical Review D **101**, 063528 (2020).

[502] L. Visinelli, S. Vagnozzi, and U. Danielsson, "*Revisiting a negative cosmological constant from low-redshift data*," Symmetry **11**, 1035 (2019).

[503] G. Ye and Y.-S. Piao, "*Is the Hubble tension a hint of AdS phase around recombination?*" Physical Review D **101**, 083507 (2020).

[504] W. Yin, "*Small cosmological constant from a peculiar inflaton potential*," Physical Review D **106**, 055014 (2022).

[505] L. Campanelli, G. Fogli, T. Kahniashvili, A. Marrone, and B. Ratra, "*Galaxy cluster number count data constraints on cosmological parameters*," The European Physical Journal C **72**, 2218 (2012).

[506] Z. Sakr, S. Ilić, and A. Blanchard, "*Cluster counts-III. ΛCDM extensions and the cluster tension*," Astronomy & Astrophysics **666**, A34 (2022).

[507] F. Simpson and J. A. Peacock, "*Difficulties distinguishing dark energy from modified gravity via redshift distortions*," Physical Review D **81**, 043512 (2010).

[508] L. Samushia, W. J. Percival, and A. Raccanelli, "*Interpreting large-scale redshift-space distortion measurements*," Monthly Notices of the Royal Astronomical Society **420**, 2102 (2012).

[509] F. Montanari and R. Durrer, "*New method for the Alcock-Paczyński test*," Physical Review D **86**, 063503 (2012).

[510] A. Hamilton, "*Linear redshift distortions: a review*," in *The evolving universe* (Springer, 1998) pp. 185–275.

[511] T. Matsubara and Y. Suto, "*Cosmological Redshift Distortion of Correlation Functions as a Probe of the Density Parameter and the Cosmological Constant*," The Astrophysical Journal Letters **470**, L1 (1996), arXiv:astro-ph/9604142 [astro-ph] .

[512] W. E. Ballinger, J. A. Peacock, and A. F. Heavens, "*Measuring the cosmological constant with redshift surveys*," Monthly Notices of the Royal Astronomical Society **282**, 877 (1996), arXiv:astro-ph/9605017 [astro-ph] .

[513] D. J. Bacon, R. A. Battye, P. Bull, S. Camera, P. G. Ferreira, I. Harrison, D. Parkinson, A. Pourtsidou, M. G. Santos, L. Wolz, *et al.*, "*Cosmology with Phase 1 of the Square Kilometre Array Red Book 2018: technical specifications and performance forecasts*," Publications of the Astronomical Society of Australia **37**, e007 (2020).

[514] A. Fialkov, R. Barkana, and A. Cohen, "*Reconstructing the nature of the first cosmic sources from the anisotropic 21-cm signal*," Physical Review Letters **114**, 101303 (2015).

List of Publications and Presentations

- **Publications in National/International Journals**

1. *Chandrachud Bijay Vaswar Dash*, Tapomoy Guha Sarkar, "Constraining dark energy using the cross correlations of weak lensing with post-reionization probes of neutral hydrogen", *Journal of Cosmology and Astroparticle Physics*, **499**, (November 2, 2020).

2. *Chandrachud Bijay Vaswar Dash*, Tapomoy Guha Sarkar, Anjan Kumar Sarkar "Intensity mapping of post-reionization 21-cm signal and its cross-correlations as a probe of $f(R)$ gravity", *Journal of Astronomy and Astrophysics*, **44**, (January 21, 2023).

3. *Chandrachud Bijay Vaswar Dash*, Tapomoy Guha Sarkar, "Probing Quintessence using BAO imprint on the cross-correlation of weak lensing and post-reionization HI 21-cm signal", *Monthly Notices on Royal Astronomical Society*, **516**, (September 09, 2022).

4. *Chandrachud Bijay Vaswar Dash*, Tapomoy Guha Sarkar, Anjan A. Sen " Post-reionization HI 21-cm signal: A probe of negative cosmological constant" *Monthly Notices of the Royal Astronomical Society*, **527**, (February 2024).

- **Schools and Workshops Attended**

1. *Chandrachud Bijay Vaswar Dash* attended *Cosmology - The Next Decade* held in *ICTS, Bangalore* during January 03 - 25, 2020.

2. *Chandrachud Bijay Vaswar Dash* attended *Observing The First Billion Years of the Universe Using Next Generation Telescope* held in *IIT, Indore* during January 27 - 31, 2020.

3. *Chandrachud Bijay Vaswar Dash* virtually attended *IUCAA Summer school and Refresher course 2020* held in *IUCAA, Pune* during May 11 - June 12, 2020.

4. *Chandrachud Bijay Vaswar Dash* attended *Physics of Early Universe - A Online Precursor* held in *ICTS, Bangalore* during August 31 - September 3, 2020.

5. *Chandrachud Bijay Vaswar Dash* virtually attended *Summer School on Cosmology 2022* held in *ICTP, Trieste* during July 04 - 15 July, 2022.

6. *Chandrachud Bijay Vaswar Dash* participated in *Gravitational Wave open Data Workshop- 2023* during May 15 - 17, 2023.

7. *Chandrachud Bijay Vaswar Dash* attended *ZTF-Summer School 2023* held in *University of Minnesota, Twin Cities* during July 24 - 28 July, 2023.

- **Conference Participation**

1. *Chandrachud Bijay Vaswar Dash* presented paper titled *Constraining Dark Energy Using The Cross Correlations of CMBR Weak Lensing With Post-Reionization HI 21-cm Signal* during bi-weekely telecon meeting in the *EoR and Post-EoR SKA India* group at December 4, 2020.

2. *Chandrachud Bijay Vaswar Dash* participated in *One day meeting (SAZERAC sip) on the estimators of the CD-EoR 21-cm signal* at January 29, 2021.

3. *Chandrachud Bijay Vaswar Dash* attended the Tehran Meeting on *Cosmology at the Crossroads* during February 22 - 25, 2021.

4. *Chandrachud Bijay Vaswar Dash* presented paper titled *Probing $f(R)$ gravity using post-reionization HI 21-cm signal* in *Workshop on 21-cm Cosmology and Reionization* during April 19 - 23, 2021.

5. *Chandrachud Bijay Vaswar Dash* presented paper titled *Probing Quintessence using BAO imprint on the cross-correlation of weak lensing and post-reionization HI 21cm signal* in *Workshop on 21-cm Cosmology in the SKA Era, ISI Kolkata* during Oct 30 - Nov 4, 2022.

6. *Chandrachud Bijay Vaswar Dash* presented poster titled *Probing $f(R)$ gravity using post-reionization HI 21-cm signal* in *Field Theoretic Aspects of Gravity (FTAG)- 2023* during March 17 - 19, 2023.

Brief Biography of the Supervisor

Prof. Tapomoy Guha Sarkar is a professor in the Department of Physics, Birla Institute of Technology & Science Pilani, Pilani Campus. He obtained the Doctorate of Philosophy from the Centre for Theoretical Studies, Indian Institute of Technology Kharagpur, India in 2011 under the supervision of Professor Somnath Bharadwaj. He also worked as a Postdoctoral fellow at Harish Chandra Research Institute, Allahabad, for a year before he joined the Physics Department of BITS Pilani, Pilani Campus, in June 2012. His research interests are in the areas of cosmological structure formation, gravity, and 21-cm cosmology.

Brief Biography of the Candidate

Mr. Chandrachud Bijay Vaswar Dash joined the Department of Physics, BITS Pilani as a Research Scholar in August 2018. He is currently pursuing a PhD in the area of Theoretical Cosmology specifically, on dark energy and 21-cm physics. He has published research articles in reputed international journals. He has attended schools on various topics during his PhD. He has also participated and presented his work in several national and international conferences.